DOCTOR OF PHILOSOPHY

New methods for in situ measurement of mechanical root-reinforcement on slopes

Meijer, Gerrit Johannes

Award date:
2016

School of Science and Engineering
Department of Civil Engineering
University of Dundee

New methods for *in situ* measurement of mechanical root-reinforcement on slopes

Gerrit Johannes Meijer

A dissertation submitted for the
degree of Doctor of Philosophy
to the University of Dundee.
July 2016

Declaration

This is to certify that, except where specific reference is made to other investigations, the work described in this dissertation is the result of the investigation of the candidate. All references cited have been consulted by the candidate, and neither this dissertation or any part of it has been previously accepted for a higher degree.

Gerrit Johannes Meijer (candidate), Dundee, July 2016

Dr A. Glyn Bengough, Dundee, July 2016

Acknowledgements

This work was made possible through a studentship provided by Forest Research, funded by ClimateXChange, the Scottish Government's Centre for Expertise on Climate Change. It was carried out as a collaboration between the University of Dundee (UoD), the James Hutton Institute (JHI) and Forest Research (FR).

I would like to take this opportunity to thank many people. First, I would like to thank my supervisors Dr Glyn Bengough (UoD/JHI), Dr Jonathan Knappett (UoD), Dr Kenneth Loades (JHI) and Dr Bruce Nicoll (FR). Your excellent guidance, encouragement and innumerable suggestions and ideas have been invaluable. My thanks extend to the technical staff of both the University of Dundee and the James Hutton Institute for their invaluable support during the design and manufacturing of experimental equipment.

In addition, thanks go to Dr Jennifer Brown (JHI), David Boldron (UoD/JHI) and Colin McEvoy (FR) for their assistance during some of the field work, and to Mengqi Zhang and Ivan Mukov, both former Civil Engineering undergraduate students at the University of Dundee, for their help with preparing and conducting some of the laboratory testing. The Forestry Commission and the Comer Estate receive thanks for providing me with access to their field sites. I also owe thanks to Philip Smith for his thorough final proofreading.

Scotland has become a wee bit of a second home for me throughout the course of my studies, and my thanks goes out to everyone who made it so. I think of the inhabitants of the fish bowl, V-block, my friends, my church congregation and especially my girlfriend Jaynie. I am grateful for the moral support all of you, together with friends and family in The Netherlands, have provided me over the last years.

Sola Deo gloria

Abstract

Vegetation can increase the resistance of slopes against landsliding. The mechanical contribution of roots to the shear strength of the soil is however difficult to measure *in situ*. Existing methodologies are time-consuming and therefore not suitable to quantify spatial variability on the slope. Furthermore, some existing methods, for example large *in situ* shear box testing, can be difficult to apply on remote sites with difficult access, e.g. steep slopes. Therefore in this thesis novel, simple and portable methods to quantify mechanical root-reinforcement in the field were developed.

The 'blade penetrometer method', one of these new methods, was based on standard penetrometer testing but used an adapted tip shape to increase sensitivity to roots. Root depths and diameters could be quantified based on characteristics of the depth–resistance trace, both in the laboratory and in the field. Several new analytical interpretive models were developed to predict the force–displacement behaviour of roots loaded under various conditions: one assuming roots broke in tension and another assuming roots broke in pure bending. Both methods did take root–soil interaction into account. Based on these models, some roots were shown to have broken in bending and others in tension, depending on plant species and root diameter.

Two new methods were developed to measure the root-reinforced soil strength directly. The 'pin vane' was an adaptation of a standard field shear vane, replacing the cruciform blades of the latter by prongs to minimise the effects of soil disturbance and root breakage during installation. This was one of the main problems encountered when using standard vanes in rooted soil. This 'pin vane' method was qualitatively shown to be able to measure the reinforcing effects of both fine and thick roots (or root analogues), both in the laboratory and the field. This method will be most useful when the strength of densely rooted surface layers is to be analysed, e.g. for erosion resistance purposes.

Another newly developed shear device was the 'corkscrew'. Rotational installation of the screw ensured minimal soil and root disturbance. During vertical extraction the root-reinforced shear strength was mobilised along the interface of the soil plug caught within the screw. The measured extraction force could be related to the reinforced soil strength. This method underestimated the strength in surface layers (especially at 0–125 mm and less so at 125–250 mm depth) but functioned well in deeper soil layers important for landsliding. Although laboratory results were promising, during *in situ* testing in deeper layers (>125 mm) local variation in soil stress, gravel content and water content, combined with low root volumes, made it difficult to accurately quantify the effect of the

roots. Where the effect of roots was pronounced, e.g. in more heavily rooted surface layers (0–125 mm), significant positive trends between the measured soil strength and root strength and quantity were found. Measured reinforcements were small compared with various root-reinforcement model predictions but comparable to direct shear tests on rooted soil reported by others.

These new methods, although still in the early stages of development, showed promising results for practical use in field conditions. The equipment was simple to use and portable, enabling measurements on sites with difficult accessibility. However, more work is required to validate the interpretive models developed and to calibrate these methods for a wider range of soil and root conditions.

Keywords: soil bio-engineering, mechanical root-reinforcement, *in situ* testing, slope stability

Contents

List of Figures

List of Tables

List of Symbols

Symbol	Unit	Parameter
α	[-]	Van Genuchten parameter
α	[°]	Slope angle
α_E		Coefficient in root diameter–tensile stiffness fit
α_σ		Coefficient in root diameter–tensile strength fit
α_1	[-]	Ratio of standard over blade penetrometer resistance (in terms of force)
α_2	[-]	Ratio of lateral root resistance over standard penetrometer resistance
β	[°]	Angle between root orientation and direction perpendicular to the shear plane
β_E		Power coefficient in root diameter–tensile stiffness fit
β_σ		Power coefficient in root diameter–tensile strength fit
γ	[kNm^{-3}]	Volumetric weight
γ'	[kNm^{-3}]	Effective volumetric weight
γ_d	[kNm^{-3}]	Dry volumetric weight
γ_w	[kNm^{-3}]	Volumetric weight of water
δ	[°]	Interface friction angle
ζ	[-]	Coefficient in analytical cable model
η	[-]	Coefficient in analytical cable model
θ	[m^3 m^{-3}]	Volumetric water content
ρ_d	[Mgm^{-3}]	Dry bulk density
σ_t	[MPa]	Tensile strength
σ_v	[kPa]	Total vertical soil stress
σ'_v	[kPa]	Effective vertical soil stress
τ	[kPa]	Soil shear strength
τ_i	[kPa]	Soil–root interface friction
τ_{cs}	[kPa]	Shear strength measured with corkscrew device
τ_{pv}	[kPa]	Shear strength measured with pin vane device
ϕ'	[°]	Soil effective angle of internal friction
ϕ^b	[°]	Angle indicating the rate of increase in soil shear strength relative to the matric suction

Symbol	Unit	Parameter
a	[-]	Load distribution coefficient in fibre bundle models
b		Gradient of linear fit
c	[kPa]	Soil cohesion
c'	[kPa]	Effective soil cohesion
c_r	[kPa]	Root cohesion
d	[mm]	Diameter
d_{cs}	[mm]	Diameter of the corkscrew device
d_{pv}	[mm]	Diameter of the pin vane device
d_r	[mm]	Root diameter
DBH	[mm]	Tree diameter at breast height
E	[MPa]	Young's modulus
E_{90}	[MPa]	Secant stiffness at 90% of peak strength
E_b	[MPa]	Young's modulus in bending
E_t	[MPa]	Young's modulus in tension
f	[-]	Ratio of root–soil interface friction over soil shear strength
f_s	[Hz]	Measurement frequency
F	[N]	Force / resistance
F_t	[N]	Maximum tensile force
F_u	[N]	Maximum external load a root can sustain before breakage (analytical models)
FOS	[-]	Factor of safety
h_{cs}	[mm]	Height of the corkscrew device
h_{pv}	[mm]	Height of the pin vane device
h_w	[mm]	Height of the water table above the sliding plane
h_z	[mm]	Height of the soil layer above the sliding plane
I	[mm^4]	Second moment of cross-sectional area
I_d	[%]	Soil relative density
k'	[-]	Ratio between root cohesion and the product of root tensile strength and root area ratio (Wu/Waldron model)
k''	[-]	Fibre bundle model root-reinforcement reduction factor due to progressive root failure
k_{cs}	[Nmm^{-3}]	Corkscrew spring stiffness
K_0	[-]	Coefficient of lateral earth pressure (at rest)
K_a	[-]	Coefficient of lateral earth pressure (active)
L	[mm]	Length
L_{crit}	[mm]	Length of displacing root in analytical bending model
m	[-]	Van Genuchten parameter

Symbol	Unit	Parameter
m	[g]	Mass
M	[Nmm]	Moment
M_u	[Nmm]	Ultimate moment capacity
n	[-]	Van Genuchten parameter
n	[-]	Amount
p	[MPa]	Soil resistance to lateral pile or root displacement
p_u	[MPa]	Ultimate soil resistance to lateral pile or root displacement
R^2	[-]	Coefficient of determination of a fit
RAR	[-]	Root area ratio
RLD	[cm cm^{-3}]	Root length density
RV	[m^{3}m^{-3}]	Volumetric root volume ratio
s	[kPa]	Soil suction
s_e	[kPa]	Air entry value
S_r	[-]	Soil saturation
S_t	[-]	Soil sensitivity
t	[s]	Time
T	[Nmm]	Torque
u	[mm]	Displacement
u_u	[mm]	Lateral root displacement at root failure (analytical models)
V	[mm^3]	Volume
V_f	[mm^3 mm^{-3}]	Fibre content (volumetric)
V_s	[mm^3 mm^{-3}]	Stone content (volumetric)
w	[mm]	Width
w	[g g^{-1}]	Gravimetric water content
w_L	[g g^{-1}]	Soil liquid limit (Atterberg)
w_t	[kPa]	Tree surcharge
w_w	[kPa]	Tangential soil stress caused by tree wind loading
w_P	[g g^{-1}]	Soil plastic limit (Atterberg)
W_n	[-]	Normalised energy dissipation
z	[mm]	Depth
z_0	[mm]	Depth of top of rooted soil layer
z_1	[mm]	Depth of bottom of rooted soil layer
z_r	[mm]	Root depth

1

Introduction

1.1 Use of vegetation in civil engineering

Vegetation influences the mechanical behaviour of the soil it grows on, and therefore can perform important engineering functions. At the soil surface, plants can restrain and protect the soil against erosion while at depth roots can increase the soil strength and therefore increase slope stability (Gray and Sotir, 1996; Norris et al., 2008). Compared to more traditional 'hard engineering' methods, such as soil nailing or the use of retaining walls, natural vegetation can be used as an alternative and more environmentally friendly solution. This approach acknowledges that a slope is part of the natural environment to which 'green' solutions might not only benefit geotechnical safety but also provide a range of other ecosystem services. For example, one can think of providing natural visual or acoustical screening, improving air quality along busy transport corridors or establishing a habitat for wildlife.

While some uses of vegetation are well documented, e.g. the use of grass on stream banks to protect the banks against scour and erosion (Coppin and Richards, 1990), coherent scientific frameworks for using vegetation for practical soil stabilisation are not well documented, likely because root–soil interaction is highly complicated and multi-faceted. However, noteworthy efforts in linking theory with practice were made by Coppin and Richards (1990), Gray and Sotir (1996) and Norris et al. (2008). Challenges for using vegetation in civil engineering, compared to more traditional methods, stem from natural variation in the character of biological material and soil. This results in large spatial and temporal variability in mechanical behaviour across a slope, with a requirement for appropriate long-term management.

1.2 Slope stability and erosion

Vegetation can help to mitigate various natural problems. Here a distinction is made between slope instabilities in natural slopes, slope instabilities in man-made slopes (embankments or cuttings) and the problem of erosion.

Landslides occurring on natural slopes are a large problem worldwide, yearly killing thousands of people (USGS, 2016). Petley (2012) identified 2620 fatal landslides worldwide over the period 2004–2010, causing over 32,000 fatalities.

Commonly, landslides are classified based on the dominant mechanisms and the type of material involved, e.g. using the classification by Cruden and Varnes (1996). They distinguished various types of failure mechanisms: 1) *falls*: material falling from sleep slopes, largely displacing by falling and rolling rather than shearing; 2) *topples*: out-of-slope movement of material by forward rotation or overturning; 3) *slides*, sliding of material along a thin sliding surface with high localised shear strain, where the sliding mass suffers no or little internal deformation. Slides can have various shapes of sliding surfaces (e.g. planar or rotational, resulting in translational or rotational failures); 4) *flows*: spatially continuous flow-like movements of material behaving like a viscous fluid. Flow materials can be saturated or dry; 5) *spreads*: slow fracturing and lateral extension of material caused by plastic flow or liquefaction. The type of material is generally categorised as either rock, debris or earth.

Most landslides in Scotland can be classed as debris flows: high velocity viscous flows consisting of a mixture of a lubricant (in the Scottish case: water), soil and debris. In many cases, the initial displacement of a small mass of soil appeared to be the trigger. When such a mass slides into a stream channel, the sediment fluidises during subsequent mixing with the available water. During further downhill movements, the slide will further erode the channel bed, increasing the flow volume (Winter et al., 2005). Although debris flows are most common, rotational or translational slides occur in Scotland as well.

Landslides cause damage in the form of loss of life, direct damage to structures or damage through loss of function. The latter case is topical in Scotland where landslides regularly cause roads or railways to shut for days or weeks until the debris has been cleared and the slope is deemed safe. The A83 trunk road through the Rest and Be Thankful pass is especially notorious, experiencing at least 16 slope instabilities between October 2007 and March 2014 (Transport Scotland, 2016b), although many other places experience frequent instabilities as well.

The most common landslide trigger in Scotland and the rest of the UK is rainfall. Precipitation increases pore pressures in the slope, thereby reducing the soil strength available to withstand gravity acting on the sliding mass. Both extended periods of rainfall and intense storms can result in the soil water conditions necessary to trigger slope instabilities (Winter et al., 2005).

Roots will add to the strength of the slope through mechanical action only when the rooting depth of plants is sufficiently deep to intersect with a potential shear plane. Therefore, the mechanical reinforcement of natural slopes by roots is likely to be only relevant when shallow landslides and/or deep-rooting plant species are considered, as most of the plant root material will be present in the top 1–2 m of the soil.

Slope instabilities may also occur on man-made slopes such as embankments and cuttings, for example those constructed for rail or road links. Although these failures involve much smaller volumes, they can still have a large economic impact by blocking important transport corridors. For example, National Rail estimated that geotechnical causes were to blame for 400,000 minutes of train delays over the period 2000–2003, costing 26 million pounds (Scott et al., 2007). Since the dimensions of these slopes are generally much smaller compared to natural slopes, the shear plane will likely occur at shallower depths. Therefore using vegetation for stabilisation purposes is likely to be more relevant for these types of slopes.

A third natural problem for which vegetation might provide an 'green' solution concerns soil erosion. Roots bind the soil together and the shoot of the plant might slow down subsurface flow (Gyssels et al., 2005). The reduction of erosion due to vegetation might be important for stream banks, which can be prone to instability for example due to undercutting, where soil at the toe of the bank is washed away by the stream, increasing the slope angle and therefore the chance of failure. Green bank protection techniques can help to protect these banks by reducing scour and erosion (e.g. SEPA, 2008). For example, willows can be used to bind bundles of brushwood to the bank and also directly reinforce the slope.

Climate change projections indicate that the mean precipitation levels in the UK will increase over the next century, especially during the winter. For example, in the west and north of Scotland, the regions with the highest landslide occurrence (Winter et al., 2005), the average winter precipitation is expected to increase by 8–16% by 2050 and 16–30% by 2080 (50% probability levels), depending on the emission scenario (UKCIP, 2009). This will increase the risk of slope instability and increase erosion rates.

1.3 Forestry

Forestry is an important economic sector in the UK. The timber production in the UK was estimated to be 10–11 million m^3 per year over the period 2011–2014. The export value of UK wood products, comprising 5–7 million m^3 per year (2005–2014), was worth roughly 1.5–1.8 billion pounds per year (Forestry Commission, 2015). Woodlands take up 3.15 million hectares (13%) of the UK's land area. In Scotland, an even larger proportion of land (18%) is classed as woodland (Forestry Commission, 2015).

Forests provide various ecosystem services. These can be classed as 1) *provisioning*

services, where the woodland provides resources such as timber or food; 2) *regulating services*, where the woodland helps to regulate ecosystem processes such as water purification, climate or pollination; 3) *cultural services*, where the woodland provides non-material benefits like recreation or education (Forestry Commission, 2011). Vegetation helping to reduce the risk of slope instability can be seen as a regulating service. Although ideally these services are complementary, often a trade-off has to be made. This is especially true when using forests to reduce slope stability, as selecting suitable species or forest management strategies might, for example, affect timber yield or forest aesthetics.

Forestry relates to slope stability problems in two ways. First, planting slopes with new vegetation might help to stabilise (unplanted) slopes which are at risk. Guidelines have been developed for selecting species and for planting techniques and strategies (Coppin and Richards, 1990; Gray and Sotir, 1996; Stokes et al., 2009; Norris et al., 2008). However, use of vegetation as a serious slope stabilisation alternative is still uncommon in civil engineering. Second, potential instability of slopes has implications for the way forests on these slopes should be managed. Planting, managing and harvesting forests should be performed in such a way that slope stability is not compromised. Slopes are at risk for example through the building of forest roads or the use of heavy equipment damaging the soils. Furthermore, it is often observed that slopes are more prone to slope instability after clearfelling (e.g. Watson et al., 1999) because of root degradation. Generally, managed forests provide less stability to slopes than natural forests, although careful forest management can minimise this discrepancy (Stokes, 2011).

Both the use of vegetation to stabilise slopes at risk and the management of existing slopes with vegetation require a good understanding of the behaviour of soil and roots .

1.4 Mechanical root-reinforcement quantification

Roots reinforce the soil through both mechanical and hydrological effects. The latter mechanisms work through reducing soil water contents and increasing soil suctions through plant evapotranspiration and changes in soil drainage (Coppin and Richards, 1990). However, since landslides often coincide with periods of intense rainfall these reinforcing effects will be low when most needed (Pollen-Bankhead and Simon, 2010). Mechanical root-reinforcement is introduced by the mechanical action of roots crossing a potential failure plane. These roots carry part of the load through tensile or bending action (Waldron, 1977). Since this process is generally considered to be independent from soil hydrology, it can increase the strength of a slope during adverse weather conditions.

Mechanical reinforcement is difficult to quantify in the field due to the discrete nature of the roots. It is difficult to install any test device without significant disturbance of the soil and the root system. *In situ* quantification is however important as there can be a large spatial variability in root architecture and soil properties. Since landslides will trigger

locally where soil strengths are low, it is important to take this variability into account. Landslides are observed to occur most frequently where vegetation covers are low (e.g. Moos et al., 2016).

Two common field measurement approaches exist. In the first, root quantities and diameters are measured using excavation of complete root systems (e.g. Di Iorio et al., 2005), core sampling (e.g. Genet et al., 2008) or counting root intersections on soil planes (e.g. Mao et al., 2012). Subsequently this data can be combined in a root-reinforcement model with data for root strength to calculate reinforcements. This method suffers from two problems: 1) it depends on the accuracy of the chosen model and 2) *in situ* root quantification is very time-consuming. In a second approach, the strength of root-reinforced soil is directly measured, for example by using a field shear box (e.g. Cammeraat et al., 2005). However, these tests are also time-consuming and require heavy equipment (e.g. for harvesting), making them less suitable to apply on difficult terrain such as steep and/or remote slopes.

1.5 Research aims and objectives

An improved understanding of the mechanical interaction between plant roots and soil is required to address the effect of plant roots on the stability of soil on a more practical level. However, currently a limiting factor is the lack of a quick yet reliable method to map mechanical root-reinforcement *in situ*. Such a method is required so that the spatial variation in soil conditions, variability in root growth and strength, as well as changes in environment can be taken into account. Furthermore, such a method will help to validate existing root-reinforcement models, something that is highly needed as these models currently yield a wide range of results.

Therefore, the main aim of this research is to develop new experimental methods to quantify the spatial distribution of roots and mechanical root-reinforcement *in situ*. Although root-reinforcement might be beneficial to reduce soil erosion, this thesis will focus on quantifying the effects of roots on slopes prone to shallow landslides.

The objectives of this study were:

1. To assess the benefits and limitations of existing methods to models used to quantify mechanical root-reinforcement;
2. To develop new root-soil interaction models to predict the reinforcement added by single roots under various loading conditions.
3. To design new measurement methods based on design criteria selected for practical use in the field;
4. To select the most promising measurement methods based on a pilot study performed under idealised laboratory conditions;

5. To compare selected shear strength measurement techniques with existing shear strength measurement devices in non-rooted soil to assess the accuracy of the new methods;
6. To compare selected methods with root-reinforcement models and existing measurement techniques to assess their accuracy under laboratory conditions using root analogues;
7. To compare selected methods with existing measurement and modelling techniques to assess their practicality, reliability and accuracy on vegetated fields and slopes;

1.6 Thesis structure

Before new experimental methods are introduced, first a background to roots and root-reinforcement as well as various existing methodologies to quantify their effect is provided in Chapter 2. Thereafter a number of novel *in situ* measurement techniques are presented (Chapter 3) and subsequently compared under controlled laboratory conditions using root analogues and recompacted soil (Chapter 4). Chapter 5 introduces numerical modelling techniques and new analytical models to study root–soil interaction of individual roots under diverse loading conditions. The next two chapters focus on 'blade penetrometer' testing, a new method to quantify root depth and diameter, both under laboratory (Chapter 6) and field conditions (Chapter 7). In the next chapter, Chapter 8, field testing of new methods developed to directly measure the strength of root-reinforced soil ('corkscrew' and 'pin vane' methods) is discussed. The thesis is concluded with a general discussion and conclusions (Chapter 9).

2

Literature review

Before new experimental methods could be developed a strong theoretical understanding of roots and soil–root interaction was required. Therefore the existing body of root-reinforcement research was investigated first. This chapter starts with introducing the various effects of roots on the strength of soil and the stability of slopes. The effect of forestry practice is treated in more detail. Subsequently the characteristics of individual roots and root systems are discussed, including root anatomy, architecture and mechanical behaviour. The mechanical interaction between soil and root is then discussed extensively since this forms the basis for understanding mechanical root-reinforcement. Various existing modelling and experimental techniques are introduced thereafter. Finally a discussion about how the stability of rooted slopes can be quantified is provided.

2.1 Influence of plants on soil strength

Roots affect the mechanical strength of soil and slope stability through both hydrological and mechanical mechanisms. These are discussed in the following sections, and a summary is presented in Table 2.1.

2.1.1 Hydrological reinforcement

Hydrological effects comprise strengthening or weakening effects by changes in water contents, water pressures and/or water fluxes.

Vegetation intercepts rainfall and stores water on the surfaces of aboveground parts of the plant (leaves, stems etc.). This water can evaporate from these surfaces, thus decreasing the total amount of water reaching the soil underneath the plant. In temperate broadleaved and coniferous forest this can cause an average annual decrease of 15–25% and 25–35% in rainfall reaching the soil surface respectively, while for grasses a reduction of 25–40% was found (Coppin and Richards, 1990). Smaller water contents in the soil correspond with increased soil strengths. However, interception might result in a local increase due

Table 2.1: Summary of the beneficial ('+') and adverse ('–') effects of vegetation on slope stability. Table remade from Coppin and Richards (1990).

Hydrological effects	Foliage intercepts rainfall causing:	
	1 absorptive and evaporative losses, reducing rainfall available for infiltration	+
	2 reduction in kinetic energy of raindrops and thus erosivity	+
	3 increase in drop size through leaf drip, thus increasing localised rainfall intensity	–
	Stem and leaves interact with flow at the ground surface, resulting in:	
	1 higher depression storage and higher volume of water for infiltration	+/–
	2 greater roughness on the flow of air and water, reducing its velocity, but	+
	3 tussocky vegetation may give high localised drag, concentrating flow and increasing velocity	–
	Roots permeate the soil, leading to:	
	1 opening up of the surface and increasing infiltration	–
	2 extraction of moisture which is lost to the atmosphere in transpiration, lowering pore water pressure and increasing soil suction, both increasing soil strength	+
	3 accentuation of desiccation cracks, resulting in higher infiltration	–
Mechanical effects	Roots bind soil particles and permeate the soil, resulting in:	
	1 restraint of soil movement reducing erodibility	+
	2 increase in shear strength through a matrix of tensile fibres	+
	3 network of surface fibres creating a tensile mat effect, restraining underlying strata	+
	Roots penetrate deeper strata, giving:	
	1 anchorage into firm strata, bonding soil mantle to stable subsoil of bedrock	+
	2 support to up-slope soil mantle through buttressing and arching	+
	Tall growth of trees, so that:	
	1 weight may surcharge the slope, increasing normal and down-slope force components	+/–
	2 when exposed to wind, dynamic forces are transmitted into the ground	–
	Stem and leaves cover the ground surface, so that:	
	1 impact of traffic is absorbed, protecting soil surface from damage	+
	2 foliage is flattened in high velocity flows, covering the soil surface and providing protection against erosive flows	+

to stem flow and leaf drip (Coppin and Richards, 1990), resulting in unfavourable local increases in surface erosion (Pollen-Bankhead and Simon, 2010).

During photosynthesis in plant shoot water evaporates from the leaves, a process named evapotranspiration. The water loss triggers an upward water flux in the plant, resulting in lower water contents in the soil and increased suction pressures near roots (Tarantino et al., 2002). The effects of matric suction can be significant and can influence soil reinforcement well below the rooted soil zone (Collison et al., 1995). Pollen-Bankhead and Simon (2010) quantified both the effects of suction and mechanical root-reinforcement for riparian young trees and switch grass and found that suction reinforcement effects were greater than mechanical reinforcements, but only during the summer months. During spring and winter mechanical effects were dominant as suction levels were low. Therefore evapotranspiration probably does not have a large effect on shallow landsliding and debris flow in temperate regions, where landsliding coincides with wet and cold seasons with low rates of evapotranspiration and soils being in (nearly) saturated conditions (Stokes et al., 2009).

Root growth increases the soil hydraulic conductivity through soil structure development. In addition, the hydraulic conductivity is significantly influenced by the emergence of preferential flow paths around roots, either through expansion–contraction cycles, root decay (Collison et al., 1995) or soil cracking (Coppin and Richards, 1990). Not only will rainwater penetrate more quickly, but the balance between infiltration and surface run-off will shift more towards infiltration. In areas covered with trees or grass, the percentage of rainfall running off is 10–20% while cultivation (30–40%) or urban development (60–80%) increases this percentage significantly (Coppin and Richards, 1990). Increased infiltration rates can have both positive and adverse effects on slope stability. Faster infiltration can result in increased rates of adverse pore water pressure build-up. This effect is more significant in soil with small permeabilities (such as clays or peats) where large pore water pressures can develop at the interface between rooted and non-rooted soil (Collison et al., 1995). On the other hand, increased permeabilities in slopes might be beneficial as the soil drains faster (Coppin and Richards, 1990). A well drained surface horizon in a slope can significantly reduce the occurrence of high soil water potentials in shallow soils (Preti, 2013).

The aboveground plant tissue increases the soil roughness, slowing down run-off water flows, and therefore can decrease surface inter-rill and rill erosion, although the effect of splash erosion is limited (Coppin and Richards, 1990; Gyssels et al., 2005). The decrease in erosion rates can be described with an inverse exponential relation between root parameters (e.g. root mass) and erosion rate (Gyssels et al., 2005). In addition, this additional roughness is able to intercept transported soil particles, thus reducing sediment travel distances. On the other hand, the presence of vegetation can increase the run-off velocity locally as water has to flow around the plant stem (Coppin and Richards, 1990),

thus increasing local flow velocities.

2.1.2 Mechanical reinforcement

Plants affect the strength of soil and slope stability through mechanical effects such as changes in soil strength, stiffness, density, stress conditions or additional external loading.

Together, roots and soil form a composite material. Similar to reinforcement of concrete by steel rebar, soil, weak in tension, is reinforced by roots, a material strong in tension. During soil deformation, roots are stretched and their tensile resistance transferred to the soil through interface friction between root and surrounding soil. The amount of mechanical reinforcement generated by mobilising root tensile strength depends on many factors, for example root length density, diameter, tensile strength, tensile stiffness, length/diameter ratio, surface roughness, root alignment (e.g. tortuosity) and the orientation of roots to the direction of principal strains (Coppin and Richards, 1990). Soil properties, such as density, pore water pressures/suctions, strength, stiffness parameters and the interface friction between soil and root affect reinforcement as well.

Commonly, the contribution of roots to the strength of soil is expressed as an increase in soil cohesion (c_r), sometimes called 'apparent root cohesion' (e.g. Wu et al., 1979; Operstein and Frydman, 2000). Typical values for different soil and plant conditions were summarised by Coppin and Richards (1990) as ranging from 1 to 17.5 kPa. The main composite reinforcement effect is commonly attributed to the influence of fine roots (Coppin and Richards, 1990). Not only is their tensile strength usually larger (see Section 2.3.3), they are also more abundant. For example, a good correlation between the fine root content (< 1 mm) and reinforcement (measured with an *in situ* shear box) was observed by Cammeraat et al. (2005), although relevant data on the influence of coarse roots was not presented. Mechanical root-reinforcement will be less effective when the slope failure mechanism is a deep failure, as root growth is commonly limited to the upper 0.5–1.0 m of the soil (see Section 2.3.2) (Collison et al., 1995; Coppin and Richards, 1990).

Roots affect the soil structure. They provide carbon to the soil via root turnover and exudation. Furthermore, soil particles in the area around the roots (the rhizosphere) are bound together by mucilage under the effect of wetting–drying cycles (Stokes et al., 2009). Field soil is known to harden in time through both thixotropic and cementation effects (Utomo and Dexter, 1981; Dexter, 1988; Mitchell and Soga, 2005), the latter often aided by the presence of organic material, e.g. decaying plant and root material (Smucker, 2005).

Vertically growing roots such as tap roots and sinker roots may penetrate into deeper soil and therefore anchor the plant and root–soil mass against lateral displacement (Coppin and Richards, 1990), similar to soil nailing (Stokes et al., 2009). Wu et al. (1979) observed pine roots penetrating into unweathered till and weathered bedrock. When anchorage is sufficient, the root–soil matrix can keep upslope soil in place by buttressing and arching effects. Buttressing is the stabilisation of a soil strip immediately upslope from the plant.

In addition, arching will develop in areas between these upslope stabilised soil 'strips'. This will however only occur if plant spacing is sufficiently close (Coppin and Richards, 1990).

The aboveground plant mass introduces additional external loading effects on the soil. The shoot weight of a plant causes an additional surcharge. This effect is usually only considered to be important in the case of trees because of the mass of their shoot (Coppin and Richards, 1990). Surcharge can have both a positive and negative effect on slope stabilisation depending on soil characteristics and slope angle. It increases the driving force (gravity) but also increases the resisting forces by increasing soil stress levels. Surcharge will be more adverse on steeper slopes. Reported surcharge magnitudes range between w_t = 1–5 kPa (O'Loughlin and Ziemer, 1982; Simon and Collison, 2002; Wu et al., 1979), but often the surcharge effect is neglected in slope stability calculations as the influence is small. Simon and Collison (2002) only found a small average decrease of 7% in the factor of safety for steep riparian stream banks when the additional weight was included.

The plant shoot also adds additional loading to the soil through wind loading on the shoot. Again this is mainly important for trees because of their large size and leaf area. Wind loading induces both moments and lateral loads in the root system. When these lateral loads act downslope, the driving force acting along a possible failure plane increases and the factor of safety is hence reduced (Coppin and Richards, 1990). In addition, wind may overturn individual trees creating local zones of weakness and increase in erosion susceptibility. The latter was observed at the A82 near Glen Gloy in Scotland in November 2011, where a landslip was triggered after a storm-felled tree detached a large part of the slope just below the motorway (Transport Scotland, 2016a).

2.2 Influence of forestry practice on slope stability

From the moment a tree dies or is harvested, root mass and root strength will start to decay over time, resulting in gradual reduction of root-reinforcement (O'Loughlin and Ziemer, 1982; Preti, 2013; Watson et al., 1999). The root systems of newly planted vegetation takes time to develop, resulting in a temporal 'window' of increased landslide risk corresponding with reduced root-reinforcements (Watson et al., 1999). The size of this 'window' decreases with slower decay rates and faster growth rates. In commercial forests, almost a decade is required for coniferous species to increase root-reinforcement to levels $c_r > 10$ kPa (Schmidt et al., 2001). The 'window size' depends also on species and forestry management (Watson et al., 1999).

Schmidt et al. (2001) found much smaller root cohesions in industrial forests compared to natural forests and attributed this to disturbance in the prior, e.g. arising from fire, herbicides and/or forest operations. Damage may have long-lasting effects. Pohl et al.

(2012) found that grading on alpine ski slopes strongly affected vegetation, despite being conducted 16–44 year ago. Vegetation was observed to be in pioneering state and aggregate stabilities were smaller.

Plant diversity can be beneficial to stop erosion. Plant diversity has a positive influence on ecosystem functioning, and studies above the tree line in the Alps demonstrated a positive influence on soil aggregate stability (Pohl et al., 2009, 2012), which is related to soil cohesion and therefore with slope stability (Fattet et al., 2011). However, the presence of understory might prohibit root growth of newly planted trees, creating zones of reduced soil strength which may last for more than 100 years (Schmidt et al., 2001). On the other hand, reducing understory might negatively impact erosion. In China, the practice of planting trees (mainly *Vernicia fordii*) to stabilise slopes while removing the understory vegetation increased inter-rill erosion and soil erodibility (Fattet et al., 2011).

Commercial forestry requires forest roads, which can be a cause of erosion (see studies cited in Imaizumi and Sidle, 2012), or negatively affect the stability of slopes below the road (Sidle and Ochiai, 2006, cited in Imaizumi and Sidle, 2012). Generally, managed forests provide smaller beneficial reinforcement effects compared to natural ones. However, when continuous cover management (e.g. selection or shelterwood systems) are used similar reinforcement might be achieved (Stokes, 2011).

Landslides will localise where the soil strength is low. Therefore, the spatial distribution of trees will have an effect on where landslides are likely to occur. Moos et al. (2016) found that the length of open gaps in the forest (in the direction of slope gradient) was larger in plots where landslides had occurred. Three-dimensional slope stability modelling by Mao et al. (2014) found that, although the safety against landslides increased significantly with the presence of roots, difference in safety between various planting scenarios (forest, old gap, new gap, tree island) was low. This shows the spatial distribution of plants is important to consider.

2.3 Root characteristics

2.3.1 Root anatomy

To understand the mechanical behaviour of a root, its anatomy needs to be taken into account.

In the root apical meristem, just behind the root tip and covered by the root cap, new cells divide and multiply. Behind this zone lies the region of cell elongation, driving root growth. Further away from the tip, in the region of maturation, cells differentiate into different functions. The stele, the central cylinder of the root comprised of vascular xylem and phloem tissue, transports water and food. It is covered by the cortex, generally occupying the largest volume in the root and made out of parenchyma tissue. The inner boundary of the cortex is called the endodermis and the outer boundary the epidermis,

from which root hairs might grow (Gregory, 2006).

Growth from the apical meristem is called primary growth. Roots of woody species also develop secondary growth. In this process, the vascular cambium, originating between xylem and phloem, forms new tissue, causing the root to expand radially. The outer layers of the new cork tissue, functioning similar to bark, is called the periderm. Because of this inside-out growth, often the endodermis, cortex and epidermis are shed in the process, resulting in a woody root (Gregory, 2006). Non-woody roots include those of grasses and herbs, as well as young shrub and tree roots which have not undergone secondary growth. More mature tree and shrub roots are classed as woody (Coppin and Richards, 1990).

2.3.2 Root architecture

Woody and non-woody plant species have different root systems.

Grasses provide a dense network of shallow roots and grow very quickly. 60–80% of the biomass of grass roots is usually found in the upper 50 mm of the soil, and the root system is highly branched and fibrous (Coppin and Richards, 1990). Similarly, herbs grow close to the ground providing a dense cover and often have shallow rooting. The majority of a herbaceous root system is generally found within the top 300–400 mm of the soil (Coppin and Richards, 1990). This tight and dense cover provided by grasses and herbs is mainly useful to prevent surface erosion, e.g. by wind or rain (Gray and Sotir, 1996).

Woody plants, such as trees and shrubs, can have deeper roots. Roots can be classed based on their function: Long, thick roots (or woody, coarse, skeleton, anchoring roots or macrorhizae) are a permanent part of the root system and provide anchorage, while the main function of thin roots (or non-woody, fine, feeding, absorbing roots or brachyrhizae) is taking up water and nutrients (Stokes et al., 2009). Roots can also be classed based on their location in the root architecture: tap roots are main vertical roots directly below the bole; sinker roots are vertical roots coming either from the bole or lateral roots, and lateral roots are roots growing from the bole in lateral direction (Gray and Sotir, 1996).

A traditional distinction for tree root systems is to divide them into plate root systems (large laterals and sinker roots), heart root systems (many horizontal, oblique and vertical roots) and tap root systems (large tap root with smaller laterals) (Gray and Sotir, 1996; Stokes et al., 2009). The resistance to tree overturning is highest for tap and heart root systems, while plate systems are more vulnerable (Dupuy et al., 2005b).

Root branching patterns can be described as herringbone (parent root remains straight and daughters branch off sideways) or dichotomous (parent root splits into two daughter branches at the end) (Dupuy et al., 2005a; Mickovski et al., 2007; Stokes et al., 1996, 2009). In reality, most patterns will lie somewhere in between the two extremes. All types can be found within one plant, depending on root age and nutrient heterogeneity (Stokes et al., 2009).

The spatial distribution of roots is affected by genetics, soil conditions and environ-

Table 2.2: Processes influencing root growth. Data from Bischetti et al. (2005), Coppin and Richards (1990), Sonnenberg et al. (2010), Stokes et al. (2009).

Plant	Soil			Environment
	Mechanical	Hydrological	Chemical	
Species	Impedance	Permeability	Nutrient availability	Loading conditions
Tree age	Density	Matric suction	pH	Management
	Texture	Water content	Toxicities	Competition
	Structure	Aeration		Climate

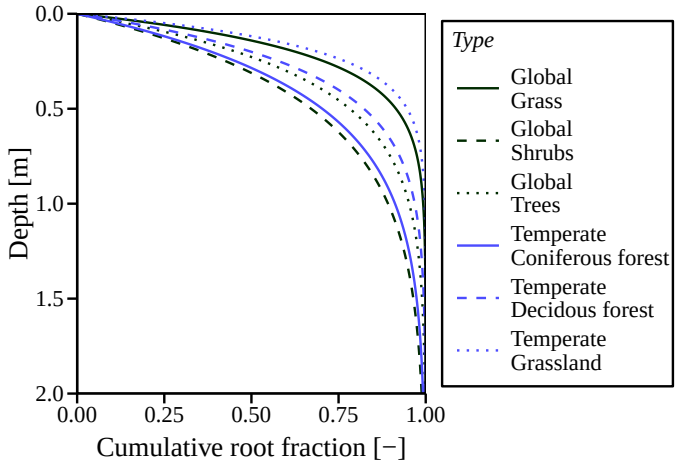

Figure 2.1: Fitted cumulative root distribution over depth for various plant types and climatic regions (Jackson et al., 1996).

mental conditions. Some important characteristics and limitations mentioned in literature are summarised in Table 2.2.

Root mass generally decreases rapidly with depth. This trend can be explained by the higher availability of oxygen (Gregory, 2006), smaller soil mechanical impedance (Bengough and Mullins, 1990) and higher availability of nutrients such as phosphorus, potassium or carbon (Jobbágy and Jackson, 2001) at shallow depth. When fitted with exponential curves, Jackson et al. (1996) found that globally and in temperate climate regions, > 75% of roots are found in the top 0.5 m, although there is variation between climatic region and plant type (Figure 2.1). Coarse roots (> 2 or 3 mm) are on average situated deeper than fine roots (Schenk and Jackson, 2002). Other root–depth distribution functions used were exponential curves (Abdi et al., 2010; Pollen-Bankhead and Simon, 2009), gamma functions (Bischetti et al., 2005), logarithms (Mattia et al., 2005) or normal distributions (Schmidt et al., 2001), all with declining root quantities with depth.

Since root growth and the resulting architecture depends on so many different factors, it is difficult to predict where the roots will be. The distance to the nearest tree might provide a decent proxy when combined with aboveground parameters such as stem thickness, plant height or canopy volume (Casper et al., 2003; Roering et al., 2003; Schwarz et al., 2010;

Docker and Hubble, 2009). The input parameters for these models are however site- and species-dependent, requiring calibration for each individual case. Furthermore, they only provide an average root distribution, ignoring spatial variability and preferential root growth.

2.3.3 Root biomechanical strength and stiffness

Root tensile strength (σ_t) and stiffness (E_t) are often found to vary with root diameter. This relationship is generally fitted using a power law:

$$\sigma_t = \alpha_\sigma \cdot d_r^{\beta_\sigma} \tag{2.1}$$

$$E_t = \alpha_E \cdot d_r^{\beta_E} \tag{2.2}$$

where α_σ, β_σ, α_E and β_E are fitting parameters. Reported fits are presented in Figure 9.1. Data on root stiffness is very sparse. Generally root strength and stiffness were found to decrease with increasing diameters. Comparison of 90 species categorised in three plant types (trees, shrubs and grass/herbs) showed significant differences in α_σ ($p = 0.003$) and β_σ ($p < 0.001$) between plant types (Mao et al., 2012). The larger tensile strength in thinner roots is attributed to increased cellulose contents, being highly resistant in tension (Genet et al., 2005), or differences in root tissue density (Coutts, 1983).

Root tensile strength and stiffness are not just dependent on species and diameter as Figure 9.1 might suggest. Different root types in fibrous barley roots (nodal, seminal or lateral roots) showed significant differences in strength (Loades et al., 2013). Root strength might be influenced by root water content (Yang et al., 2016), root age (Genet et al., 2008) or by soil conditions such as water content (Loades et al., 2013). The influence of environmental factors was not always found to be significant. Hudek et al. (2010) did not find differences for *Mahonia aquifolium* roots grown in cultivated and non-cultivated clay loam. Similar results were found by Bischetti et al. (2005) for 8 plant species in Northern Italy and by Vergani et al. (2012), who only found a weak relationship between elevation and tensile strength, and no correlation with mean annual rainfall, steepness, drainage, tree stem diameter, forest type, soil type or distance to the trunk. However, environmental differences were found by Schiechtl (1980), Burroughs and Thomas (1977) and Stokes (2002) (all as cited by Abdi et al., 2010).

Some of the variation in reported values for root tensile strength could have been caused by variation in the measurement procedure. Many different methods to store roots, root diameter measurements, prepare roots for testing, clamping, testing with or without root bark, root length and strain rate were reported which all might effects the results. The effect of only some of these has been studied. For example, an increase in the elongation rate from 10 to 400 mm min^{-1} was shown to lead to a 8–20% increase in measured tensile strength for beech roots (Cofie and Koolen, 2001).

The root stress–strain curve can be resembled by a bilinear curve (e.g. Loades et al., 2013): before reaching the yield point the material behaves linear elastic. After yielding, the stiffness is reduced and the root deforms plastically until failure is reached. For a number of broadleaf and conifer trees, the yield strain is approximately 4% (σ_t = 9–16 MPa) and the failure strain 11–20% (σ_t =15–63 MPa) (Coutts, 1983). Other reported strains at failure were in the order of 5–10% (Operstein and Frydman, 2000; Schmidt et al., 2001). Very dry roots were shown to possess more linear rather than bilinear stress–strain curves, with much smaller to failure strains than moist roots (Yang et al., 2016).

Values for root elasticity measured in element testing might be higher than those observed during *in situ* root pull-out because of the tortuous root shape. Therefore Commandeur and Pyles (1991) made a distinction between 'form modulus', occurring when a tortuous root straightens out, and 'material modulus', which is the material Young's modulus (E_t). They found that the form modulus might be as small as one third of the material modulus.

The mechanical properties of roots change during the lifetime of a plant. Changes can occur in shape, e.g. depending on environmental conditions (Nicoll and Ray, 1996), chemical characteristics, e.g. lignin content (Scippa et al., 2006), or diameter, e.g. by root secondary growth. For example, the mean tensile strength of Japanese cedar (*Cryptomeria japonica* D. Don) increased from 22.6 ± 1.1 for 9 year old trees ($0.25 < d_r < 3.50$ mm) to 25 ± 1.2 for 20 year old trees ($0.45 < d_r < 4.20$ mm) to 31.7 ± 1.3 for 30 year old trees ($0.30 < d_r < 4.30$ mm), the cause of which was hypothesised to be increased cellulose contents or changes in internal structure (Genet et al., 2008).

Roots will slowly decay after a plant dies, influencing the mechanical characteristics. Small Douglas fir roots lost 0.3–0.5 MPa of tensile strength per month and the root biomass rapidly decreased after clearfelling. The reduction in maximum tensile force (F_t, in kg) of roots up to d_r = 14 mm was fitted as $F_t = 1.04 \cdot (2.51 \cdot d_r)^{1.8-0.06 \cdot \sqrt{t}}$, where d_r is the root diameter [mm] and t the time since clearfelling [months] (O'Loughlin and Ziemer, 1982). The tensile strength of kanuka and *Pinus radiata* trees decreased with an averages rate of 5.9 and 9.2 MPa y^{-1} respectively, although the mean tensile strength of kanuka increased in the first 12 months after clearfelling (Watson et al., 1999). This latter effects was attributed to root shrinkage caused by loss of water. Ziemer and Swanston (1977) (cited in O'Loughlin and Ziemer, 1982) contributed the measured strength increase in western hemlock and Sitka spruce between respectively 2–4 and 4–6 years after clearfelling to the increased importance of decay-resistant resinous roots in the remaining root fraction. Beech roots (*Fagus sylvatica L.*) were found to yearly lose 9.1% of their original tensile strength (Preti, 2013). Wu et al. (1979) measured that only $1/6^{th}$ of the tensile strength was left four years after clear-cutting in trees on the Prince of Wales Island in Alaska, USA. Root thickness can serve as an indicator for root longevity (Stokes et al., 2009), with

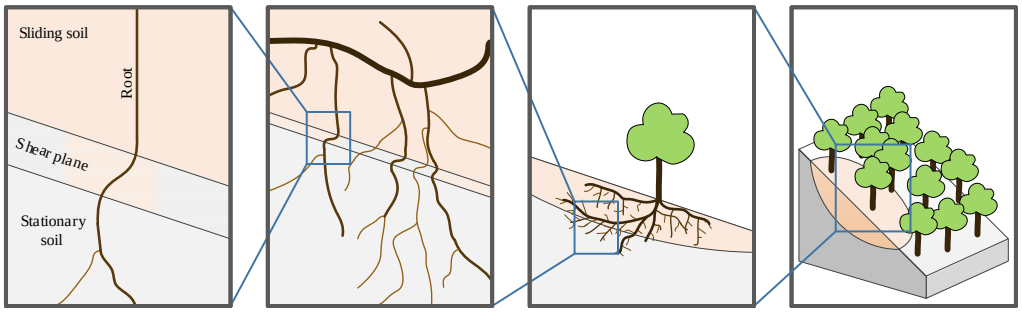

Figure 2.2: Illustration of upscaling sequence of root-reinforcement considering different scales, after Schwarz et al. (2010).

thinner roots having a shorter lifespan.

Not only does the tensile strength decrease during decay, the elasticity is affected as well. The joint effect of root decay, decrease of the elasticity and water decrease in the root (increasing the elasticity) resulted in a 4% net elasticity decrease per year for beech roots (Preti, 2013).

2.4 Mechanical root-reinforcement

2.4.1 Scales

When studying the interaction between roots and soil the scale on which the effects are studied is important to take into account. For example, when studying the reinforcement caused by a single root, roots might be treated as discrete elements, each with different characteristics, whereas when considering landslides using the continuum behaviour of the root–soil composite is a more common approach. Schwarz et al. (2010) distinguished between single root, bundle of roots, single tree root system and forest stands scales, see Figure 2.2.

2.4.2 Failure mechanisms of individual roots in soil

On the scale of single root, failure of the root–soil composite can be characterised as one of the following three failure mechanisms (Dupuy et al., 2005a):

1. *Root failure*: forces in the root exceed the maximum root strength. This results in *breakage* of the root.

2. *Root–soil interface failure*: internal root forces cannot be fully transferred to the surrounding soil, for example because the root is not firmly embedded in the surrounding soil or had a limited length, resulting in *slippage* of a root.

3. *Soil failure*: forces in the soil are larger than the soil resistance, and the soil fails before the root does. This results in merely *stretching and/or displacement* of the

root.

Which failure mechanism will occur depends on the interaction between external loading conditions, soil strength and stiffness, root mechanical characteristics, root–soil interface strength as well as the root architecture.

However, although these three failure mechanisms are clearly distinct in theory, numerical simulations of pull-out of simple root architectures showed that a strong interaction existed between the three mechanisms and that failure of a single root element is a consequence of the combined effects of soil failure, tensile failure and slippage (Dupuy et al., 2005a). Is is expected that on higher scales (root bundles, whole root systems) the behaviour is even more complicated.

Several attempts have been made to relate whether breakage or slippage occurs to a root diameter threshold. *In situ* direct shear tests showed that all roots that failed in tension had diameters smaller than 7 mm (Wu et al., 1988). These observations are reinforced by field observations of landslide scarps, often showing numerous broken roots whose diameter was generally smaller than diameter of unbroken roots (Schmidt et al., 2001). In laboratory shear box tests, (Mickovski et al., 2009) observed that thinner willow roots broke more frequently, similar to observations by Operstein and Frydman (2000) on rosemary, *pisacia lentiscus* and *meoporum parvifolium* roots. In contrast, Pollen (2007) reported based on *in situ* pull-out tests on riparian river birch trees that there is a threshold root diameter above which no roots fail by slippage. They concluded that increasing the soil shear strength led to a greater proportion of roots failing in breakage rather than slippage.

Using theoretical models (discussed in more detail in Section 2.5) to define the diameter threshold also showed this diffuse picture. Wu et al. (1988), using mechanical beam theory, calculated a threshold at level at $d_r = 7$ mm, similar to their observations in the field, above which no roots crossing a shear zone would fail in tension unless very stiff resulting in bending failure. On the other hand, Pollen (2007), using a fibre bundle model, while taking into account both a tensile strength–diameter (Equations 2.1) and a root length–diameter relation, concluded that no roots should pull-out above a certain threshold diameter.

Both experimental testing and modelling will have suffered from limitations. Experimental testing might have been influenced by the test conditions. For example, laboratory shear box tests showed that many roots are merely stretched at the end of the tests (Mickovski et al., 2009; Operstein and Frydman, 2000; Wu and Watson, 1998) suggesting that the displacement of the apparatus was too small to reach failure or that the embedded root length was insufficient, resulting in root slippage rather than breakage. It is known that rooted soil requires a much larger displacement to mobilise the maximum strength (Section 2.4.4). Modelling on the other hand will have been highly influenced by the choice of model and assumed relationships, and has difficulty taking variability into account. Moreover, both approaches have difficulties taking the effect of root architecture into account.

2.4.3 Influence of root architecture on failure mechanisms

So far the mechanical root behaviour has been discussed at a single root scale. However, in reality, single roots are part of larger root systems, and at the higher scales of root bundle and single root systems root architecture effects are expected to have a large influence on the root–soil composite behaviour. The complex influence of architectural effects can be most readily seen from uprooting or pull-out tests (e.g. Dupuy et al., 2005a; Ennos et al., 1993; Hamza et al., 2007; Mickovski et al., 2007; Operstein and Frydman, 2000; Reubens et al., 2007; Stokes et al., 2009).

A parametric two-dimensional numerical study by Dupuy et al. (2005a) using simplified root architectures (tortuous single tap root, herringbone, dichotomous architectures) showed large differences in pull-out behaviour. Relating the uprooting resistance to single parameters led to poor correlations (R^2 ranged from 0.05–0.58; root system width and number of lateral branches yielded the best fits). The best association for dual parameter fits were found for number of lateral branched + stem diameter (R^2 = 0.73) and number of lateral branches + total root volume (R^2 = 0.70). Soil cohesion, interface friction and soil pressure were shown to influence uprooting resistance only slightly, except for cohesion in the case of (unbranched) tap roots. The strong influence of lateral branching was also observed in experimental work by Ennos et al. (1993) on maize roots, Mickovski et al. (2007) on rubber model root and willow root systems and Stokes et al. (1996) on copper coated steel wire model root systems. Dichotomous systems had a larger resistance than herringbone systems, which in turn were more resistant to pull-out than single roots (Mickovski et al., 2007; Stokes et al., 1996).

During the failure of root systems in pull-out, single root failure, soil failure and slippage of roots occurred all at the same time (Dupuy et al., 2005a). This was visually observed by Mickovski et al. (2007) using PIV. The root displacements during pull-out varied between different materials (rubber or wood), architectures (simplified straight single root, herringbone and dichotomous pattern) and water contents (dry and wet sand), suggesting different resistance mechanisms. The pull-out resistance was larger in wet sand than in dry sand, attributed to suction pressures in the wet sand. The stiff woody branched root systems generally moved upwards as a rigid structure, displacing the soil above the joints upwards, while the flexible rubber root branches displaced more axially rather than laterally, i.e. more like a cable. Hamza et al. (2007) observed using PIV that whether root pull-out, root breakage or soil failure in tension occurred during their laboratory pull-out tests depended on test and root characteristics.

While single roots show a rapid decrease in pull-out resistance once the root breaks, branched or forked roots can show multiple peaks (sudden drops in resistance) in the load–displacement graph, indicating successive failure in the branches. This was for example observed by Norris (2005) during *in situ* pull-out tests on lateral oak and hawthorn roots in

a London clay cutting. A displacement of 50–100 mm was required before the first peak in the load–displacement curve occurred. Laboratory pull-out tests on idealised rubber root systems showed, using PIV, that branches were mobilised progressively. Laterals closest to the point of load application broke first (Hamza et al., 2007). The uprooting resistance decreased in the order: dichotomous > herringbone > tap root systems, and increased resistances corresponded with larger displacements at peak resistance. (Mickovski et al., 2007).

Similar complicated dynamics can be expected during shearing of rooted soil, in which the root axial stress–strain behaviour is important, similar to pull-out tests. However, no studies were found addressing the effect of root architecture and branching on the shear strength of root-reinforcement soil.

2.4.4 Root strength mobilisation

A certain amount of displacement is required for a single root to fully mobilised its strength, depending on the root stiffness and tortuosity. This dependency of stress on displacement also holds for root systems.

As will be discussed in more detail in Section 2.6, the shear strength of root-reinforced soil can be determined using direct shear tests. Roots significantly increase the the soil shear strength. Compared to fallow soil, in rooted soil the displacement at which the peak strength is reached is higher. For example, laboratory direct shear tests performed by Mickovski et al. (2009) on willow roots showed that the average displacement at peak strength in fallow soil took was 31–35 mm, compared to 75–84 mm in rooted soils. *In situ* shear box tests by Ekanayake et al. (1997) for kanuka trees on silty clay required 22–52 mm (rooted) or 6–20 mm displacement (fallow) to reach peak reinforcement, while tests using sandy clay planted with *Pinus radiata* required 18–48 mm (rooted) and 10–16 mm (fallow) respectively. Similar results were found by Fan and Su (2008) for prickly sesban on sandy soils (12 / 5 mm). *In situ* shear box tests on soils with Australian juvenile riparian trees required 50–100 mm displacement before the peak strength was reached (Docker and Hubble, 2008). (*In situ*) shear box testing often shows spiky force–displacement behaviour (e.g. Docker and Hubble, 2008), associated with roots failing at different displacement levels.

The shear band (or shear zone) is the narrow zone of intense soil deformation ('strain localisation') forming during shear deformation. The thickness of this band depends on the soil type (frictional soils having thicker bands), and was observed to increase with the amount of roots and a diversity of branching angles (Abe et al., 1991, in Stokes et al., 2009; Shewbridge and Sitar, 1989). Furthermore, increasing fibre bending stiffness (Abe et al., 1991, in Wu, 2007; Jewell and Wroth, 1987; Shewbridge and Sitar, 1989) and soil–root interface bond strength (Shewbridge and Sitar, 1989) increased the shear band thickness as well. The thickness in laboratory shear box tests ranged between 5 and 50 mm, but

depended strongly on the boundary conditions of the test (Gray, 1991; Shewbridge and Sitar, 1991), and therefore on the dimensions of the shear box and root sizes.

Some reported values for shear band thickness measured during *in situ* shear box tests on root-reinforced soil are 100–200 mm (Abernethy and Rutherfurd, 2001), 70–250 mm (Burroughs and Thomas 1977, cited in Abernethy and Rutherfurd 2001), >200 mm (Wu and Watson, 1998) or 80–120 mm (Fan and Su, 2008). The latter authors showed that the shear band thickness also increased with larger soil water contents. Although these values were reported as being 'large', all mentioned studies failed to provide the shear band thickness of similar non-rooted soil. The dimensions of the shear boxes used and test conditions are presented in Table 2.3. Finite element modelling confirmed that roots increase the shear band thickness (Mickovski et al., 2011).

Most root-reinforcement models assume that roots follow the behaviour of the soil perfectly like very flexible elements, and therefore that the behaviour of the soil is independent from the roots. However, both experimental and modelling work showed that roots have an effect on the thickness of the shear band, showing that this assumption is not correct. The large deformations required to reach failure and the thick shear bands indicate that the soil behaves like a composite material with interactions between the various components.

2.5 Root-reinforcement quantification models

Mechanical root-reinforcement can be quantified in various ways. This section introduces common methodologies to model the increase in soil strength based on root and soil properties.

2.5.1 Wu/Waldron model (WWM)

The most commonly used mechanical root-reinforcement model was developed by Wu and Waldron (Wu, 1976; Waldron, 1977; Wu et al., 1979). They developed a force-equilibrium model to describe the reinforcement of a single root perpendicularly crossing a shear plane, see Figure 2.3. The tangential component of the root tensile force causes an increase in shear resistance, whereas the normal component causes an increase in confining stress, resulting in additional soil shear resistance. Both effects are combined to find the increase in soil cohesion c_r:

$$c_r = k' \cdot \sigma_t \cdot RAR \tag{2.3}$$

where σ_t is the root tensile strength and RAR the root area ratio. The factor k' [-] is given by

$$k' = \cos\beta \tan\phi' + \sin\beta \tag{2.4}$$

where β is the angle between mobilised root and a line perpendicular to the shear plane, and ϕ' the soil angle of internal friction. In Equation 2.4, the first term reflects the influence

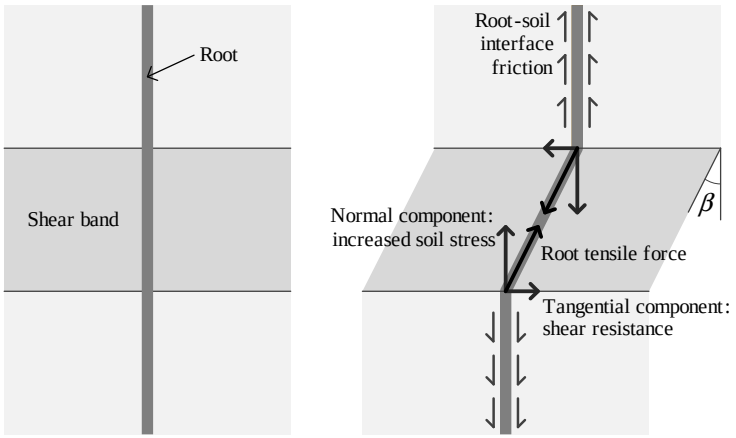

Figure 2.3: Schematic view of the Wu/Wadron model.

of the normal component of the tensile force in the fibre and the second term the influence of the tangential component. Often, $k' = 1.2$ is assumed (Wu et al., 1979), found by averaging Equation 2.4 for realistic ranges of β and ϕ'.

When the tensile strength varies with respect to root diameter, the reinforcement of each diameter class can be calculated individually and summed to yield more accurate reinforcement values. When applied to a bundle of roots, this type of models assumes that the tensile strength of all roots crossing the failure plane is fully mobilised simultaneously.

Experimental studies showed that the Wu/Waldron model overestimates the actual reinforcement. Some reported values in literature for the value of k' are 0.25 (Operstein and Frydman (2000), laboratory direct shear tests on *Meoporum parvifolium*, rosemary, *Pistacia lentiscus* and alfalfa roots), 0.40–0.99 (Comino et al. (2010), *in situ* direct shear tests on five grass species), 0.4 (Wu and Watson (1998), *in situ* direct shear tests on *Pinus radiata*), 0.4 (Preti (2006), cited in Preti (2013)).

Multiple explanations have been put forward to address the inaccuracies in the WWM. Firstly, roots do not always fail in tension. When the embedded length of the root in the surrounding soil is to short to transfer the axial load to the surrounding soil, the root will slip before breakage might occur, resulting in smaller maximum root tensile forces and therefore in less resistance. Although this was addressed in the original model formulation (Waldron, 1977), slippage is generally neglected in favour of a more simple model. Secondly, in reality roots will not all mobilise at the same time due to variation in root orientation and elasticity, resulting in sequential breakage rather than a single catastrophic failure (Pollen and Simon, 2005). Also the interaction between individual roots is disregarded.

2.5.2 Fibre bundle model (FBM)

To take progressive rather than simultaneous root failure into account, Pollen and Simon (2005) applied a fibre bundle model (FBM). In this type of model, the total load is distributed among all roots according to a user-defined function. Once the tensile force exceeds the strength in a single root the root is considered to be broken and the load it carried is distributed over all intact roots. Incrementally increasing the load until all roots have failed yields the maximum force the bundle can sustain.

An important modelling choice is how to distribute the load over all intact roots in the bundle, all having different properties. This choice alone can account for 60% variation in peak root-reinforcement values (Thomas and Pollen-Bankhead, 2010). Mathematically, the force in root i (F_i) can be described by:

$$F_i = F \cdot \frac{d_{r,i}^a}{\sum_{j=1}^{n} d_{r,j}^a} \tag{2.5}$$

where $d_{r,i}$ the diameter of root i, n the total number of intact roots, F the total applied force and a a dimensionless distribution factor. Common choices for a are $a = 0$, meaning that the load is equally distributed over all roots regardless of the root diameter, and $a = 2$, resulting in equal stresses in all roots. When $a > 2+\beta_\sigma$ (β_σ in the tensile strength–diameter relation of Equation 2.1), the thickest roots will break first, while when $a < 2 + \beta_\sigma$ thin roots will break first. When $a = 2 + \beta_\sigma$, all roots will fail at the same time, equalling the WWM solution. As experiments showed that smaller roots broke first, often equal load sharing ($a = 0$) is adopted (e.g. Comino and Marengo, 2010; Thomas and Pollen-Bankhead, 2010), although these authors appear to overlook that any value $a < 2 + \beta_\sigma$ might accomplish similar dynamics. Others suggested distributing the load based on root elasticity (e.g. Schwarz et al., 2010). In terms of Equation 2.5, this means $a = 2 + \beta_E$, where β_E is the power coefficient in the root diameter–elasticity equation (Equation 2.2).

A second important modelling choice is to decide to which intact roots the load of a failed root should be transferred. Either a Global Load Sharing (GLS, the load is equally distributed over all intact roots) or a Local Load Sharing scheme (LLS, the load is spread over nearby roots) can be adopted. Pollen and Simon (2005) argue that in the case of slope instability calculations it would be better to use a LLS scheme, as is is unlikely that redistribution of stresses will be equal over large shear plane surfaces. However, probably because of simplicity, GLS is commonly used (Bischetti et al., 2009; Comino and Marengo, 2010; Mao et al., 2012; Schwarz et al., 2010; Thomas and Pollen-Bankhead, 2010).

Studies showed that the results from FBM were more in line with laboratory direct shear test results than the Wu/Waldron model (Comino et al., 2010; Loades et al., 2010;

Mickovski et al., 2009; Pollen and Simon, 2005). Pollen and Simon (2005) found that the FBM underestimated the measured strength at low root densities and overestimated at higher densities. The reduction factor for predicted root-reinforcement due to progressive root failure in FBMs (k'') was reported to be k''=0.55–1.00 (Mao et al., 2012), 0.45–0.82 (Pollen and Simon, 2005), 0.3–0.7 (Hales et al., 2009, cited in Mao et al., 2012), 0.35–0.56 (Adhikari et al., 2013) or 0.56 (Hammond et al., 1992, cited in Bischetti et al., 2009). Bischetti et al. (2009) reported $k'' = 0.32$–0.50 at high root densities (400–1200 roots m^{-2}) and k'' =0.50–1.00 at lower densities (< 400 roots m^{-2}). Taking this reduction factor into account, the root cohesion can be expressed as:

$$c_r = k' \cdot k'' \cdot \sigma_t \cdot RAR \tag{2.6}$$

Later additions to the FBM included pull-out failure mechanics (Pollen, 2007), root growth curves (Pollen-Bankhead and Simon, 2009) or random root orientations (Thomas and Pollen-Bankhead, 2010). Equation 2.5 suggests that all roots with the same diameter show exactly the same stress–strain response and therefore fail simultaneously. Since in reality this assumption is not true and roots will mobilise at different displacements despite having the same diameter, the use of Weibull curves has been successfully used by Schwarz et al. to predict the force–displacement behaviour of a bundle of roots, accounting for sequential mobilisation of roots with the diameter (Schwarz et al., 2013, 2015; Moos et al., 2016). This extended version of the FBM has been referred to as 'FBMw'.

2.5.3 Laterally loaded pile model

Both the WWM and FBM consider roots as very flexible elements, able to easily follow the displacements of the soil, and therefore loaded in pure tension. This limits their application to the finest roots which can be considered as cable elements (Stokes et al., 2009). However, thicker structural roots, similar to beams in structural engineering, develop longitudinal shear stresses (Reubens et al., 2007). This increases the thickness of the shear zone and makes the root no longer deform similarly to the soil (Wu, 2007). In this case the displacement of the root and the accompanying forces can be described using solutions for laterally loaded piles or spring-supported beams.

According to Wu (2007), a root can be simplified as a flexible element when $\eta \cdot L > 2.5$ or as an elastically supported beam when $\eta \cdot L < 1.5$, where $\eta = \sqrt{T_x/(E \cdot I)}$ and L the half-length of the root (Wu, 2007). In the latter equation, E and I are the Young's modulus and second moment of inertia of the root respectively, and T_x the component of the root axial tensile force T in the non-displaced axial direction. Wu (2007) provided analytical solutions. However, these do not take non-linear displacement effects into account.

In situ shear box tests with strain gauged roots showed that this approach estimated the actual forces in the root accurately within 30% (Wu and Watson, 1998). However, to

successfully apply this solution to real root-reinforcement predictions, the characteristics and positions of each root must be known on beforehand (Wu and Watson, 1998), which in practice proved to be difficult (Wu et al., 1988).

Wu et al. (Wu, 2007, 2013) proposed analytical beam models for calculation of the root contribution to soil shear resistance, taking into account root bending resistance and axial force. Root forces and displacement could be found by solving the beam differential equation:

$$E \cdot I \cdot \frac{d^4u(x)}{dx^4} - T_x \cdot \frac{d^2u(x)}{dx^2} = k \cdot d_r \tag{2.7}$$

where x the distance to the shear plane along the root axis, u the lateral root displacement, T_x the axial force in the root in the x-direction, k the linear elastic soil spring resistance (force per unit volume) and d_r the root diameter. Wu et al. (1988) used linear elastic soil springs instead of modelling soil resistance as a constant. However, these methods were not able to take large non-linear displacement effects into account and therefore had to assume that u was small compared to the length of the displaced root.

Duckett (2014) and Liang et al. (2015) used a numerical framework to model roots as spring-supported beams using non-linear springs, allowing for non-linear effects and the modelling of large relative root–soil deformations. The properties of these springs were derived from methods adopted for laterally loaded piles, so called p-y curves (e.g. American Petroleum Institute, 2000; Randolph and Gourvenec, 2011; Reese and Van Impe, 2011). In addition, adopting a numerical framework allows for more complicated root architectures. This approach might therefore allow studying the behaviour of root bundles rather than single roots, although this has not been attempted yet.

2.5.4 Constitutive modelling

To model the stress–strain behaviour of fibre-reinforced soil with finite elements, constitutive models and failure criteria are required. Diambra et al. (2010) developed a constitutive model for fibre-reinforcement using the rule of mixtures (assuming fibres and soil behaved independently). The fibres were assumed to behave linear-elastic and the variation in fibre orientation was taken into account. By adding the fibre contribution to a elastic–perfectly plastic soil model with a Mohr-Coulomb failure criterion, the stress–strain behaviour of the composite could be modelled. Comparison with triaxial testing showed that the model was able to reproduce the main features of fibre-reinforced sand behaviour, although there were quantitative discrepancies between numerical and experimental results attributed to the simplicity of the adopted soil model.

Failure criteria for both randomly (Michalowski and Çermák, 2003) and preferentially orientated fibres (Michalowski, 2008) have been derived. These are based on mechanical dissipation of work in fibres during the deformation process. The derived criteria take both fibre slip and fibre breakage into account, and have been shown to accurately predict

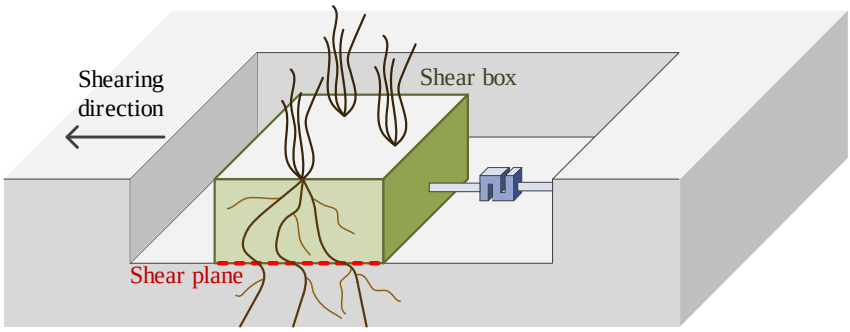

Figure 2.4: Schematic view of *in situ* shear box testing.

the strength of the sand–fibre composite.

Constitutive modelling has only been used for soil reinforced with small diameter fibres. Its suitability for rooted soil with large variations in root properties, diameters and architectures is unknown.

2.6 Root-reinforcement measurement techniques

Various methodologies exist to quantify mechanical root-reinforcement in the field or in the laboratory. These are discussed in the following sections.

2.6.1 *In situ* testing methods

Shear box

Shear box (or direct shear) testing is the most used method to determine the strength of root-reinforced soil *in situ*. A direct shear apparatus (DSA) measures the force required to overcome the friction on the sides of a block of soil sampled in the shear box. Since the shear plane is pre-defined and the shear surface area known, the measured force can be used to calculate the shear strength. In root-reinforced soils, in general a square box with an open bottom and top is used. It is vertically inserted, sometimes after excavation of surface layers. After insertion a horizontal displacement or force is applied, while measuring both displacement and load (Figure 2.4).

Some details of reported equipment and test conditions are presented in Table 2.3. Differences in apparatus, test size, test conditions, soil conditions and species make comparison between devices very difficult.

The size of the box will influence the measurement results. Smaller sized devices not only suffer more from boundary effects (Gray, 1991; Shewbridge and Sitar, 1991), but smaller boxes will cut relatively more roots when installed as the ratio between circumference and area is larger for smaller boxes, and therefore introduce more disturbance. When shear box tests are used to model the strength of a real slope, a correction must be made for cut roots (Wu et al., 1988).

Table 2.3: *In situ* shear box properties and test conditions.

Author	Location	Vegetation	Soil conditions	Moisture conditions	Size (W×L×H) [cm]	Test conditions [mm min^{-1}]	Normal load [kPa]	Max displacement [mm]	Max depth [m]
Cammeraat et al. (2005)	Alcoy basin, Spain	Aleppo pine, grass / annuals / small herbs	Weathered marl	Natural moisture	60 × 60 × 40	4	3.3/4.1	N/A, but >25% strain	0.40
Comino and Marengo (2010)	Pellice valley, Italy	5 Grasses	Alluvial deposits	Natural moisture	30 × 30 × 10	Force controlled, rate N/A	0	±110	0.10
Docker and Hubble (2008)	Nepean River, Australia	Juvenile (16–27 months) riparian trees, 1–3 trees per tested block[a]	Alluvial loam, sandy loam	Saturated, allowed to drain during tests	40×40 / 50×50 × 21–44	1.5	0	100–200	0.21–0.44
Ekanayake et al. (1997)	East Coast, North Island, New Zealand	Kanuka / *Pinus radiata*	Silty clay / Poorly graded sandy clay	Saturated before tests	30 × 30 × 15	10	148 kg	90	≈0.5
Hengchaovanich and Nilaweera (1996)	Malaysia	Vetiver grass	N/A	N/A	50 × 50 × 50	Force controlled, rate N/A	N/A	N/A	1.50, steps of 0.25
Fan and Su (2008)	Kaoshiung City, Taiwan	Prickly sesban	Sand, mixed with some gravel, silt and clay	Dry conditions	30 × 30 × 20	18	0	90	0.08–0.10
Wu et al. (1979)	Prince of Wales Island, Alaska, USA	Sitka spruce forest	Sand and silt, with varying amounts of gravel	Natural moisture	30.5 m^2 (area)	N/A		N/A	N/A
Wu and Watson (1998)	East Coast, South Island, New Zealand	*Pinus radiata* (6–8 years)	Silty sand	N/A	10000 cm^2 (area) × 50 (depth)	N/A	0	400	0.5

[a] *Casuarina glauca*, *Eucalyptus amphifolia*, *Eucalyptus elata*, *Acacia floribunda*. 1–3 trees per tested block

Although shearing along the bottom interface of the soil block is the most commonly used design, other direct shear devices have been reported as well. Van Beek et al. (2005) used, in addition to a 'conventional' four-sided box, a device with only two vertical plates placed perpendicular to the loading direction. Thus the combined shear force on the bottom and the sides was measured. During testing some arching was observed, resulting in increased shear stresses. However, because these movements are small compared to the displacement of the enclosed soil block, they argued that this setup is still feasible. Wu et al. (1988) used a similar device as Van Beek et al. but with an additional bottom plate, slid under the soil block after excavation, so that only side friction was measured.

In case of (partially) saturated soils, the displacement rate is an important parameter, as the ratio between loading rate and excess pore water pressure dissipation determines whether the test results should be interpreted as drained or undrained soil behaviour (e.g. Verruijt, 2012).

In situ shear box testing has some advantages. The rooted soil can be tested as it is without the need for potentially destructive sampling. Secondly, the soil is sheared parallel to the soil surface, which is similar to the general displacement direction of landslides. Testing equipment is however large and heavy, making this testing less suitable for areas with difficult access. Furthermore, setting up of a test takes significant time, especially for testing in deeper soil layers, due to both the need to excavate the soil around the test to allow for horizontal displacements and the careful installation of the box to minimise disturbance.

Shear vane tests

With a vane apparatus the frictional resistance along the interface of a soil cohesion can be determined by measuring the maximum torque required to rotate the cylinder. The size of this cylinder follows from the size of the cruciform blade. Only few examples for the use of vane apparatus to measure root-reinforcement were found in the literature. Osman and Barakbah (2006) used a field inspection vane tester (Eijkelkamp Agrisearch Equipment, model 14.05, 0–260 kPa (±10%)) to measure the strength of five slopes in Malaysia, grown with diverse vegetation. Measurements in the top 10 cm resulted in a positive relation between shear strength and root length density ($R = 0.95$, $p < 0.05$).

A second example is a study by Chen et al. (2012), who reported using a pocket vane (Geotest E-285) to measure the strength of saltmarsh tidal creek banks. These consisted of uniform clays and silts and were covered with sea purslane and/or sea rush. Vane shear results yielded 'remarkable similarity in terms of vertical variation and influence of roots, consolidation and microalgae' compared to measurements using a cohesive strength meter (which measures the erosion threshold strength). They contributed 23–27% of the variation in measured shear strength to the effect on roots.

Other studies used vane tests as a qualitative measure for root-reinforcement. For

example, Cammeraat et al. (2005) used a simple field vane test (tor vane) to preliminary investigate spatial variability in root-reinforced soil strength to select typical sites to perform *in situ* shear box tests. They noticed a close similarity between the mean vane readings and the effective cohesion measured using laboratory drained direct shear tests using the same surficial root-reinforced soil.

Although the field shear vane is easy and quick to use, its use in rooted soil is limited. Testing in peaty soil showed that installation caused a lot of soil disturbance as the device dragged the fibrous soil down. Cutting of fibres during installation was also observed (Landva, 1980). These effects will be problematic when root-reinforced soil is to be measured, as either the soil will be disturbed or roots broken prior to shearing phase, both resulting in inaccurate measurements and underestimations of the actual strength.

Erosion resistance

Scour is an important mechanism to take into account when assessing the stability of stream banks. Chen et al. (2012) measured the erosion resistance of saltmarsh tidal creek banks with a cohesive strength meter (CSM). This device applies an increasingly strong jet of water on a soil interface while measuring the turbidity of the residual water. A sudden change in turbidity indicates the erosion shear stress threshold has been reached. They found a clear influence of roots on the erosion threshold and a similarity between CSM and vane results. Pollen-Bankhead and Simon (2010) used a jet device and found a negative trend between root volume and the volume of eroded soil material, as well as a negative relation between root biomass and scour hole volume. They showed that even small root volumes may significantly reduce erosion.

Measurement methods for use in the soil surface

In agriculture, the use of ribbed plates ('grouser plates') can be used to determine the soil strength parameters of the surface soil layer (Johnson et al., 1987). A ribbed plate is pushed into the soil and a normal load applied on top. Subsequently, the plate is horizontally translated while measuring the required force. By repeated measurements at different soil stress levels the Mohr-Coulomb strength parameters can be obtained. A similar approach, using a 20×20 cm plate with 89 nails (with a length of 11 cm) instead of ribs, equally spaced in 10 staggered rows, was proposed by Farabegoli et al. (2012). This device, called the 'turf's comb', operates in a similar fashion as a conventional *in situ* shear box. Measurements were however time-consuming; it proved only possible to conduct three tests per day.

Tests such as these only work near the surface, making them less useful when a soil strength profile, required for slope stability analyses, is to be measured.

2.6.2 Laboratory methods

Shear box

Shear box (or direct shear) testing is not only an *in situ* test but also a common standard geotechnical laboratory test. As is the case with *in situ* testing apparatus (see Section 2.6.1), there is a wide variety in apparatus characteristics, test conditions, root characteristics and soil characteristics reported in the literature (Gray and Ohashi, 1983; Jewell and Wroth, 1987; Loades et al., 2010; Normaniza et al., 2008; Mickovski et al., 2009; Operstein and Frydman, 2000; Pollen and Simon, 2005; Shewbridge and Sitar, 1989; Waldron, 1977; Waldron and Dakessian, 1981; Wu et al., 1979, amongst others). Commonly, plants grown in cores or blocks of rooted soil are sampled in cores, followed by shearing of these cores (e.g. Loades et al., 2010). Shear box sizes ranged from conventional 65 mm diameter (Pollen and Simon, 2005) up to 200 mm diameter (Operstein and Frydman, 2000). Due to their smaller size compared to field devices, edge effects such as root cutting will have a stronger influence.

Using laboratory shear box testing for determining the properties of field soil requires time-consuming and costly sampling to ensure soil samples are not disturbed, making them unsuitable for measuring field soil properties on a large scale.

Triaxial tests

The triaxial shear test is a common geotechnical laboratory test to measure soil stress–strain behaviour. A cylindrical soil specimen is vertically loaded in compression or tension while the lateral pressure is kept constant using pressurised water. No examples of root-reinforced triaxial tests have been found in literature, apart from unrealistic tests using reconstituted samples reinforced with individual cut roots (Zhang et al., 2010). However, triaxial testing on fibre-reinforced soils is more common (Ibraim and Fourmont, 2007; Michalowski and Çermák, 2002, among others). Explanation for the lack of triaxial tests on root-reinforced soils might be the complexity of these tests or the large size of triaxial samples required to realistically test the soil behaviour because of root boundary effects.

Centrifuge tests

Using a geotechnical centrifuge to model and measure the behaviour of a root-reinforced slope is a relative new approach. By increasing the acceleration to N times the earth acceleration g, a model slope can be scaled down N times while the stress distribution remain similar to *in situ* conditions. Sonnenberg (2008) and Sonnenberg et al. (2010) investigated the stability of a 45° slope reinforced with willow roots or root analogues, led to failure by increasing the water table level in the slope. Scaling problems were reported, especially for root diameters and properties. They found that the best way to simulate roots is to use natural root systems, grown before centrifuge flight. Although the failure mechanism was observed to change from a progressive block-wise failure to an intact

sliding block, minimal reinforcement was measured. Other reported centrifuge studies involved earthquake-loaded slope stability tests using soil reinforced with root analogues (Liang et al., 2015).

2.6.3 Combining root counts with interpretive models

Instead of directly measuring the shear strength of rooted soil, mechanical root-reinforcement can also be estimated indirectly through measurements of root quantities, root strengths and application of a root-reinforcement model.

Various methods exist to quantify root spread and diameters *in situ*. Firstly, entire root systems can be excavated. For larger root systems, this can for example be done using manual excavation (Di Iorio et al., 2005; Henderson et al., 1983b), high pressure water (Watson et al., 1999; Tosi, 2007) or air (Danjon et al., 2008; Stokes et al., 2002) or pulling complete plants over (Nicoll and Ray, 1996; Stokes et al., 2007). Subsequent to excavation or pull-over, roots can be mapped. However, many roots will be broken or lost (Danjon et al., 2007; Stokes et al., 2007), especially finer roots, making these methods more useful to study coarse root architecture. Secondly, root distribution can be measured by counting root intersections and measuring root diameters on the vertical plane of a soil pit or trench wall (e.g. Abdi et al., 2010; Abernethy and Rutherfurd, 2001; Mao et al., 2012; Pierret et al., 2000; Moos et al., 2016), see Figure 2.5. However, this method is very labour-intensive. Thirdly, soil cores can be used (Ammer and Wagner, 2005; Børja et al., 2008; Danjon et al., 2008; Genet et al., 2008; John et al., 2001; Steele et al., 1997; Wang et al., 2006). After coring and subsequent washing to remove soil particles, the root biomass can be determined or roots can be scanned and analysed using image analysis software to extract individual root lengths and diameters. Finally, geophysical method such as ground penetration radar (GPR) can be applied to find roots depths and spread (e.g. Stokes et al., 2002; Hirano et al., 2009), using wave reflection patterns to find soil–root interfaces. A trade-off has to be made between resolution and penetration depth, making it more useful to study coarse root architecture. Although these methods are non-intrusive, costs are high (Stokes et al., 2002) and accuracy is seriously degraded in soils with high water and/or clay contents (Hirano et al., 2009). Root counts in soil pits and soil coring are most commonly adopted for quantification of the number and diameters of roots.

Once the root quantities are known, interpretive models (Section 2.5), for example the Wu/Waldron model, can be used to translate this information into values for additional soil strength. This additional resistance can then be added to the fallow soil strength estimated or measured using conventional geotechnical methods.

A disadvantage of this approach is that the actual root-reinforced soil strength at the locations of the sampled roots is only indirectly established.

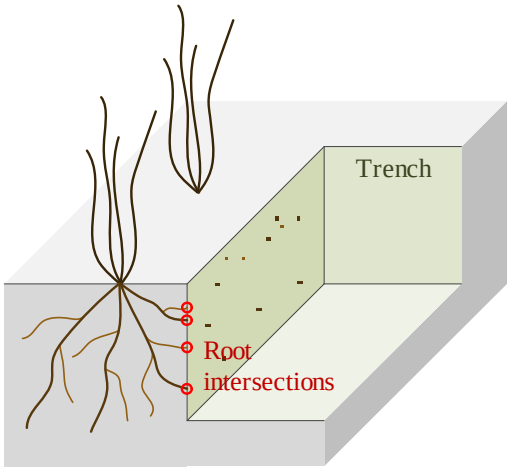

Figure 2.5: Schematic view of root quantification using the trench wall technique.

2.7 Root-reinforced soil landslide potential

Modelling is required to make an assessment of the slope stability. Two approaches can be used to model root-reinforced soil. Either the roots are modelled as discrete elements (discrete approach, e.g. when using a beam solution), or their effects are 'spread' out over the surrounding soil considering the rooted soil into account as a single material (continuum approach, e.g. when using the Wu/Waldron model). With either approach traditional slope stability analysis or numerical analysis can be used, in two or three dimensions.

2.7.1 Analytical slope analysis with factors of safety

Analytical slope stability models are based on force equilibrium, and express the stability of a slope as a factor of safety (*FOS*), defined as the ratio between resisting and driving forces. When modelling root-reinforcement, the effect of roots is usually taken into account as an increase in soil strength, generally using the Wu/Waldron model (Section 2.5.1). Commonly, the stability is analysed in two dimensions, although it is possible to analyse 3-D stability (e.g. Chen et al., 2003). 2-D analysis can be seen as a conservative approach as it neglects additional soil resistance on the planes parallel to the plane of analysis.

Common slope stability models use either an infinite or finite slope approach. An infinite slope approach is generally chosen in case of shallow slope stability, in which case the slide length to depth ratio is high (e.g. $L/z > 20$, Gray and Sotir, 1996). The (beneficial) soil strength effect is only assumed to be working on an infinitely long sliding interface parallel to the surface. In these type of analyses the stability of a slope is expressed as a factor of safety (*FOS*):

$$FOS = \frac{\sum \text{Resisting forces}}{\sum \text{Driving forces}} \tag{2.8}$$

A slope can be considered stable when the sum of resisting forces (strength) exceeds the sum of driving forces (load), i.e. when $FOS > 1$. The mechanical effects of roots cause an increase in resisting forces, and therefore a beneficial increase in FOS.

An example of a infinite-slope stability formulation, taking into account wind loading and tree overburden effects, is (Coppin and Richards, 1990; Wu et al., 1979):

$$FOS = \frac{(c' + c_r) + (\gamma \cdot h_z - \gamma_w \cdot h_w + w_t) \cdot \cos^2 \alpha \cdot \tan \phi'}{((\gamma \cdot h_z + w_t) \cdot \sin \alpha + w_w) \cdot \cos \alpha} \tag{2.9}$$

where c' is the effective soil cohesion [kPa], c_r the additional apparent root cohesion [kPa], ϕ' the soil angle of internal friction [-], h_z and h_w the height of soil and water table above the sliding plane [m], α the slope angle [-], γ and γ_w the volumetric weights of the soil and water [kNm^{-3}], w_t the additional vertical stress caused by the tree [kPa] and w_w the additional tangential stress caused by wind loading on the aboveground tree parts [kPa].

Many variations of Equation 2.9 exist. For example, Ekanayake et al. (1997) used a similar equation excluding wind loading and assuming fully saturated soil (the most negative soil condition), whereas Gray and Sotir (1996) included a seepage flow direction parameter while excluding the effect of vegetation surcharge and assuming full saturation. The infinite slope approach is thought to underestimate the effect of mechanical root-reinforcement as the effect of roots along the perimeter of the slide mass are neglected. Lateral reinforcement might greatly exceed the basal reinforcement effects (Schmidt et al., 2001).

In a finite slope approach a full slip interface is assumed. Two-dimensional slip surfaces can have many shapes, for example planar, circular, log-spiral or bi-linear (wedge). A common method, Bishop's method of circles, assuming circular slip planes, subdivides the sliding mass into vertical slices. For each slice the driving and resisting forces are found. These are subsequently summed to find the factor of safety.

In this type of analysis, regardless of using a infinite or finite slope approach, the critical failure surface (the one having the smallest FOS) is iteratively found by quantifying FOS for a large number of potential failure planes. When the critical shear plane is stabilised, for example by roots, the factor of safety for this plane will increase. Although even after adding reinforcement this plane might still have the smallest global value of FOS, it is possible that another plane now has become the critical shear plane. In practical terms, this means adding reinforcement might move the critical shear plane to elsewhere in the slope. This effect has been observed by Liang (2015) in 2-D finite element numerical analyses, where the critical shear plane was 'pushed' down to depths below the rooted zone once reinforcement was added to the analysis. These observations suggest that there might be a theoretical reinforcement threshold above which adding additional reinforcement does not lead to an increase in FOS as the shear plane will be pushed to depths below the rooted zone.

2.7.2 Finite element methods

Finite element methods (FEM) subdivide the modelled soil into numerous small elements. By solving force and displacement equilibrium equations for each of these soil elements, the full stress–strain behaviour of the slope can be modelled. Numerical methods take into account not only the strength of the soil, but also the strains and displacements, making it a powerful tool to model the behaviour of a slope prior to and during failure. Generally, both a failure criterion, determining the yield stress conditions of the material, and a constitutive model, relating stresses and strains, have to be specified.

When using a numerical model, the effects of roots might be modelled either as separate root elements (discrete approach) or by incorporating their effects in the behaviour of the soil, thus modelling rooted soil as a composite (continuous approach). The work by Dupuy et al. (2005b) is an example of a discrete approach, investigating the overturning resistance of single trees with various root architectures in idealised soils, using a 3-D finite element program (ABAQUS) and an elastic perfectly plastic Mohr-Coulomb soil model. Discrete modelling of root pull-out is reported as well (Dupuy et al., 2005a). No examples of root-reinforced landslide modelling modelling roots as discrete elements are found in literature, probably because of the high computational power required.

The continuum approach to model root-reinforced slope-stability problems using finite elements is more common (e.g. Van Beek et al., 2005; Genet et al., 2008; Tiwari et al., 2013)). Usually, the root-reinforcement is taken into account as an increase in soil cohesion, and this reinforcement is assumed to be independent from the soil strain. A more sophisticated continuum approach was used by Van Beek et al. (2005), who used a root-reinforcement model in the FLAC 2D finite element program. Root input consists of the measured spatial distribution (diameters, depths, orientations) and root tensile strength and elasticity. During each step in the numerical calculation the actual root-reinforcement is calculated based on the stress and strain in each root. This benefit of this approach is a more realistic reinforcement based on actual levels of soil deformation.

2.8 Conclusion

Vegetation affects the strength of the soil in various ways. One of these is through mobilising the mechanical strength of roots, therefore enhancing the strength to the root–soil composite material. This is a highly complicated process. The mechanical characteristics of single roots and the architecture of a root system are highly variable, both in space and time. The interaction between soil and roots, especially on a larger scale, is poorly understood, resulting in a wide selection of reported root-reinforcement models and and a large range in root-reinforcement values measured or predicted.

Existing methods to quantify root-reinforcement *in situ* are either time-consuming and require heavy equipment (field shear box testing) or rely on time-consuming root

measurement methods (e.g. core sampling or trench wall mapping) and the need for an interpretive model to link these to an increase in soil strength, introducing additional inaccuracies. Laboratory methods require expensive and difficult non-destructive soil sampling in the field.

Because of the limitations of existing models and measurement methodologies, there is a need to develop new *in situ* measurement techniques which are able to quickly establish an estimate for root-reinforced soil strength. This equipment should be easy to transport so that locations difficult to access can be investigated. This will be the focus for the remainder of this thesis.

3

Measurement methods

Large sections of this chapter have been published as part of a journal paper, see Meijer et al. (2016c).

3.1 Introduction

Existing methodologies to quantify root-reinforcement in the field are limited. In this chapter, new design for devices to measure root-reinforcement *in situ* are introduced. For every device the design rationale is discussed, technical details are presented and the method used to interpreted measurement data is presented. This chapter thus introduces the methodology for the experimental work in subsequent chapters, in which these new methods will be tested under various laboratory and field conditions to assess the accuracy, reliability and practicality of the proposed devices and interpretative methods.

All new measurement methods were developed based on the following design criteria:

- *Portability:* Many locations on slopes are difficult to reach, for example because of difficult or steep terrain or locations being remote. Therefore the devices should be portable (i.e. light and small), and preferably it should be possible to dis- and reassemble them easily.
- *Quick to use:* Soil characteristics, hydrological conditions and root distributions vary significantly spatially. Since landslides will initiate locally, it is important to take this variability into account and localise the most vulnerable part of the slope. This requires many *in situ* measurements to find local weak zones. To enable this the new methods should be able to acquire data quickly.
- *Easy to use:* To ensure the device is user-friendly and has widespread potential, operation should not require specialistic knowledge of roots and soil. Therefore devices which are easily usable and require little expert knowledge to use (and interpret) are preferable.

In this thesis, four methods have been developed and studied. The first two methods can be used to quantify the depth and diameter of individual roots:

1. *Blade penetrometer:* Device to measure root depth and diameters by pushing a penetrometer with an adapted tip into the soil. The characteristics of the depth–resistance trace, as the penetrometer pushes and subsequently breaks roots, are used to acquire root depth and their properties.
2. *Pull-up device:* Similar to the blade penetrometer, but with this device roots in the soil are mobilised during upward extraction of the device rather than downwards installation.

The other two methods can be used to directly measure the shear strength of the root-reinforced soil:

3. *Pin vane:* Device to measure the root-reinforced shear strength by mobilising a cylinder of soil, similar to a standard field vane shear device. The blades in a standard vane are replaced by prongs to minimise root and soil disturbance during installation.
4. *Corkscrew:* Device to mobilise the combined root–soil resistance. A screw-like device is rotationally screwed into the soil and then vertically extracted. The extraction force is used to calculate the root-reinforced shear strength along the interface of the extracted soil plug.

These methods are discussed in more detail in the following sections.

3.2 Blade penetrometer

In standard soil cone penetrometer test (CPT) interpretation, tip resistance is correlated to soil strength and type (e.g. Lunne et al., 1997). The same principle can be applied to rooted soil. When a penetrometer hits a root, additional resistance will be measured until the root fails in breakage or slippage (Figure 3.1). Similar to root pull-out tests, main root or side branch failure might be observed from the shape of the force–displacement curves (Riestenberg, 1994; Norris, 2005; Docker and Hubble, 2008; Giadrossich et al., 2013). Alternatively, when roots and soil act more as a composite material, an increased resistance over longer displacement ranges is expected, similar to the observed increase in shear strength in fibre-reinforced sands measured with triaxial, direct shear or ring shear tests (Gray and Ohashi, 1983; Jewell and Wroth, 1987; Michalowski and Çermák, 2002; Heineck et al., 2005; Ibraim and Fourmont, 2007; Tang et al., 2007; Diambra et al., 2010)

A penetrometer fitted with an elongated tip increases sensitivity to measuring root effects. This can be understood by simplifying roots as one-dimensional line objects. For a single root with azimuth θ, the chance it will be hit by the penetrometer is proportional

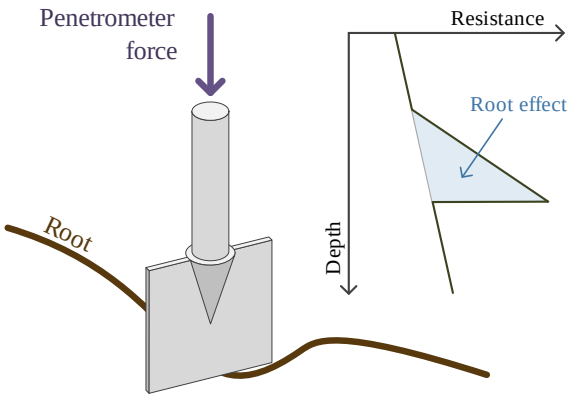

Figure 3.1: Schematic view of root quantification using the blade penetrometer method.

to the projected width (d) of the penetrometer in the transverse direction to the root:

$$d(\theta) = \max(y_i \cdot \cos\theta - x_i \cdot \sin\theta) - \min(y_i \cdot \cos\theta - x_i \cdot \sin\theta) \tag{3.1}$$

where (x_i, y_i) are the coordinates of any point i in the horizontal cross-section of the penetrometer (Figure 3.2). When the root azimuths are assumed to be uniformly distributed, the chance a penetrometer hits a root is proportional to the 'average' width of the tip (d_{avg}):

$$d_{avg} = \frac{1}{2 \cdot \pi} \cdot \int_0^{2\pi} d(\theta) \cdot \mathrm{d}\theta \tag{3.2}$$

When soil resistance is assumed to be proportional to tip area A_{tip}, the relative sensitivity to roots can be expressed in dimensionless terms as the ratio between d_{avg} and $\sqrt{A_{tip}}$, see Figure 3.2. This figure shows that the sensitivity is much larger for oblong shapes, and that the ratio of the major to the minor dimension is more important than the shape (rectangular or ellipsoidal). Although this simplified analysis does not take soil friction or tip shape effects into account, it clearly indicates the advantages of adapting a penetrometer tip for root measurements. A second advantage of an elongated shape is the opportunity this offers for studying root growth direction anisotropy by varying the plane of orientation of the penetrometer.

The main advantage of this method is its ability to quickly obtain strength data over a depth profile. Secondly, by making only a small adaptation to a well-known method, it can build upon a large body of existing knowledge and experience. The main advantage of this method is its ability to quickly obtain strength data over a depth profile. Secondly, by making only a small adaptation to a well-known method, it can build upon a large body of existing knowledge and experience. On the other hand, this method needs reliable correlations between profile results and soil shear strength currently not existing. Furthermore, to minimise errors induced by dynamic installation effects, a rig is required with sufficient weight to counteract installation resistance.

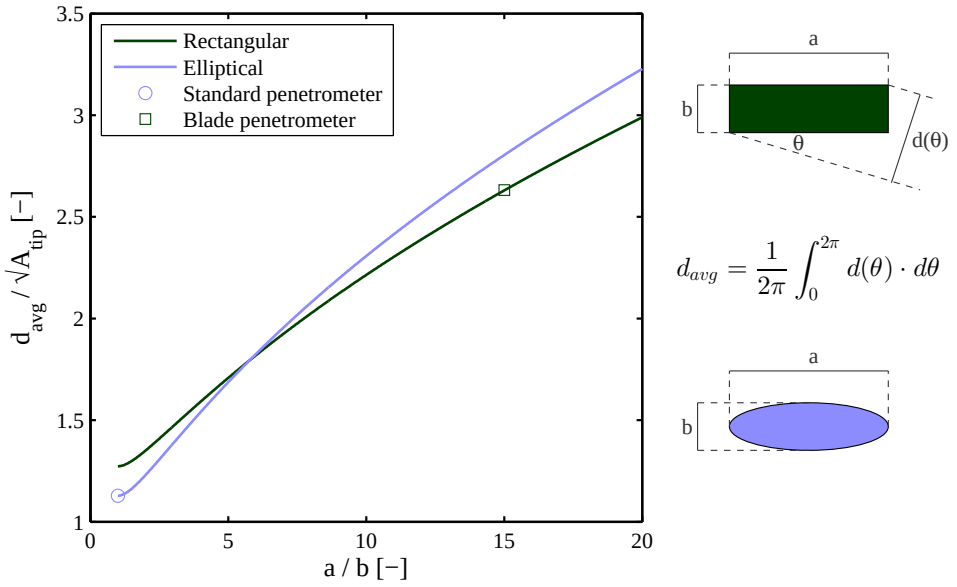

Figure 3.2: Sensitivity of one-dimensional object for various penetrometer tip shapes.

In this study, a rectangular 30×2 mm stainless steel tip was used. To ensure structural rigidity, the height was chosen as 35 mm. This 'blade' was welded to a 30° ∅12.5 mm standard penetrometer tip screwed to a ∅10 mm shaft, see Figure 3.3a.

3.3 Root pull-up

Similar root-reinforced penetration profiles as measured by a blade penetrometer can be obtained during upwards rather than downwards movement (Figure 3.4). To yield reliable results, soil disturbance during installation needs to be minimised, while during upwards extraction the tip shape should have increased sensitivity to roots (Figure 3.2). In this thesis, a standard agricultural 30° ∅12.5 mm CPT with a ∅10 mm shaft is used. This device is pushed down to depth. Once reached, a 2 mm thick blade (width × breadth: 60×12.5 mm) is expanded out of a recess in the shaft (Figure 3.3b). Thus, during installation the test is similar to normal penetrometer testing but during extraction (almost) all of the resistance will act on the expanded part.

The main benefit of measuring root resistance during upwards movement is the ability to use the overlying soil surface to apply reaction force, reducing the need for counterweight. Secondly, the installation phase yields a secondary set of data for the same soil profile but less influenced by roots, which might help to establish both the fallow and root-reinforced soil strength.

3.4 Pin vane

Field shear vane devices are well established to measure soil undrained shear strength in cohesive soil (e.g. Knappett and Craig, 2012). However, a major limitation to use in

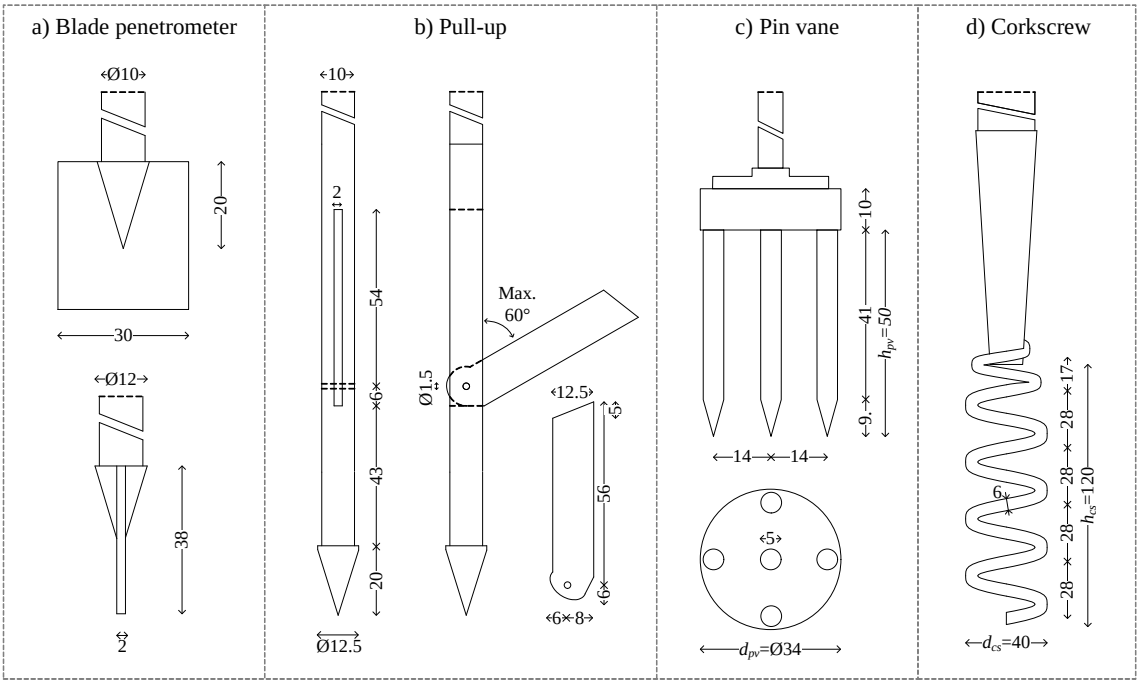

Figure 3.3: Technical drawings of new root-reinforcement measurement devices. All measurements in millimetres.

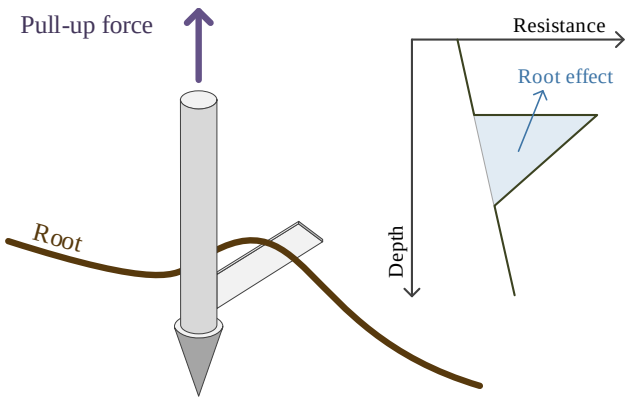

Figure 3.4: Schematic view of root quantification using the root pull-up method.

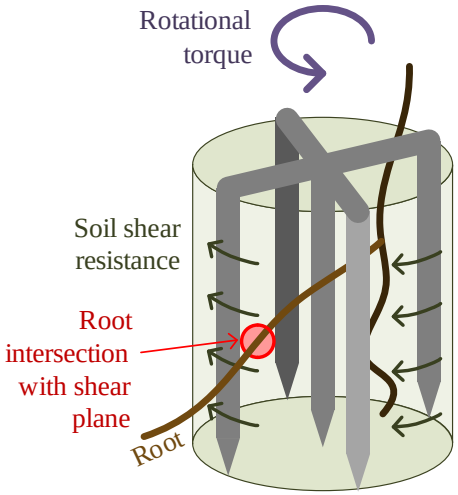

Figure 3.5: Schematic view of root-reinforced shear strength measurement using the pin vane method.

root-reinforced soil is the tendency to cause root breakage and soil disturbance during installation, as for example observed during vane testing in fibrous peats (Landva, 1980). The solution proposed here is to replace the vane blades by prongs, see Figure 3.3c. During installation, the roots can slide between the prongs without breaking. The unbroken roots passing through the shear plane will be mobilised during the subsequent rotational shearing phase, adding reinforcement (Figure 3.5).

To prevent root accumulation or soil disturbance or compacting while pushing the device to depth, the soil just above the desired test depth has to be excavated first. A drawback of this is that it might lead to a reduction of vertical stress in the soil, therefore underestimating the shear stress. The effect of excavation should be checked in the field. Because of excavation, no shear resistance will be present on the top interface of the sheared cylinder. Assuming cylindrical failure, the soil shear stress τ_{pv} [kPa] can be evaluated as fallows:

$$\tau_{pv} = \frac{12 \cdot T}{\pi \cdot d_{pv}^2 \cdot (6 \cdot h_{pv} + d_{pv})} \tag{3.3}$$

where T [kNm] is the measured torque and h_{pv} and d_{pv} the height and exterior diameter [m] of the soil cylinder trapped in the vane device respectively.

Since the pin vane directly measures the shear strength of the rooted soil, both mechanical and hydrological root-reinforcement will be measured at the same time. If the the mechanical reinforcement is to be analysed independently, additional measurements are required. For example, one might estimate hydrological root-reinforcement using pore water pressure transducers in the field combined with measured or estimated soil parameters to obtain the corresponding increase in shear strength due to hydrological effects.

Care must be taken to ensure the prongs are spaced sufficiently close to mobilise sufficient lateral soil resistance. Otherwise, local soil failure around individual prongs might occur rather than the typical cylindrical failure of the soil in conventional vane tests.

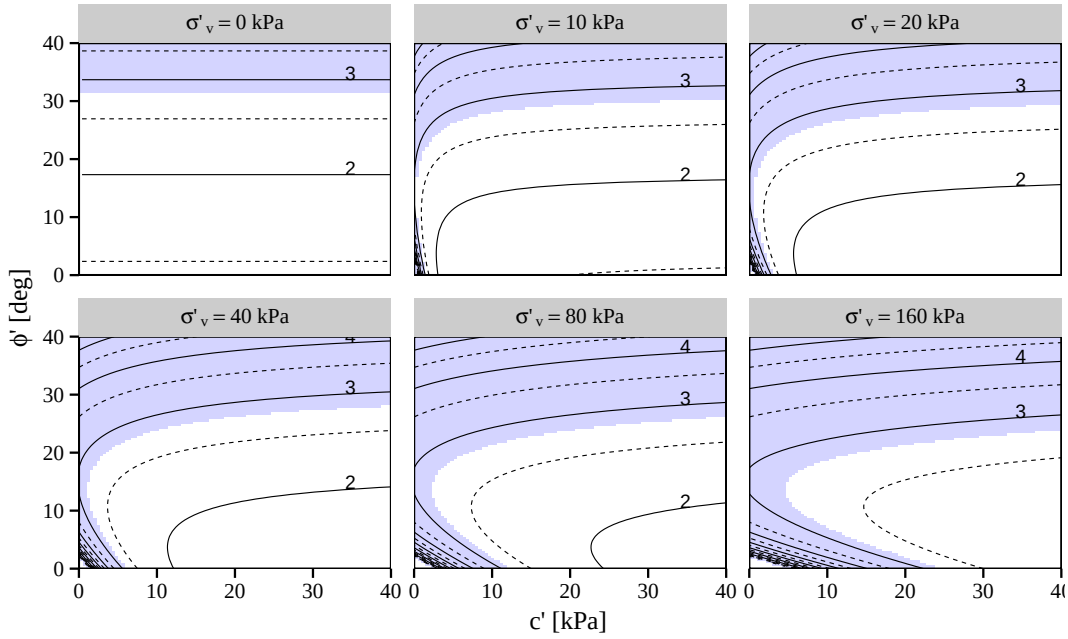

Figure 3.6: Contour plots of the minimum required pin vane prong spacing for various soil strength parameters (ϕ' and c') and effective vertical stress levels. Spacing is normalised as prong centre-to-centre distance s over diameter d_{prong}). Effective stress levels are given in subplot titles. The shaded zone indicates the 'zone of applicability' for the adopted pin vane spacing $s/d_{prong} = 2.8$.

The plastic deformation model derived by Ito and Matsui (1975) was used to study the effect of prong spacing. This model was originally derived to quantify the soil resistance for a group of laterally displacing foundation piles. By comparing model results to the soil resistance on the cylindrical shear surface, the minimum required prong spacing can be deduced. Details of this analysis can be found in Appendix A.

The results showed that the minimum required ratio between prong centre-to-centre distance s and prong diameter d_{prong} is a function of both the soil vertical effective stress σ'_v and soil strength parameters ϕ' and c' (Figure 3.6). Higher soil frictional resistance (increasing ϕ' and σ'_v) resulted in a larger minimum required spacing s/d_{prong}. This was in line with soil arching theory, where more arching takes place when there is more frictional strength. Increasing the soil cohesion c' reduced the minimum required spacing. When this analysis is to be used for rooted soils, root effects might be taken into account as an increase in soil cohesion. However, it is unclear whether this model is reliable in this case as the presence of roots not only increases the soil's shear strength but also adds significant tensile strength and changes the soil stress–strain behaviour.

The device used in this thesis consisted of five $d_{prong} = 5$ mm diameter stainless steel prongs: one central and four equally spaced along the outer perimeter with a centre-to-centre distance of 14 mm ($2.8 \cdot d_{prong}$) to the central axis. Pins were 50 mm long and had 30° conical tips (Figure 3.3c). The corresponding 10.8% area ratio (ratio of device

versus soil cross-sectional area, i.e. $5 \cdot d_{prong}^2 \cdot d_{pv}^{-2}$) is lower than the maximum value of 12% prescribed by the British Standard for normal shear vane devices (British Standards Institution, 2007). To make the device sufficiently rigid, the top sides of the prongs were held in place by a 10 mm thick steel disc. Because of this disc, soil had to be excavated to just above the desired test depth prior to each test, to prevent root accumulation and soil compaction.

Using this pin vane design, Ito and Matsui's model suggested that the device would function well in frictional soil (where $\phi' \gtrsim 30°$) but would not yield the desired failure mechanism in purely cohesive soil unless the spacing was reduced.

3.5 Corkscrew

Similar to the pin vane device, the proposed corkscrew device mobilises shear strength along a cylindrical interface. The strength however is mobilised during upwards rather than rotational displacement. Rotational installation (similar to inserting a corkscrew into a wine bottle) minimises soil disturbance; only soil and roots close to the path of the screw tip are likely to be affected and the corkscrew helix can be installed 'around' the roots. During translational extraction shear resistance along the outer sides of the cylinder of soil trapped within the screw is mobilised. This includes the effect of undisturbed roots passing through this interface (Figure 3.7). The root-reinforced soil shear resistance τ_{cs} was derived from the measured extraction force F when tensile forces on the bottom interface are neglected (i.e. no tensile strength and no suction):

$$\tau_{cs} = \frac{F}{h_{cs} \cdot \pi \cdot d_{cs}} \tag{3.4}$$

where h_{cs} and d_{cs} are the height and diameter of the displaced soil cylinder [m] respectively. It has to be ensured that the support the screw gives to the trapped cylinder is sufficiently large so that soil does not drop out of the screw, resulting in underestimation of the shear strength.

Similar to the pin vane, the cork screw will measured the combined effect the non-rooted soil shear strength, hydrological reinforcement and mechanical reinforcement. If only the mechanical reinforcement is to be studied, additional measurements are required to subtract the hydrological root-reinforcement from the measured total shear strength.

Installation torque might be related to soil strength. For example, tests with screw anchors have shown that installation torque can be related to pile bearing capacity (Hoyt and Clemence, 1989; Pack, 2009) and therefore to soil strength. Screw anchors provided for the initial inspiration in the developmental process of the corkscrew method. Although likely more rigid than the corkscrew, they will introduce more soil disturbance and root breakage during installation because of the central shaft and helices, and this concept was therefore discarded.

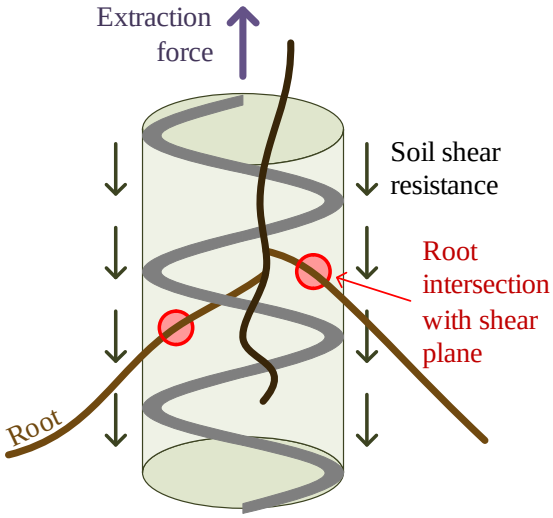

Figure 3.7: Schematic view of root-reinforced shear strength measurement using the corkscrew method.

Figure 3.8: Picture of the corkscrew device used.

In this thesis, d_{cs} = 40 mm (outer diameter) steel corkscrew weeders (De Wit, The Netherlands) were used (Figure 3.8). The screw height h_{cs} was approximately 120–125 mm, the screw pitch approximately 28 mm and screw thickness 6 mm (Figure 3.3d). To prevent root accumulation in the device during installation, prior to each test soil had to be excavated to a depth corresponding with the target top level of the screw. This might have two drawbacks: 1) this leads to a potential reduction of vertical pressure in the soil, thus resulting in an underestimation the shear strength; 2) the device gets more difficult to use at greater depth, as it gets more difficult to extract the device perfectly axially. In this thesis, no serious extraction problems were encountered, although the maximum depth that could be reached did not exceed 0.625 m due to the presence of very stony soil layers or bedrock. It is therefore not know how the device would function in deeper soil layers.

Corkscrew displacements (u_{cs}), measured at the top of the device, were corrected for the axial stiffness of the screw. The screw stiffness was determined in compression using an universal testing machine (Instron 5966) fitted with a 2 kN load cell. The corkscrew was guided around a ∅28 mm 100 mm wooden high cylinder to minimise buckling during

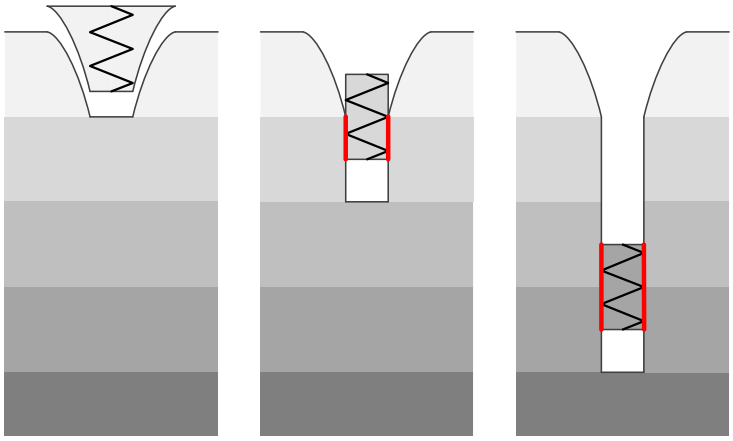

a) surface level: Wedge failure

b) 125 – 250 mm: Reducing shear area during extraction

c) > 250 mm: Shear area constant during extraction

Figure 3.9: Development of shear area during corkscrew displacement at various depths.

compression and loaded at a rate of 250 Nmin^{-1} to a maximum load of 600 N. At higher loads buckling mechanisms started to form near the connection between the screw and the shaft. The force–displacement curve was highly linear, with an average stiffness of $k_{cs} = 54.3\ \mathrm{Nmm}^{-1}$. When the shear strength was assumed to be evenly distributed along the shear plane, the 'average' soil displacement u_{soil} in the screw (measured in the middle of the corkscrew) could be expressed as:

$$u_{soil} = u_{cs} - \frac{1}{2} \cdot \frac{F(u_{cs})}{k_{cs}} \tag{3.5}$$

where $F(u_{cs})$ is the measured extraction force at displacement level u_{cs}. Corkscrew displacements for the remainder of this thesis are presented in terms of this corrected u_{soil} rather than u_{cs}.

The residual strength measured with the corkscrew ($\tau_{cs,res}$) was defined as:

$$\tau_{cs,res} = \min\left(\frac{F(u_{soil})}{\pi \cdot d_{cs} \cdot h_{cs}}\right), u_{peak} \leq u_{soil} \leq h_{cs} \tag{3.6}$$

where u_{peak} is the displacement associated with the measured peak shear strength. In tests performed at the very surface of the soil, the extracted core might have a conical or wedge shape, making it too difficult to determine the residual strength accurately (Figure 3.9a). This will also affect the test just below this surface test since the shear area will gradually decrease during the test (Figure 3.9b). In this case the residual strength was defined as:

$$\tau_{cs,res} = \min\left(\frac{F(u_{soil})}{\pi \cdot d_{cs} \cdot (h_{cs} - u_{soil})}\right), u_{peak} \leq u_{soil} \leq h_{cs} \tag{3.7}$$

3.6 Summary and test plan

In this chapter, four new devices were proposed. The 'blade penetrometer' and root 'pull-up' device can be used to infer root depth and properties from characteristics of the measured depth versus resistance trace. These devices therefore do not directly measure the shear strength of root-reinforced soil. In contrast, the 'corkscrew' and 'pin vane' devices measure the strength of root-reinforced soil by mobilising a cylinder of soil in translation or rotation respectively.

In Chapter 4, all four devices will be qualitatively evaluated through laboratory testing in field soil with various inclusions (plastic root analogues, fibres and stones). These tests will provide insight in the type of response each device yields in a variety of conditions. Based on the outcome of these experiments, some methods will be taken forward for further development and others will be abandoned.

For the most suitable devices that can be used to quantify the depth and diameter of individual roots, interpretive models will be developed to infer root properties from the measured force–displacement traces (Chapter 5). Subsequently, a more comprehensive laboratory study will be performed to study the effect of various root properties, root architecture and soil parameters on the root response (Chapter 6), followed by experiments in the field to study the behaviour of the device in realistic conditions (Chapter 7).

For devices that directly measure the shear strength of the root–soil composite, selected devices will be compared to existing shear strength measurements to study whether they yield reliable results (Section 8.2). Subsequently, they are trialled in rooted field soil (Section 8.3). Based on the results of these experiments, the best device will be selected and tested in various field soils to derive correlations between root properties and measured reinforcement (Section 8.4). Finally, a large scale field experiment on steep slopes will be performed to study determine how the device performs under field conditions for which the device was initially designed (Section 8.5).

4

Laboratory comparison

The contents of this chapter have been published as part of a journal paper, see Meijer et al. (2016c).

4.1 Introduction

In this chapter, the four measurement methods introduced in Chapter 3 were tested under laboratory conditions using various root analogues and loose, recompacted, unsaturated field soil. This study mainly served as a pilot study to identify which devices were most promising to take forward for further development, so that efforts to developed new methods could be focussed on a smaller subset of devices. Additionally, it provided insight in the type of force–displacement responses each measurement method yielded in field soil with a variety of inclusions. Finally, it was used to identify practical problems that needed to be solved before taking the devices for more detailed laboratory or field investigations.

4.2 Methods

4.2.1 Soil and root analogues

Root analogues and recompacted soil were used to minimise variability in the initial testing and to facilitate inter- and intra-device comparison. Two different root analogues were used.

Straight acrylonitrile butadiene styrene (ABS) plastic rods with circular cross-sections were used as an analogue material for relatively thicker roots (diameters 1 and 4 mm). Rods were printed using a rapid prototyper ('3D-printer', Liang et al., 2014, 2015). The benefits of using ABS are twofold: first, it enables creating 'roots' with reproducible characteristics, and second, material characteristics are comparable to real roots (Figure 4.1). The tensile strength was comparable to the highest reported values for roots in the

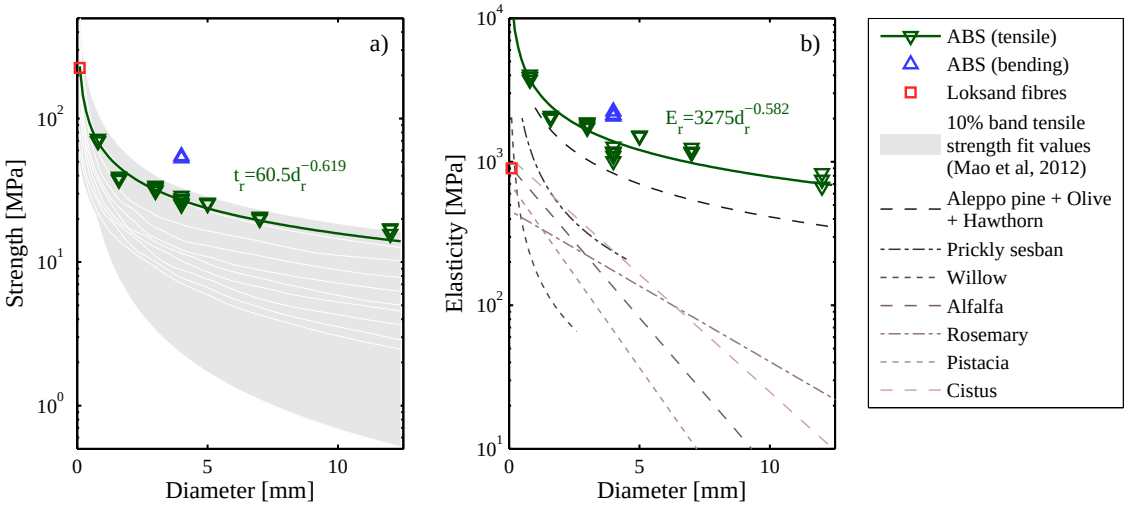

Figure 4.1: Comparison of (a) strength and (b) Young's modulus between root analogues and plant root data from the literature. In the strength plot, 40 fitted tensile strength–diameter relationships for tree roots (Mao et al., 2012) are used to construct bands, each containing 10% of reported data. Data sources: ABS: present study; PP fibres: Diambra et al. (2010); Aleppo pine + olive + hawthorn: Van Beek et al. (2005); prickly sesban: Fan and Su (2008); willow, alfalfa, Pistacia and Cistus: Operstein and Frydman (2000).

literature. The Young's modulus of ABS had the same order of magnitude as available data for tree roots, but was greater than values for other plant types. The printing process introduces anisotropy (Ziemian et al., 2012), as the model was printed in thin lines of molten plastic. Therefore here it was ensured that during printing the root axis is aligned with the printing direction.

To model dense fibrous root systems, such as those of grass, 35 mm long, 0.1 mm diameter Loksand polypropylene (PP) crimped fibres were used, similar to those used by Diambra et al. (2010). The tensile strength is similar to values for real roots (Figure 4.1).

Slightly clayey sand (Atterberg limits w_L = 32% and w_P = 23%) was collected from Bullionfield near the James Hutton Institute (Dundee, UK; Mickovski et al. (2009)). It was chosen to use real field soil rather than more traditional laboratory soils such as kaolin clay or sands to better represent real field conditions (more realistic soil density, particle size distribution and matric suction levels).

The particle size distribution was determined using a combination of laser diffraction (particles < 2 mm; British Standards Institution, 2010) and dry sieving (particles ≥ 2 mm), see Figure 4.2.

Particles with diameters > 5 mm were removed using a rotary sieve. The gravimetric water content after sampling averaged w = 20%. Soil was air dried to w = 10–17%, sieved again (≤ 2 mm) and packed into polyvinyl chloride (PVC) tubes (150 mm internal diameter, 400 mm long).

To some tubes gravel of two different sizes was added: 4–5 mm diameter subrounded gravel (Bullionfield) and angular 10–30 mm diameter broken road gravel.

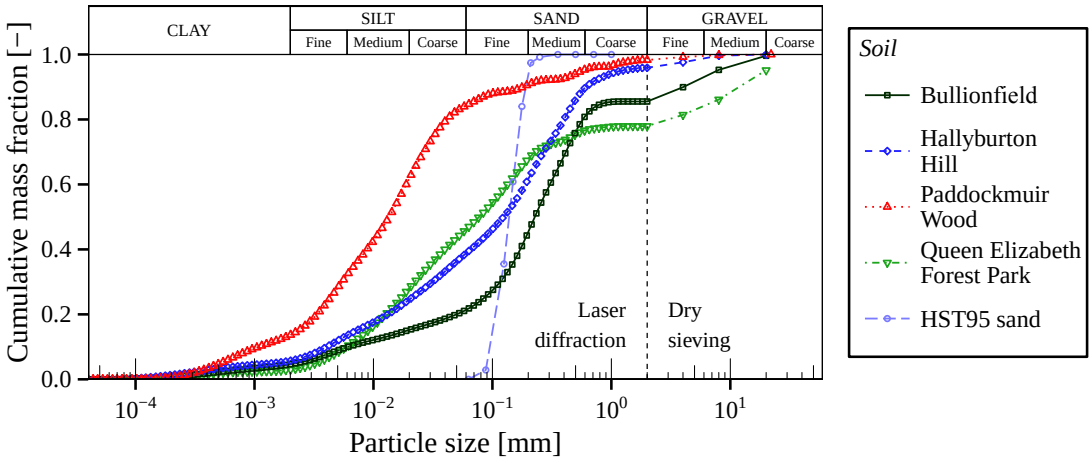

Figure 4.2: Particle size distributions for soils used in this thesis. Laser diffraction (British Standards Institution, 2010) was used to quantify the amount of particles smaller than 2 mm, while dry sieving was adopted for particles > 2 mm. Field soils were sampled between 150 and 250 mm depth. Particle sizing for (laboratory) HST95 sand was determined using dry sieving only, see Lauder (2010).

4.2.2 Sample preparation

Soil was packed to a dry density of $\rho_d = 1.35\ \mathrm{Mgm^{-3}}$ in seven layers, each with a thickness of 50 mm, using a standard 2.5 kg Proctor hammer and a 150 mm diameter hammering plate. The 5 mm wide outer rim of this plate protruded 5 mm to compact to a higher density around the edges and to discourage preferential water flow along the core–soil boundary during saturation and drainage. On average, 166.5 $\mathrm{kJm^{-3}}$ was applied to each layer (20 blows). Before adding a new layer, the top 5 mm of the previous layer was abraded to ensure layer bonding.

After compaction, cores were saturated from the base in large plastic containers for 48 h. During the first 24 h the water level was 150 mm below the soil surface. On the following day, this was raised to 20 mm above the soil surface. Full saturation was reached after approximately 36 h (confirmed by free water on top of the samples and volumetric water content measurements (using a theta probe, model ML2x, Delta T).

Following saturation, cores were drained on sand tables to 1.5 kPa suction at their base. With a soil height of 350 mm in the core, this is equivalent to field conditions where the water table is 500 mm below the soil surface. All cores were drained for at least four full days to reach equilibrium (checked using mini tensiometers at the top of the core).

Water retention characteristics were determined using four samples packed in 100 $\mathrm{cm^3}$ steel rings (average dry density $\rho_d = 1.34\ \mathrm{Mgm^{-3}}$). Samples were saturated for 2 days and subsequently equilibrated on ceramic plates (0.5, 1.0, 2.0, 5.0, 10, 20, 50 kPa suction). The corresponding results were fitted to the Van Genuchten model (Van Genuchten, 1980) in terms of saturations rather than volumetric or gravimetric water contents. Saturation is

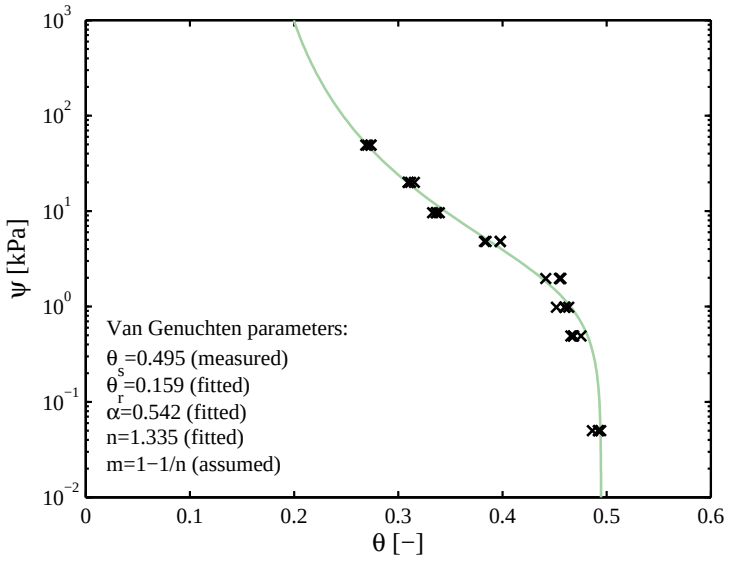

Figure 4.3: Water retention curve for recompacted Bullionfield soil at dry density $\rho_d = 1.34$ Mgm^{-3}.

less sensitive to variations in soil dry densities.

$$S_r(s) = S_{r,r} + \frac{S_{r,s} - S_{r,r}}{(1 + (\alpha|s|)^n)^m} \tag{4.1}$$

where S_r is the saturation [%], s the suction level [kPa], $S_{r,s} = 100\%$ the saturation at saturated conditions (measured prior to testing), $S_{r,r} = 31.9\%$ the residual saturation (fitted), and α, n and m dimensionless model parameters, fitted as 0.542, 1.335 and $(1-1/n)$ respectively ($R^2 = 98.9\%$), see Figure 4.3. Based on these water retention parameters, saturation levels of $S_r = 77\%$ (top) to 91% (bottom) were expected in the soil cores.

Because of the limited size of the sand tables, 4–6 cores were prepared at a time ('batch'). Cores from the same batch were used for testing the same device in cores containing different inclusions (ABS, PP fibres, stones) rather than varying the device type and keeping the inclusion type constant. This choice was made to be better able to compare the behaviour of a single device between cores with various inclusions.

Dry bulk densities in cores were checked using standard 100 cm^3 steel sampling rings. Gravimetric water contents were determined using conventional oven drying (105°C). Measurements were corrected for the presence of stones, assuming a stone bulk density of 2.65 Mgm^{-3}.

For classification purposes and to check whether the adopted compaction method yielded a homogeneous soil, the strength of the soil was measured in two cores with no inclusions, using a standard penetrometer (standard agricultural penetrometer, 30° 12.5 mm diameter cone connected to a 10 mm diameter shaft pushed at 300 mm min^{-1}) using an Instron 5966 universal testing machine.

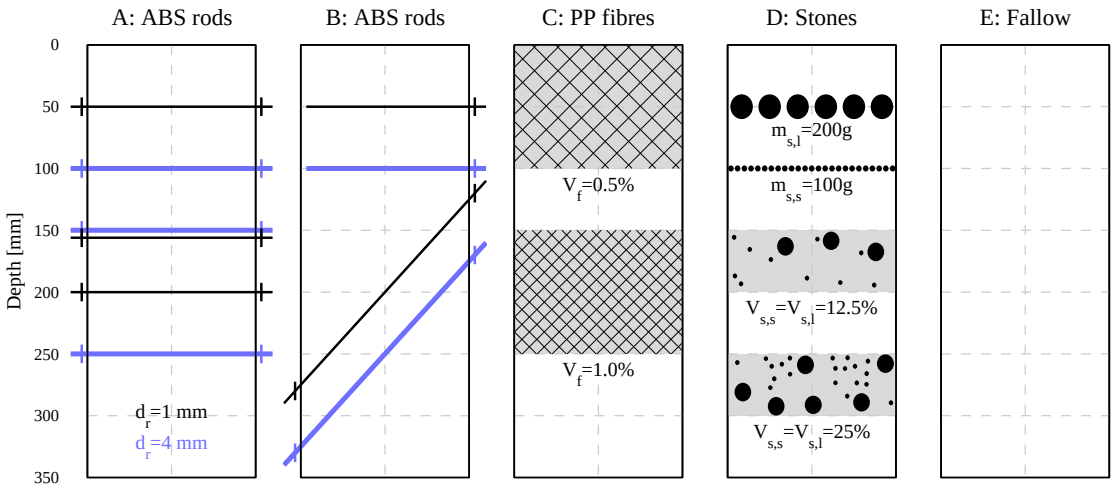

Figure 4.4: Schematic overview of used laboratory soil and root test conditions. In cores with fibres (C) or stones (D), quantities of fibres (V_f), small stones ($V_{s,s}$) and large stones ($V_{s,l}$) are expressed in volume fractions [%]. In the uppermost half of stony cores (D) two single stone thick stone layers are placed. Of these the total mass of stones (m_s) is given.

4.2.3 Test conditions

Cores containing inclusions were made to test the various measurement devices under a range of conditions (Figure 4.4).

Cases A and B were prepared to study the behaviour of individual horizontal woody tree root analogues (1 and 4 mm diameter). Many tree roots grow in the (sub)horizontal direction, as tree roots explore the resource-rich topsoil layer (e.g. see Reubens et al., 2007). In the present testing, straight root analogues were generally vertically spaced 50 mm apart so that root analogues would not affect each other (Figure 4.4). Therefore, in blade penetrometer, pull-up and vane testing, the effects of a single root could be studied. This was more difficult for corkscrew tests because of the larger height of the device.

In case A, sections of horizontal, thin (1 mm diameter) and thicker (4 mm diameter) roots were modelled using printed ABS. Translation was restricted at both rod ends by leading them through drilled holes in the side of the core and gluing a Perspex disc around the rod on the outside, preventing axial movement. This is intended to represent the tensile restraint at the ends of longer sections of root or short regions of branched roots. Individual rods were installed during packing when the soil level reached the level of the inclusion. At depth $z \approx 150$ mm, one 1 mm diameter rod and 4 mm diameter rod were placed 5 mm apart to see whether interaction would occur between the closely spaced root analogues.

In case B, the top half of the core was used to model root ends with potential pull-out failure. When a root is loaded near its tip, reinforcement is expected to be smaller, as the root will slip at one end rather than break. In the bottom half, ABS rods were oriented at 45° to study the effect of root angle on the test results. Both ends of these angled rods were restrained and pushed in after the cores were filled to a level corresponding with the

top end of the rod.

In case C, dense fibrous root mats were modelled using PP fibres. Two 100 mm thick rooted layers were modelled at different depths: one with a fibre volume fraction of 0.5% and the other, deeper layer, with 1.0% fibres. These percentages are in line with root fractions in the top soil layer (0–500 mm) found for tree species in northern Italy (Bischetti et al., 2005). Fibres and soil were premixed by hand in small quantities (1/70 of the total soil mass) until by visual examination the fibres were considered to be well distributed (similar to Ibraim and Fourmont, 2007). Then the mixture was carefully deposited in the core. After each ten batches, together forming one 50 mm thick core layer, the soil in the core was compacted as described earlier.

In case D, a stony soil was modelled. This was done for two reasons: first to study whether the developed methods can be reliably used in gravelly soil, and second to see whether gravel and roots yield distinct behaviour, as both may be present in real soils. In the top half, for both gravel size classes, a single layer of stones was manually deposited between two soil layers using 100 g (4–5 mm gravel) or 200 g (10–30 mm gravel), respectively. In the bottom half, two 50 mm thick stony soil layers were premixed with soil, carefully deposited in the core and compacted. Both contained equal volumes of both gravel size classes (assuming a density of ρ_d = 2.65 Mgm^{-3}). In the shallowest layer, the ratio of stone volume to total bulk volume equalled 12.5% and in the deeper layer 25% for each gravel size class. Different quantities are used in different layers to study the sensitivity of measurements to various amounts of stones.

Case E was a fallow soil sample, which served as the control treatment.

4.2.4 Test setup

Tests were performed using universal testing machines. For blade penetrometer, pull-up tests and CPT tests, an Instron 5966 fitted with a 2 kN load cell (Instron 2530-418) was used. For pin vane and corkscrew testing, an Instron 4204 fitted with a 50 kN load cell (Instron 2525-802) was used. All Instron load cells were accurate to the maximum of either 0.25% of the indicated load or 0.025% of the maximum capacity. Forces and displacement were measured at 20 Hz (Instron 4204) or 100 Hz (Instron 5966).

The Instron 4204 setup was enhanced with a rotational rig to apply rotation, see Figure 4.5. A DC shunt motor (Parvalux) was mounted in line with the shaft, the speed of which was controlled using a voltage controller. Torque was measured using a 15 Nm load cell (Novatech F311-Z3862; sampling frequency 1000 Hz, resampled to 100 Hz by averaging every ten measurements).

Displacement rates were chosen to reflect both expected application rates for *in situ* use (Table 4.1) and typical shear displacements of landslides (Figure 4.6).

Test devices were inserted centrally at the top of the core. For pull-up tests, the cone was installed slightly off-centre so that the centre of the expanded wing coincided with the

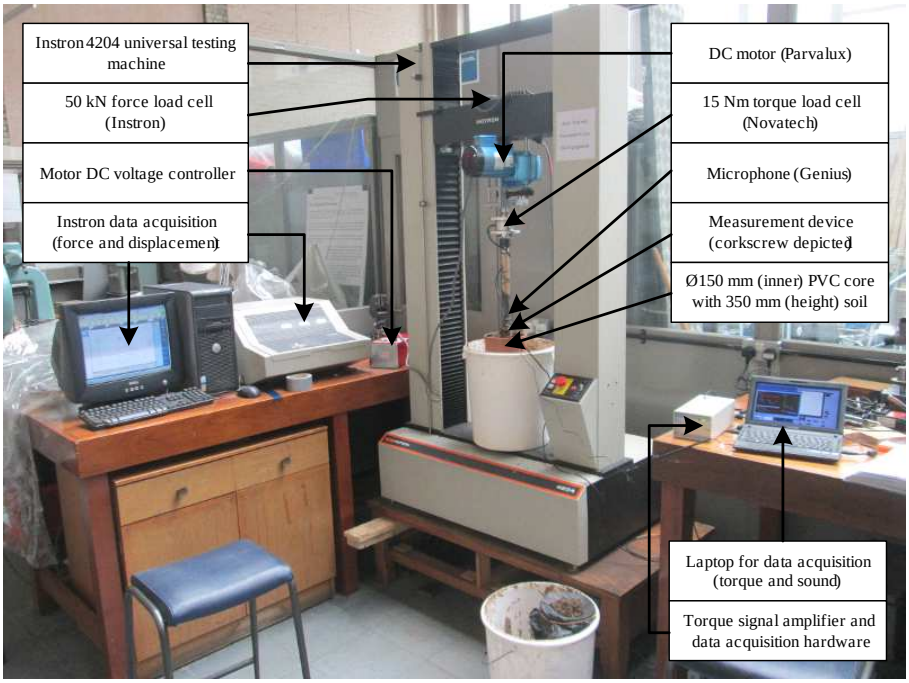

Figure 4.5: Laboratory test setup for pin vane and corkscrew (depicted) tests.

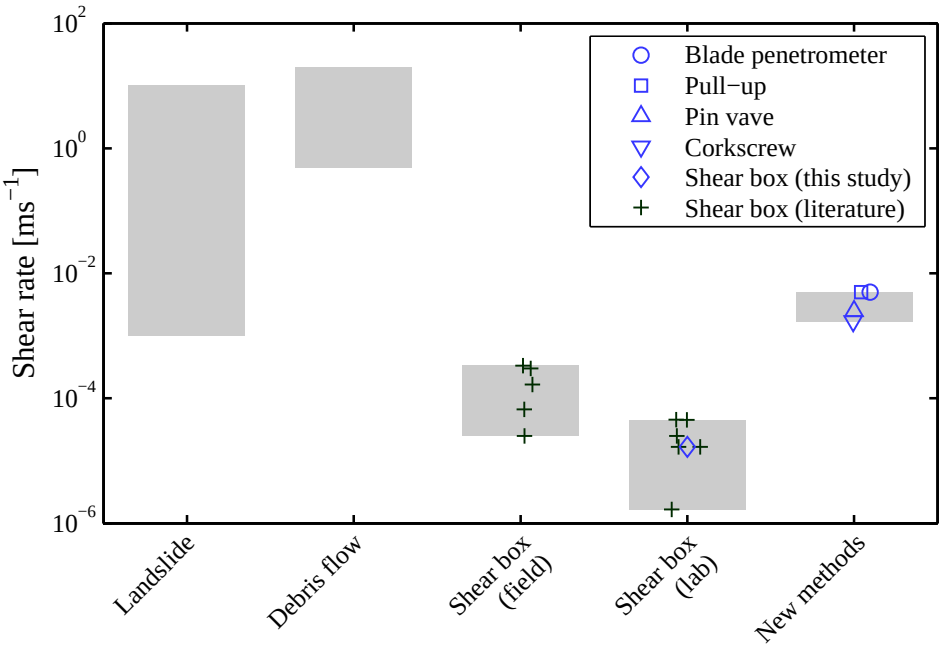

Figure 4.6: Typical shear rates for landslides, debris flows, field testing, laboratory testing and rates adopted in this study. Sources: landslides and debris flows (Davies et al., 2010), field shear box testing (Ekanayake et al., 1997; Cammeraat et al., 2005; Docker and Hubble, 2008; Fan and Su, 2008; Mickovski and Van Beek, 2009, many other studies do not provide adopted rates), laboratory shear box testing on root-reinforced soil (Waldron, 1977; Waldron and Dakessian, 1981; Operstein and Frydman, 2000; Normaniza et al., 2008; Mickovski et al., 2009; Loades et al., 2010).

Table 4.1: Translation, rotation and shear rates in laboratory testing.

Test	Translation		Rotation	Test rate
	Downwards [mm min^{-1}]	Upwards [mm min^{-1}]	[rpm]	[ms^{-1}]
Blade penetrometer	300*	—	—	0.0050
Pull-up	300	300*	—	0.0050
Pin vane	300	—	1.43*	0.0025
Corkscrew	116**	100*	4.23**	0.0017

* Main shear test phase
** Rates are linked based on corkscrew pitch, to minimise soil disturbance during installation

core central axis.

During blade penetrometer, pull-up and CPT tests, a single continuous measurement profile was taken per core. In vane tests, measurements were taken every 50 mm between 25 and 325 mm depth (six tests per core). In corkscrew tests, measurements were taken at 0–125, 125–225 and 225–325 mm depth. Each pin vane or corkscrew test was performed just beneath the hole excavated during the previous test.

4.2.5 Reference tests

Direct shear tests were performed using a shear table custom built to shear the 150 mm diameter cores (Mickovski et al., 2009, Figure 4.7). A load cell (Tedea Huntleigh 615, 2 kN capacity, accuracy 1 N) was mounted between the screw jack and upper braces. Displacements were measured using a linear variable differential transducer (LVDT) (RDP LDC6000C). Force and displacement were sampled at 10 Hz using a USB data acquisition unit (National Instruments USB-6008) and LabView software (National Instruments). All samples were sheared at a rate of 1 mm min^{-1} in correspondence with root-reinforced soil shear box rates reported in the literature (Figure 4.6), until a maximum displacement of around 50 mm was reached. Equipment limitations did not allow faster shear rates.

The PVC pipes surrounding soil cores for shear box testing were cut at the appropriate depths and re-joined using tape before packing. To ensure water tightness, the seams were filled with petroleum jelly and the inside lined with a plastic sheet. The tape was removed before shearing; the top part of the core was slid approximately 3 mm vertically, maintaining a solid soil core, and the plastic lining was cut with a scalpel blade.

Cores were sheared at various depths (see Figure 4.15). Most cores were prepared with fallow soil, although for the core types with PP fibres (case C) and stones (case D) a single core was also prepared. Each core was sheared at two or three different depths.

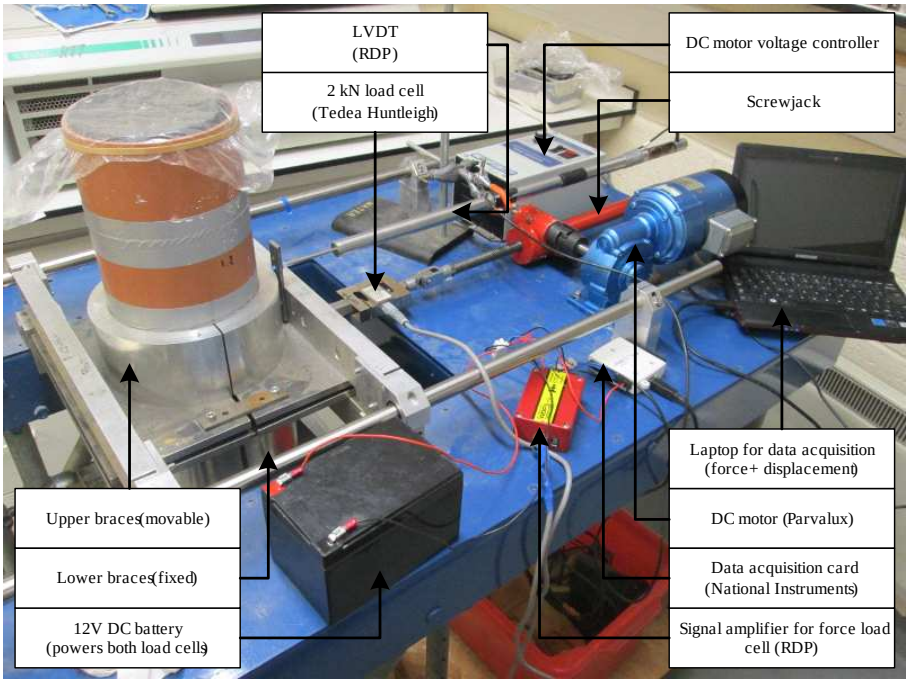

Figure 4.7: 150 mm diameter core laboratory direct shear apparatus.

4.3 Results

4.3.1 Sample preparation

Dry density measurements in 32 PVC tubes showed a very constant density over a 0–275 mm depth range (Figure 4.8a). The best linear fit resulted in $\rho_d = (1.36 \pm 6.1 \cdot 10^{-3}) + (5.94 \cdot 10^{-5} \pm 3.73 \cdot 10^{-5}) \cdot z$ Mgm^{-3} (values of coefficients ± standard error, number of tests $n = 104$, $R^2 = 0.024$), where z is the measurement depth (mm). In the bottom 75 mm, the density trend (Figure 4.8b) was linearly increasing to approximately 1.46 Mgm^{-3}. This increase in dry density corresponded with a decrease in water content. Gravimetric water content (w) samples taken from 33 PVC tubes showed an increasing water content over 0–275 mm depth ($w = (29.4 \pm 0.447) + (0.0142 \pm 0.00285) \cdot z$, $R^2 = 0.133$, $n = 162$) but below 275 mm the trend was linearly decreasing to roughly $w \approx 27\%$ at the bottom.

Measured water contents and saturation levels were larger than expected based on measured water retention characteristics. Many of the outliers in water contents corresponded with fibrous and stony layers. Although this trend could be observed in dry densities as well for successful measurements in stony soils, it was impossible to confirm for fibrous layers because it proved impossible to insert a steel sampling ring without significant disturbance.

Standard penetrometer resistance (measured with the standard cone penetrometer) decreased from 0.12 to 0.06 MPa with increasing depth (Figure 4.9). Although there were some signs of soil layering, due to the compaction procedure (50 mm thick layers), the influence on soil strength variation was small.

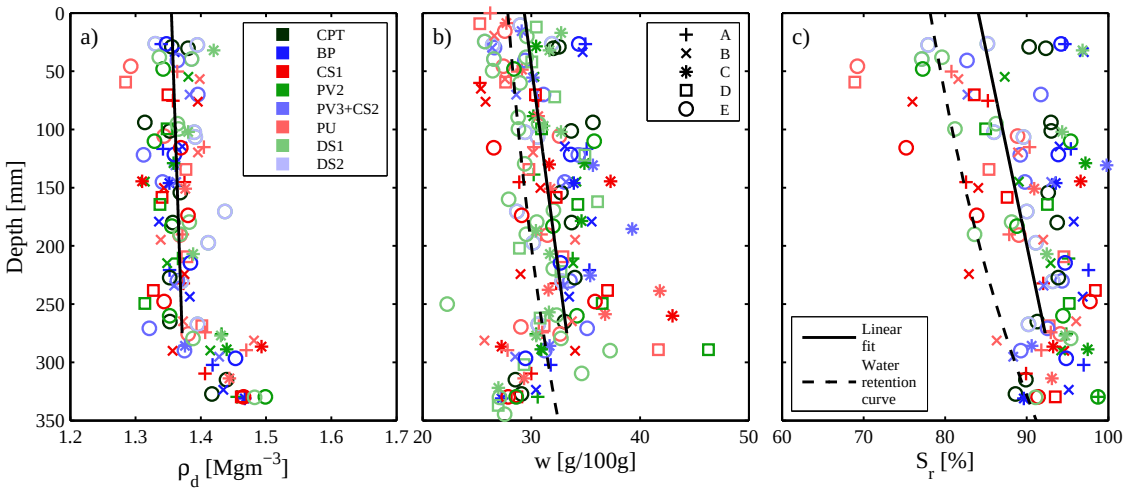

Figure 4.8: a) Dry bulk densities (ρ_d), b) gravimetric water content (w) and c) saturation levels (S_r) for various depths in soil cores after testing. Different symbols indicate core type. Different colours indicate different preparation batches (CPT = Standard penetrometer tests, BP = Blade penetrometer, CS = corkscrew, PV = pin vane, PU = pull-up, DS = direct shear). Solid lines represent least-square linear fitting over the depth the line spans, and dashed lines are predictions based on measured water retention characteristics.

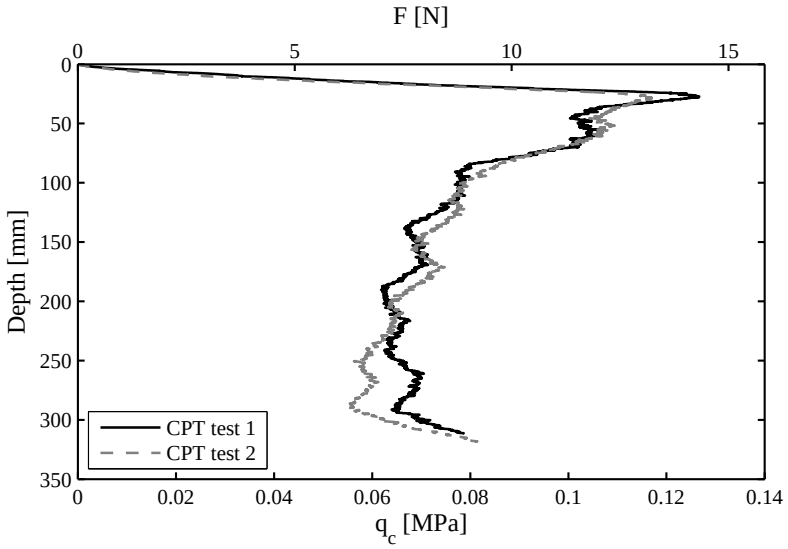

Figure 4.9: Standard penetrometer test profiles in fallow laboratory soil cores (E).

4.3.2 Blade penetrometer method

The blade penetrometer test (Figure 4.10) showed distinct behaviour for each core type. ABS roots showed force 'peaks' at levels where roots were present. The sudden drops in penetration resistance corresponded with root breakages. All ABS rods broke during tests, all directly below the penetrometer tip.

The results with ABS rods showed that both the penetration force increase and maximum root displacement varied with different diameters, orientation and clamping conditions. In core A, where all roots were clamped, thinner roots yielded a smaller increase in penetration resistance, with breakage occurring at larger relative displacements compared to thick roots. In case B, the shallowest 1 mm diameter root broke at much greater displacements compared with its counterpart in case A (50 and 13 mm, respectively). The force–displacement gradient was much smaller for the 4 mm diameter root at $z = 100$ mm in core B, and effect of the root on the increase in penetration resistance was much smaller. This demonstrated the importance of axial constraint. The 45° roots in core B broke at smaller forces than their horizontal counterparts in core A, a result which stemmed from either orientation or distance to anchoring point.

In contrary to ABS rods, the fibrous roots (case C) resulted in a large increase in penetration resistance without apparent breakages. The resistance gradually built up over the first 75 mm of the fibrous layers. Thereafter, the resistance decreased as the blade tip penetrated deeper, even in fallow soil directly below reinforced layers.

Stones (case D) increased penetration resistance (relative to the fallow case), but, in contrast to ABS rods, there were no sudden force drops and the force–displacement behaviour was more variable. Similarly to fibres, a larger stone volume fraction resulted in higher penetration resistances.

In all tests, in regions of soil where there were no inclusions, resistances were similar to those measured in cores with no inclusions (case E).

4.3.3 Pull-up method

Pull-up test results for both the installation (down, 'dn') and extraction ('up') phase are given in Figure 4.11. Installation resistances in cores for cases A, B and E were similar, but fibres (C) and stones (D) increased the installation resistance. This resistance was much smaller than for the blade penetrometer resistance, except for the very fibrous layer in case C ($z = 150$–250 mm).

During extraction ABS rods resulted in distinct force peaks with sudden drops in force corresponding to root breakages, similar to the blade penetrometer results. All ABS rods broke at the point of loading in case A. In case B, all rods broke apart from the top 1 mm diameter rod, which slipped out. The lowest, skewed 4 mm diameter rod could not be tested because it was located below the level of the expanding blade. Interestingly, the

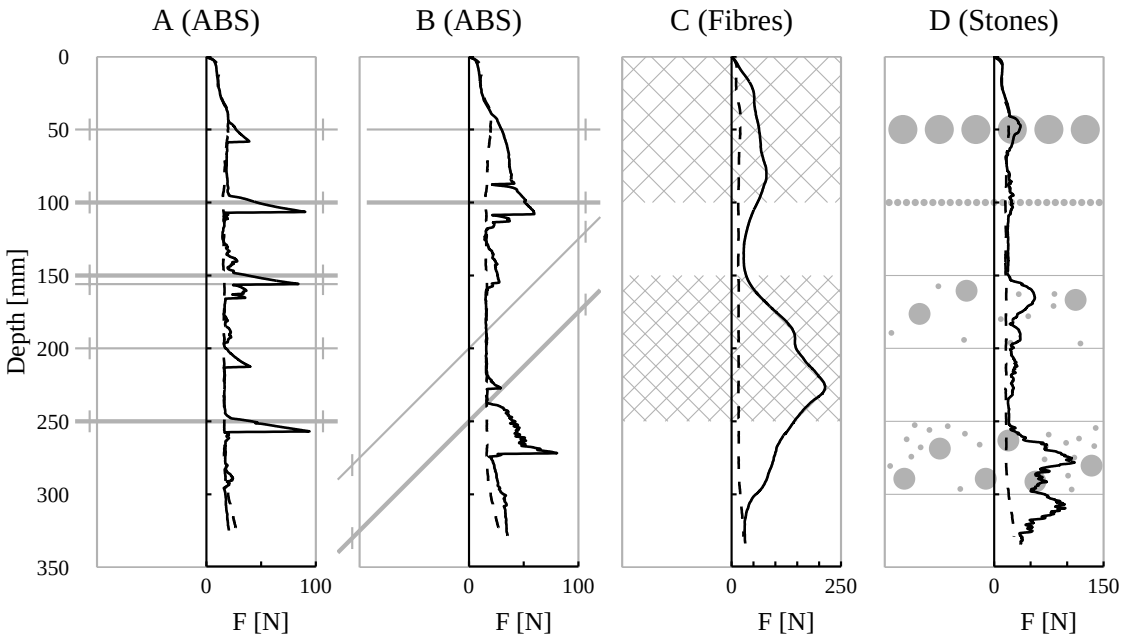

Figure 4.10: Laboratory blade penetrometer test results: depth versus installation force. In each core A–D the fallow behaviour (E, dashed line) is plotted for reference.

resistance during extraction in the deepest fibrous layer (case C) was not much larger than the resistance in the top fibrous layer despite containing double the amount of fibres. The additional resistance caused by stones seemed to be small compared to blade penetrometer installation forces.

4.3.4 Pin vane method

Pin vane test results yielded not only root-reinforced soil peak shear strengths; rotation–shear strength traces (examples given in Figure 4.12) contained additional information useful to distinguish between core types. All ABS rods (cases A and B) broke, resulting in sudden drops in measured resistance (Figure 4.12a). Most rods broke at a single point within the pin vane device, although some broke at multiple points. In these six cases (out of 24), for five of them breakages were located between 14 and 26 mm apart, near the middle of the rod. Residual strengths were similar for fallow and ABS-rooted soil once rods had broken.

Fibrous samples (Figure 4.12b) showed a very smooth response with a gradual rise to peak strength and slow decline to residual strength. The lack of sudden force decrease suggested that the fibres did not break. The peak strength was much higher and occurred at larger displacements compared with the fallow soil.

Soil with stones (Figure 4.12c) returned very spiky force–displacement plots. Force declined more smoothly than for ABS rods. In these results, and also in the test in core B at 75–125 mm depth, local maxima beyond 75° rotation lay approximately 90° apart, suggesting they were caused by the same broken root end or stone being mobilised every

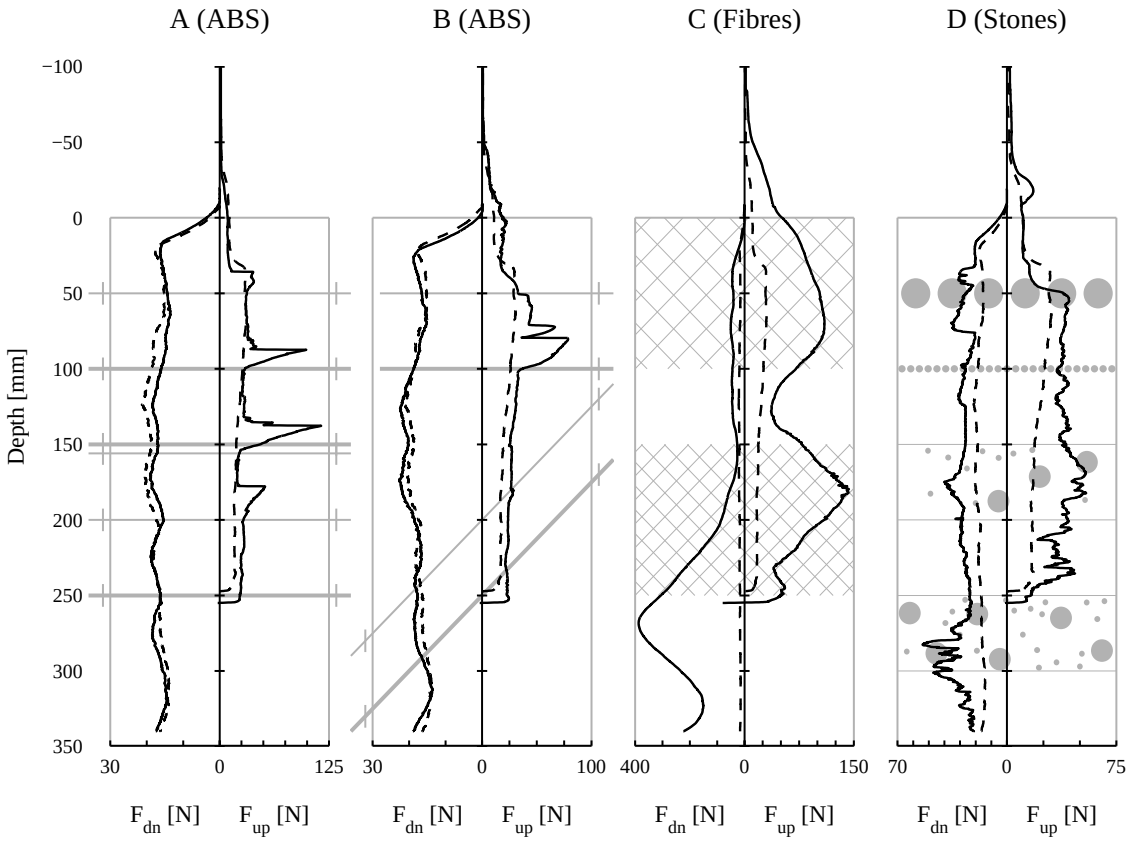

Figure 4.11: Pull-up device test results. For each core type, the installation force F_{dn} (left) and extraction force F_{up} (right) are plotted. Fallow results (core E) are plotted using dashed lines. For the installation phase, depth corresponds with tip depth. During extraction, depth corresponds with the depth of the wing along the central core axis.

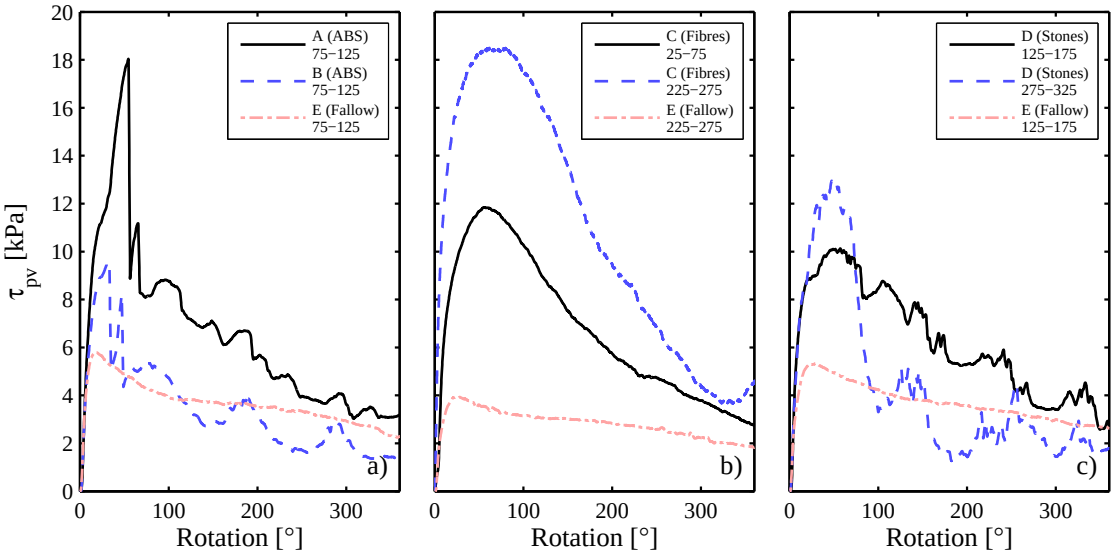

Figure 4.12: Example pin vane test results in cores with (a) woody root analogues, (b) fine root analogues and (c) stones. Core type and test depth range (in mm) are given in the keys.

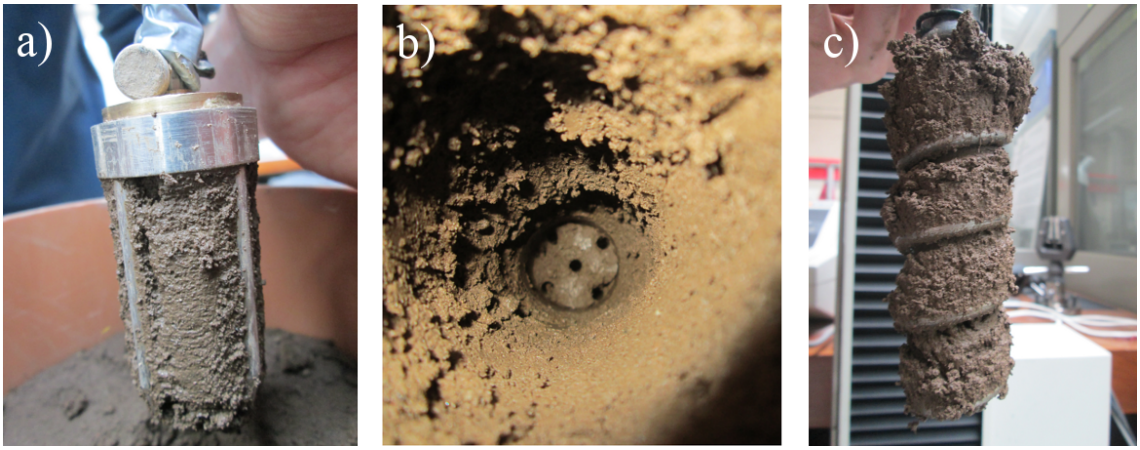

Figure 4.13: Soil failure mechanism: a) pin vane with soil plug extracted, b) pin vane with soil plug not extracted, c) corkscrew soil plug after test at 125–225 mm depth.

time an outermost pin passed.

In most tests a cylindrical plug of soil was still trapped within the device after testing (Figure 4.13a). This shows that a failure mechanism occurred similar to that in standard field vane testing. In approximately a third of all tests, primarily in the wetter, deeper layers, no soil plug was extracted and the soil remained in the hole. Inspection of the hole however showed clear, circular-shaped cavities where the prongs had been (Figure 4.13b). This suggests that the soil had rotated as an intact block with the pins, rather than pins moving relative to the soil plug, again justifying the assumptions of a coring failure mechanism.

4.3.5 Corkscrew method

Force–displacement plots for corkscrew extraction differed between core types. Extraction shear strength behaviour was similar to that observed in pin vane torque–rotation plots: ABS rods broke (Figure 4.14a), resulting in distinct force peaks. The presence of fibres (case C) resulted in ductile behaviour, with increased resistances over a large displacement range (Figure 4.14b). Both peak strength and displacement to failure increased with increasing fibre volume fractions. Stones (case D, Figure 4.14c) resulted in spiky profiles, whereas fallow (case E) soils resulted in a smooth profile with smaller peak displacements and a smaller width of the maximum strength peak.

Complete cylinders were extracted during almost all tests (Figure 4.13c), including those in deeper and wetter soil. In tests closest to the surface (z = 0–125 mm), the top of the extracted soil had a conical rather than a cylindrical shape. This was especially pronounced in the first batch of tests, where at the top the width of the cone could be as wide as the core. The plug diameter gradually diminished with depth until $z \approx 50$ mm, where the soil plug diameter was as wide as the corkscrew device. In later tests this effect was smaller, with maximum cone diameters of 90 mm observed at the top 20 mm of the soil plug. In deeper tests, this effect was not observed.

An interesting feature occurred in one of the fallow tests at 225–325 mm depth (Figure 4.14b). A sudden drop in force occurred after 50 mm displacement. This behaviour was observed in two other fallow tests (at 125–225 mm and 225–325 mm depth tests, after extracting 20 and 35 mm, respectively). It was hypothesised this was caused by a sudden loss of suction at the void that opened up below the device during extraction. In other tests, this suction probably dissipated more gradually.

In some of the tests belonging to the first series of corkscrew tests, larger resistances were measured because the corkscrew was not inserted perfectly vertically yet vertically extracted. During installation, instead of the installation force and torque increasing linearly, an additional sinusoidal pattern in the installation resistance was observed. Because of this, the fallow results from this series were discarded. These observations showed that, for field applications, it is important to extract the corkscrew in line with the installation orientation, and also that potential misalignment can easily be observed from installation measurement torque and force.

4.3.6 Comparison to reference shear box testing

Direct shear tests of fibrous layers yielded greater shear strengths than in fallow tests. However, the reinforcement effect was small compared to both the pin vane and corkscrew methods (Figure 4.15). Differences may be explained by fibre orientation and test direction. During preparation fibres will be orientated mainly horizontally and therefore add less reinforcement to the horizontally oriented shear plane in the shear box tests (Ibraim et al.,

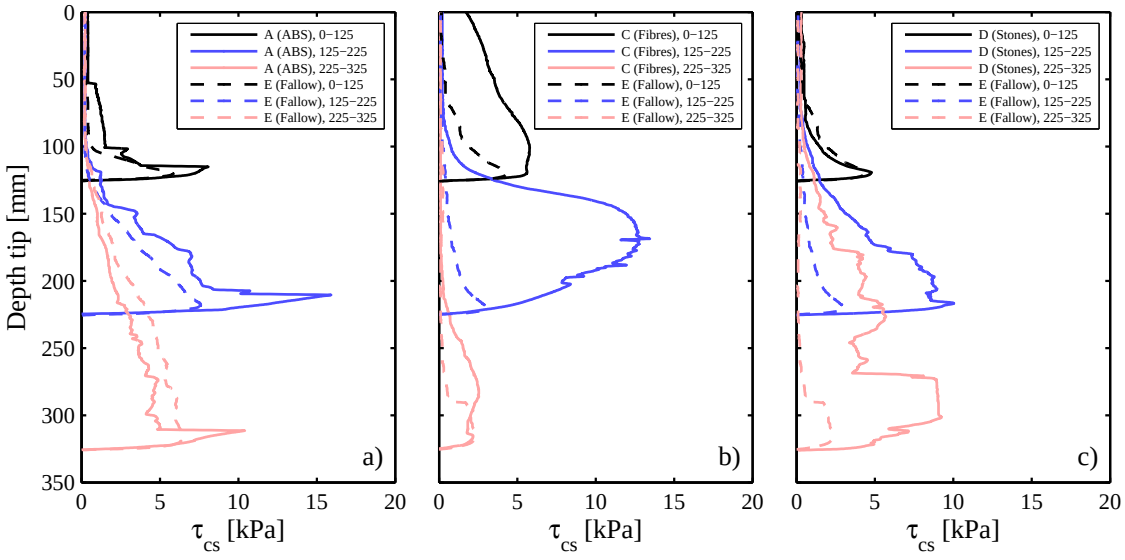

Figure 4.14: Example corkscrew test results for extraction in cores with (a) woody root analogues, (b) fine root analogues and (c) stones. Core type and test depth range (mm) are given in the keys. Depths were not corrected for corkscrew spring stiffness and directly based on the cross head displacement of the testing machine.

2012). In pin vane and corkscrew tests the shear plane was orientated vertically, resulting in more fibres crossing the shear plane at angles favourable for tensile reinforcement. Shear planes were also located close to the boundary between two compacted soil layers. Fibre reinforcement will probably be lower at these interfaces because of fewer fibres crossing between layers, despite abrasion of the soil prior to adding a new soil layer during compaction. Shearing in cores with stones significantly increased the shear strength. Larger stone contents resulted in greater reinforcements.

Both the corkscrew and pin vane tests showed decreasing strength with increasing depth in fallow soil. This trend was also observed in standard penetrometer tests (Figure 4.9) corresponding with decreasing suction with depth. Direct shear strengths were similar to corkscrew and pin vane tests at 250–300 mm; however, at shallow depths they were smaller.

4.4 Discussion

4.4.1 Quantifying root presence by resistance profile

In blade penetrometer and pull-up testing the best indication for the presence of individual (thicker) roots was a sudden drop in resistance. This distinct phenomenon contrasted with the gradual decrease in force, and a more noisy behaviour, associated with stick–slip between blade penetrometer and stones (case D). In field conditions, the force build-up prior to root failure may be masked by the presence of debris, variation in soil strength, overlapping of root force peaks or composite action between soil and roots as observed

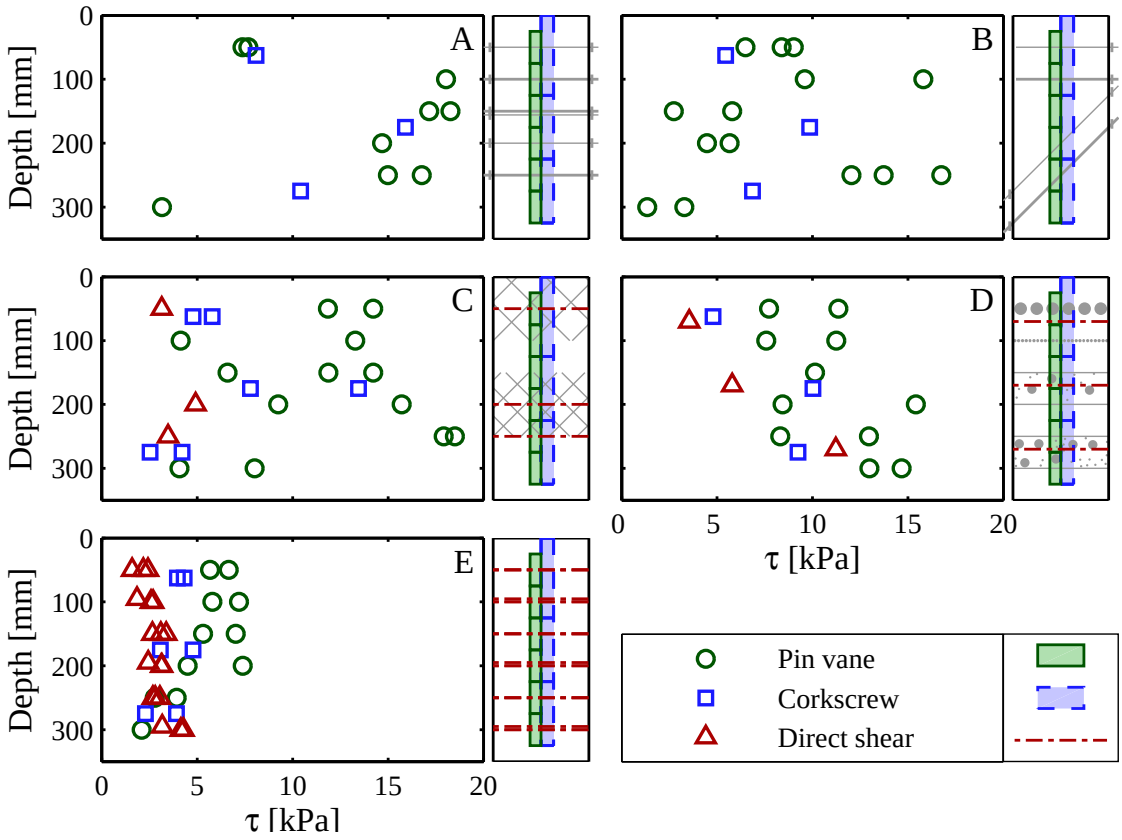

Figure 4.15: Laboratory peak shear strength values measured using pin vane, corkscrew and direct shear tests. Tests are sorted per core type. Per test the depth over which the shear strength is determined is indicated in the small core geometry plots. Shear strength values are averaged over test depth. Because the corkscrew device is larger than the pin vane, spatial resolution is lower and values are averaged over a larger depth range, smoothing out reinforcement effects more.

in fibrous experiments (case C). Linking the magnitude of sudden force decrease to root properties such as diameter and strength is similarly complicated. Experiments showed increasing resistances with increases in both root diameter and axial constraint. This made it difficult to differentiate between these effects using the test method. This behaviour can be investigated further assuming ABS analogues behave as spring-supported beams (e.g. using p-y curves, see Chapter 5). It is expected that the force–displacement response depends on the complicated interaction between root (diameter, tensile strength, bending strength), soil (resistance) and constraint characteristics (root branching, tortuosity), making careful selection of parameters and model calibration necessary.

Instead of studying the response of individual roots, the general increase in resistance compared to tests in fallow soil might be used as a proxy for soil strength. This would require similar correlations as routinely used in CPT testing where tip resistance and sleeve friction can be correlated to soil strength parameters. No attempts to derive such a correlation were made because of the small data set.

Both the blade penetrometer and pull-up device are heavily dependent on reliable post-test interpretation of the data. Because these interpretations are either dependent on availability of input parameters or reliable correlations, it is concluded that these are not the most suitable methods for quantifying the shear strength of the soil. However, they might prove to be a simple and useful tool for studying root occupancy as they provide information about depth of roots and an indication of their strength where incidences of breakage can be detected as a drop in force.

Although the blade penetrometer and pull-up methods employ the same mechanism and yield similar force–displacement traces, the increased installation force and relatively low extraction force in the fibrous soil for the pull-up device suggested that installation of this device might have lead to significant disturbance. Disturbance will result in a potential underestimation of root presence and reinforcement. However, it will be easier to use in the field compared to the blade penetrometer because it does not require as large a counterweight for installation and the soil itself can counteract extraction forces.

When these methods are to be adopted for measuring real roots *in situ*, similar force peaks are expected as measured in tests with ABS because root strength and stiffness are similar. However, traces are likely to be more difficult to interpret because of variations in root architecture (branching, orientation). Furthermore, the effect of various roots and/or debris might be superimposed, making it more difficult to quantify their individual contributions. Studies in more realistic soil and root conditions are required to further develop these methods, see Chapters 6 and 7.

4.4.2 Quantifying root resistance by shear strength measurements

The presence of discrete ABS rods increased peak force with peak strength occurring at greater displacements. Sudden drops in force or torque indicated root presence, similar to

the blade penetration and pull-up tests. Presence of fibrous roots (modelled with PP fibres) showed that the soil behaves in a more plastic manner with reinforcement over larger shear ranges, with peak strength occurring at larger displacements.

Direct shear peak strengths were significantly smaller than pin vane and corkscrew results at shallow depths. Several explanations can be provided. First, this may be due to loss of suction, introduced by the slight lifting of the outer PVC core and cutting the inner plastic liner prior to the direct shear test. In the time between cutting and testing (around 15 min.) and the subsequent shearing phase (50 min. duration), negative pore pressures might have dissipated. This can explain why direct shear strengths measured at the top of samples were roughly similar to those measured at larger depths in the core, and why the latter values were similar to those measured with pin vane and corkscrew measurements at the same depth. Water contents in the samples were close to the liquid limit (w = 28–34%, while w_L = 32%), so when assuming the soil behaved in an undrained fashion typical shear strengths around 1.7 kPa are expected (Wroth and Wood, 1978), similar to shear strengths measured. Second, in direct shear tests at 50 mm depth surface cracking was observed, suggesting a different failure mechanism and strength underestimation. Third, shear rates in direct shear tests were smaller than those in the other tests, providing another explanation for the observed differences when rate effects were present and tests could be considered to be undrained.

In fallow soil pin vane shear strengths yielded the highest shear strengths. This was more pronounced near the surface. In corkscrew tests a conical, rather than cylindrical, failure shape was observed in tests near the surface. This explained why near the surface measured corkscrew shear strengths were smaller than those measured using the pin vane, while at the same time at greater depths results were similar. In some of the pin vane tests a slight angular offset was observed, resulting in a swirl of the vane around the vertical axis. Larger resistance forces were measured due to the vane being pushed through the surrounding soil rather than only mobilising shear forces around the soil plug interface. Although the tests where this effect was obvious were discarded, it might still have influenced the remaining results to a smaller extent.

Boundary effects might have played a role due to the relatively small diameter of the soil cores used (150 mm diameter). In pin vane tests, a soil layer only 1.71 times vane diameter thick was surrounding the device and in corkscrew tests the cover was 1.38 times diameter. The vicinity of the boundaries might have resulted in stiffer soil behaviour prior to reaching peak strength. The peak strength itself was not thought to be influenced because the failure mechanisms for both methods were observed to be located closely around the devices (Figures 4.13a and 4.13c). Only in some of the corkscrew tests at 0–125 mm depth intersection between the failure surface (conical shape) and boundary was observed. In these tests peak strength was likely underestimated. Boundary effects could be reduced through the use of larger cores; however, due to the maximum printable

length of the ABS rods (200 mm) this was not possible.

The resistance–displacement profiles, in both corkscrew and pin vane tests, gave information important for landslide analysis. Only the peak strength is considered in most current analyses, for example, when using a Mohr-Coulomb model with Bishop circles or an infinite slope approach. However, local mobilised strength depends on local displacement, which will vary along the shear plane. The real average maximum strength over the full slide interface will therefore always be less than or equal to the average of local peak strengths. Furthermore, stress–strain behaviour affects landslide propagation. A larger area under the stress–strain curve results in more energy dissipation during sliding and, probably, less violent slides. Both corkscrew and pin vane methods provided stress–strain information instead of only peak strength measurements. The adopted shear rates in the presented work were typical of those observed within landslides and differ from those used within *in situ* shear box tests, and especially laboratory shear box tests, which are one or more orders of magnitude slower. It is advised that the potential effects of shear rate are investigated in future work to assess the sensitivity of the new measurement devices to such effects.

Intact soil cylinders observed in pin vane and corkscrew tests suggested that the assumed cylindrical failure mechanisms were valid. It is likely that there is a sheared zone of soil surrounding the central cylinder due to the soil being partially saturated and containing a significant sand fraction. Fibres, or roots, will increase the shear zone thickness as observed in shear vane testing of peats (Landva, 1980) and reinforced direct shear tests of sand (Jewell and Wroth, 1987; Shewbridge and Sitar, 1989). Shear strengths measured with the pin vane and corkscrew may therefore be overestimated, necessitating further study.

Both pin vane and corkscrew devices measure root-reinforcement primarily on vertical planes and therefore primarily measure the reinforcement introduced by more or less horizontally orientated roots. In landslides, however, the shear plane will be more horizontal; this issue can be partially addressed by inserting the measurement devices perpendicular to the root angle. Alternatively, assumptions or measurements on the distributions of root orientations can be used to verify or correct the root-reinforcement from mathematical root architecture models (e.g. Danjon et al., 2008).

Here, tests were performed in idealised conditions. Because the root analogues used had similar material characteristics to real roots, similar stress–strain patterns are expected in the field. The simplicity of the equipment and the beneficial results regrading soil stress–strain behaviour are key advantages of the pin vane and corkscrew methods. However, one downside is the need for pre-drilling of soil to prevent accumulation of root material and potential compaction prior to testing. More work is required to correlate *in situ* measurement results with the strength and quantity of roots. The inclusion of root-reinforced shear tests will better assess how the proposed new methods relate to existing

approaches and models.

4.5 Conclusions

- Four methods (blade penetrometer, pull-up, pin vane and corkscrew) were developed and tested under laboratory conditions with repacked field soil at field capacity. Various inclusions were inserted to model behaviour resulting from discrete roots, fine root mats and stones within soil. All methods yielded distinct behaviour when roots were present with both fibrous and thicker roots distinct from stones. Although idealised conditions and only one soil type were considered, the results provided insight into how the devices might perform in the field.
- The blade penetrometer and pull-up method are best used for root localisation purposes. Relating measurements to soil shear strength, or root properties, requires reliable empirical correlations or the use of complicated modelling. Although the latter method can be versatile and powerful, it requires many soil and root parameters, which is problematic without extensive field investigation, making it potentially less suitable for making quick and easy estimates for slope stability analysis. The blade penetrometer performed much better than the pull-up device, and therefore the pull-up device will not be considered in the remainder of this thesis.
- Both the corkscrew and pin vane can be employed to directly measure rooted shear strengths. They can be installed without damaging the roots, yield valuable stress–strain information, they are quick and easy to use, and can be performed with a mobile and light experimental setup, making them suitable for use in remote areas. Detailed follow-up study, particularly in the field, is required to validate the failure mechanisms and to correlate the measured reinforcement with root traits. Because both appear to be suitable, both will be considered in subsequent field testing.

5

Root–soil interaction modelling

The contents of Sections 5.2–5.7 have been written up as part of a paper and submitted for revision, see Meijer et al. (2016a).

5.1 Introduction

The laboratory tests using model ABS roots described in Chapter 4 showed a clear response of the root under penetrometer or pull-out loading: from the moment a root was hit, the resistance rapidly increased until the point the root suddenly broke. Such breakages were visible as distinct and sudden drops in the measured force. Similar drop were observed in corkscrew and pin vane tests.

The characteristics of these force peaks, for example the magnitude of the drop or the displacement range over which the resistance increased, can be used to derive root characteristics such as root diameter or strength. Currently, there is no established method to do this. Therefore, in this chapter several interpretive models are developed to predict characteristics of these peaks based on root and soil properties. Separate models will be derived for roots loaded by a penetrometer or roots loaded by shearing soil. In subsequent chapters these models will be compared with a more comprehensive set of blade penetrometer experiments in the laboratory (Chapter 6) and with field experiments (Chapter 7). In Chapter 8 some of these models will be used to study the force–displacement behaviour of roots loaded by the corkscrew device.

The following interpretive models were developed:

1. *Numerical Abaqus model:* finite element model, assuming the root as a homogeneous circular beam, supported by non-linear springs to model soil resistance.
2. *Analytical bending model:* analytical model assuming the root broke due to bending effects, ignoring any root tension or root shear effects.

3. *Analytical cable model:* analytical model assuming the root behaved like a cable element, i.e. purely loaded in tension, ignoring any root bending and root shearing.

The laboratory blade penetrometer tests in soil reinforced with fibrous root analogues showed that increasing amounts of fibres resulted in larger reinforcements although no distinct peaks were observed. Therefore an additional model was developed in an attempt to model this ductile behaviour:

4. *Root mat model:* model to study the behaviour of a bundle of roots, e.g. a densely fine rooted soil mat, by smearing out the behaviour of each individual root over the depth interval of the rooted zone.

These models are discussed in the next sections. In addition, analyses performed to study the influence of certain model assumptions and to compare various models are discussed.

5.2 Soil resistance to root displacement

To accurately model the load and displacement behaviour of a root it was important to model root–soil interaction. One of the important interaction aspects is the soil resistance acting against lateral root displacement. In the models described here, quantification of the soil resistance acting against laterally displacing roots was estimated using p-y theory (e.g. Randolph and Gourvenec, 2011). This theory was initially derived to estimate the lateral soil resistance acting on horizontally loaded foundation piles.

The soil resistance was estimated using methods derived by Reese and Van Impe (2011) and the American Petroleum Institute (2000). To generate p-y curves for dry sand, as used in subsequent penetrometer experiments described in Chapter 6, both methods required the soil angle of internal friction ϕ', soil unit weight γ', pile diameter d and depth z. In addition, Reese and Van Impe's method required an additional input value for the spring's initial stiffness based on soil density. In this work, sands were classified as 'loose' when $\phi' < 30°$, as medium dense when $30° \leq \phi' < 36°$ and as dense when $\phi' \geq 36°$, based on the classification used in the API method (American Petroleum Institute, 2000).

Both methods apply correction factors when curves are determined at shallow depth to account for different soil failure mechanisms such as wedge failure. Because in blade penetrometer tests the root was pushed downwards, vicinity to the surface will not have such a strong influence. Therefore for both methods, when evaluating these correction factors, it was assumed that $z/d = \infty$. Because of this simplification p and y in both methods scale linearly with diameter d and the ultimate soil resistance p_u (after Reese and Van Impe), expressed as a force per unit area, can be expressed as:

$$p_u = \overline{A}_s \cdot \left(K_a \cdot \gamma' \cdot z \cdot \left(\tan^8 \beta - 1 \right) + K_0 \cdot \gamma' \cdot z \cdot \tan \phi' \cdot \tan^4 \beta \right) \tag{5.1}$$

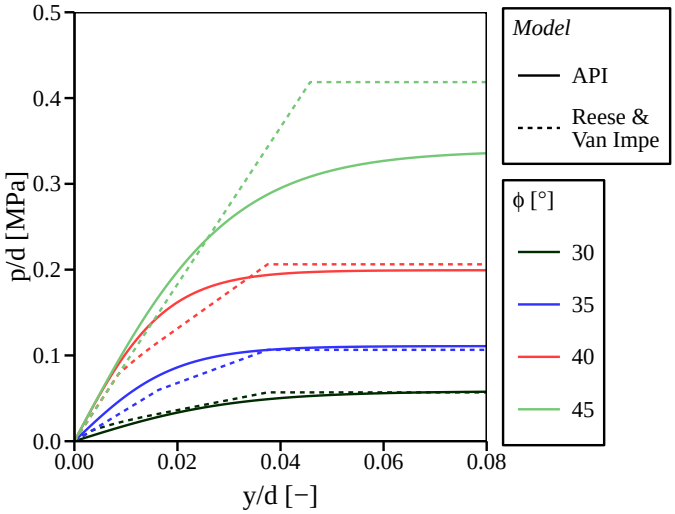

Figure 5.1: Example p-y curves for piles at 150 mm depth in dry sand generated using methods derived by Reese and Van Impe (2011) and the American Petroleum Institute (2000) (API). p is the lateral soil resistance per unit pile length [Nmm^{-1}] acting on a circular pile with with diameter d [mm], while y indicates the lateral pile displacement [mm].

where $\beta = 45 + \phi'/2$ [°], K_a and K_0 the coefficients of lateral earth pressure in the active case and at rest [-], and $\overline{A}_s$ a model constant equal to 0.88 [-]. Example curves for both methods are presented in Figure 5.1. Both models yielded similar curves when $\phi' \lesssim 40°$ but started to diverge at larger values. This was mainly due to some charts in the API method only being usable when $\phi' \leq 40°$ In this analysis, when $\phi' > 40°$ values corresponding with $\phi = 40°$ were used, resulting in underestimation of soil resistance. Because of this limitation in the API method, Reese and Van Impe's method was adopted during the remainder of this study.

5.3 Numerical modelling using Abaqus

Root behaviour under blade penetrometer loading was numerically modelled using Abaqus/ Standard) version 6.13-1 (Simulia) finite element software. Roots were modelled as one-dimensional beams with non-linear springs attached to account for soil resistance and extra resistance introduced by side branching, see Figure 5.2.

The root material was numerically modelled as linear elastic–perfectly plastic using the maximum root strength as yield stress. The root itself was modelled using 1-dimensional circular 3-node quadrilateral Timoshenko beam elements to allow for shear strain (Abaqus reference: 'B22'). Non-linear effects of large displacement were taken into account (Abaqus: 'NLGEOM = on').

A soil resistance spring, using p-y curves, was applied to each node. Because soil p-y curves yielded a resistance per unit length, the soil resistance is multiplied by the length of the segment between two nodes projected on to the plane normal to the direction of penetrometer loading (w), see Figure 5.2.

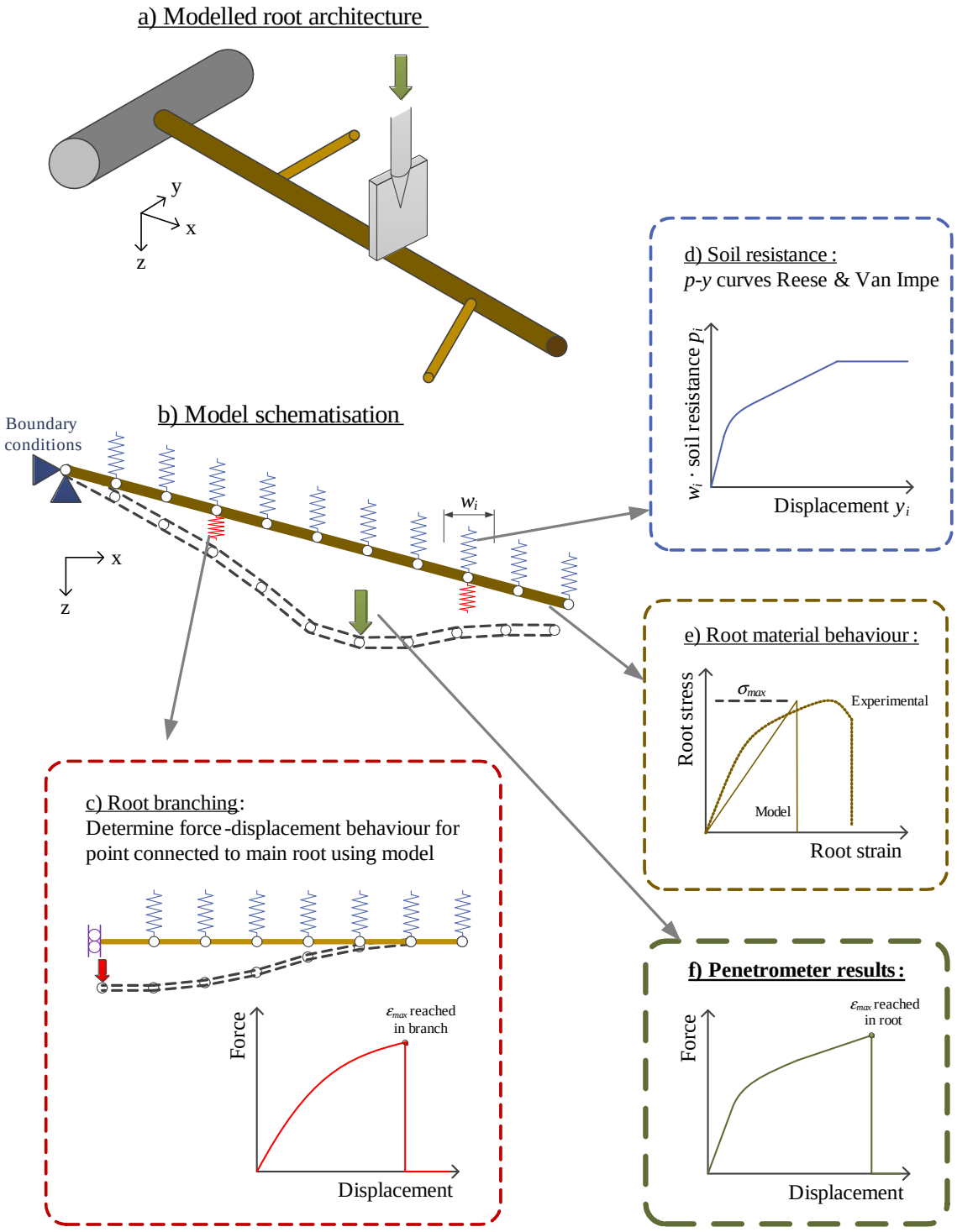

Figure 5.2: Schematic representation of the numerical modelling procedure. A root with linear-elastic material properties (e) is discretised in small elements (b). To every node a soil resistance spring is attached (d). To some nodes additional springs are attached to model root branching (c). Model results include the penetrometer force and corresponding displacements (f).

The penetrometer behaviour was modelled by varying the displacement of the closest node. By step-wise increasing this displacement and analysing residual forces on this node, the full force–displacement behaviour of the penetrometer was simulated. The adopted displacement step size was 0.5 mm. The root was assumed to be broken once the Von Mises stress exceeded the yield stress anywhere in the root.

The friction on the interface between root and soil (τ_i) is difficult to incorporate in a spring-supported beam model. It depends on many factors, e.g. root type, root tortuosity, root hairs or the presence of mucilage in the rhizosphere. Therefore, two extreme cases were modelled. In the first (Case A), the non-root ends of the soil resistance springs were connected to nodes directly below the root, so the spring force was active along the axis of the nodal displacement. Therefore these springs also provided resistance to root axial movement. In this case:

$$\tau_i \approx \frac{p}{\pi} \cdot \cos\beta \tag{5.2}$$

where p is the soil resistance [MPa] and β the angle between the root axis and the nodal displacement direction. In the second case (Case B), the soil resistance springs were modelled as very long and parallel to the direction of loading so that root deformation does not have any significant influence on the orientation of the spring. Therefore it had no component in the root axial direction, so:

$$\tau_i \approx 0 \tag{5.3}$$

The anchoring of a root to a larger parent root or tree stump was modelled by fixing all degrees of freedom at end of the root.

Root branches were not directly modelled, but represented by additional non-linear springs attached to the modelled ‘main’ root, see Figure 5.2. For each branch a force–displacement curve was generated for the node at the parent root side of the branch using the same numerical model as used for the ‘main’ root. The properties of this spring were then used in the model for the ‘main’ root. The branch was assumed to be broken once the peak strength was reached, after which the branch resistance was set to zero.

5.4 Simplification of soil *p-y* curves

To simplify the modelling of the soil resistance, it was investigated whether it could be assumed that the full soil resistance was mobilised after infinitely small lateral root displacements instead of gradually, i.e.:

$$\begin{cases} p = 0 & \text{when } |u| = 0 \\ p = p_u & \text{when } |u| > 0 \end{cases} \tag{5.4}$$

p-y theory (Reese and Van Impe, 2011) suggested that the soil reaches its maximum resistance after a finite displacement of $3/80 \cdot d_r$. The effect of this simplification was studied by comparing numerical model simulations in Abaqus using both the full p-y curves (Figure 5.1) and the simplified approach using perfectly plastic springs (Equation 5.4). Soil and root parameters used in this analysis were based on the experimental blade penetrometer laboratory test conditions adopted, see Chapter 6. Results were compared for 2 and 4 mm diameter ABS rods in dry sand with relative densities ranging between 10 and 90% in increments of 10%. The root depth was varied between 50, 100, 200 and 500 mm. This combination of relative density and depth yielded a large range of soil resistances: p_u ranged between 0.0211 and 2.16 MPa. The root length was set to 250 mm to both sides of a point loading (e.g. a blade penetrometer) and all degrees of freedom were restrained at both root ends. Because of symmetry, only one half of the root was modelled.

The difference between results obtained with the simplified p_u approach or full modelling of the p-y curve was considered to be related to the ratio of lateral displacement at which the full curve reaches its maximum resistance ($y_u = 3/80 \cdot d_r$) and the penetrometer displacement at root failure (u_u, using the analytical bending model). Using Table 5.1, this ratio was proportional to:

$$\frac{p_u \cdot E}{\sigma^2} = 2.615 \cdot \frac{y_u}{u_u} \tag{5.5}$$

The smaller this ratio, the smaller the expected inaccuracy caused by simplifying the p-y behaviour, as the lateral root displacement will be much larger than the lateral displacement required to mobilise the full soil resistance according to p-y theory by Reese and Van Impe (2011).

The results (Figure 5.3) showed that the simplified approach almost yielded the same results as obtained by modelling the full p-y curve, especially for the peak force. The accuracy decreased with increasing root bending and soil stiffness and with decreasing root strengths. For the worst case in the laboratory testing programme (ABS in dry sand, $d_r = 4$ mm, $p_u \approx 0.5$ MPa, see Chapter 6) the predicted peak force was only 0.8% higher and the displacement 3.3% lower by using the simplified approach compared to modelling the full p-y curve. This analysis showed that, because roots displace large distances compared to the displacement required to reach the full soil resistance, the simplified soil resistance approach was valid for the experimental conditions tested in the laboratory.

For realistic conditions in the field ($0.5 \leq p_u \leq 2.0$ MPa, Sitka spruce roots ($\sigma \approx 6$ MPa and $E_{90} \approx 66$ MPa) or pedunculate oak roots ($\sigma \approx 12$ MPa and $E_{90} \approx 165$ MPa), see Chapter 7, the value $p_u \cdot E \cdot \sigma^{-2}$ ranges from approximately 0.5 to 3.7, introducing potential errors of 2–15%in the predicted peak force and 12% to potentially exceeding 100% in the predicted displacement. This means that for field conditions, the p-y simplification could have a significant effect on the predicted displacement, depending on the exact conditions

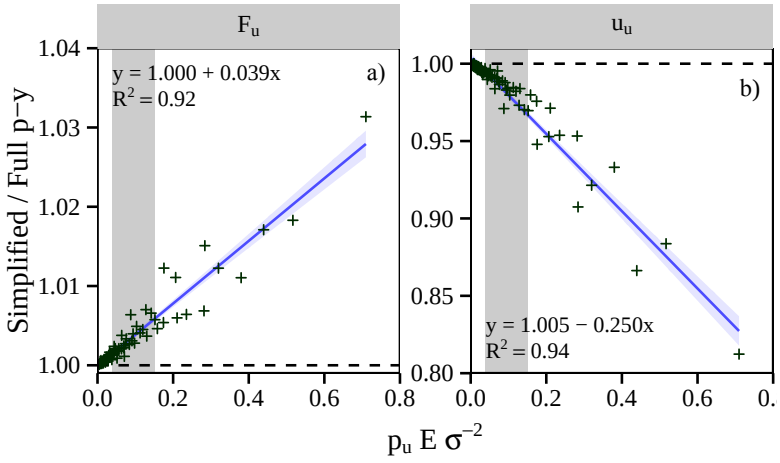

Figure 5.3: Differences between numerical simulations using the full p-y curve and the simplified approach for a) root peak reinforcement (F_u) and b) lateral root displacement at peak (u_u). The grey band indicates the range of experimental conditions (Chapter 6) while the blue line indicated the best linear fit and the 95% confidence interval of this fit. p_u, σ and E indicate the soil resistance, root strength and root stiffness respectively.

present.

5.5 Analytical bending model

Thicker roots are thought to reinforce the soil through mobilising their bending strength (e.g. Wu, 2007). To model this effect, the behaviour of roots crossing a shear plane or loaded by a point load (e.g. blade penetrometer) was approximated using analytical beam bending theory (e.g. Hibbeler, 2014). Simplifying assumptions made in the modelling, the validity of which will be explored later through comparisons with the numerical modelling using Abaqus, were:

- The beam/root fails in pure bending. Axial deformations, axial and shear stresses are neglected.
- Non-linear geometric effects are neglected.
- Root behaviour is linear elastic up to failure.
- The full soil resistance is mobilised after infinitely small lateral root displacements.
- The root is straight and loaded perpendicular to the root axis.

Under these conditions, the beam displacement can be described using a simplified form of the Euler–Bernoulli differential equation for beam bending:

$$E_b \cdot I \cdot \frac{\mathrm{d}^4 u(x)}{\mathrm{d}x^4} = -d_r \cdot p_u \tag{5.6}$$

where E_b is the beam bending stiffness [MPa], u the lateral deformation [mm], x the distance from the point of loading along the beam [mm], p_u the ultimate soil resistance

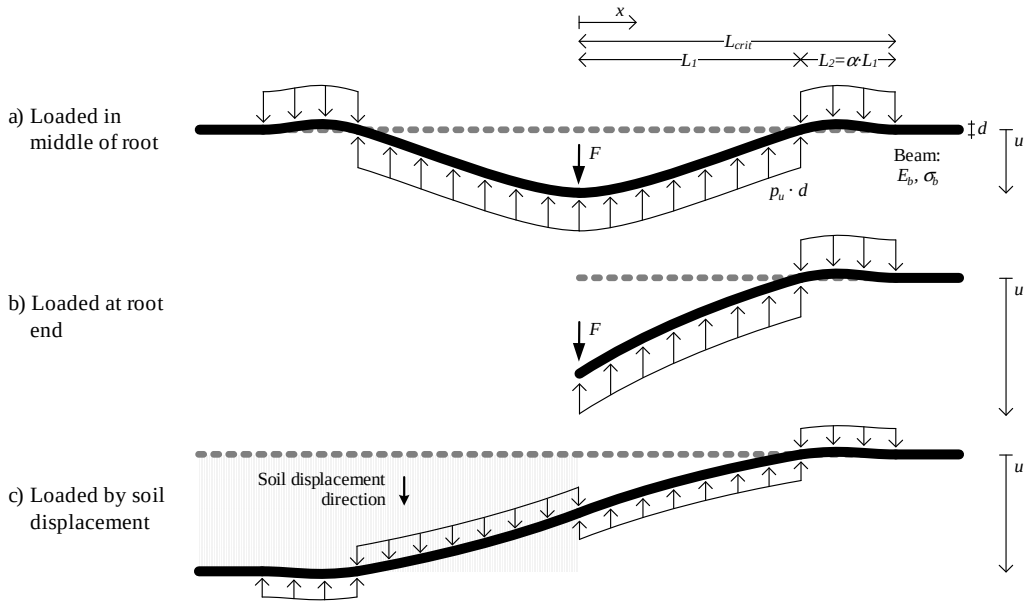

Figure 5.4: Assumptions and parameters used to solve the analytical beam bending differential equation for different loading conditions. a) infinitely long root loaded by a point load, b) root loaded by a point load at the root end, and c) root loaded by shear displacement of the surrounding soil. The dotted line indicates the original position of the unloaded root. Thin arrows indicate the direction and location of lateral soil resistance (p_u) against root displacement (u).

[Nmm^{-2}] and I the second moment of area [mm^4], for a circular beam with diameter d_r equal to:

$$I = \frac{1}{64} \cdot \pi \cdot d_r^4 \tag{5.7}$$

Where the beam is deformed ($|u| > 0$), a constant soil resistance p_u is assumed to be present in the opposite direction to the deformation. Initial numerical simulations indicated the root displacement follows a wave-like pattern, the amplitude of which decreases with increasing distance from the point load. The displaced root shape is therefore simplified as schematised in Figure 5.4.

The following boundary conditions were used in case the beam was laterally loaded by a point load in the middle section of the root (Figure 5.4a):

$$\begin{cases} \frac{\mathrm{d}u(0)}{\mathrm{d}x} = 0 & \text{no rotation at point of loading} \\ u(L_1) = 0 & \text{no displacement at } x = L_1 \\ \frac{\mathrm{d}u(L_{crit})}{\mathrm{d}x} = 0 & \text{no rotation at } x = L_{crit} \\ u(L_{crit}) = 0 & \text{no displacement at } x = L_{crit} \\ \frac{\mathrm{d}^3u(L_{crit})}{\mathrm{d}x^3} = 0 & \text{no shear force at } x = L_{crit} \\ \frac{1}{2} \cdot F = d_r \cdot p_u \cdot (L_1 - L_2) & \text{vertical load equal to total soil resistance} \end{cases} \tag{5.8}$$

When the root was loaded at a root end, the following boundary conditions were assumed (Figure 5.4b):

$$\begin{cases} \frac{d^2u(0)}{dx^2} = 0 & \text{no bending moments at } x = 0 \\ u(L_1) = 0 & \text{no displacement at } x = L_1 \\ \frac{du(L_{crit})}{dx} = 0 & \text{no rotation at } x = L_{crit} \\ u(L_{crit}) = 0 & \text{no displacement at } x = L_{crit} \\ \frac{d^3u(L_{crit})}{dx^3} = 0 & \text{no shear force at } x = L_{crit} \\ F = d_r \cdot p_u \cdot (L_1 - L_2) & \text{vertical load equal to total soil resistance} \end{cases} \tag{5.9}$$

The same boundary conditions as in Equation 5.9 applied for roots passing through shear planes within soil. This can be seen as two root end solutions combined (Figure 5.4c).

Solving Equation 5.6 once for both $0 \leq x \leq L_1$ and $L_1 \leq x \leq L_{crit}$ with these boundary conditions yielded the beam displacement as a function of location on the beam ($u(x)$). The beam was assumed to fail when the maximum bending strength σ_b was exceeded. The maximum bending moment a circular beam can sustain (M_u) is equal to:

$$M_u = \frac{\sigma_b \cdot I}{\frac{1}{2} \cdot d_r} \tag{5.10}$$

The bending moment can be expressed in terms of beam displacement:

$$M(x) = E_b \cdot I \cdot \frac{d^2u(x)}{dx^2} \tag{5.11}$$

Using Equations 5.10 and 5.11, both the location where bending stresses will be highest and the magnitude could be found. Thus the beam deformations associated with failure in bending could be obtained.

Results for the critical length (L_{crit}), maximum penetrometer force (F_u) and displacement (u_u) associated with beam failure in bending, the location of bending failure (x_u, x-coordinate) and the penetrometer or soil displacement associated with penetrometer or shear resistance $u(F)$ are summarised in Table 5.1.

The length of root that displaces as an effect of the applied load (L_{crit}) increases with diameter and bending strength, and decreases with increased soil resistance. The force required for bending failure (F_u) goes up with increasing bending strength, increasing soil resistance and especially with increasing diameter. The corresponding displacement (u_u) increases when bending strength and diameter are increased, and decreases when bending stiffness and soil resistance are increased.

Table 5.1: Analytical beam bending solutions. α and L_{crit} are defined in Figure 5.4. F_u and u_u are the maximum external force and corresponding displacement (of the point load or shearing soil) associated with beam failure in bending. The maximum root stress is reached first at $x = x_u$. $u(F)$ indicates the force–displacement behaviour of the point load or shearing soil.

	Formula			Multiplication factor ξ
	Penetrometer		Shear plane	
	Middle of root	Root end		
α	0.2695	0.4248	0.4248	
L_{crit}	0.8311 ξ	1.0976 ξ	1.0976 ξ	$d_r \cdot \sigma_b^{0.5} \cdot p_u^{-0.5}$
F_u	1.0231 ξ	0.4431 ξ	0.8862 ξ	$d_r^2 \cdot \sigma_b^{0.5} \cdot p_u^{0.5}$
u_u	0.09808 ξ	0.5247 ξ	1.0493 ξ	$d_r \cdot \sigma_b^{2} \cdot E_b^{-1} \cdot p_u^{-1}$
x_u	0	0.4431 ξ	0.4431 ξ	$d_r \cdot \sigma_b^{0.5} \cdot p_u^{-0.5}$
$u(F)$	0.08954 ξ	13.61 ξ	1.7011 ξ	$F^4 \cdot d_r^{-7} \cdot E_b^{-1} \cdot p_u^{-3}$

5.6 Comparison between analytical bending and numerical Abaqus model

To study when the analytical bending model yielded accurate results, model predictions were compared to two runs of numerical simulations using the numerical model described in Section 5.3. First it was investigated for which combinations of soil and root parameters the analytical bending model yielded similar results compared to the more sophisticated numerical modelling. In a second set of simulations, the effect of loading in close proximity to a root end was studied.

5.6.1 When are roots loaded in bending?

To study when the analytical bending model yielded similar results to numerical modelling multiple simulations were performed. Parameters that were varied were the distance to the root end on either side ($L \in \{0.5, 1, 2, 4, 8\} \cdot L_{crit}$), root strength ($\sigma \in \{2, 5, 10, 20, 50, 100\}$ MPa), root Young's modulus ($E \in \{100, 200, 500, 1000, 2000\}$ MPa) and ultimate soil resistance ($p_u \in \{0.1, 0.2, 0.5, 1.0, 2.0\}$ MPa). Two different models were run. In the first, axial constraints were high (axial deformation prevented at root tips + high root–soil interface friction case (Case A friction, see Section 5.3)), while in the second axial constraints were low (axial deformation possible at root ends + no root–soil interface friction (Case B friction)). In the latter case, a smaller number of parameter combinations was adopted to decrease the numerical workload. Lateral soil resistance was modelled using the simplified approach (Equation 5.4).

Comparison between the numerical simulations showed that the analytical bending solution yielded similar results when (Figure 5.5):

$$\frac{u_u}{L_{crit}} \leq 0.05 \tag{5.12}$$

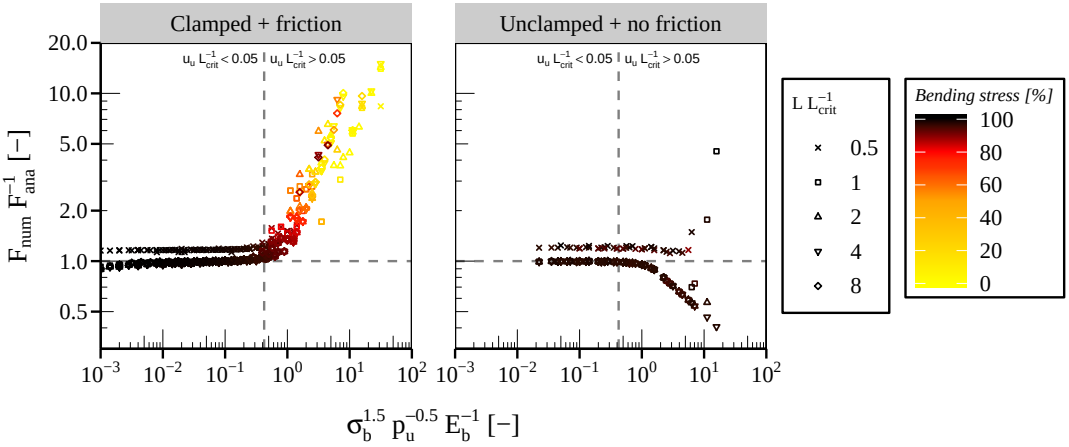

Figure 5.5: Comparison between predicted numerical (F_{num}) and analytical bending model (F_{ana}) for penetrometer force required to break a root, using various root parameters, soil resistances and soil–root interface friction assumptions.

When Equation 5.12 is expressed in terms of soil and root parameters using Table 5.1:

$$\frac{\sigma_b^{1.5}}{p_u^{0.5} \cdot E_b} \leq 0.424 \tag{5.13}$$

The dimensionless parameter group $\sigma_b^{1.5} \cdot p_u^{-0.5} \cdot E_b^{-1}$ can therefore be seen as a measure of the ratio between maximum root lateral displacement and length of laterally displacing root. It is therefore also a measure for the validity of the analytical bending model assumption that non-linear geometric effects can be ignored (lower values of the dimensionless parameter group correspond with smaller non-linear effects).

In the case where the root was axially constrained, when $\sigma_b^{1.5} \cdot p_u^{-0.5} \cdot E_b^{-1} > 0.424$ predicted root peak resistances were higher and a smaller proportion of the root stress was caused by bending effects, indicating a build-up of tensile forces. In the unconstrained case, the resistance was less sensitive to changes in the dimensionless parameter group $\sigma_b^{1.5} \cdot p_u^{-0.5} \cdot E_b^{-1}$. In both cases, the ratio between numerical and analytical bending model forces was relatively independent from the length of the modelled root, provided that $L \geq L_{crit}$.

For realistic values of soil conditions ($1 \leq p_u \leq 5$ MPa) and root conditions (weak roots: $\sigma_b = 10$ MPa and $E_b = 100$ MPa, or strong roots: $\sigma_b = 100$ MPa and $E_b = 1000$ MPa), the value $\sigma_b^{1.5} \cdot p_u^{-0.5} \cdot E_b^{-1}$ ranges from approximately 0.14 to 1.00. These values are close to the identified threshold value of 0.424, indicating the analytical bending solution is usable in some field conditions, but might underestimate the real force at higher values of $\sigma_b^{1.5} \cdot p_u^{-0.5} \cdot E_b^{-1}$ (Figure 5.5a).

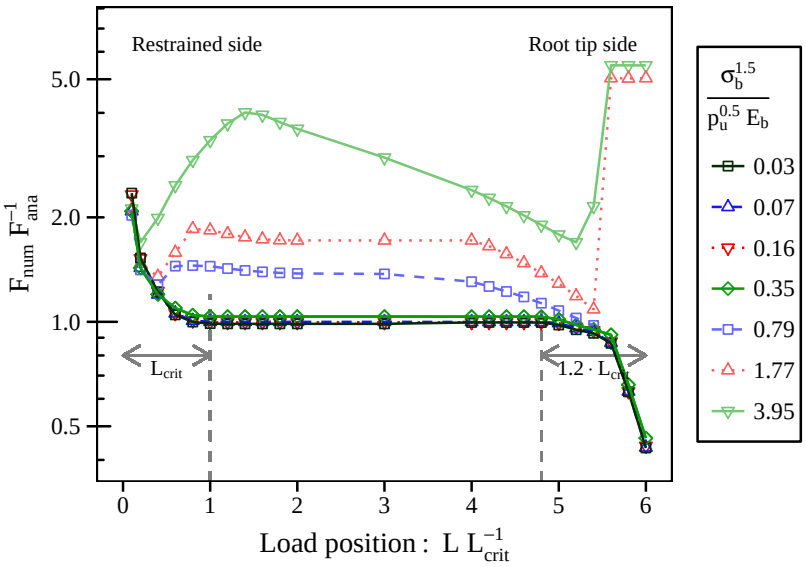

Figure 5.6: Comparison between predicted numerical (F_{num}) and analytical bending model (F_{ana}) for penetrometer force required to break a root, using various root and soil parameters and distances to a root boundary.

5.6.2 Loading close to a root end

The analytical bending model assumes infinitely long roots. However, in reality roots might be loaded close to a root tip or close to the trunk or parent root. The behaviour of roots loaded close to a boundary was investigated using the numerical model. A root with length $6 \cdot L_{crit}$ was modelled. The left end was fully restrained (parent root) and the right end unsupported (root end). The distance between the point of loading and either boundary was varied between 0 and $2 \cdot L_{crit}$ in steps of $0.2 \cdot L_{crit}$ for various root and soil properties ($d_r \in \{2, 10\}$ mm; $\sigma \in \{10, 50\}$ MPa; $E \in \{200, 1000\}$ MPa; $p_u \in \{0.2, 1\}$ MPa).

When Equation 5.13 was met, the simplified bending method was accurate as long as the point load was applied within $1.2 \cdot L_{crit}$ of either end of the root (Figure 5.6). When an error of approximately 10% is deemed acceptable, the analytical solution was valid when the root is loaded at least approximately $0.5 \cdot L_{crit}$ from either end.

5.7 Analytical cable model

An alternative mechanism by which the root may add additional resistance to the soil is through tensile action. This is be more likely to occur than bending for roots with low resistance to bending, under which conditions relative lateral soil–root deformations will be large. Existing tension-based models which consider roots to act as rods (i.e. neglecting lateral displacements) may be insufficient to capture such behaviour and so an analytical model was developed assuming roots behave as buried laterally flexible cable elements

loaded in tension. The effects of root axial strain are incorporated in this model.

5.7.1 Model derivation

This modelling approach assumed that:

- The cable fails in pure tension;
- The cable can only support axial tension forces. Compression, bending and shear forces and stiffnesses were neglected;
- The cable behaviour is linear elastic with axial tensile stiffness E_t;
- The full soil resistance is mobilised after infinitely small lateral root displacements (as with the bending model);
- The cable is straight and loaded perpendicular to the cable axis.

The force a horizontal cable vertically loaded by a point load can sustain in tension can be estimated using force vector decomposition once the maximum angle between the deformed root under the penetrometer tip and the horizontal axis (β, see Figure 5.7) is known:

$$F_u = 2 \cdot F_t \cdot \sin(\beta) \tag{5.14}$$

where the factor 2 originates from tensile loading to both sides of the penetrometer and where F_t is the root tensile force at failure, equal to:

$$F_t = \frac{\pi}{4} \cdot d_r^2 \cdot \sigma_t \tag{5.15}$$

where σ_t is the root tensile strength. However, β depends on the root–soil interaction and was therefore not known *a priori*.

A solution for β was found using analytical modelling. Only half of the root was modelled because of symmetry. At the location of point loading, horizontal deformations were assumed to be restrained and at the other end of the root both vertical and horizontal displacement were fixed, see Figure 5.7. The half-cable was split into two zones. In zone I, closest to the point of load application, vertical soil resistance is mobilised. Since this is the only force counteracting the external loading, the length of this zone can be expressed as:

$$L_I = \frac{1}{2} \cdot \frac{F_u}{p_u \cdot d_r} \tag{5.16}$$

Over the length of zone II, it was assumed that the root only strained in the axial direction and no lateral soil resistance was mobilised. The length of this zone is equal to:

$$L_{II} = L - L_I \tag{5.17}$$

The horizontal component of the cable axial force is constant over the whole cable length since all external forces act vertically. Therefore, the maximum axial force occurred where

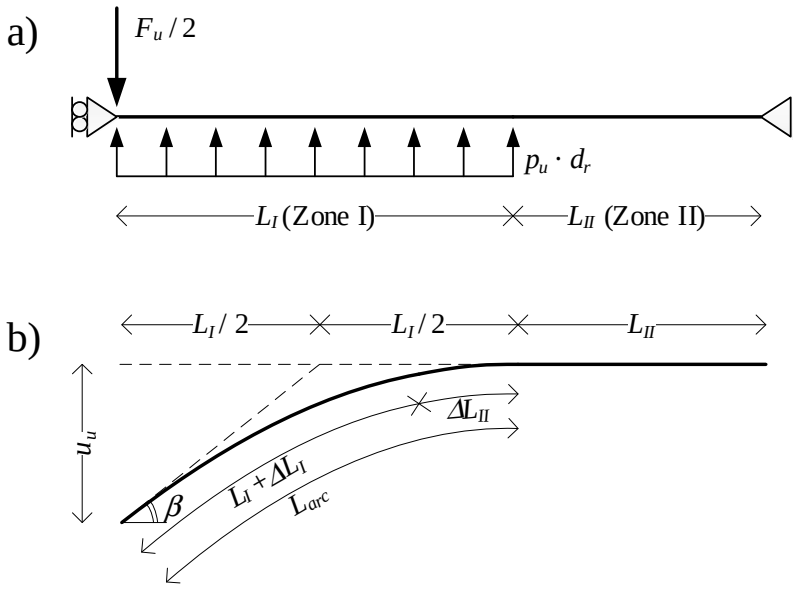

Figure 5.7: Schematic analytical cable model. a) schematic loading and boundary conditions, b) schematic cable deformation. The external point load (F_u) is counteracted by lateral soil resistance (p_u) over a length L_I. As a result, the cable displaces both laterally and axially in zone I, but only axially in zone II.

the root deformation angle was largest, i.e. directly under the point of loading. Equation 5.14 described this maximum angle.

The maximum axial stress in zone II can then be expressed as:

$$\sigma_{II} = \sigma_t \cdot \cos\beta \tag{5.18}$$

The increase in length due to this axial stress is:

$$\Delta L_{II} = \frac{\sigma_{II}}{E_t} \cdot L_{II} \tag{5.19}$$

The deformations in zone I were more difficult to model due to non-linear effects, and were estimated as follows. Since the root is modelled as a cable and the soil resistance is constant over length L_I, the cable will deform in a parabolic shape. The length of this parabolic section can be estimated using the analytical solution for parabola arc length (Weisstein, 2016):

$$L_{arc} = \sqrt{\frac{L_I^2}{4} + u_u^2} + \frac{L_I^2}{4 \cdot u_u} \cdot \sinh^{-1}\left(\frac{2 \cdot u_u}{L_I}\right) \tag{5.20}$$

where u_u is the vertical deformation under the point load. This parameter could be estimated in turn using another property of a parabola, stating that the maximum gradient is equal to twice the average gradient:

$$u_u = \frac{L_I}{2} \cdot \tan\beta \tag{5.21}$$

The average stress in zone I was estimated by averaging the stress at the beginning and end points of the parabola:

$$\sigma_I = \frac{1}{2} \cdot (\sigma_t + \sigma_{II}) \tag{5.22}$$

and the total increase in length in this zone is then:

$$\Delta L_I = \frac{\sigma_I}{E_t} \cdot L_I \tag{5.23}$$

Now two different derivations to predict the length of the deformed root have been obtained: one through root axial deformation under root stress and one through the arc length of the deforming root. Both predictions should give similar results, so:

$$L_{arc} \approx L_I + \Delta L_I + \Delta L_{II} \tag{5.24}$$

All parameters in Equation 5.24 can be expressed in terms of root (d_r, σ_t, E_t and L) and soil characteristics (p_u), along with the external force required to reach root tensile failure (F_u).

There was no closed-form solution for Equation 5.24 rewritten in terms of F_u. Therefore, the equation was numerically solved for every combination of a large number of parameters: $d_r \in \{0.5, 1, 2, 4, 8\}$ [mm], $\sigma_t \in \{5, 10, 20, 50, 100\}$ [MPa], $E_t \in \{50, 100, 200, 500, 1000\}$ [MPa], $L \in \{10, 20, 50, 100, 200, 500, 1000\}$ [mm] and $p_u \in \{0.1, 0.2, 0.5, 1, 2, 5\}$ [MPa], totalling 4375 combinations. Root parameters were chosen to cover a large range of reported root properties (e.g. Mao et al., 2012) and soil properties to cover a large range of possible soil resistances.

The results (Figure 5.8) showed that the angle between the cable and the horizontal increases with increasing root length and soil resistance and with decreasing cable diameter and tensile stiffness. The results for β were fitted in the following form:

$$\tan\left(\frac{\beta}{2}\right) = \sqrt{\eta} \tag{5.25}$$

where:

$$\eta = \sqrt{\frac{\zeta - 2 \cdot \sqrt{\zeta + 1} + 2}{\zeta}} \tag{5.26}$$

$$\zeta = \frac{L \cdot p_u}{d_r \cdot E_t} \tag{5.27}$$

This shape ensures that the solution yields realistic values at extreme values of ζ. β approaches 0 at low values of this parameter (no root deformation) and $\pi/2$ at high values (root oriented almost vertically under the penetrometer tip). Using Equations 5.15, 5.16,

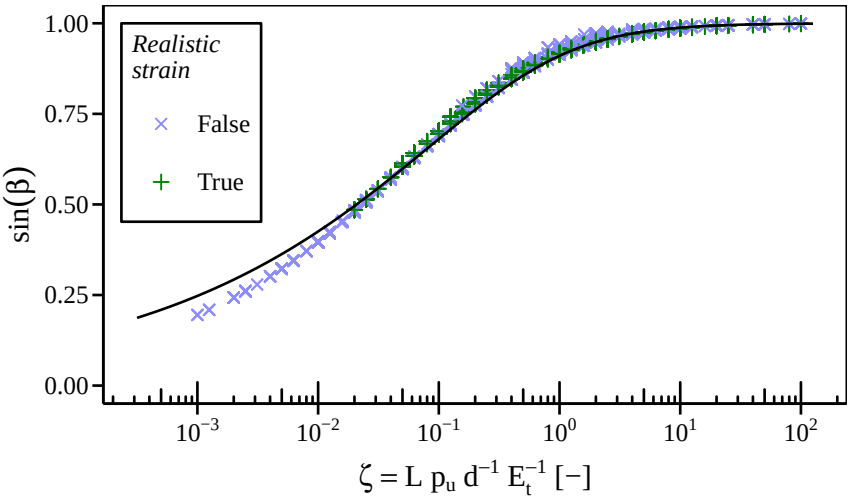

Figure 5.8: Analytical cable model solutions for the maximum angle between the deformed and undeformed root. Realistic strain values are defined as $0.05 \leq \sigma_t \cdot E_t^{-1} \leq 0.20$ (Coutts, 1983; Operstein and Frydman, 2000; Schmidt et al., 2001).

5.21 and 5.25, the penetrometer deformation at failure simplified to:

$$u_u = \frac{\pi}{4} \cdot d_r \cdot \frac{\sigma_t}{p_u} \cdot \sqrt{\zeta} \tag{5.28}$$

and the penetrometer force to:

$$F_u = \frac{\pi}{4} \cdot d_r^2 \cdot \sigma_t \cdot \frac{4 \cdot \sqrt{\eta}}{1 + \eta} \tag{5.29}$$

In reality, there will be friction between the root and the surrounding soil (τ_i), limiting axial strain and therefore influencing the cable deformation. Since in this model the fixed model boundary at $x = L$ has a similar restraining effect, τ_i was expressed in terms of L. Assumptions were that the total cable elongation in both cases was equal. The maximum friction force was assumed to be equal to the tensile force corresponding with failure. τ_i was assumed to be constant over the length of the cable, so the axial force decreased linearly with x and reached 0 at a distance:

$$L_\tau \approx \frac{F_t}{\pi \cdot d_r \cdot \tau_i} = \frac{d_r \cdot \sigma_t}{4 \cdot \tau_i} \tag{5.30}$$

The total axial root elongation was then equal to:

$$\Delta u_{x,1} = \frac{1}{2} \cdot L_\tau \cdot \frac{\sigma_t}{E_t} \approx \frac{d_r \cdot \sigma_t^2}{8 \cdot \tau_i \cdot E_t} \tag{5.31}$$

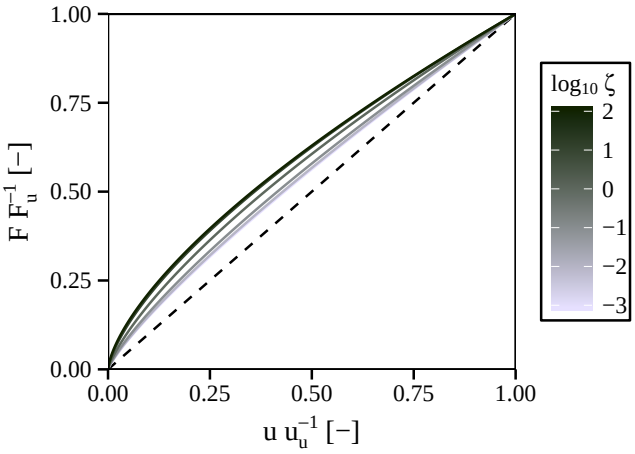

Figure 5.9: Normalised analytical cable model force–displacement curves for various values of ζ. The dashed line indicates linear behaviour.

The corresponding model length L can be found when $\Delta u_{x,1}$ is compared to the increase in cable length ($\Delta u_{x,2}$) computed using the cable stiffness and stress in the cable:

$$\Delta u_{x,2} \approx L \cdot \frac{\sigma_t}{E_t} \tag{5.32}$$

Solving $\Delta u_{x,1} = \Delta u_{x,2}$ resulted in:

$$L \approx \frac{d \cdot \sigma_t}{8 \cdot \tau_i} \tag{5.33}$$

Therefore:

$$\zeta \approx \frac{\sigma_t \cdot p_u}{8 \cdot E_t \cdot \tau_i} \tag{5.34}$$

Equation 5.34 can then be used instead of Equation 5.27 to find ζ, from which η can be found from Equation 5.26 and then F_u and u_u from Equations 5.29 and 5.28 respectively.

By changing the root tensile strength σ_t by an intermediate stress level σ_i in Equations 5.28 and 5.29, ranging between $0 \leq \sigma_i \leq \sigma_t$, the full force–displacement behaviour of the root can be modelled. The shape of these curves is slightly dependent on the value of ζ, see Figure 5.9, but for reasons of simplicity can be approximated using a linear curve, especially for smaller values of ζ.

The cable model can also easily be used to calculate the additional reinforcement a root perpendicularly crossing a shear plane adds to soil. Because of symmetry, the force required to fail a root in shearing will be half that of a point load, and the soil displacement twice that of the displacement under point loading. The multiplication factor in Wu and Waldron's root-reinforcement model (Equation 2.4), generally assumed as $k' = 1.2$, can then be expressed in terms of the analytical cable model as:

$$k' = \sin\beta + \cos\beta \cdot \tan\phi' = \frac{2 \cdot \sqrt{\eta}}{1+\eta} + \frac{1-\eta}{1+\eta} \cdot \tan\phi' \tag{5.35}$$

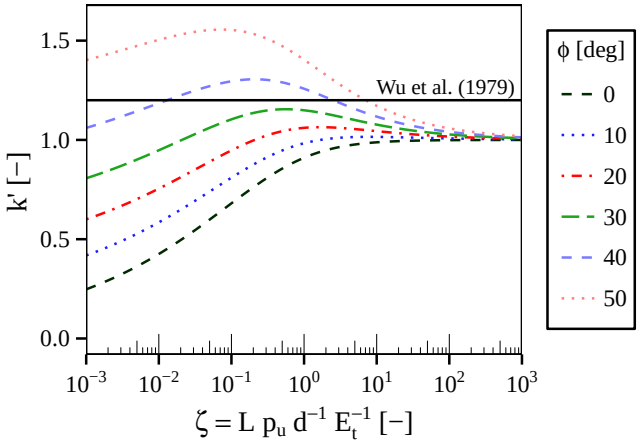

Figure 5.10: Comparison between the analytical cable model and Wu/Waldron model (Waldron, 1977). ϕ denotes the soil angle of internal friction.

Equation 5.35 shows that the peak root contribution to soil shear strength through tensile action is not only a function of root diameter, tensile strength and soil angle of internal friction, but also of soil–root interface friction, root tensile stiffness and soil resistance. Depending on the exact values of ϕ' and ζ, the root contribution to shear strength predicted using the analytical cable model will be smaller or larger compared to the WWM (Figure 5.10). An additional advantage over the WWM is that the analytical cable model provides insight into the root displacements required to reach tensile failure, which were shown to increase with increasing root diameter and strength and decreasing soil and root stiffnesses.

5.7.2 Comparison of analytical cable solution to a numerical cable model

To check the accuracy of the analytical cable model, a numericalnumerical scheme was developed to estimate cable forces and displacement (Figure 5.11).

Because of symmetry reasons only half of the cable was modelled. The beam was loaded by a force $F/2$ at $x = 0$. At this point horizontal deformations were restrained, and at $x = L$ both vertical and horizontal displacements were prohibited. The soil resistance was modelled as vertical point loads acting on nodes between $x = 0$ and $x = F/(2 \cdot p_u \cdot d)$ or $x = L$ (in the undeformed state), whichever of the latter two values was smaller. After discretisation into n nodes, the axial force between two nodes was simply determined by first calculating the axial strain and from that the axial stress and force.

At every node, horizontal and vertical forces had to be in equilibrium. This resulted in a system of equations with $(2 \cdot n - 3)$ equations and unknowns (x and y positions of the displaced roots, minus the three boundary conditions), and therefore could be solved for a given value of F. From the displaced shape the maximum axial stress could be computed.

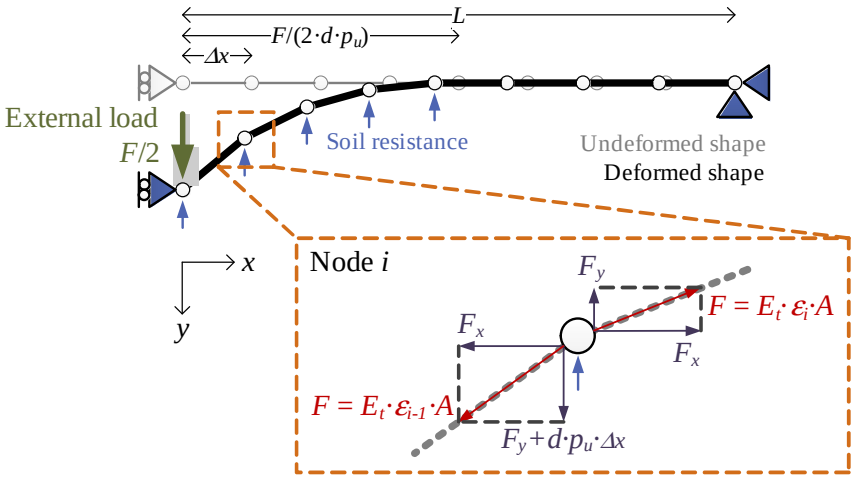

Figure 5.11: Schematic view of the numerical cable model.

The penetrometer force and displacement corresponding with root tensile failure (F_u and u_u) were then determined by iterating over F using a Newton-Raphson scheme until the maximum stress in the beams equalled the prescribed maximum tensile stress.

The difference between peak forces and displacements predicted using the analytical and numerical cable were 7% and 20% at most when $\zeta \geq 0.01$. When ζ was smaller, the analytical model predicted higher forces and displacements, up to 28% (F_u) and 66% (u_u) higher when $\zeta = 0.001$. This situation corresponded with low soil stiffness, in which case the root will deform a relative large amount. In realistic situations ζ will probably not be that low, and therefore it can be concluded that the analytical solution approximated the equivalent numerical scheme well.

5.8 Root mat penetrometer model

When a penetrometer is pushed through soil reinforced with lots of fine roots, individual root breakages might not be visible, as observed in the laboratory blade penetrometer tests in fibre-reinforced soil (Figure 4.10c). The soil and roots behaved as a continuum instead. This behaviour was approximated by superimposing the behaviour of lots of roots. Assumptions made were:

- The extra penetrometer resistance introduced by a single root increases linearly over a distance u_u until the maximum reinforcement F_u is reached (triangular shape).
- The penetrometer is a 2-dimensional element with width w and an infinitely small blade thickness.
- Roots are uniformly distributed over the rooted layer.
- The behaviour of every single root is independent from the behaviour of nearby roots.

Under these assumptions, the number of roots (n_r) hit over penetration depth interval Δz is only dependent on the root length density (RLD) and penetrometer width (w):

$$\frac{n_r}{\Delta z} = RLD \cdot w \tag{5.36}$$

Over the zone where new roots are picked up ($z_0 \leq z \leq z_1$, where z is the depth of the penetrometer tip and z_0 and z_1 the depths of the top and bottom of the rooted layer respectively) and none of the roots have broken yet ($z \leq z_0 + u_u$), the depth–resistance gradient will increase with depth as more and more roots are being strained under the tip. This gradient can be expressed as:

$$\frac{\mathrm{d}F(z)}{\mathrm{d}z} = n_r \cdot (z - z_0) \cdot \frac{F_u}{u_u} \tag{5.37}$$

where $F(z)$ is the root-reinforcement force at depth z. Integrating Equation 5.37 over depth z and substituting n_r using Equation 5.36 then yields:

$$F(z) = \frac{1}{2} \cdot RLD \cdot w \cdot \frac{F_u}{u_u} \cdot (z - z_0)^2 \tag{5.38}$$

When the displacement is sufficient for the first roots to break ($z \geq z_0 + u_u$) and the penetrometer has passed the root layer ($z > z_1$) the same approach yields that the resistance decreases in the following form:

$$F(z) = \frac{1}{2} \cdot RLD \cdot w \cdot \frac{F_u}{u_u} \cdot \left(u_u^2 - (z - z_1)^2\right) \tag{5.39}$$

Over the depth range between these two cases, the resistance gradient will be linear since the number of roots strained by the penetrometer is constant; the number of roots breaking will be equal to the number of new roots picked up by the penetrometer.

Figure 5.12 shows the idealised penetrometer response in the case of a relatively thick ($u_u \leq z_1 - z_0$) or thin root mat ($u_u > z_1 - z_0$). When the mat is classed as ‘thin’, the maximum penetrometer resistance is dependent on the mat thickness, whereas this is not the case with ‘thick’ mats.

In thick root mats, the maximum resistance can be simplified to:

$$F_{max} = RLD \cdot w \cdot \left(\frac{1}{2} \cdot F_u \cdot u_u\right) \tag{5.40}$$

The bracketed term is equal to the energy required to lead a single root to failure, whereas $RLD \cdot w$ equals the number of roots strained per unit depth.

Both the analytical bending and analytical cable bending can be used in conjunction with this root mat model, as both can yield the required predictions for F_u and u_u. The model can also be used for roots loaded by shearing soil when F_u and u_u are calculated

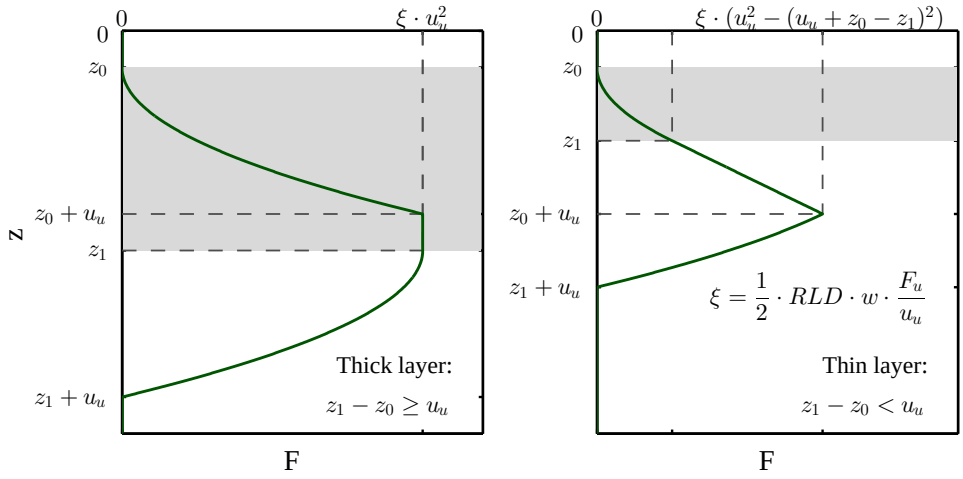

Figure 5.12: Schematic blade penetrometer resistance in case the penetrometer is pushed through a root mat with depth $z_0 \leq z \leq z_1$.

using the derived solutions for roots loaded in shear rather than loaded by a point load.

In both the analytical bending model (Section 5.5) and the cable model (Section 5.7) the product of F_u and u_u is correlated with d_r^3. Thicker roots therefore will have a large influence compared to smaller roots. It is therefore recommended to split the roots into multiple diameter classes, analyse the contributions of each class separately and sum the results in a final step.

5.9 Discussion

In some existing analytical root models incorporating soil resistance, the soil resistance was taken into account as a linear spring (e.g. Wu et al., 1988), while in others a constant resistance was adopted independent from the root lateral behaviour (Wu, 2007, 2013). The new models introduced in this chapter, based on (simplifications of the) the *p-y* method (Reese and Van Impe, 2011), showed that the latter approach was more realistic because root displacements required to reach failure were much larger than those required for the soil to reach its maximum resistance value.

The analytical bending model provides simple solutions for root resistances and displacements based on root mechanical properties and soil resistance. The analytical model results in similar reinforcement compared to numerical modelling when root strengths are relatively low and root stiffnesses and soil resistances high. Similar to limitations for existing models (Wu et al., 1988; Wu, 2007, 2013), roots are assumed to be infinitely long, straight, unbranched, loaded perpendicular to the root axis and linear elastic with no plastic deformation.

The analytical cable model improves over existing cable models (e.g. Wu et al., 1988; Wu, 2007, 2013) because of its ability to take non-linear deformation effects and axial elongation into account. Similar to bending models, however, it suffers from similar major

simplifications with respect to root architecture and root properties.

The applicability of all models to real roots should be tested to establish whether they are accurate and to find out when roots primarily fail in bending and when in tension.

Both analytical models were derived for point loading and shear loading. Point-loading solutions can be used when analysing the behaviour of roots loaded by a blade penetrometer or root pull-up device, see Chapter 3, because of the small size of the device. For small roots loaded by a corkscrew or pin vane device, the shear solution might be more appropriate. However, for thicker roots loaded by corkscrew or pin vane devices, the length of roots embedded in the device is relatively small compared to the diameter (i.e. small $d_r \cdot L_{crit}^{-1}$ (analytical bending model) or small $d_r \cdot L_I^{-1}$ (analytical cable model)). Therefore, in these cases the real root behaviour is expected to be somewhere between the point-load and shear solutions. Solutions for the peak reinforcement for both cases lay roughly a factor 2 apart in both models, whereas solutions for the root lateral displacements range more (factor 10 for the analytical bending model though 2 for the analytical cable model).

6

Blade penetrometer: laboratory testing

The contents of this chapter have been written up as a paper and submitted for revision, see Meijer et al. (2016a).

6.1 Introduction

In Chapter 3 the blade penetrometer method was introduced. Laboratory testing with various root analogues in low-strength, unsaturated, recompacted field soil (Chapter 4) showed that a fibre-reinforced soil (modelled with thin polypropylene fibres) caused 'smooth' increase in penetrometer force over the rooted depth range. Thicker roots (modelled with ABS plastic) showed distinct reinforcement peaks in the penetrometer trace; from the moment the penetrometer hit an ABS root analogue, the resistance gradually increased until the analogue broke, visible as a sudden decrease in resistance. This study however only showed qualitative results. No attempt was made to use these peak characteristics to infer root properties.

Before the blade penetrometer method was tested in the field, a larger set of laboratory experiments was performed in idealised to investigate the behaviour of roots under blade penetrometer loading. This laboratory study is the subject of this chapter. Individual buried ABS root analogues with various architectures were tested in dry sand with two different densities to study the effect of root length, root diameter, root angle, root branching, soil density and the position at which the root is loaded with respect to a root tip or parent root.

The study aimed to:

- Find out which of the tested variables (root diameter, root length etc.) had the largest effect on the observed force and displacement corresponding with root failure under penetrometer loading.
- Find out which of the models derived in Chapter 5 yielded the most reliable predictions.

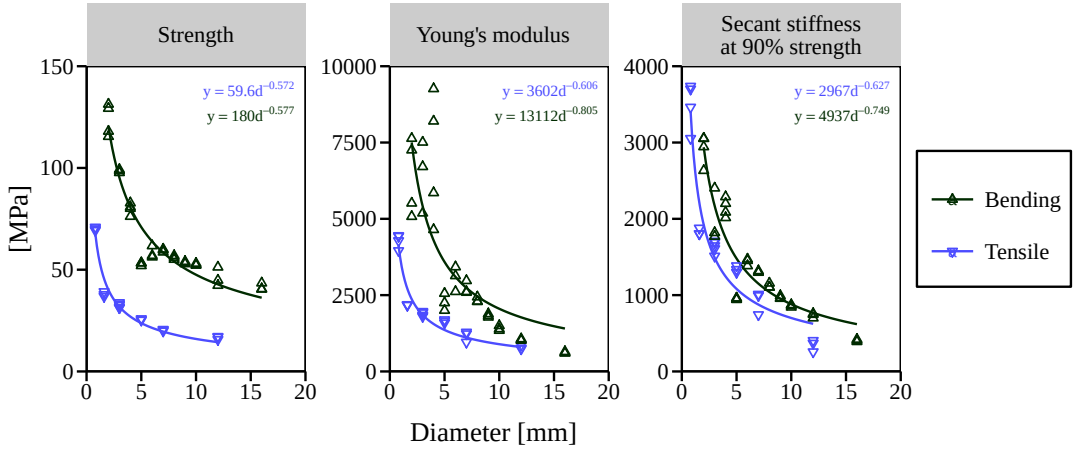

Figure 6.1: Tensile and bending strength and stiffness of acrylonitrile butadiene styrene (ABS) plastic. Data obtained from testing by Liang et al. (2015). Lines indicate best power law fits.

- Investigate how the combination of experimental results and modelling techniques can be used to back-calculate the root diameter. Root diameter is a useful parameter both when root architecture is to be studied and when root-reinforcement is to be quantified using any of the models described in Section 2.5.

6.2 Methods

6.2.1 Root analogues

Acrylonitrile butadiene styrene (ABS) plastic was selected as root analogue material. This material has been shown to have comparable mechanical characteristics to plant roots (Liang et al., 2014, 2015). A rapid prototyper ('3D-printer') was used to print roots in various configurations.

Material strength and stiffness was measured in both tension and bending by Liang et al. (2015) using a universal testing machine (Figure 6.1). The secant stiffness at 90% of the peak strength (E_{90}) was determined from stress–strain curves. E_{90} was chosen due to yielding a good representation of the non-linear stress–strain curve when using a linear elastic material model, see Figure 6.2. Using the Young's modulus would lead to the modelled stiffness being too high, which is especially a problem for real roots (Figure 7.4). It was decided to use the secant stiffness at 90% strength rather than the secant stiffness at peak strength as some ABS root analogues showed considerable plastic strain before the peak strength was reached (e.g. Figure 6.2b), which would have resulted in a large uncertainty in the adopted model stiffness.

Root analogue diameters were 2 and 4 mm with lengths of 200 or 400 mm. Because of the limited print volume of the 3D-printer, 400 mm rods were made by connecting two

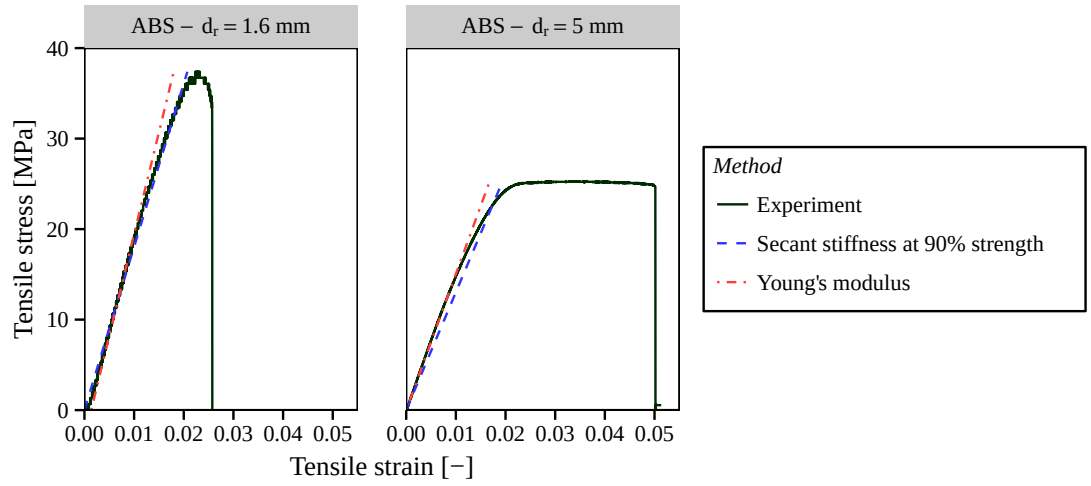

Figure 6.2: Example stress–strain curves for ABS root analogues testes in uniaxial tension. d_r indicates the tested root diameter.

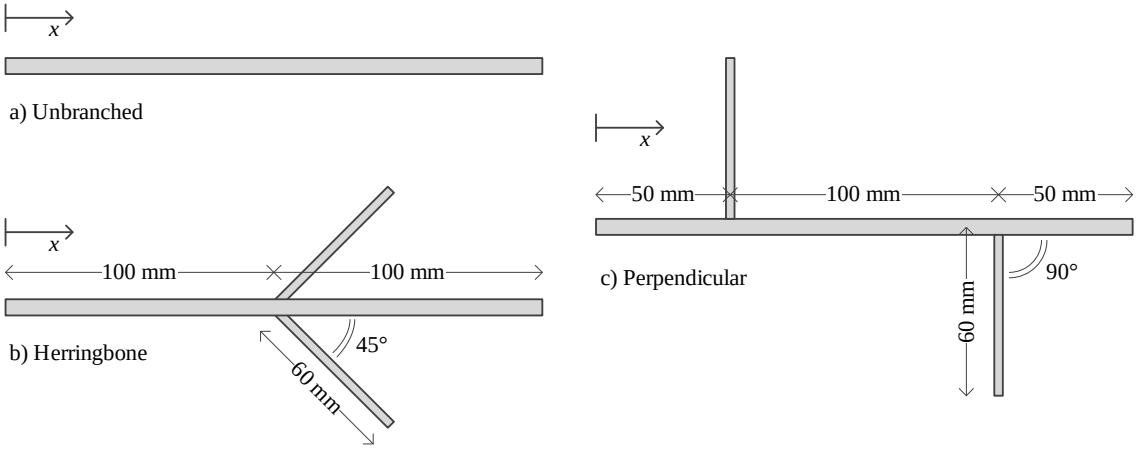

Figure 6.3: a) Unbranched, b) herringbone and c) perpendicular branching patterns for 200 mm long analogue root sections.

200 mm rods by means of epoxy resin and a printed ABS coupler with a length of 15 mm and an external diameter 3 mm larger than that of the rod.

Roots with three commonly modelled architectures were tested: a) unbranched, b) herringbone branching, and c) perpendicular branching (Figure 6.3) (Dupuy et al., 2005a; Hamza et al., 2007; Mickovski et al., 2007). The adopted branching angle for the herringbone pattern was 45°, similar to values found *in situ* (Henderson et al., 1983a; Riestenberg, 1994). Branch length was chosen as 60 mm and distance between branches as 200 mm (herringbone) or 100 mm (perpendicular), close to the 150 mm reported for 1–5 mm diameter Norway spruce (*Picea abies*) roots (Giadrossich et al., 2013). All tested 2 mm diameter roots were unbranched. Branch diameter was 2 mm, so that the child–parent diameter ratio for branched cases was 0.5, similar to the 0.45 used by Dupuy et al. (2005b) for Maritime pine.

All tests were performed at a root depth $z = 150$ mm. One root end was securely anchored to the side of the model container to simulate the root being connected to a

larger parent root. Roots were oriented in the horizontal plane or under an angle (30° dipping down). 400 mm long horizontal root analogues were loaded at either 100 or 300 mm distance from the 'parent root' (measured along the root axis) while 200 mm long horizontal analogues were loaded only at 100 mm distance. Angled roots were only loaded at 300 mm (400 mm long roots) or 100 mm distance (200 mm long roots) from the 'parent root'.

6.2.2 Soil and sample preparation

Dry Congleton silica sand (HST95) was used as soil. The particle size distribution is presented in Figure 4.2. Tests were performed in medium dense (relative density I_d = 50%) and dense sand (I_d = 80%). From previous experimentation the following correlations were derived for soil peak angle of internal friction ϕ' [°] and dry density γ'_d [kNm^{-3}] (Lauder, 2010; Al-Defae, 2013):

$$\phi' = 20 \cdot I_d + 29 \tag{6.1}$$

$$\gamma'_d = 3.0 \cdot I_d + 14.5 \tag{6.2}$$

where I_d is expressed as a fraction. A plastic box was filled with dry sand to a height of 300 mm using pluviation. The plastic box was lined with 10 mm thick adhered wooden panels to provide walls that could easily be drilled for mounting roots. Internal dimensions were 530×330×310 mm (length×width×height). Roots were glued into pre-drilled holes, matching root analogue diameter, in the side of the box and supported by wires (cut prior to testing). Following analogue placement sand was pluviated into the box using a slot pluviator from a fixed height (Lauder, 2010; Al-Defae, 2013). Each box contained multiple roots. The main root axes were spaced at least 80 mm apart to prevent interference between tests, while branched roots were never put next to each other.

Two Civil Engineering undergraduate students at the University of Dundee (Ivan Mukov and Mengqi Zhang) prepared boxes for testing and collected raw test data as part of their honours projects, under supervision of the author of this thesis. Test design, data post processing and data analysis were all performed by the author of this thesis.

6.2.3 Test equipment

The blade penetrometer shape was identical to the one used in previous experiments, see Figure 3.3.

The penetrometer was pushed down vertically using an universal testing machine (Instron 5980) fitted with a 30 kN load cell (Instron 2580 Static series, accurate to 0.5% of a reading down to 1/500th of the load cell capacity) (Figure 6.5) with force and displacement logged at 20 Hz.

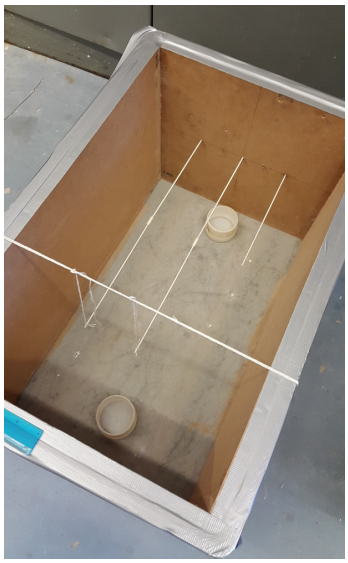

Figure 6.4: Box ‘rooted’ with ABS root analogues before pluviation.

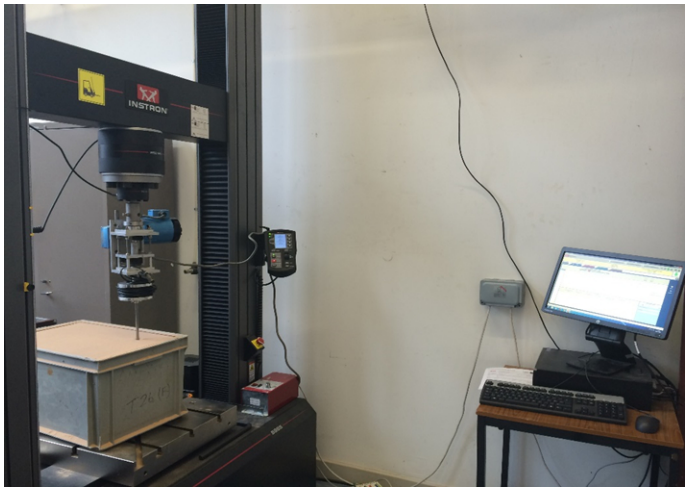

Figure 6.5: Laboratory blade penetrometer test setup. A universal testing machine (left) pushes a shaft with attached blade penetrometer tip into a box filled with dry sand and ‘rooted’ with ABS root analogues. Penetrometer force and displacement are logged using a computer (right).

The installation rate was 300 mm min^{-1}, in line with expected rates to be adopted in the field to obtain a practical and fast test method. This rate is also representative of landslide velocities and similar to previous testing (Figure 4.6).

For reference testing, 10 blade and 11 standard penetrometer (no plate) tests were performed in non-rooted ('fallow'), 50% relative density sand. In I_d = 80% sand, 14 and 8 tests were performed respectively.

6.2.4 Data processing

In each depth–resistance trace, soil and root effects were superimposed. Furthermore, due to the experimental nature there was some variability in soil resistance. Root effects were isolated first by calculating the mean soil resistance without root effects at each depth level, resulting in a single 'average' fallow trace for each relative density. Subsequently, for each test the average ratio between the resistance measured during the test and the average fallow resistance was determined over a depth range 100 $\leq \leq$ 140 mm (i.e. over the depth range just before the penetrometer encountered the buried root analogue). The root effect ('reinforcement') was then found by subtracting the product of this ratio and the average fallow resistance from the resistance trace measured in each test.

Reinforcement was only studied until the root broke, visible as a sudden decrease in penetrometer resistance in the force–displacement diagram. Additional peaks were visible over a displacement range of 0–40 mm following failure, see Figure 6.7. Peaks evident following failure may be attributed to stick–slip, broken root ends sliding along the blade, and by broken root ends getting stuck behind the shoulder of the cone. These additional peaks were therefore discarded.

Exact root depth was required for accurate determination of the the root displacement corresponding with root failure. Root depths were never exactly 150 mm due to experimental variation introduced during sample preparation. The depth could not be determined from the displacement–reinforcement plot due to increased resistance prior to touching the actual root. Both uniaxial tensile tests and 3-point bending tests showed highest root analogue stiffnesses at zero strain. Assuming this was also the case during blade penetrometer testing, for every test the magnitude and location of the largest gradient on the measured depth–root resistance curve was determined. Subsequently, the 'real depth' was defined as the depth at which the the tangent at this location intersects the depth axis (Figure 6.7).

All data processing and statistical analyses were performed using R statistical software (R Core Team, 2013). Statistical significance of p-values is denoted as: $p = 0 < ^{***} \leq 0.001 < ^{**} \leq 0.01 < ^{*} \leq 0.05 < ^{\cdot} \leq 0.1 < ^{n.s.}$

6.2.5 Predictions for forces and displacements

Predictions of both the peak reinforcement (F_u) and root lateral displacement required to reach peak reinforcement (u_u) were made using the numerical model (see Section 5.3), the

analytical bending model (assuming the root analogues broke in bending, see Section 5.5) and the analytical cable model (assuming analogues broke in tension, see Section 5.7).

In the analytical cable model, ABS tensile parameters were used whereas in the analytical bending model bending parameters were used. Numerical modelling was performed separately for both bending and tensile parameters. In the numerical model, soil–root interface friction was modelled assuming Equation 5.2. The connection of the model root to the box was modelled by fixing all degrees of freedom at this node. In all analyses, the root stiffness was modelled using the secant stiffness at 90% strain (E_{90}) rather than the Young's modulus (E) to more accurately capture the non-linear stress–strain behaviour of the root.

For all models, predictions were only made for horizontal roots due to model limitations. Predictions for angled roots were made instead by assuming they were horizontally oriented. Since both analytical models assume infinitely long unbranched roots, no separate analytical model predictions could be made for roots with various lengths, loading positions and branching patterns.

6.3 Results

Standard cone penetrometer resistance, in non-rooted samples, was approximately half (0.497) of that recorded for the blade penetrometer (In terms of force, Figure 6.6), with a surface area only 24% smaller when compared to the blade penetrometer. This suggests shape effects and/or frictional resistance on the sides of the blade influenced total resistance. Predictions for soil resistance (Equation 5.1) yielded on average 37.7% lower resistances than measured using the standard penetrometer, when averaged between z = 50 mm (to avoid near-surface effects) and z = 250 mm (to avoid bottom boundary effects, Figure 6.6).

Root-resistance versus depth traces (Figure 6.7) showed the same type of clearly defined root reinforcement peaks as observed in previous laboratory tests (Figure 4.10).

Measured peak reinforcement increased with increasing root diameter and soil density (Figure 6.8). Branching increased resistance compared to unbranched roots, with the herringbone type yielding approximately 23% higher reinforcements than perpendicular branching. When comparing roots with different lengths and loading positions, tests with 400 mm long roots loaded at 100 mm distance from the fixed point generally gave the highest results, although the effect of length and loading position was small in comparison.

The analytical cable model overestimated predictions of force while the analytical bending model results closely resembled experimentally measured peak forces (Figure 6.9). Highest coefficients of variation were observed in the analytical bending model (R^2 = 0.7), indicating ABS rods are likely to have failed in a bending rather than tension

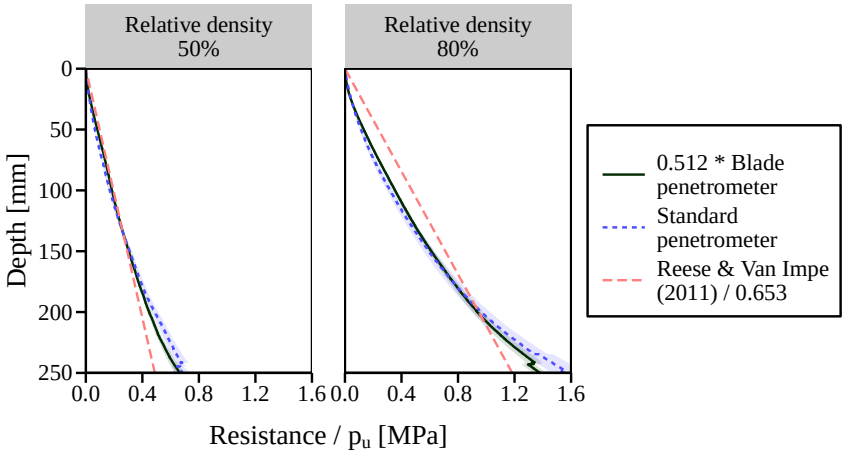

Figure 6.6: Average soil resistance over depth measured using the standard penetrometer and blade penetrometer and predicted using the model described by Reese and Van Impe (2011). For both penetrometer types, resistances are calculated assuming load is distributed over the tip area of the standard penetrometer. Shaded areas indicate the standard error of the mean for experimentally measured results. Note the linear scaling factors for the measured blade penetrometer resistance (0.512) and the resistance predicted using Reese and Van Impe's model (1/0.653) to make them coincide with the experimentally measured standard cone penetrometer resistance.

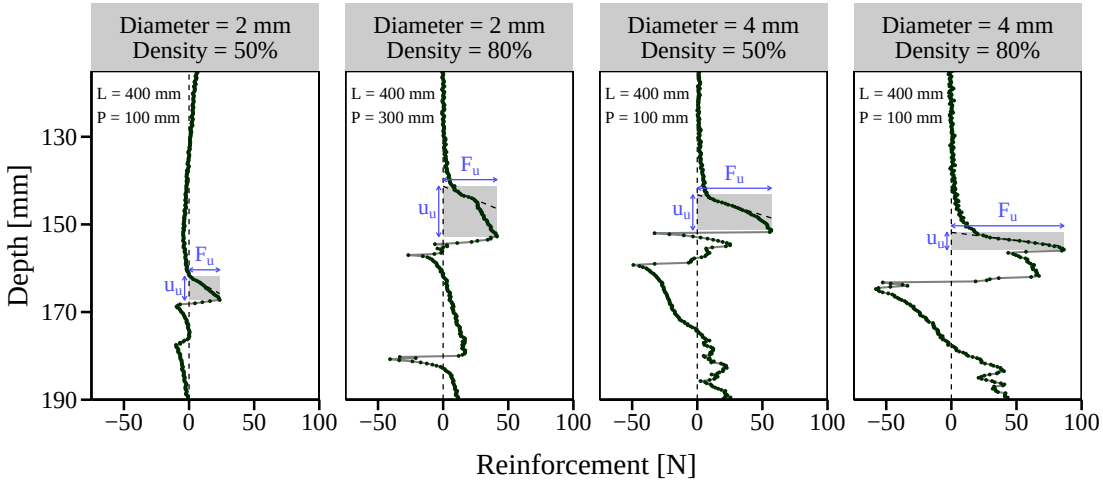

Figure 6.7: Example laboratory blade penetrometer root resistance versus depth traces for horizontal roots. L indicates root length and P the distance between the trunk and the point of loading. F_u and u_u indicate the peak force and root displacement at maximum peak force.

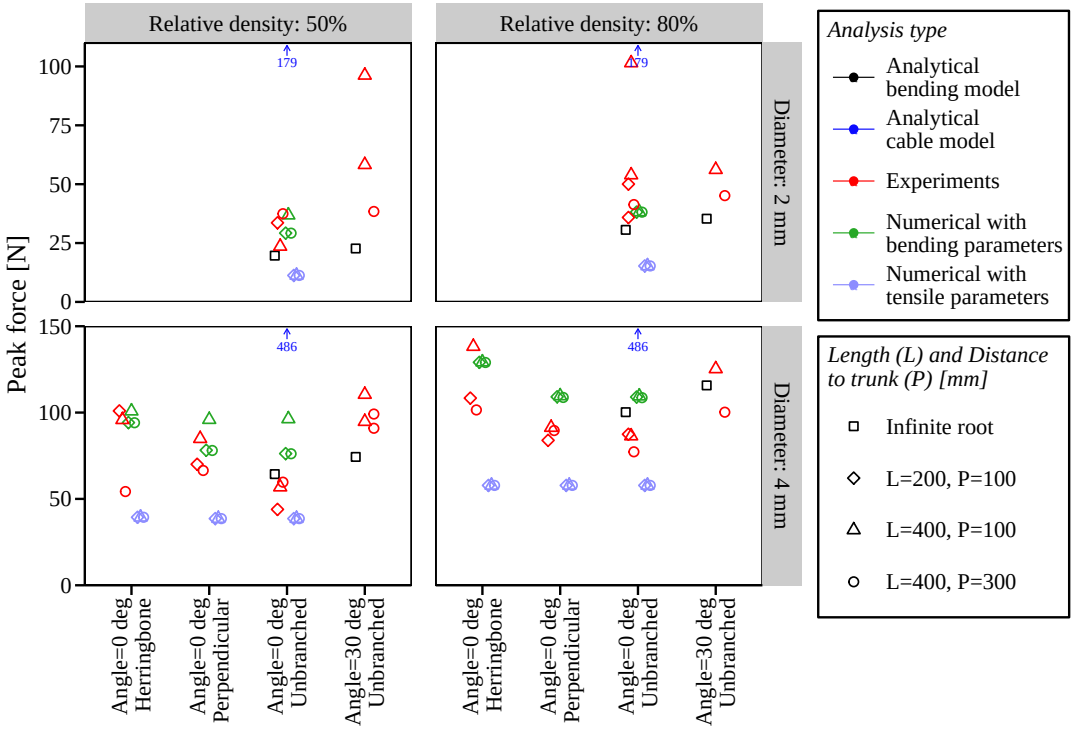

Figure 6.8: Experimental and predicted root peak forces in laboratory blade penetrometer tests. Predicted values for the analytical cable model were so high their magnitudes are indicated using arrows and numbers on the graph.

failure mechanism. Numerical simulation results also indicated that using bending bending parameters resulted in much better predictions than using tensile parameters.

Two outliers were observed in some of the tests on 400 mm long 2 mm diameter roots loaded at 100 mm distance from the fixed point. Both had much higher peak forces (101.5 and 96.2 N) and displacements (19.1 and 17.2 mm) compared to repeat tests. It is hypothesized that this was the result of variation in sample preparation. The density below the root might have been lower due to the root 'shielding' the area just below the root from pluviated sand, resulting in lower densities. This explains the higher displacements. Since the soil resistance is lower, a larger length of the root will displace, increasing the peak force. Because of the proximity of the 'parent root', the root will also be (partially) loaded in shear instead of bending, enhancing the higher resistances.

Root analogues at a 30° angle resulted in higher peak forces (0–100%) compared to their horizontal counterparts, especially for thicker roots and those in lower density soils. These dependencies suggest that the failure mechanism might be different from the failure mechanism for horizontal roots. It is suggested that future work focusses on studying this effect of root angle and on developing better predictive models taking this effect into account.

Perpendicular branching resulted in a smaller increase of the peak resistance when

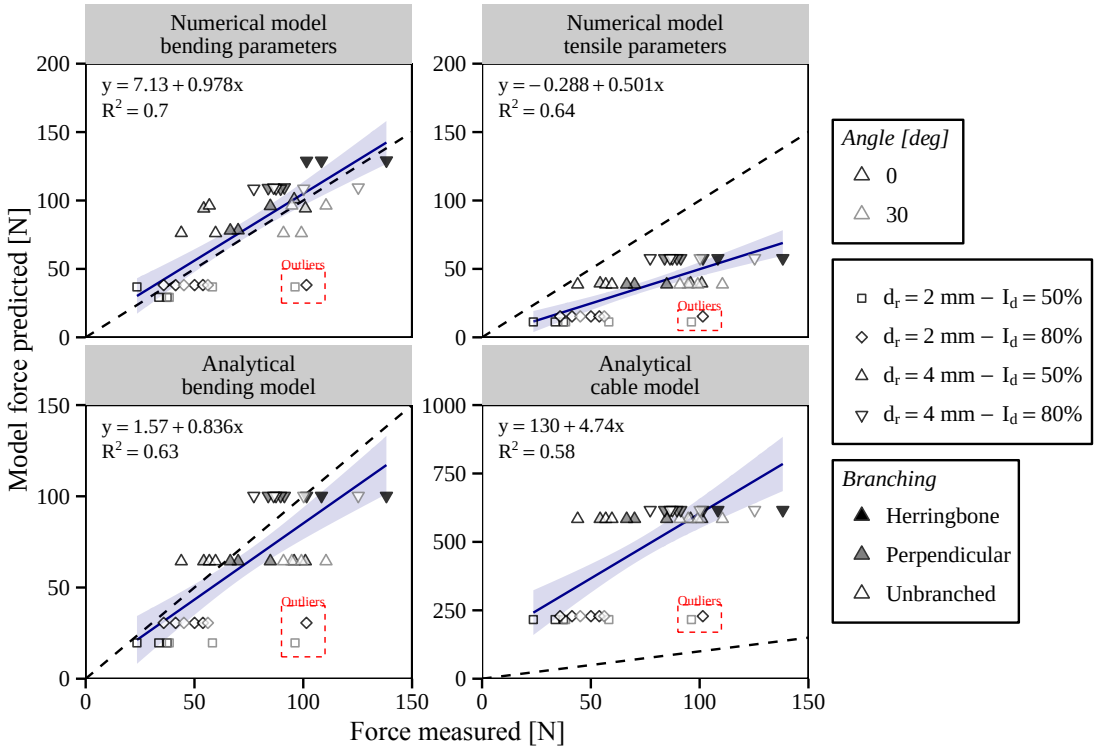

Figure 6.9: Comparison between experimentally measured and predicted peak force values. Solid lines indicate best linear fits, shaded areas the 95% confidence interval of this fit and the dashed line parity. Identified outliers, not taken into account in the fit, are indicated by a red box.

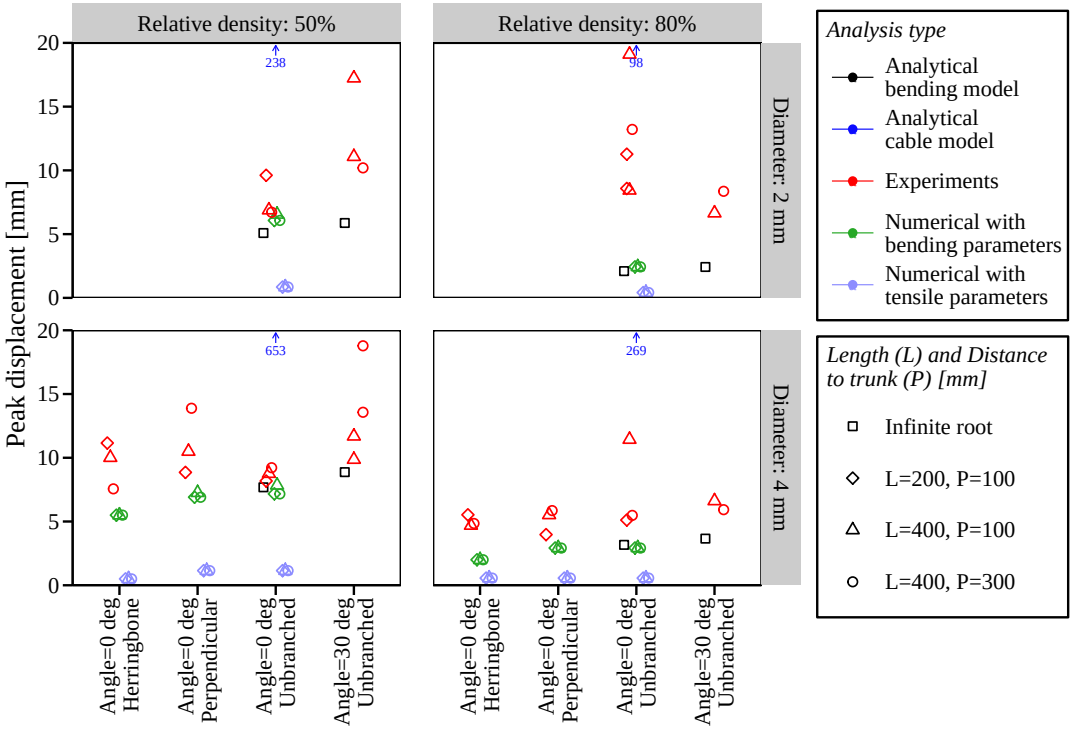

Figure 6.10: Experimental and predicted root displacement at peak forces in laboratory blade penetrometer tests. Predicted values for the analytical cable model were so high their magnitudes are indicated using arrows and numbers on the graph.

compared to herringbone branching. This may be caused by the distance between branches and the loading point. Herringbone branches were located directly below the loading point and therefore strained more. Perpendicular branches were located further from the loading point, reducing strain. This distance also explains why in dense soil (I_d = 80%) there was almost no difference in peak reinforcement between perpendicularly branched roots and unbranched roots, as due to the higher soil resistance, branches might have been too far away from the point of loading to be mobilised.

Roots located at an angle required larger displacements to reach failure than horizontal roots (Figure 6.10). Both root diameter and branching pattern had a small influence on the displacement at peak reinforcement.

The analytical bending model and numerical model using bending parameters yielded the best predictions and the best fits between experimentally measured and predicted lateral root displacements at peak reinforcement (u_u) (Figure 6.11). However, predictions were lower than displacements measured, and the variability in predictions was higher than those for peak reinforcement F_u (R^2 = 0.40–0.41 for u_u compared to 0.63–0.70 for F_u). This suggests large variation in experimental results or inaccuracies in the models.

Higher soil densities generally resulted in lower displacements, although 2 mm diameter roots in dense sand displaced much further compared to other roots even though

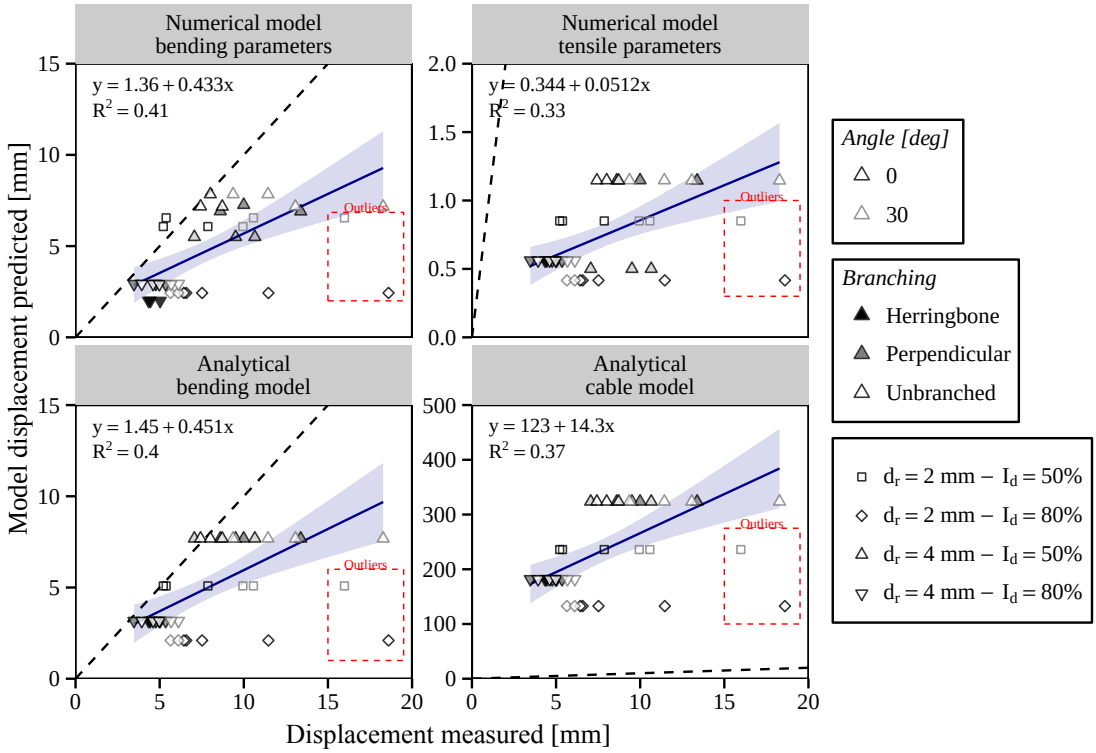

Figure 6.11: Comparison between experimentally measured and predicted displacement at peak reinforcement. Solid lines indicate best linear fits, shaded areas the 95% confidence interval of this fit and the dashed line parity. Identified outliers, not taken into account in the fit, are indicated by a red box.

Table 6.1: Effect of various root and soil properties on the magnitude of the laboratory blade penetrometer peak reinforcement force F_u. 'Data subset' indicates which experimental results were taken into account for deriving the mean and standard deviation ('SD') of the differences. The statistical significance was determined using paired t-tests.

Factor	Comparing	Data subset	Increase in root resistance			n
			Mean [%]	SD [%]	Significance [-]	[-]
Diameter	4 v.s. 2 mm	Horizontal & Unbranched	72.2	48.1	**	6
Relative density	80 v.s. 50%	Horizontal & Unbranched	74.7	81.8	*	6
Branching	Herringbone v.s. unbranched	Horizontal & d_r = 4 mm	50.8	47.6	*	6
	Perpendicular v.s. unbranched	Horizontal & d_r = 4 mm	23.0	25.5	·	6
Angle	30 v.s. 0°	Unbranched	47.2	49.1	**	8
Distance to trunk	100 v.s. 300 mm	Horizontal & Length = 400 mm	25.0	41.7	·	8
Length	400 v.s. 200 mm	Horizontal & Distance to trunk = 100 mm	16.4	32.6	*n.s.*	8

reinforcements were similar. It is unclear what caused this effect. Force–displacement traces (Figure 6.7) suggest a more gradual, plastic failure mechanism might have occurred. When these measurements were ignored, both the analytical bending model and numerical model using bending parameters resulted in decent predictions, although lower than measured. This is attributed to roots being modelled using a linear-elastic material using the secant stiffness at 90% strength. Since these models ignore any plastic deformation, the modelled strain to failure and therefore the predicted displacements will be lower than observed in experiments.

Since predictions for peak reinforcement values were shown to be better predicted than displacements, variability in peak force was further analysed. Replicated tests for combinations of branching, diameter, angle, relative density, length and loading position values were averaged so that a balanced dataset was obtained.

The effect of various factors (e.g. root diameter, branching type etc.) was studied by pairwise comparison using two-sided Welch's t-test. For example, when quantifying the influence of root diameter, with the same angle, branching, length, distance to trunk and relative density but different diameters were compared. The results (Table 6.1) showed that the variation in diameter and relative density had the strongest effects on the magnitude of the peak force. Root branching and angle had a lesser effect, while the effect of distance to trunk and especially root length was small.

In addition, a type III analysis of variance test (ANOVA) was performed on the same dataset using the same factors. This analysis suggested that most of the variation in the data

is explained by variation in root diameter (39%***), followed by relative density (14%***), root angle (12%***), branching (11%**) and the distance to the trunk (5%**). Root length was non-significant (1%$^{n.s.}$). The importance of each factor on the measured variation in peak reinforcement as determined using the ANOVA roughly corresponds with that found using t-tests.

6.4 Discussion

The analytical bending model force predictions were close to the experimentally measured values, suggesting the ABS root analogues failed in bending. The highest value for $\sigma_b^{1.5} \cdot p_u^{-0.5} \cdot E_b^{-1}$ equals approximately 0.80 (I_d = 50%, d_r = 2 mm) and the lowest 0.48 (I_d = 80%, d_r = 4 mm). These values are just above the identified threshold level of 0.424, derived using numerical modelling (Equation 5.13), below which numerical and analytical bending models yielded similar reinforcements. This magnitude of this dimensionless group of parameters explained why the root analogues failed due to bending rather than tension mechanisms (Figure 5.5). The magnitude of $\sigma_b^{1.5} \cdot p_u^{-0.5} \cdot E_b^{-1}$ being slightly higher than the derived threshold level of 0.424 explained why the numerical bending model yielded similar but slightly higher predictions than the analytical bending model, as previous modelling work showed that for values of $\sigma_b^{1.5} \cdot p_u^{-0.5} \cdot E_b^{-1}$ exceeding $\approx$ 0.424 peak force predictions using the numerical model were larger than those using the analytical bending model (see Figure 5.5).

Numerical modelling showed that the analytical bending solution should be accurate when the roots area loaded at least $1.2 \cdot L_{crit}$ from a root boundary (e.g. root end or parent root, see Section 5.6.2). In the laboratory experiments reported here, predicted values for L_{crit} ranged between 26.8 and 68.4 mm while the minimum distance to the trunk or root tip was 100 mm, thus fulfilling this condition. This explained why the statistical analyses showed that both the root length and the position of loading had hardly any influence on the results. Whether the root was loaded at 100 or 300 mm from the trunk, the nearest boundary was always at a distance of 100 mm.

Practical application of the blade penetrometer, characteristics of root peaks identified in the measured depth–resistance trace may be used to back-analyse the root diameter. Rewriting the analytical bending model equation (point load, Table 5.1) to find the root diameter based on the measured peak force yields:

$$d_{predicted} = 0.9886 \cdot F_u^{0.5} \cdot \sigma_b^{-0.25} \cdot p_u^{0.25} \tag{6.3}$$

This shows that the diameter prediction is relatively insensitive to changes in root strength and soil resistance compared to changes in the measured reinforcement. When the equation

for root displacement (analytical bending model) is rewritten:

$$d_{predicted} = 10.20 \cdot u_u \cdot \sigma_b^{-2} \cdot E_b \cdot p_u \tag{6.4}$$

Comparing Equation 6.4 to Equation 6.3 indicates that predictions based on displacement are likely to be less accurate. Small variations in root stiffness, soil resistance and especially root strength will have large effects on the predicted diameter compared to the effect of variation in u_u. The same conclusion holds for the analytical cable model. This explained why the experimentally measured root-reinforcements could be predicted much more accurately than the accompanying displacements.

The variation in experimentally measured reinforcement was best explained by variations in root diameter and soil relative density. Branching and root angle were of limited importance, while the effects of root loading distance and root length were less so. This explained why the analytical bending model yielded reliable predictions for the peak reinforcement for horizontal root analogues despite ignoring root length, branching and distance to trunk.

The few parameters required for both analytical models makes them easy to use in practical applications and minimises the need for time-consuming numerical modelling. Both analytical models require estimates for root strength and stiffness. Biomechanical data can be easily acquired using standard material testing (tensile and bending tests), and for many species tensile data has been published before (e.g. Mao et al., 2012) although data for root stiffness is sparse and data for bending properties almost non-existent. A third required parameter, soil resistance p_u, can be estimated for dry sand when soil properties (ϕ' and γ') are known using Equation 5.1. In the field however it might be easier to estimate p_u from standard cone penetrometer testing or even from blade penetrometer testing (see Chapter 7). This study showed that in that case correction factors are required to compensate for the difference in shape between the penetrometer and the root. The cable model requires an additional value for root–soil interface friction (τ_i). In field conditions, this value can be estimated from *in situ* shear tests (e.g. vane testing) or from penetrometer resistance when penetrometer resistance–shear strength correlations are available. However, a correlation factor will be required taking into account the difference between soil–soil friction and soil–root friction. Alternatively, *in situ* pull-out testing of roots can be adopted to estimate the resistance of a root to axial displacement (e.g. see Van Beek et al., 2005; Docker and Hubble, 2008; Norris, 2005; Tosi, 2007).

The analytical cable model is an improvement compared to existing cable models (e.g. Wu et al., 1988; Wu, 2007, 2013) because of its ability to take non-linear deformation effects and axial elongation into account. However, since root analogues in the experiments described here were relatively stiff and failed in bending, model predictions were inaccurate. Because many real roots are more flexible than ABS analogues (Figure 4.1),

the analytical cable model is expected to yield better predictions than the bending model for many real root cases.

6.5 Conclusions

- Experimental penetrometer results for buried ABS root analogues in dry sand show that the force required to break horizontal root analogues is mainly a function of root diameter. The second most important parameter is soil resistance (p_u). Root branching, root length and the position of loading all have a smaller effect.
- The force required by a penetrometer fail an ABS root analogue was best predicted using the numerical model (using strength and stiffness parameters derived from 3-point bending tests rather then uniaxial tensile tests) or the analytical bending model, showing that the root analogues failed in bending rather than tension.
- All models poorly predict root lateral displacement required for root failure (u_u).
- Root angle potentially has a strong effect on both force and displacements. However, the experimental results could not be compared to modelling predictions because of model limitations.
- Root diameters can be predicted from the penetrometer force–displacements when root mechanical properties and soil resistance are known or accurately estimated, given that the correct root failure mechanism (bending or tension) is known. Predictions based on the magnitude of root-reinforcement were more reliable than those based on lateral root displacement to reach peak force.
- Having developed the analytical models and validated them against experimental data collected in controlled laboratory conditions, the next chapter will apply and further validate these methods against field data collected for two contrasting sites/species. This will yield data for more realistic soil (real field soil instead of dry sand) and root conditions (real plant roots instead of ABS root analogues).

7

Blade penetrometer: field testing

The contents of this chapter have been written up as a paper and submitted for revision, see Meijer et al. (2016b).

7.1 Introduction

Laboratory blade penetrometer experiments (Chapter 6) showed that the behaviour of ABS root analogues under penetrometer loading could be accurately predicted, given the correct predictive model was adopted (in this case, a model assuming root analogues broke in bending). In this chapter, the blade penetrometer is applied *in situ* in two forests with different soil conditions and tree types. The diameters of roots broken by the penetrometer was measured and compared to model predictions using the analytical interpretive models developed in Chapter 5.

7.2 Methods

7.2.1 Field sites

Field testing was performed at two different sites covering a range of soil and root conditions.

The first site was Hallyburton Hill forest, a Forestry Commission owned woodland in the Sidlaw Hills, near Dundee, UK (56°31'10.3"N, 3°11'29.9"W), planted with Sitka spruce (*Picea sitchensis*) in 1961, see Figure 7.1. Sitka spruce is the most common conifer in UK woodlands, accounting for 51% of the growing stock (Forestry Commission, 2015). The soil was classified as sandy silt, see Figure 4.2 for the particle size distribution.

The second site was Paddockmuir Wood, a Forestry Commission owned woodland near St Madoes, UK (56°21'55.3"N, 3°16'13.0"W), planted with mature pedunculate Oak (*Quercus robur*) and interspersed with young Sycamore (*Acer pseudoplatanus*), see

Figure 7.1: Sitka spruce forest at Hallyburton Hill.

Figure 7.2: Blade penetrometer testing near oak tree at Paddockmuir Wood.

Figure 7.2. Oak is one of the most common broadleaf species in UK woodlands (16%); only birch is grown more (18%) (Forestry Commission, 2015). The soil was classified as clayey silt, see Figure 4.2 for the particle size distribution.

An both sites, soil dry densities and water contents were measured close to the testing locations using 100 cm^3 steel core samples (56 mm internal diameter, 40 mm deep), and these were collected within 0.5 m distance of a blade penetrometer measurement location. Soil suctions were measured *in situ* using field tensiometers (model SWT4R, Delta-T). Horizon depths were manually determined based on visual observation in soil pits and compared with the Soil Information for Scottish Soils database (James Hutton Institute, 2016). Results for both sites can be found in Figure 7.3.

7.2.2 Root biomechanical characteristics

Root strength and stiffness were determined from tensile tests and 3-point bending tests. Roots were collected from soil excavated from a trench. Fine roots were collected by excavation of soil block samples which were subsequently washed in the laboratory to expose the roots. Roots with diameters exceeding approximately 10–15 mm were not sampled as these proved to be difficult to test in uniaxial tension due to difficulties with gripping the roots during a test. After sampling, roots were bagged and stored in a fridge at 4°C for a maximum of 4 days prior to testing to minimise potential decomposition effects.

Intact root diameters were measured using a microscope magnifying 4.0 times and fitted with a eyepiece graticule. When the graticule (fitted with 100 0.1 mm ticks) was not large enough to measure the root diameter the magnification was reduced to 3.0, 2.0, 1.0 or even 0.7 times. All diameters were measured overbark.

Seventy-six Sitka and 53 Oak samples with a length of 100 mm were tested in tension using a loading rate of 5% strain per minute (5 mm min^{-1} for 100 mm long roots), in line with loading rates reported in literature (1–10 mm min^{-1}, e.g. Genet et al. (2008); Loades et al. (2010)). A further 24 shorter oak samples (60 mm long) were tested at the same strain rate. All roots were clamped by hydraulic clamps using 100–300 kPa of pressure,

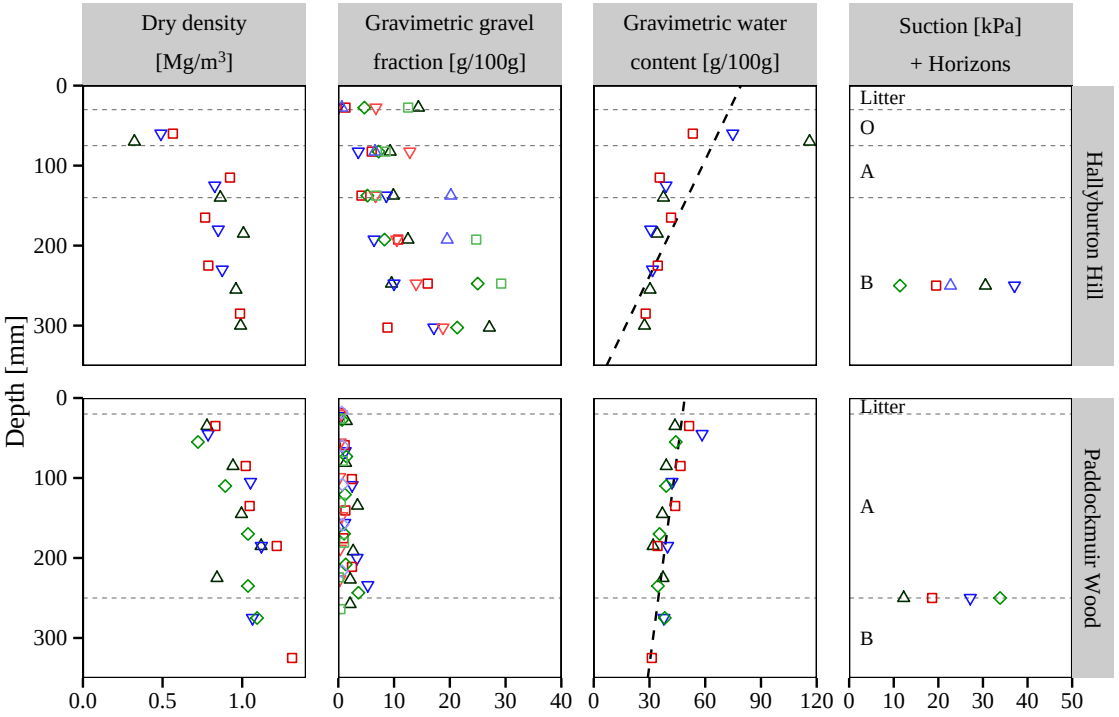

Figure 7.3: Soil properties for blade penetrometer testing at Hallyburton Hill and Paddockmuir Wood forests. 'Gravel' is defined as particles with sizes exceeding 2 mm. Different markers indicate replicates.

with more pressure used for thicker roots. For roots thicker than approximately 3 mm, the bark was stripped near the clamps to ensure good grip between the clamps and the root stele. The presence of the bark was not expected to influence the tensile strength, as it cracked and peeled prior to reaching the peak tensile strength, i.e. failing well before the stele. The diameter range of roots tested in tension was 0.39–10.2 mm for Sitka spruce and 0.48–9.1 mm for oak roots.

Eighty-two Sitka and 53 Oak samples were tested using three-point bending tests, loaded at 5 mm min^{-1} to a maximum deflection of 50 mm. The span length was varied in such as way that it exceeded $10 \cdot d_r$ to minimise the effects of shear on the results. Only for the two thickest oak ($d_r > 11$ mm) and Sitka samples ($d_r > 25$ mm) this ratio was slightly smaller (7.5–8.5) due to limited root length. Although a value of $L/d_r = 20$ was recommended for testing of wood and timber (Rowe et al., 2006), root lengths were insufficient to satisfy this criterion due to limited root lengths that could be collected and/or changing root properties over the length of the root, e.g. excessive tapering. The constant displacement rate meant that rates of strain in the extreme fibre of the root varied with root diameter and span length between approximately 0.9 and 6.0% strain per minute. The diameter range of roots tested in bending was 0.52–26.5 mm for Sitka spruce and 0.35–13.3 mm for oak roots.

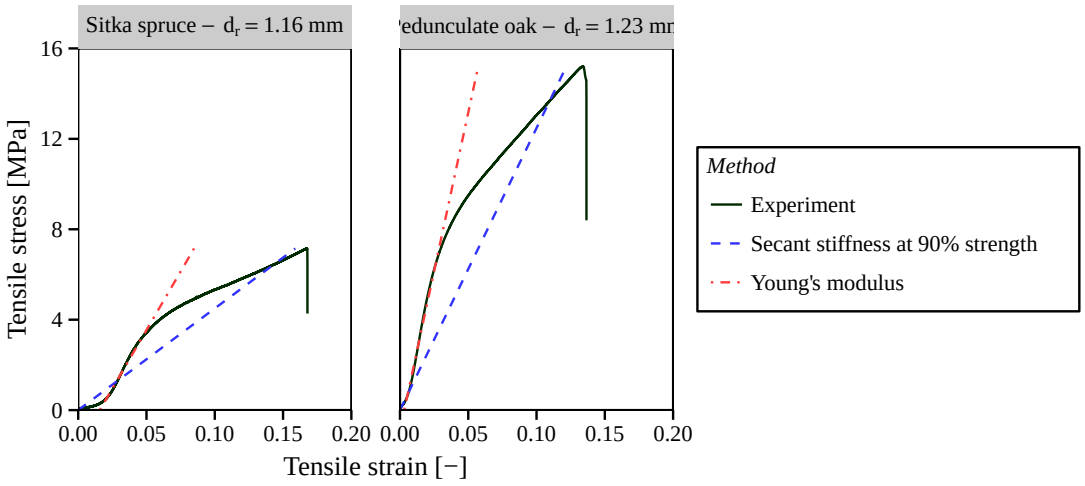

Figure 7.4: Example stress–strain curves for a Sitka spruce and pedunculate oak root tested in uniaxial tension. d_r indicates the tested root diameter.

Two stiffness parameters were determined from the test results: the initial tangent stiffness (Young's modulus, E), defined as the stiffness in the elastic region, and the secant stiffness at 90% of peak strength (E_{90}). The secant stiffness was more useful as a model input parameter (which assumed linear elastic root material properties) since it represented the real non-linear root stress–strain behaviour better, see Figure 7.4. Strength and stiffness parameters were fitted using exponential curves commonly adopted in root research, see Equations 2.1 and 2.2.

7.2.3 Field penetrometer testing

The blade penetrometer shape was similar to that used in previous laboratory testing, see Figure 3.3. The ∅10 mm penetrometer shaft was 500 mm long and connected via a 5 kN load cell to a screwjack. The screwjack was powered by a battery powered power drill (55 Nm maximum torque) to maintain a constant penetration rate. This resulted in a steady penetration rate of approximately 150 mm min^{-1}, of the same order of magnitude as the 300 mm min^{-1} as used before in the laboratory experiments described in Chapter 6. Details and a picture of the setup can be found in Figures 7.5a and 7.5b. Force and displacement were measured at 100 Hz using a data logger (CR3000 Micrologger, Campbell Scientific). The body mass of two operators, one on each side of the frame, served as a reaction mass. At each site, 8 blade penetrometer tests were performed.

Standard cone penetrometer tests were performed using the same standard agricultural penetrometer tip as used in laboratory experiments (∅12 mm 30° cone), mounted on the same frame as used for blade penetrometer tests. At Hallyburton Hill three successful traces were acquired and at Paddockmuir Wood four.

At Paddockmuir Wood, all tests were performed at 0.7–1.5 m distance from a dominant oak tree (diameter at breast height $DBH \approx 770$ mm). At Hallyburton Hill, tests were performed in the middle of the tree stand, with distances to the nearest tree ranging

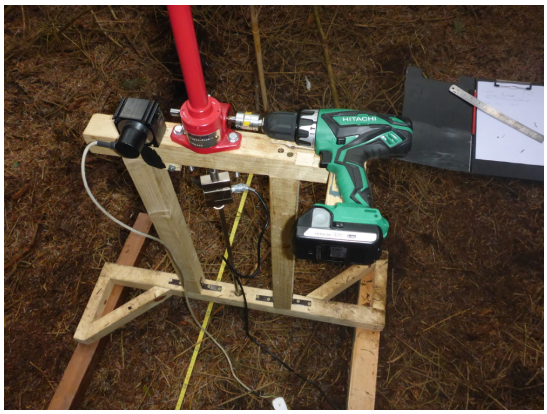

(a) Picture of the setup at Hallyburton Hill forest

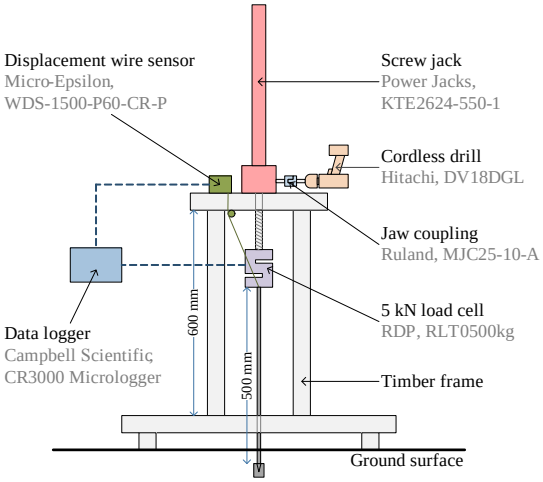

(b) Schematic

Figure 7.5: Blade penetrometer field measurement setup.

between 0.5 and 1.4 m. The maximum penetration depth was approximately 300 mm at Paddockmuir and 350 mm at Hallyburton Hill. Below these depths, soils were too stony for penetration.

In blade penetrometer tests performed at Paddockmuir Wood an acoustic microphone (Genius Multimedia Microphone MIC-01A) was placed in the soil at approximately 100 mm depth and at a distance of approximately 150 mm from the test location to study whether it was possible to record sounds associated with root breakage. Using microphones to detect root breakages has been successfully adopted before by Coutts (1983).

7.2.4 Root and stone measurements

Soil samples were collected to correlate penetrometer results to root and stone characteristics. At both sites, a large core sampler (height 110 mm, diameter 100 mm) with a cutting rim fitted with three 20 mm high cutting edges was subsequently used to extract large soil cores at the locations of each blade penetrometer test. A large ∅10 mm metal spike in the centre of the corer helped to keep the sampler in line with the hole left open by the penetrometer. The extracted cores were frozen after sampling and cut in two using a diamond saw to create two approximately 55 mm high samples. The total dry mass of each half was determined by weighing the frozen core and using the (fitted) soil water content measured using the 100 ml cores (see Figure 7.3 for the adopted fits).

During gentle washing with warm water on a 2 mm sieve, roots broken by the blade penetrometer could be identified. A root was classed as broken when the breakage occurred near the vertical centre line of the core. Breakages within 20 mm of the core side were assumed to be created by the sampling procedure and therefore discarded. The depth of broken roots was recorded and their diameters measured using the same procedure as used during root mechanical testing (Section 7.2.2).

Roots extracted from these large core samples were scanned and their diameters and lengths analysed using WinRhizo (Regent Instruments, version 2003b), using 0.1 mm wide diameter classes. During root washing, soil particles > 2 mm were collected and subsequently dried and sieved using 2, 4, 8 and 22 mm sieves to determine the mass fraction of gravel in the soil.

7.2.5 Data processing

In the measured depth–resistance profiles, a 'force drop' (sudden drop in blade penetrometer resistance) was defined as a zone where:

- The force continuously decreased over the whole range of the 'drop'.
- The force drops were at least 2 N, and was at least 4 times larger than the median value of drops encountered in a zone of 2 mm above and below the drop. This filtered out drops generated by signal noise without smoothing out potential force drops introduced by roots. A minimum threshold of 2 N was set because for smaller values it proved difficult to assess whether to drop was caused by a real root or by noise in the signal.
- The force drop gradient was larger than 200 Ns^{-1}. This threshold was decided based on an initial analysis of force drops that were recorded at the same time as a root was audibly heard snapping.
- The force did not rapidly increase before or after the potential drop. This filtered out electrical noise spikes in the measurements.

Numerous peaks were identified this way. For every drop, roots identified during root washing as broken were associated with this drop when the root depth was within a 20 mm distance of any point on the force peak. A margin was required since core sampling did not always provide good quality cores, introducing uncertainty in the actual root depths. When it was unclear at which depth resistance started to increase due to the presence of a root, this depth was estimated using $z_r = z_u - \alpha_f \cdot \Delta F$, where z_r and z_u are the depth levels associated with the start of the peak and the force drop, ΔF the magnitude of the force drop and α_f the gradient (assumed to be 15 Nmm^{-1} for Hallyburton Hill and 10 Nmm^{-1} for Paddockmuir Wood), based on peaks that could easily be identified.

Where single or multiple force drops could be related to single of multiple roots, the most likely force drop candidate was selected based on the shape of the peak and visual observations of broken root ends.

7.2.6 Interpretive models

Predictions of the root diameter were made based for every root identified as broken by the penetrometer, based either on measured force drop (F_u) or root displacement at the force drop (u_u), using the analytical bending model (assuming roots break in pure bending)

and analytical cable model (assuming flexible roots, breaking in tension) introduced in Chapter 5.

Both models required an estimate of the soil resistance parameter p_u (essentially the ultimate capacity of a p-y curve used to model the root–soil interaction, see Section 5.2). These estimations were based on the blade penetrometer resistance (F_{blade}) just after the force drop. The blade penetrometer resistance was multiplied by a factor α_1 to find the equivalent force for the standard penetrometer. This value was divided over the standard penetrometer tip area ($A_{std.tip}$) to find standard penetrometer resistance q_c [MPa]. The value for α_1 was found by comparing the average *in situ* measured blade penetrometer and standard penetrometer traces. Because the shape of the standard penetrometer (conical) was different from the root (circular), a second factor α_2 was used to estimate p_u. Here $\alpha_2 = 0.623$, based on comparing penetrometer results in laboratory testing with Reese and Van Impe (2011)'s model (Figure 6.6). Thus:

$$p_u \approx \frac{F_{blade} \cdot \alpha_1 \cdot \alpha_2}{A_{std\,tip}} = q_c \cdot \alpha_2 \tag{7.1}$$

The tensile model required an additional estimate for the soil–root interface friction (τ_i). For Hallyburton Hill, this value was based on an experimentally determined linear relation between vane shear strength in the soil (τ_{sv} [kPa], measured using a 50×34 mm cruciform blade, Edeco Pilcon hand vane) and standard penetrometer resistance (q_c [kPa]), see Figure 8.23.

$$\tau_{sv} \approx 13.4 + 0.0330 \cdot q_c,\ R^2 = 0.50 \tag{7.2}$$

To compensate for the root–soil interface friction being lower than the soil–soil friction, the soil frictional strength was reduced by a factor $f = 0.5$ (Gray and Sotir, 1996; Mickovski et al., 2009):

$$\tau_i = f \cdot \tau_{sv} \tag{7.3}$$

Because such a penetrometer versus shear strength dataset was not available for Paddockmuir Wood, predictions were made using the same shear strength–penetrometer relation as established at Hallyburton Hill.

The third and final model used assumed that the root peak force as measured with the penetrometer was equal to twice the root tensile strength. This model was only used to make predictions based on magnitude of the force drops and not from the peak displacement. The model assumed the root resistance is independent from the soil behaviour, and can be seen as a particular case of the analytical cable model where $\zeta \rightarrow \infty$, i.e. where the root is extremely flexible compared to the soil:

$$F_{u,\sigma_t} = 2 \cdot \frac{\pi}{4} \cdot d_r^2 \cdot \sigma_t \tag{7.4}$$

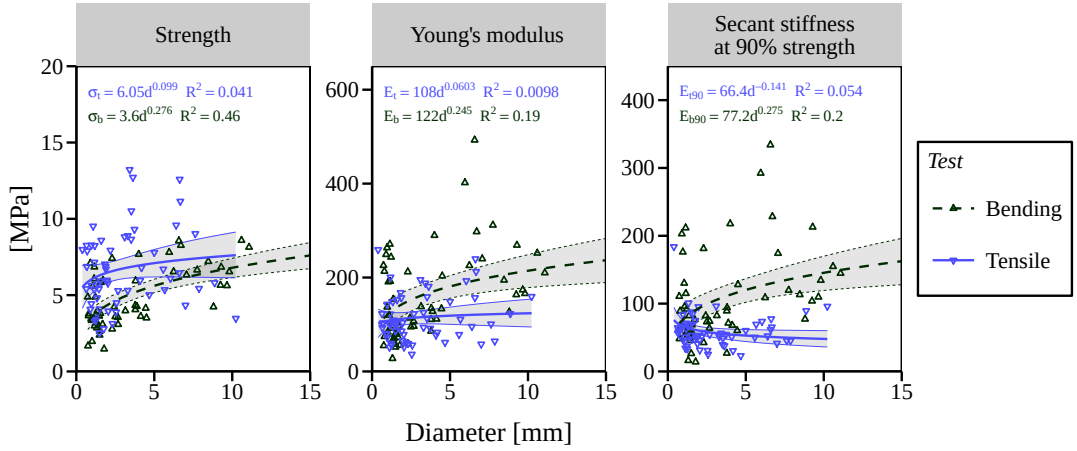

Figure 7.6: Root strength and stiffness for Sitka spruce roots from Hallyburton Hill, measured in uniaxial tension and three-point bending. The lines indicate the best power law fit and 95% confidence interval of the fit parameters.

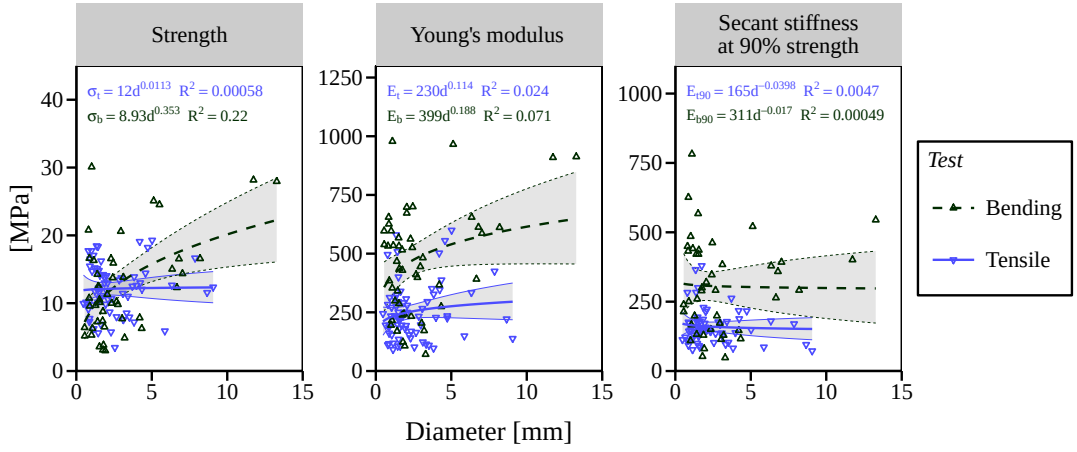

Figure 7.7: Root strength and stiffness for oak roots from Paddockmuir Wood, measured in uniaxial tension and three-point bending. The lines indicate the best power law fit and 95% confidence interval of the fit parameters.

7.3 Results

7.3.1 Root biomechanical characteristics

Tensile and three-point bending tests for both species showed weak strength–diameter and stiffness–diameter relationships (Figures 7.6 and 7.7). R^2 values were small, showing only weak diameter trends. Fitted power coefficients in tension test all were close to zero. The only statistically significant ($p \leq 0.05$) trend in tension was found for E_{90} for Sitka spruce (negative β coefficient). In bending tests, all power coefficients were positive and statistically significant, apart from E_{90} for oak roots.

The ratio between the secant stiffness at 90% strength (E_{90}) and Young's modulus (E) was on average 0.648 ± 0.020 (mean ± standard error, tension) and 0.558 ± 0.020 (bending)

Figure 7.8: Three-point bending test on barkless Sitka spruce root.

Figure 7.9: Three-point bending test on oak root.

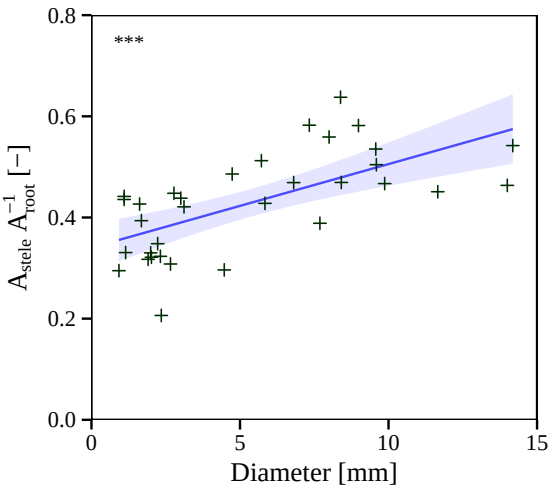

Figure 7.10: Ratio of stele (A_{stele}) over total root cross sectional area (A_{root}) for Sitka spruce roots with varying diameters.

for Sitka spruce roots. For oak roots, these ratios were 0.708 ± 0.025 and 0.778 ± 0.043 respectively. This showed root stress–strain behaviour is considerably non-linear.

None of the Sitka roots broke in bending despite significant post-peak strain. They behaved more like a bundle of fibres, where the fibres realigned during bending rather than ruptured. The material on the concave side buckled (Figure 7.8), suggesting that the root will not snap in pure bending. In contrast, in three out of seven bending tests on thick oak roots ($d_r > 6$ mm) tensile failure was observed on the convex side (Figure 7.9).

The cross-sectional area of 33 Sitka spruce roots was measured both before and after removal of the bark. This showed that for roots with larger overbark diameters a significantly ($p \leq 0.001$) larger part of the cross-section was taken up by stele (Figure 7.10).

7.3.2 Penetration resistances

When compared in terms of force, the blade penetrometer resistance was generally higher than the standard cone penetrometer resistance (Figure 7.11). Between 10 and 150 mm

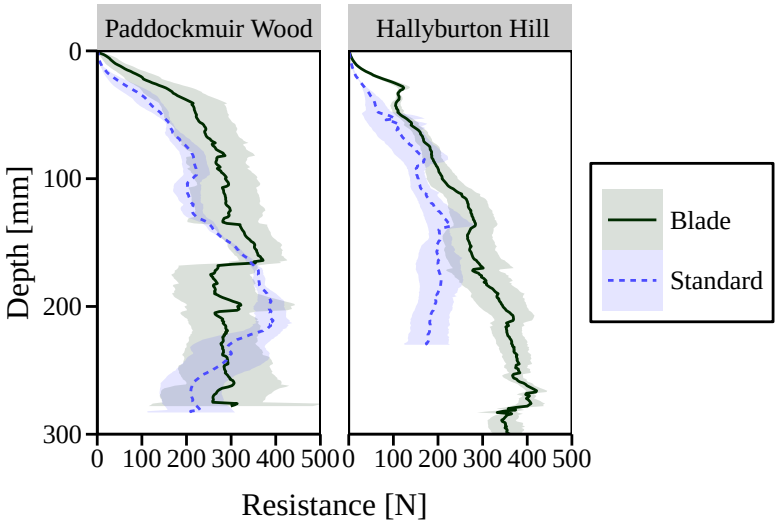

Figure 7.11: Average blade penetrometer and standard penetrometer resistance at Hallyburton Hill and Paddockmuir Wood. The shaded area indicates the mean resistance ± one standard error for each depth level.

depth, the blade penetrometer resistance force was roughly 70% higher (Hallyburton Hill: 72%, Paddockmuir Wood: 67%). Based on these results, during modelling $\alpha_1 \approx 0.588$ was assumed (Figure 7.12). Although the standard penetrometer resistance at Paddockmuir Wood was relatively greater between 150–250 mm depth, this was attributed to spatial variation in soil resistance and ignored while determining α_1. Below 250 mm depth the ratio between standard and blade penetrometer resistance reverted back to $\alpha_1 \approx 0.70$. Neither the blade penetrometer traces nor visual inspection of the soil horizons could explain this increased resistance between z = 150–250 mm.

7.3.3 Blade penetrometer results

Blade penetrometer traces for both sites are presented in Figures 7.13 and 7.14. The data for test 5 at Paddockmuir Wood was discarded because of faulty force measurements over part of the trace caused by an error in the data logger. Some traces at Hallyburton Hill (5, 7, 8) and Paddockmuir (2, 3, 4) exceeded the maximum penetration force (limited by the mass of the setup and body weight of the operators) before the target depth could be reached.

Many of the sudden force drops at Paddockmuir Wood were accompanied by a short spike in recorded sound levels. The short duration was considered to be indicative of root breakage. If the resistance would have been caused by something else, e.g. stones, sound peak with longer durations were expected, e.g. due to scraping between the stone and penetrometer.

The results for diameter predictions based on either the magnitude of force drop (F_u) or the lateral root displacement to failure (u_u) are presented in Figures 7.15 and 7.16 for

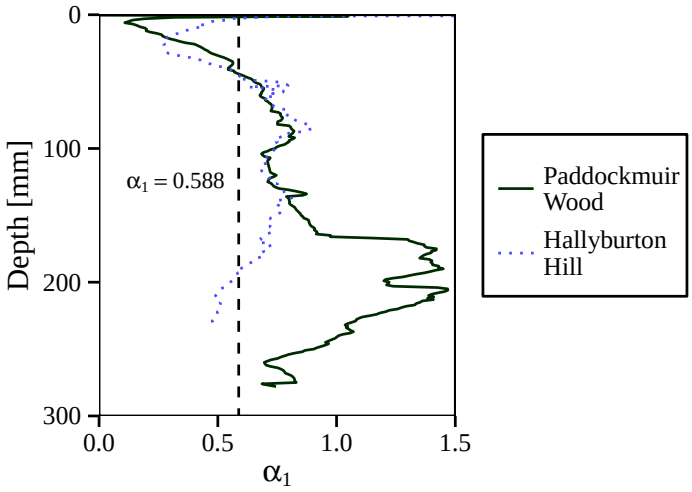

Figure 7.12: Ratio between standard and blade penetrometer resistance (force) α_1 as function of depth.

Hallyburton Hill and Figures 7.17 and 7.18 for Paddockmuir Wood.

At Hallyburton Hill, the best diameter predictions based on peak force were made using the cable model. These predictions were close to the simple 2× tensile strength approximation, indicating that the roots were flexible with respect to the soil resistance. The same held for predictions based on peak force at Paddockmuir Wood, but only for small diameter roots (d_r ≤2 mm). Thicker root diameters were better predicted using the bending model.

Predicted diameters based on the bending model displacement proved to be extremely inaccurate for both sites. Cable model displacements were more accurate at both sites, although still less accurate than diameter predictions based on F_u and showing more scatter. The predicted diameter based on u_u (analytical cable model) tended to be smaller than diameters measured, indicating that real root displacements were probably smaller than predicted, suggesting the soil resistance or root axial resistance might have been higher than predicted.

7.3.4 Surface reinforcement

At Hallyburton Hill forest, the blade penetrometer measured distinct peaks in reinforcement close to the surface (0–50 mm depth). These were absent in standard penetrometer traces (Figure 7.19). Similar results were found during initial blade penetrometer trials at the School Field near the James Hutton Institute (Dundee, UK, 56°27'28.6"N 3°4'2.7"W) which was covered with grass (Figure 7.20).

At Hallyburton Hill, positive and significant trends were found between the reinforcement, root volume (RV) and root length density (RLD), suggesting these reinforcement peaks were caused by roots (Figure 7.21). For School Field no correlations could be de-

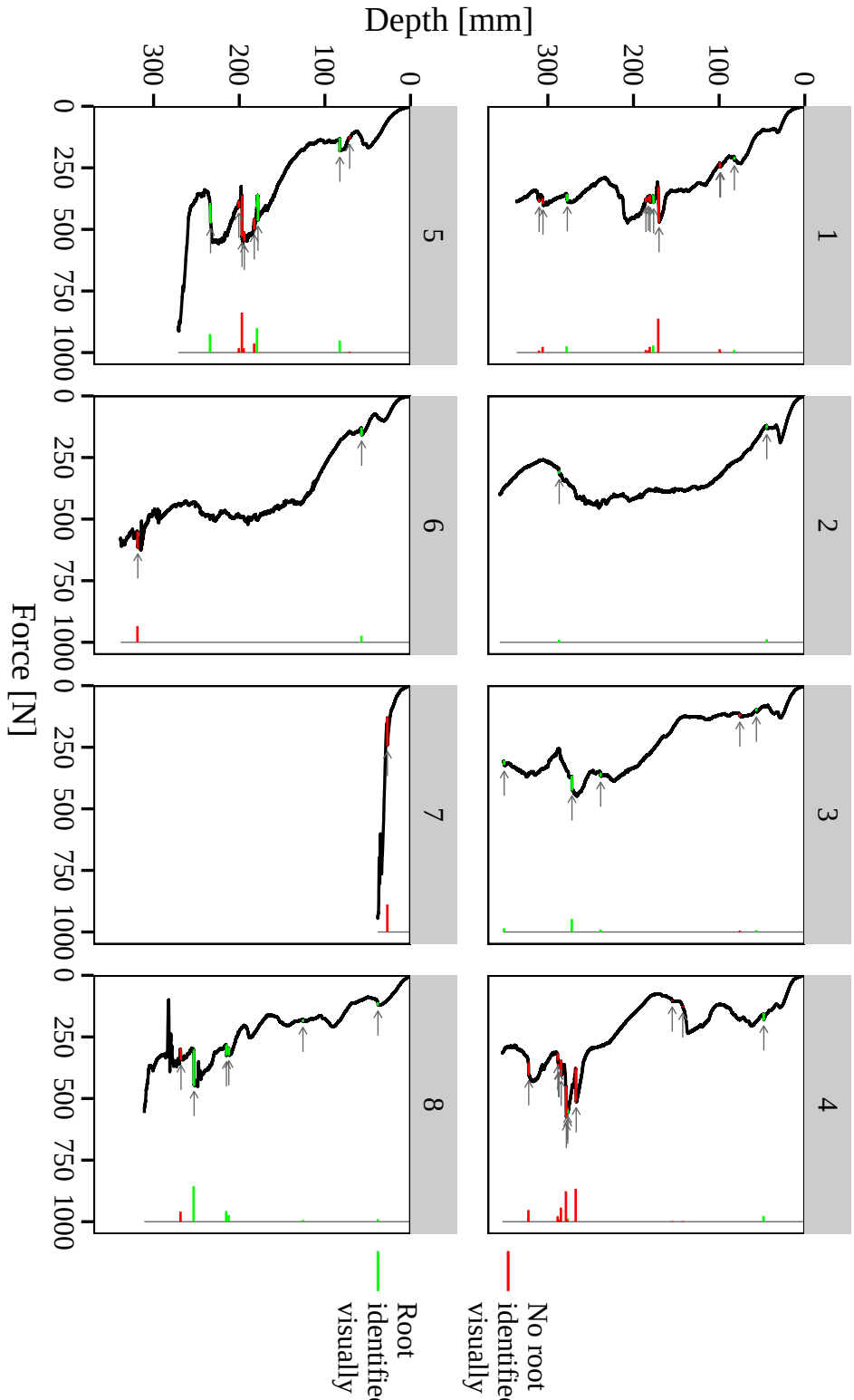

Figure 7.13: Blade penetrometer depth–resistance traces at Hallyburton Hill. Sudden drops in force are indicated in the graph with arrows. Colours indicate whether a drop was related to a root.

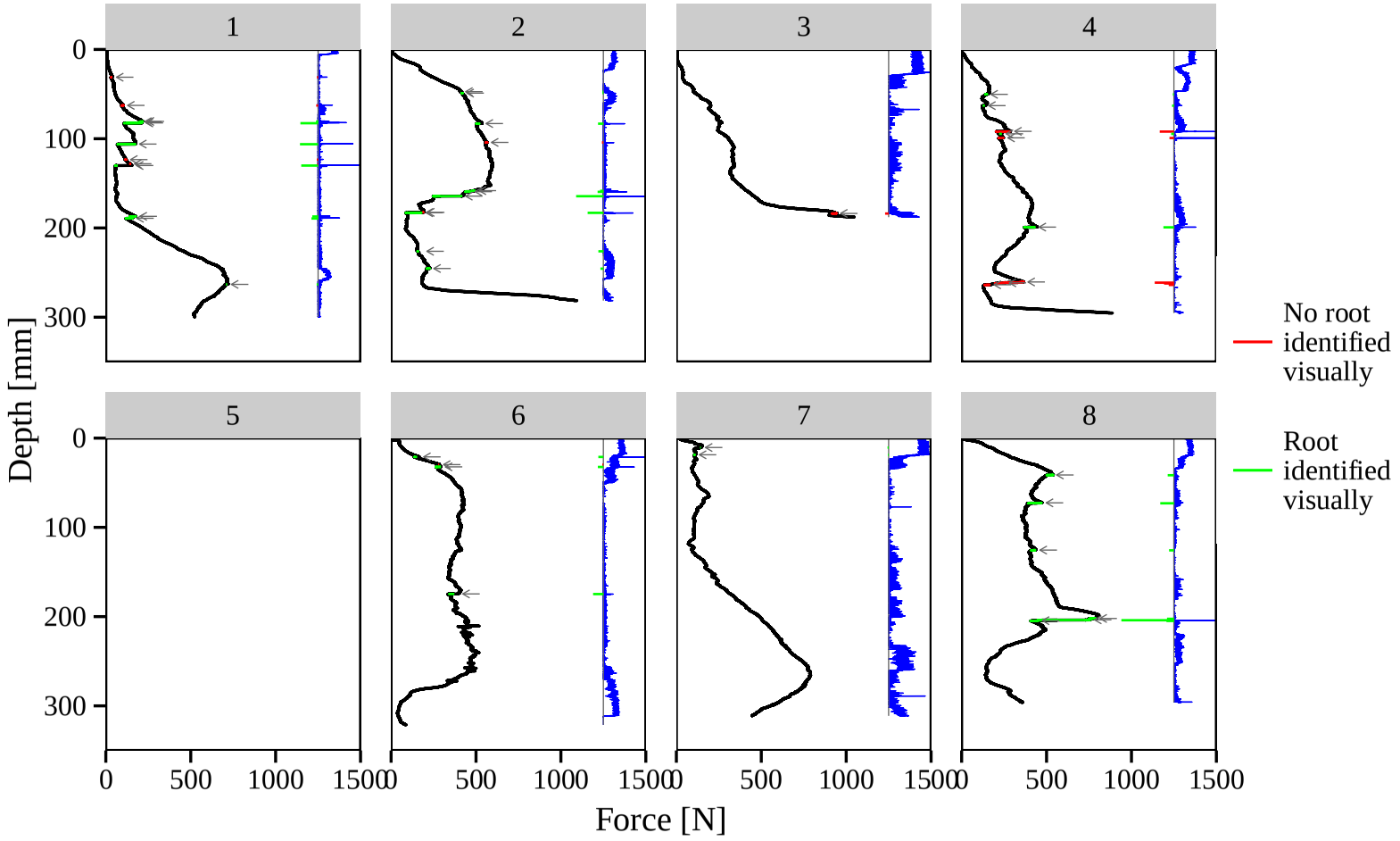

Figure 7.14: Blade penetrometer depth–resistance traces at Paddockmuir Wood. Sudden drops in force are indicated in the graph with arrows. Colours indicate whether a drop was related to a root. Blue traces (on the right of each plot window) are scaled $\log_{10}$-transformed measurements of the absolute value of the sound amplitude.

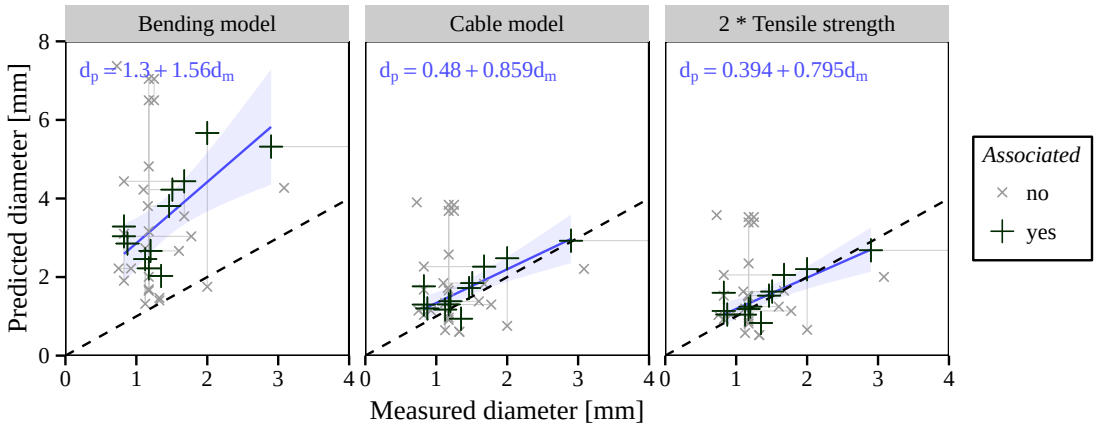

Figure 7.15: Root diameter prediction based on peak force at Hallyburton Hill. 'Associated' data points indicate the manually selected most likely combinations of root and force drop. Other points indicate all other possible combinations of root and force drop. Combinations belonging to the same root or force drop are connected by vertical and horizontal lines respectively.

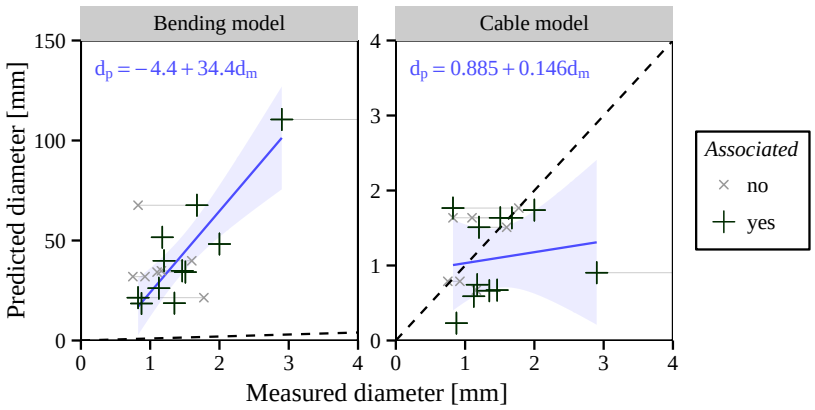

Figure 7.16: Root diameter prediction based on peak displacement at Hallyburton Hill. 'Associated' data points indicate the manually selected most likely combinations of root and force drop. Other points indicate all other possible combinations of root and force drop. Combinations belonging to the same root or force drop are connected by vertical and horizontal lines respectively.

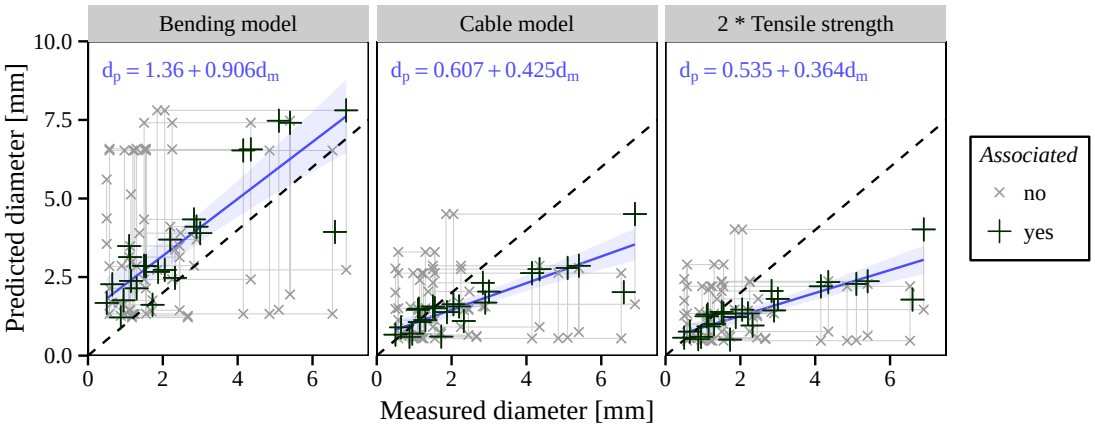

Figure 7.17: Root diameter prediction based on peak force at Paddockmuir Wood. 'Associated' data points indicate the manually selected most likely combinations of root and force drop. Other points indicate all other possible combinations of root and force drop. Combinations belonging to the same root or force drop are connected by vertical and horizontal lines respectively.

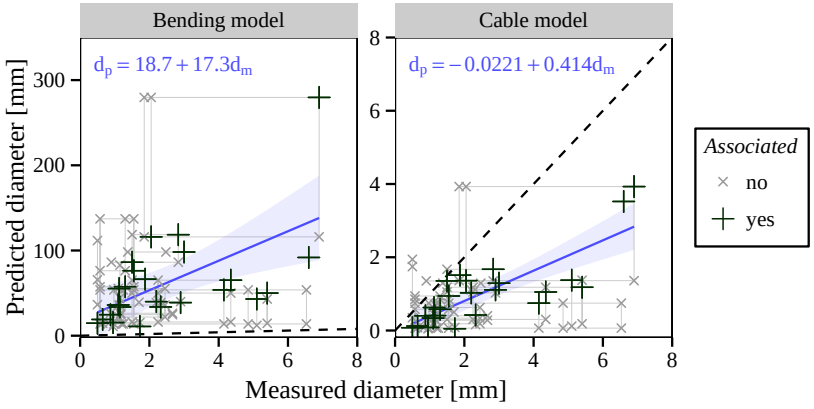

Figure 7.18: Root diameter prediction based on peak displacement at Paddockmuir Wood. 'Associated' data points indicate the manually selected most likely combinations of root and force drop. Other points indicate all other possible combinations of root and force drop. Combinations belonging to the same root or force drop are connected by vertical and horizontal lines respectively.

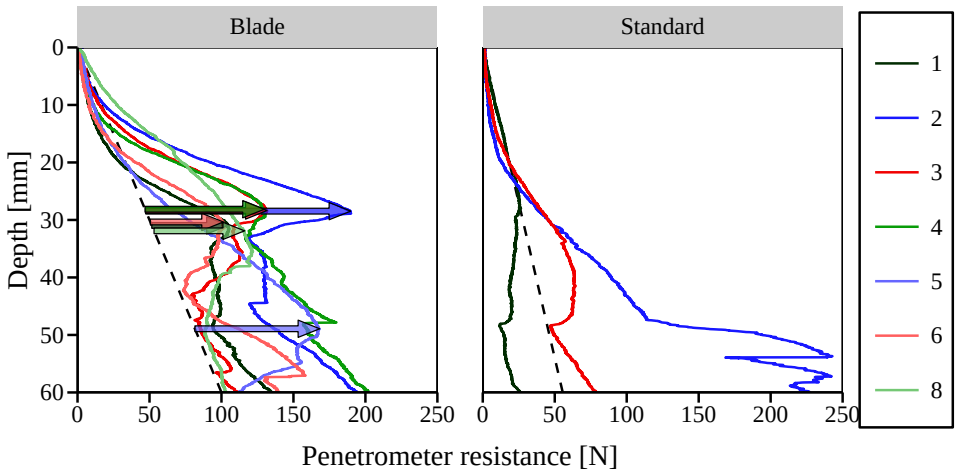

Figure 7.19: Blade and standard penetrometer resistance in the surface layer of Hallyburton Hill forest. Dashed lines indicate the estimated penetrometer resistance in 'fallow' soil. Coloured arrows indicate the depth and magnitude of the resistance peak.

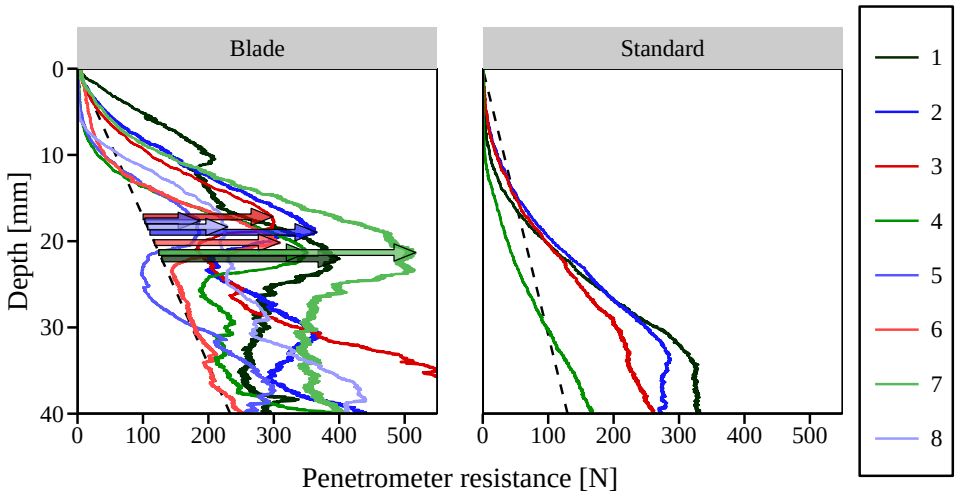

Figure 7.20: Blade and standard penetrometer resistance in the surface layer of School Field. Dashed lines indicate the estimated penetrometer resistance in 'fallow' soil. Coloured arrows indicate the depth and magnitude of the resistance peak.

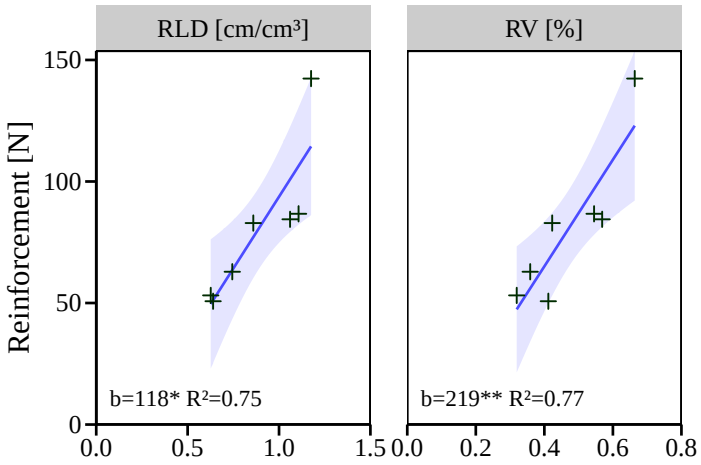

Figure 7.21: Correlations between surface blade penetrometer root-reinforcement and root length density (*RLD*) and root volume (*RV*). b indicated the gradient of the best linear fit through the origin. '*' indicates a statistical significance $p \leq 0.05$ and '**' means $p \leq 0.01$.

rived because root properties were not measured at every penetrometer hole. The average root length density in the top 50 mm of School Field was approximately 107 cm cm^{-3} and the average root volume 5.35%. Values for *RV* and *RLD* were determined by scanning and analysing roots collected from 100 cm^3 soil core samples, using WinRhizo.

These reinforcement peaks did not show any obvious sudden drops in force and therefore these could not be used to infer individual root diameters and properties. In fact, the behaviour under the penetrometer was much more similar to that observed in the laboratory tests using soil reinforced with polypropylene fibres (Figure 4.10). Therefore predictions for the magnitude of these peaks were made using measured root properties and the 'root mat penetrometer model', see Section 5.8. F_u and u_u were derived using the analytical cable model rather than the analytical bending model because blade penetrometer testing at Hallyburton Hill showed that distinct root breakages were much better predicted using the analytical cable model.

At Hallyburton Hill, root length densities and root volumes were determined from the frozen sample cores over depth intervals of 55 mm, see Section 7.2.4. Therefore, to take into account that roots were most likely to be found near the surface, separate model analyses were run assuming all roots were concentrated in the top 20, 30 or 50 mm. The model required an assumption for root orientation. If all roots were thought to be orientated horizontally, then $RLD_{model\ input} = RLD_{measured}$. If a random orientation was assumed then $RLD_{model\ input} = 0.5 \cdot RLD_{measured}$ (Bengough et al., 1992). Model predictions for both cases were made. Since no obvious force drops were observed, large roots ($d_r > 2$ mm) were disregarding in the analysis, i.e. the reinforcement was thought to be solely caused by fine surficial roots.

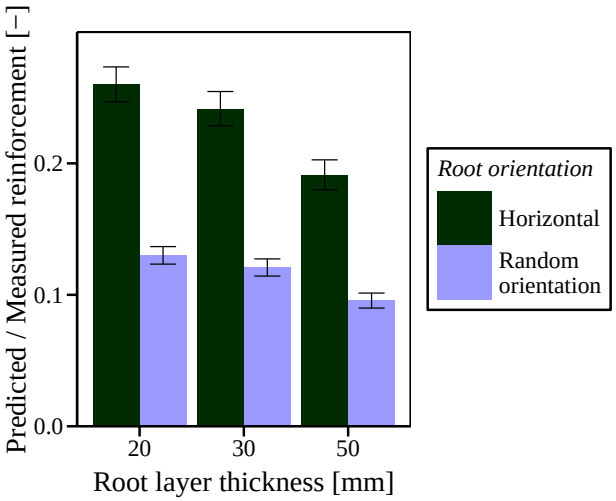

Figure 7.22: Comparison between surface reinforcement predictions (using the root mat model) and field measurements at Hallyburton Hill.

All model predictions were much smaller than reinforcements measured in the field (Figure 7.22). This suggests the root mat model did not accurately predict the reinforcement. This could be explained in various ways: 1) penetrometer experiments in the laboratory showed that analytical cable model struggled to predict the lateral root deformation u_u (see Figure 6.11). In the field, with real roots, the analytical cable model yielded lower values for u_u then measured (Figures 7.16 and 7.18). Potential explanations for these differences are discussed in Section 7.4. Since the root mat model required u_u as one of its input parameters, the model results might be inaccurate; 2) the root mat model assumed that there is no interaction between individual roots. However, these fine roots form intricate networks and it is therefore likely that this assumption was not valid.

7.4 Discussion

No root strength or stiffness data was found in the body of literature for either Sitka spruce or oak. Almost all reported tensile strength power coefficients for tree species are negative (Figure 9.1), in contrast to the values found here. However, none of these studies report statistical significance of their fitting parameters. A notable exception to the general negative trend is data for Norway spruce (*Picea abies*) reported by Vergani et al. (2014b) with power coefficients ranging between $-0.17 \leq \alpha_{\sigma,t} \leq 0.13$, depending on the sampling site (original fits reported in terms of force).

All of the tested roots were woody. Possible explanations for the increased strengths and stiffnesses of roots with larger diameters are: 1) thicker roots are generally older, and therefore stronger or denser tissue might have developed. Tensile strength increase with age has been observed before for tree roots (e.g. Genet et al., 2008); 2) the ratio of bark area over stele area was higher for thicker roots (as measured for Sitka spruce roots). Since strength and stiffness parameters were determined using the overbark diameter,

this approach might have resulted in higher apparent strength or stiffness values in thicker roots. Both predictive analytical models assume that root cross sections are homogeneous, i.e. strength and stiffness are equally distributed over the cross-sectional area. However, tensile testing showed that both strength and stiffness were concentrated in the lignified stele of the root.

The bending model assumed that the root fails when the strength of the outermost point of the cross-section is exceeded (i.e. elastical beam theory). While this type of failure was observed during three-point bending tests on thick oak roots, which ruptured in tension on the convex side, this was not observed for Sitka spruce roots. Instead, Sitka spruce roots buckled, explaining why the bending model does not work well for Sitka spruce roots.

This indicates that it is important to study the effects of root structure and biomechanics in more detail, as the root structure might govern the failure mode of roots under penetrometer loading and therefore define the most appropriate interpretive model to use.

Thin root diameters ($d_r \leq 2$ mm) broke in tension regardless of tree species. A possible explanation is that the axial stress scales less strongly with diameter ($\sigma_t \sim F \cdot d_r^{-2}$) than bending stress ($\sigma_b \sim F \cdot d_r^{-3}$) in a circular beam/rod. Therefore it is more likely that small diameter roots will be loaded to failure in tension more than thicker roots.

Root diameters predicted using peak force were more accurate than those predicted by peak displacement. Several explanations for this are put forward. Firstly, root displacement was more difficult to determine from the resistance trace than force, introducing additional inaccuracies. For many force drops, especially at Hallyburton Hill, the peak displacement could not be accurately determined resulting in a smaller dataset. Secondly, root displacement u_u depends greatly on assumed soil resistance p_u in both bending (Table 5.1) and cable models (Equation 5.28). The method for estimating p_u introduced many uncertainties, e.g. the assumed ratio between standard penetrometer resistance and resistance against root displacement (α_2) or the assumption that the penetrometer resistance just after a force drop is equivalent to the penetrometer resistance in fallow soil. In contrast, the force drop magnitude F_u in both models (Table 5.1, Equation 5.29) was much less affected by changes in p_u, making these diameter predictions more reliable. Thirdly, analytical models used the secant stiffness at 90% strength (E_{90}) and a linear elastic material model instead of using the real root stress–strain behaviour. This led to the modelled root strain to failure being underestimated in models, resulting in lower predicted values for u_u. Fourthly, roots in the field could have been tortuous. In that case, an additional root displacement would have been required to 'straighten' the roots, therefore resulting in larger measured values for u_u compared to those predicted using the analytical models, which assumed straight roots. These results corresponded with the results found for penetrometer testing with ABS root analogues in dry sand (Chapter 6), where the magnitude of the resistance peak could be predicted much more accurately than the displacement required to reach this peak.

At Hallyburton Hill, many drops in force were found that could not be associated with nearby roots, but were found in layers containing lots of gravel. This site had a higher gravel content than Paddockmuir Wood (Figure 7.3). This suggests that large stones might influence the test results. The results for Paddockmuir Wood indicate that using microphones, providing an additional independent measurement, might prove to be a useful tool in addressing this problem. Root breakages were shown to be audible as short duration bursts in sound amplitude. It is expected that stones will show a longer duration, scraping-like noise. This hypothesis should be tested in future work.

The root sampling methodology could not always establish which root corresponded to which force drop. Therefore each root could potentially be associated with several force drops and vice versa; this can introduce arbitrary elements into the interpretation process through manual association of roots with drops. Furthermore, not every drop was caused by roots, especially at Hallyburton. Despite this, clear trends could be observed in the data, especially at Paddockmuir Wood. Future work however should focus on the development of more reliable methods to identify which root corresponds to which force drop. In the laboratory, this might be performed using X-ray CT scanning during testing. *In situ* this will be more difficult. Potential methods might be 1) freezing the ground with subsequent block sampling, or 2) filling the penetrometer hole with resin or plaster to fix broken root ends in place, followed by block sampling.

Further development of this experimental methodology should focus on 1) applying this method to more soil and root types; 2) investigating the influence of root anatomy on its the mechanical behaviour, so that it is better understood when exactly roots might fail, especially in bending; 3) more accurate identification of which root belongs to which force drop; and 4) deriving a method to distinguish between root breakages and other artefacts in the soil, e.g. stones. For the latter, sound recording using microphones appears promising.

Combining in-situ measurements and interpretive models shows promising results and can be an easy in situ method to quantify root distribution.

7.5 Conclusions

- The diameter of roots broken during installation of the blade penetrometer can be estimated with reasonable accuracy from the sudden decrease in penetration resistance, given a good estimate for root strength, stiffness and soil resistance. Predictions based on penetrometer displacements required to break roots are less accurate.
- For the two sites and species tested, the analytical cable model provided the best results overall compared to the analytical bending model, indicating that roots (especially Sitka spruce roots) failed in tension rather than bending. Oak roots

thicker than roughly 2 mm at Paddockmuir Wood however failed in bending and the analytical bending model gave much better predictions. The difference in behaviour between oak and Sitka root behaviour could be attributed to differences observed during 3-point bending tests in the laboratory. These differences showcase the importance of root biomechanics.

- At Paddockmuir Wood, the breakage of roots could be detected from sound recordings made during penetration. This might be a useful, cheap and simple additional tool to distinguish between root breakages and other artefacts affecting the depth–penetration trace, for example stones.
- Where root-reinforcement was identified but without distinct force drops (e.g. in soil reinforced with a 'mat' of fine roots), the magnitude of the root-reinforcement was shown to be correlated to root quantities measured. However, the used 'root mat' predictive model was not able to accurately predict the reinforcement.
- The blade penetrometer, combined with interpretive models, can be a straightforward method to assess the spread and diameters of a root system without the requirement for extensive excavation. Tests are quick to perform. However, more calibration work and a better understanding of the root behaviour is required.

8

Shear strength methods: field testing

Large parts of Sections 8.2 and 8.3 have been published as a conference paper, see Meijer et al. (2015).

8.1 Introduction

Laboratory testing (Chapter 4) showed that both the pin vane and corkscrew device have potential for directly determining the shear strength of reinforced soil. To study the behaviour of these new methods in more realistic conditions, they were tested in various field conditions.

In subsequent experiments the level of complexity was increased. First, both new methods were compared with existing shear strength measurement techniques in non-rooted field soil to establish whether they yield reliable results (Section 8.2). Thereafter, a small experiment was performed to qualitatively study the behaviour of both devices in rooted soil (Section 8.3). The corkscrew method was then applied at two different field sites (agricultural field and conifer forest) with different vegetation (blackcurrant shrubs and Sitka spruce trees) to quantitatively study its behaviour in rooted soil (Section 8.4). Finally, the corkscrew was taken to a vegetated slope for larger scale field trials (Section 8.5).

8.2 Comparison with existing methods in fallow soil

8.2.1 Introduction

Since both the pin vane and corkscrew methods were newly developed, it was not known *a priori* whether both the corkscrew and pin vane methods yielded reliable shear strength results. Therefore their behaviour was compared in non-rooted soil to two existing shear strength testing techniques: field shear vane testing and laboratory direct shear testing.

Figure 8.1: Resting agricultural field used to compare new test methods in fallow soil.

The aim of this experiment was to establish whether the new and established measurement methods yielded similar strength results in non-rooted soil. This would determine whether the new methods could reliably measure the soil shear strength.

8.2.2 Methods

Test were performed at Bungalow Field near the James Hutton Institute, Dundee (56°27'26.1"N, 3°3'58.2"W), in August 2014. This site was an agricultural field in fallow. No vegetation was present apart from some small and shallow rooting weeds with small root systems which were easily avoided (Figure 8.1). The soil was classified as a low plasticity sandy clayey silt (57% sand, 32% silt, 11% clay) based on unpublished soil survey data held by the James Hutton Institute. Four days prior to testing the site was irrigated to decrease the soil strength because initially the soil was very dry and hard.

Soil density and gravimetric water content were measured immediately after testing using 100 ml steel cores. Field suctions were measured using field tensiometers at various depths (model SWT4R, Delta-T), see Figure 8.2.

Tests were performed over the course of two days on the central 2×2 m area of the irrigated plot, with two test locations for each test method (corkscrew, pin vane and standard vane) in each 1×1 m subplot to account for spatial and temporal variability.

The corkscrew device was manually screwed into the soil. Once the desired depth was reached, a wooden tripod (model GST101, Leica Geosystems, selected for its rigidity, see Nindl and Wiebking, 2010), was placed over the top to facilitate extraction. A manual winch was aligned vertically above the corkscrew on top of the tripod. The target extraction rate was 100 mm min^{-1}, in line with the displacement rates of landslides and previous laboratory studies in this thesis (Figure 4.6). A 3 mm diameter steel wire connected the winch to the corkscrew via a 5 kN load cell (model RLT0500kg, RDP Group) with a linearity of ±0.03% of the full scale output. Displacements were measured using a draw

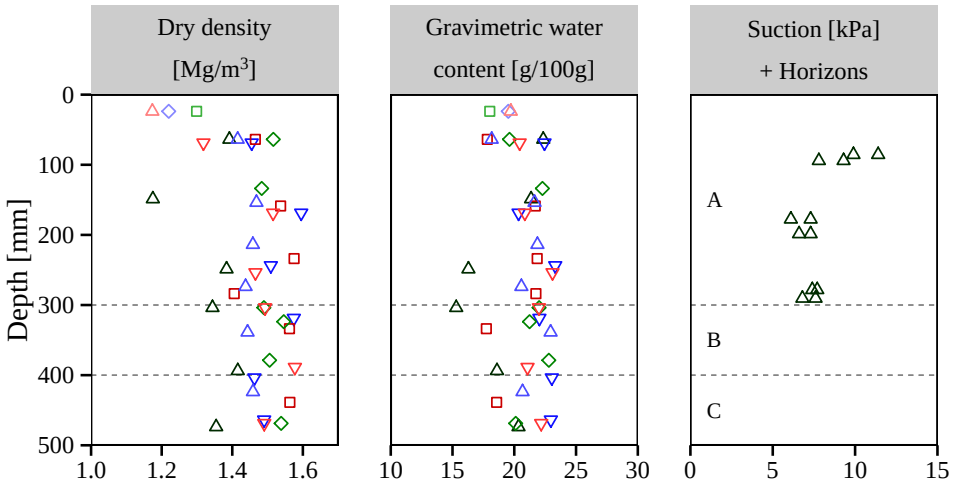

Figure 8.2: Dry bulk density, gravimetric water content, suction pressures and soil horizons at Bungalow Field. 'A' indicates the topsoil layer, 'B' the subsoil layer and 'C' the layer of parent rock material.

wire sensor (model WDS-1500-P60-CR-P, Micro-Epsilon, linearity ±1.5 mm). Both force and displacement were logged at a frequency of f_s = 100 Hz using a data logger (model CR3000 Micrologger, Campbell Scientific). A schematic of the test setup is presented in Figure 8.3. Corkscrew tests were performed at four depth levels (0–125, 125–250, 250–375 and 375–500 mm) with eight replicates per depth level.

Pin vane shear strength was measured using a digital torque wrench (Clarke PRO235 3–30 Nm) while an hand vane (Edeco Pilcon) was used to measure residual shear strength. Residual strengths were defined as the maximum measured strength between 360 and 720° rotation. For comparison purposes, soil shear strength was also measured using a standard 34 mm diameter 50 mm high cruciform vane blade, using the same equipment as used for pin vane measurements. Each vane test was replicated 8 times for each depth (50, 150, 250, 350 and 450 mm, measured at the centre of the vane).

Soil core samples (100 mm diameter × 130 mm height) were collected for laboratory direct shear tests. Steel cores were driven into the soil using a hammer and hammer block. Less destructive techniques could not easily be adopted because of high soil strength. Samples were subsequently dug out and stored at 4°C in sealed bags for a maximum of 7 days to minimise evaporation. Samples were extruded from their sampling cores using a hydraulic press and sheared in a custom laboratory direct shear apparatus (DSA) with the same diameter. The bottom (moving) part and top (fixed) part were 80 and 50 mm high respectively. Such a large shear box was adopted because similar or even larger devices are typically used to measure root-reinforcement (e.g. Waldron, 1977; Waldron and Dakessian, 1981; Operstein and Frydman, 2000; Normaniza et al., 2008; Mickovski et al., 2009; Loades et al., 2010). All samples were subjected to similar overburden pressures as experienced in the field by stacking small weights on top of the top cap.

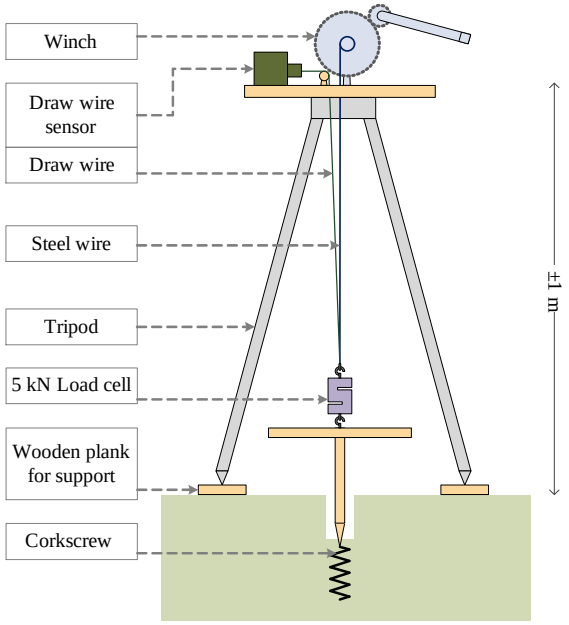

Figure 8.3: Schematic drawing of corkscrew field setup.

Force and displacement were measured using a 1 kN load cell (RLT0100kg, RDP Group) and a PD20 displacement sensor (Pioden Controls). Samples were sheared to 25 mm at a displacement rate of 2 mm min^{-1}, the fastest rate that could be adopted. Residual strengths were defined as the average strength over the 20–25 mm displacement interval.

8.2.3 Results and discussion

Below approx. 250 mm depth, the pin vane, standard vane and corkscrew methods all produced comparable results (Figure 8.4). This suggests that the potential stress reduction due to excavation in pin vane and corkscrew (as tests were performed in holes left open by testing at shallower depth) has a small effect. Near the soil surface, corkscrew results were smaller by comparison.

Peak strengths measured using the direct shear apparatus were much lower than those measured with the other three devices. This was probably caused by soil disturbance because of hammering cores during sampling. The residual strength of both vane tests and direct shear tests were similar, reinforcing this soil disturbance hypothesis.

The residual strength measured using the corkscrew tests was significantly higher at depths below 250 mm, compared with the vane readings. The most likely explanation was that the corkscrew was not extracted purely vertically, creating extra friction on one side of the corkscrew. This effect was thought not to have influenced the peak strength since the peak resistance was mobilised at small displacements ($u_{peak} < 15$ mm in all but 4 tests).

Typical failure mechanisms observed during tests in the fallow soil (Figure 8.5) suggested that the assumed cylindrical failure for both pin vane and corkscrew tests (Equations 3.3 and 3.4) were valid.

Soil heave was observed during corkscrew tests in the surface layer (Figure 8.6), similar

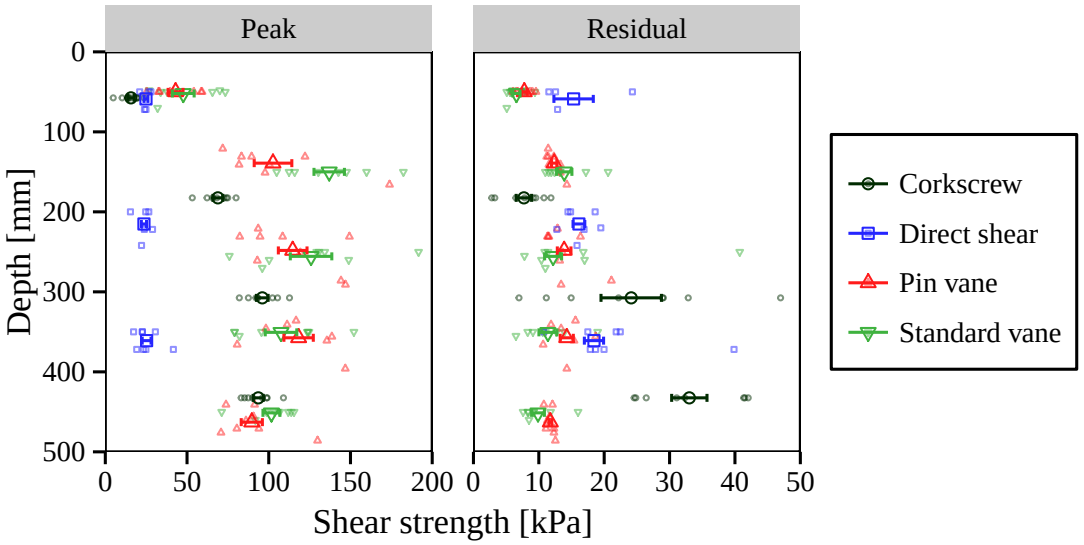

Figure 8.4: Peak and residual shear strength measurements in fallow soil at Bungalow Field. Per cluster of data points, the mean (large symbol) and standard error to the mean (horizontal line) are plotted over the raw data (small symbols).

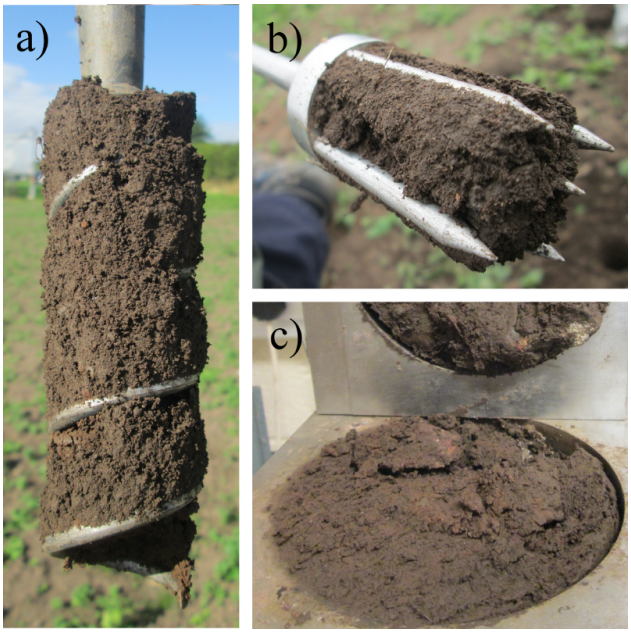

Figure 8.5: a) Corkscrew, b) pin vane and c) laboratory direct shear failure mechanisms in fallow soil.

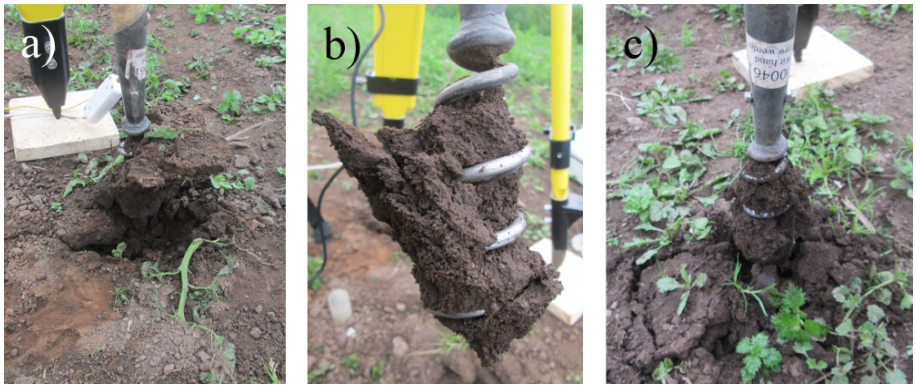

Figure 8.6: Heave in corkscrew tests at 0–125 mm depth in fallow Bungalow Field soil.

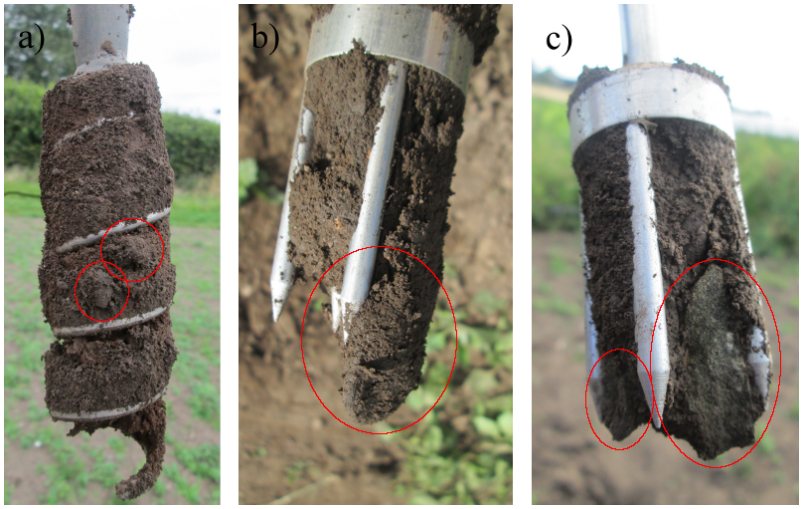

Figure 8.7: Stones in extracted corkscrew and pin vane soil plugs.

to corkscrew testing in the laboratory (Chapter 4). This provides an explanation for lower measured peak strengths near the surface compared with vane readings.

The relatively large scatter in pin and standard vane peak shear strength could not be explained by spatial shear strength variation (comparing nearby pin vane and standard vane tests) or by variation in the soil bulk density and water content. Variations in shear strength were therefore possibly caused by local variations in soil strength, especially through the presence of small (< 20 mm diameter) stones, see Figure 8.7. In some tests, scraping noises were heard during vane rotation and stones were observed in extracted corkscrew and pin vane soil plugs.

During interpretation of the corkscrew and vane tests, the shear band thickness was assumed to be negligible as d_{cs} and d_{pv} were assumed to be equal to the diameter of the device. Shear strength might therefore be slightly overestimated as the soil was sandy and only partially saturated, making a finite shear band thickness likely. However, no large soil disturbance was observed around the cylinders, indicating that this effect was probably small in the tested soil.

Both corkscrew and pin vane methods appeared to be suitable for use in quantifying

root-reinforcement of soil. Peak and residual strength readings were similar to standard vane readings in fallow soil. Corkscrew tests were shown to be less reliable when used near-surface, because the assumed cylindrical failure mechanism was not valid due to conical heave failure.

Pin vane testing proved to be more difficult at larger depth. Holes had to be excavated prior to testing, potentially disturbing the soil. Furthermore, pushing the pin vane down might have compacted the soil because of the solid disk on top of the pins and because it was difficult to verify when the pin vane had reached the right depth. Furthermore, because of its smaller size compared with the corkscrew it was more difficult to use in layers where gravel and cobbles were present. Because of these effects, it was concluded that corkscrew testing is more viable when the strength of deeper layers ($z > 250$ mm) is to be assessed. At shallow layers ($0 \leq z \leq 125$ mm) however the pin vane was considered to be the superior device because the corkscrew underestimated the soil strength values because of a different failure mechanism near the surface (conically shaped heave).

8.3 Qualitative field tests in rooted soil

8.3.1 Introduction

The previous experiment showed that both the pin vane and corkscrew measurement devices yielded similar results to standard vane testing in fallow soil. In the following experiment, the behaviour of both the corkscrew and pin vane device was qualitatively studied in rooted soil to study how they function in field soil containing real roots.

8.3.2 Methods

Testing was done on a grass-rooted plot at one metre distance from a row of mature Scots pine (*Pinus sylvestris*), see Figure 8.8, on the western side of School Field, near the James Hutton Institute, Dundee (56°27'30.4"N, 3°4'2.7"W), in October 2014. Trees were spaced approximately 2 m apart. Two days prior to testing the site was irrigated to reduce the soil strength as the soil was very dry and hard. Because of the close proximity to the tests at School Field, the same soil type was assumed (sandy clayey silt).

Soil bulk density, water content, suction and soil horizon data are presented in Figure 8.9. Root were samples using 100 ml steel cores, subsequently washed, scanned and analysed for length and diameter using WinRhizo (version 2003b). In the surface layer (0–50 mm depth) root volumes ranged between approximately 2 and 4%. Between 50 and 220 mm depth, the average root volume was 1.24% with no clear depth trend. The average root diameter was $d_r = 0.79 \pm 0.18$ (mean ± standard deviation), again with no clear depth trend.

No attempts were made to correlate the variation in measured strengths to the variation in root quantity because root quantities were determined from core samples taken at

Figure 8.8: Field site used for qualitative field trials in soil rooted with grass and Scots pine roots (School Field).

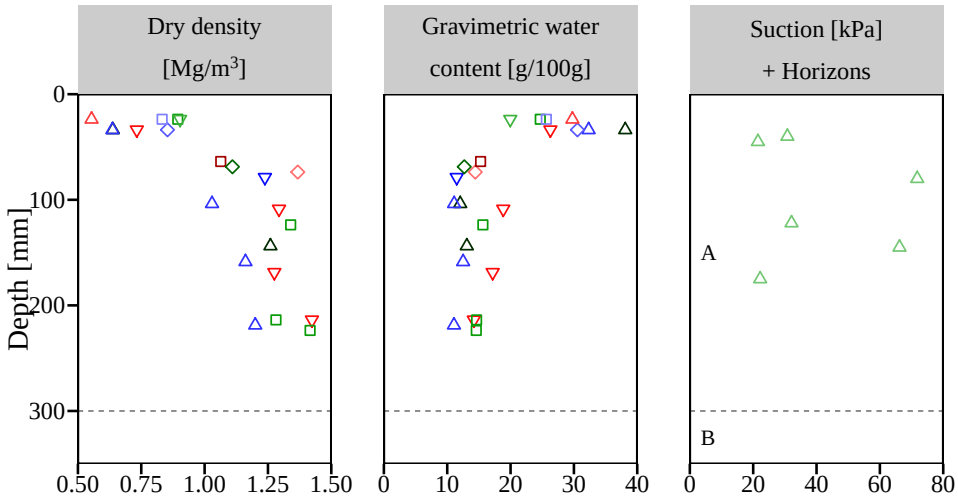

Figure 8.9: Dry bulk density, gravimetric water content, suction pressures and soil horizons at School Field.

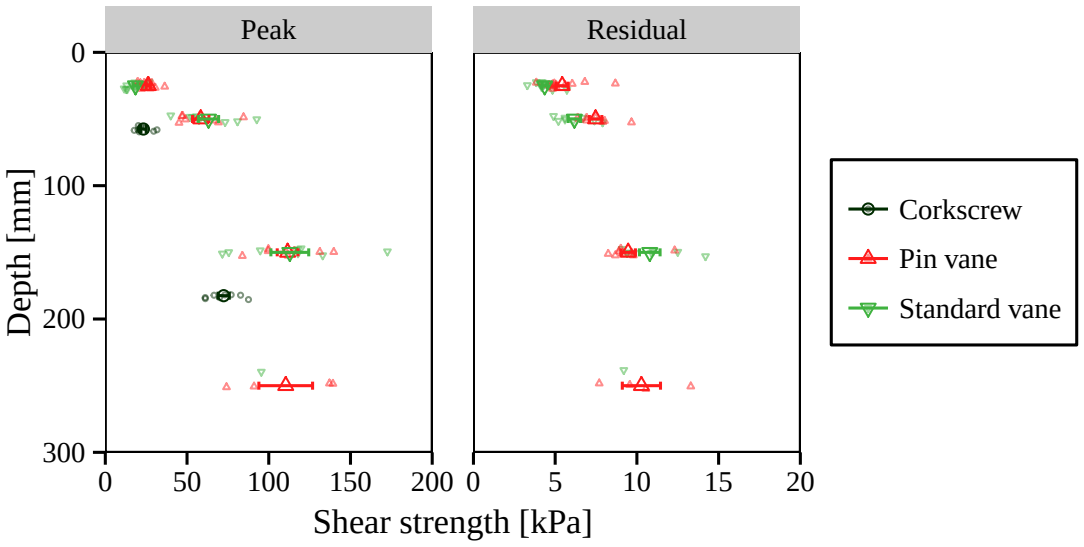

Figure 8.10: Peak and residual shear strength measurements in rooted School Field soil. Per cluster of data points, the mean (large symbol) and standard error to the mean (horizontal line) are plotted over the raw data (small symbols).

different locations (though near to the shear strength measurements). The experiments described here purely functioned to gain qualitative insight in the behaviour of the test methods in rooted soil.

Eight corkscrew, pin vane and standard vane tests were performed per depth up to a depth of approximately 300 mm. Corkscrew tests were performed at 0–125 or 125–250 mm depth, and vane tests at 50, 150 and 250 mm depth (soil below 300 mm was too difficult to penetrate). Twelve additional standard and pin vane readings were taken in the surface layer (0–50 mm) to study their behaviour in densely rooted grass. In this case, the standard vane shear strength was corrected for the lack of shear resistance on top of the shearing cylinder.

The same equipment and measurement procedure as used during the experiments in fallow soil (Section 8.2) were used.

8.3.3 Results and discussion

The results for both peak and residual strength measured in the rooted soil are presented in Figure 8.10. At first glance, pin and standard vane results appeared to be very similar. Corkscrew results were smaller, especially at 0–125 mm depth, just like in the fallow field (Section 8.2). Observed soil heave, similar to mechanisms observed in laboratory testing and fallow field testing, was the most likely cause.

When pin and standard vane results were statistically compared using t-tests, significant differences showed for tests done in the surface layer (0–50 mm). Pin vane peak strength results were 43% higher (n = 12, p = 0.0005) and residual strengths 25% higher (n = 12,

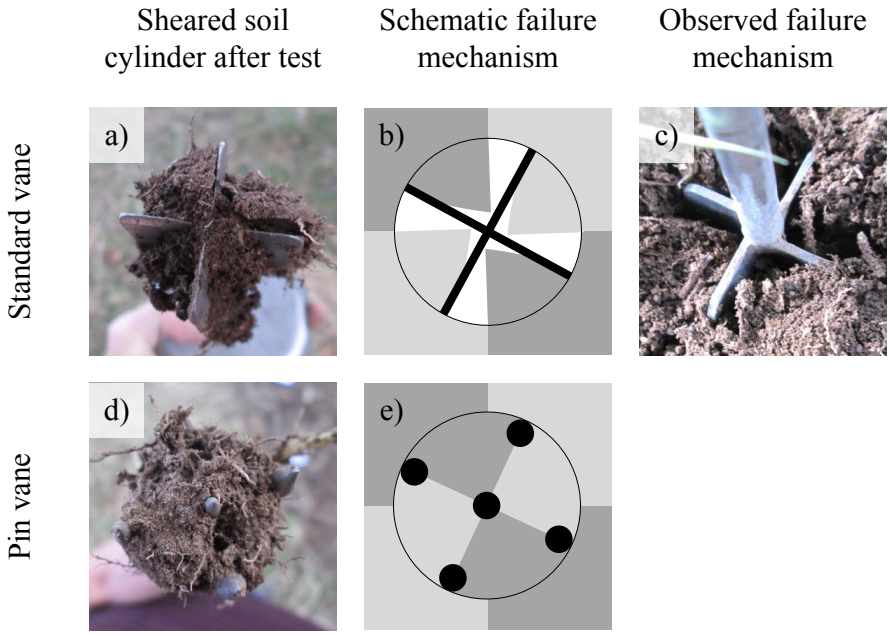

Figure 8.11: Schematic and observed pin vane and standard vane failure mechanisms during tests at 0–50 mm depth.

$p = 0.017$). At other depths, no significant differences were found apart from at 50 mm depth where the residual strength measured using the pin vane was 21% higher than those measured with the standard vane ($n = 8$, $p = 0.030$). Two phenomena providing an explanation for this effect were observed. First, during standard vane installation in the heavily rooted top layer disturbance was observed. Secondly, during the shearing phase in the surface layer (0–50 mm depth) in standard vane test voids opened up behind the vane blade and the soil in each vane quadrant was heavily distorted, in contrast to pin vane tests (Figure 8.11). Therefore it was concluded that the extra tensile strength introduced by the roots keeps the soil cylinder intact during pin vane shearing. The pin vane method was therefore thought to be more accurate than the standard vane device in heavily rooted layers.

The depths where significant differences occurred coincided with heavily rooted zones, therefore suggesting that the pin vane gave higher readings in rooted soil. The observed disturbance during installation and shearing of standard vane tests was in line with similar observations for fibrous peats (Landva, 1980).

Both the pin vane and corkscrew method yielded soil cylinders containing roots ends (Figure 8.12). This demonstrated that both methods did not suffer much from disturbance problems during installation of the device, making them suitable to use in root-reinforced soil because many roots will still be intact prior to shearing.

Inspection of the holes after corkscrew testing revealed some larger diameter roots ($d_r \geq 2$ mm) broken during testing. The effect of these roots could be observed in the corkscrew shear strength–displacement traces (Figure 8.13). After a certain displacement,

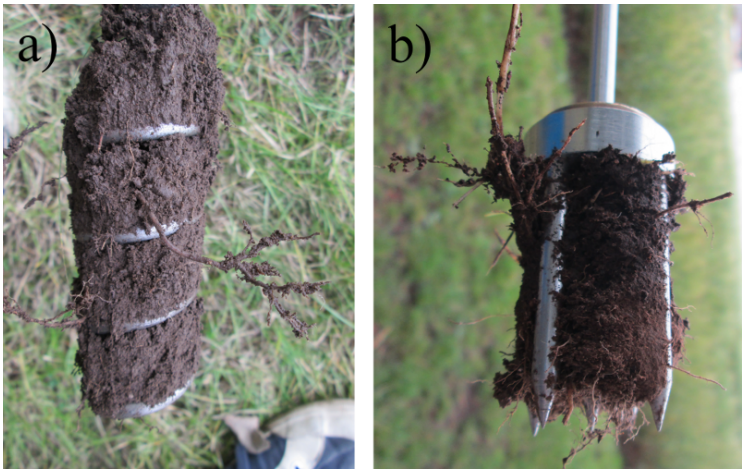

Figure 8.12: Failure mechanisms in rooted soil, measured with a) corkscrew and b) pin vane device.

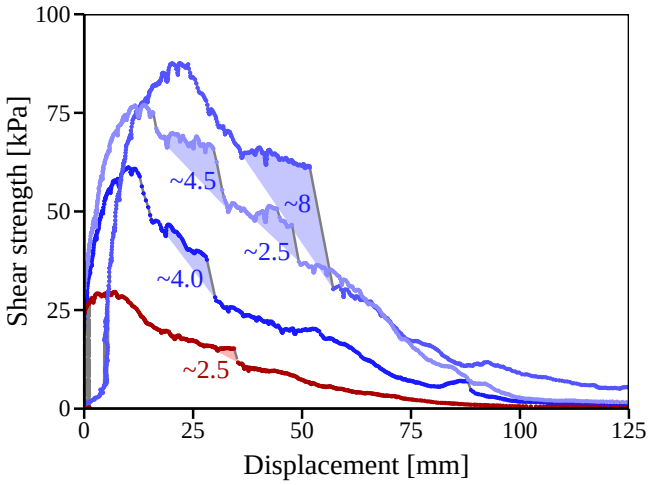

Figure 8.13: Example corkscrew extraction traces in rooted soil (School Field). Blue solid traces indicate tests performed over 125–250 mm depth and red dashed traces indicate tests at 0–125 mm depth. Shading indicates assumed mobilisation of a root and the number the measured diameter of the associated root.

root resistance was mobilised. After some more displacement, roots suddenly broke, observable as a sudden decrease in resistance only lasting a couple of tens of milliseconds. This is similar to observations during corkscrew testing using ABS rods under lab conditions (Figure 4.14) and root breakages observed in blade penetrometer testing. However, in these field tests the roots had no effect on the peak shear strength since they only mobilised after a displacement larger than the displacement required to reach the peak strength of the soil. The extra resistance the roots added did not compensate for the loss in soil resistance caused by large soil strains. This showed the importance of taking both soil and root stress–strain effects into account while quantifying root-reinforcement.

This experiment showed that the pin vane worked well in shallow soil, even when densely rooted with fine fibrous roots. The strength in these surface layers, important for erosion resistance, was underestimated using the corkscrew device because of heave near

the surface.

8.4 Detailed corkscrew field trials

8.4.1 Introduction

The previous two experiments showed that the corkscrew was easier to use in deeper soil layers (e.g. $z > 250$ mm) compared with the pin vane. Because these deeper layers are important for analysing landslide susceptibility, the behaviour of the corkscrew device was studied in more detail. Measurements were performed at two field sites rooted with contrasting species (one with shrubs and one with trees). Root mechanical properties and root size distributions were measured to compare the measured root-reinforcements to existing root-reinforcement models (Wu/Waldron model (WWM) and various fibre bundle models (FBM)). This experiment aimed to quantify the mechanical effect of roots on the strength of field soil.

8.4.2 Methods

Corkscrew device

For both sites, a similar corkscrew was used as in previous testing (Figure 3.3). The adopted field setup was similar to the one used in previous field experiments (Section 8.2), see Figure 8.3. The average pull-out rate was 120 mm min^{-1} (established using logged displacement data), in line with the displacement rate of slow landslides (Davies et al., 2010) and previous experiments.

To capture the increased ductility of the soil (as observed during previously described laboratory tests using soil rooted with polypropylene fibres, see Chapter 4) with a parameter independent from the peak strength, the normalised energy dissipation parameter (W_n) was introduced. This dimensionless parameter was defined as the total work required to move the corkscrew from displacement $u = u_1$ to $u = u_2$, normalised over the product of the peak extraction force (F_{peak}) and the displaced distance, i.e.:

$$W_n = \frac{1}{F_{peak} \cdot (u_1 - u_0)} \cdot \int_{u_0}^{u_1} F(u) \cdot \mathrm{d}u \tag{8.1}$$

In this study, $u_0 = 0$ mm and $u_1 = 100$ mm was adopted. The chosen value for u_1 was considerably larger than the displacement required to reach the soil yield point and roughly coincided to the corkscrew displacement required to lead (almost) all roots to failure.

Field sites

Measurements were performed at two sites.

The first site was Bullionfield (Figure 8.15), near the James Hutton Institute, Invergowrie, UK (56°27'31.3"N, 3°04'15.1"W). Testing was performed over three successive

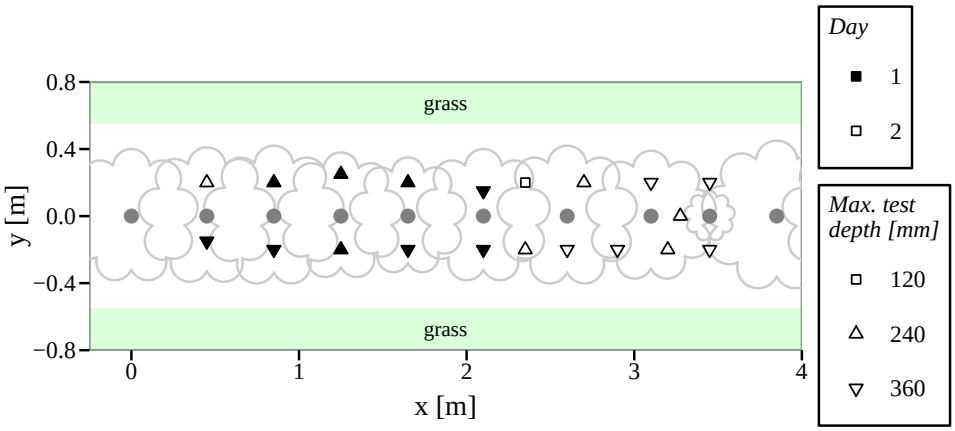

Figure 8.14: Locations corkscrew tests and nearby blackcurrant shrubs (solid grey squares) for shear strength testing at Bullionfield. Solid and hollow shapes indicate tests performed on day 1 and 2 respectively.

days in December 2015. This field was planted in April 2012 with 1 year old potted blackcurrant (*Ribes nigrum*) shrubs. Shrubs were planted in lines with 0.4 m between each plant. The distance between each line was approximately 2.8 m. Between each line, a 1.7 m wide strip of grass was present (Figure 8.14). No other vegetation was present near the shrubs. The soil was classified as slightly clayey sand, see Figure 4.2 for the particle size distribution (Atterberg limits: w_P = 18%, w_L = 25%).

The second site was Hallyburton Hill forest (Figure 8.17), a Forestry Commission owned woodland in the Sidlaw Hills, near Dundee, UK (56°31'10.3"N, 3°11'29.9"W), planted in 1962 with mature Sitka spruce (*Picea sitchensis*). Testing was performed at approximately 20 m distance from the location where blade penetrometer tests were performed (see Chapter 7). The soil was classified as sandy silt, see Figure 4.2 for the particle size distribution (Atterberg limits: w_P = 35%, w_L = 56%). Testing was performed on two plots over the course of four days in December 2014. On the first day, corkscrew tests were performed in a relatively open forest patch (Plot 1). On days 2–4, testing was performed in a denser region of forest (Plot 2). The plots were spaced approximately 10–15 m apart (Figure 8.16).

At both sites soil dry bulk density and water content were measured adjacent to the testing locations using 100 ml steel cores. Soil suctions were measured *in situ* using field tensiometers (model SWT4R, Delta-T). At Bullionfield, suctions were not measured and assumed to be <2 kPa because of abundant rainfall in the weeks before testing, resulting in high water tables (visually present at 150–250 mm depth below the soil surface). Soil horizon depths were manually determined based on visual observation in soil pits and compared with the Soil Information for Scottish Soils database (James Hutton Institute, 2016). Results for both sites are presented in Figure 8.18.

Figure 8.15: Picture of test location at Bullionfield.

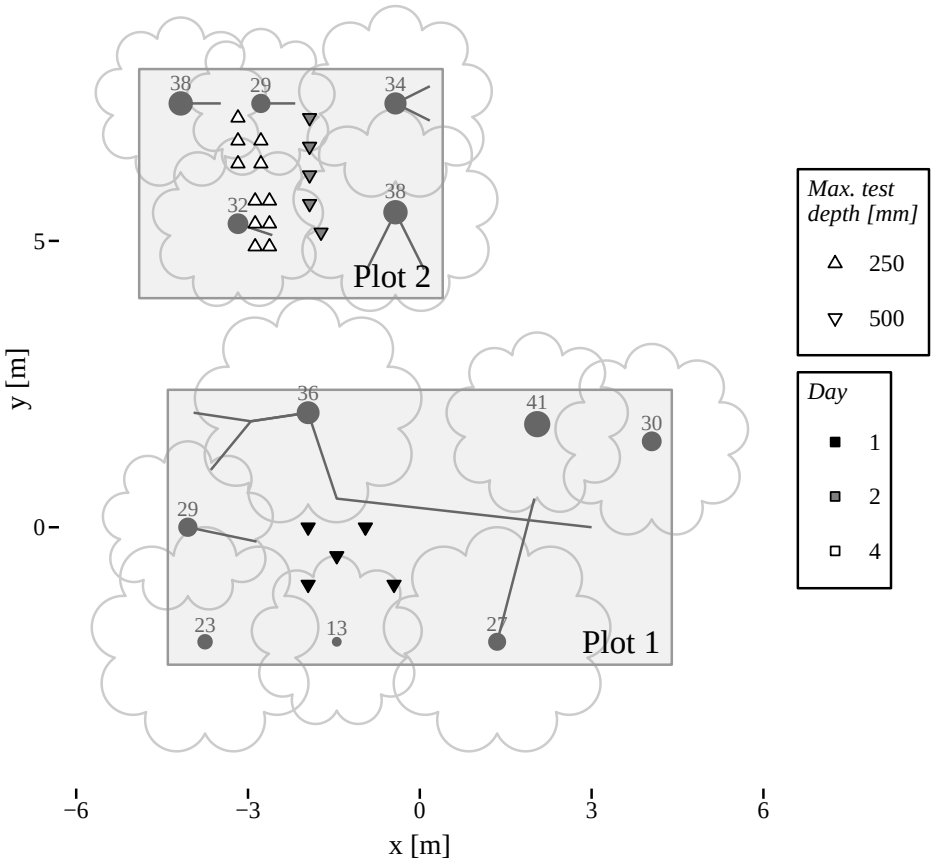

Figure 8.16: Locations of plots, corkscrew tests and nearby trees for shear strength testing at Hallyburton Hill forest. Solid dark grey circles indicate nearby trees (diameter at breast height given in centimetres) and straight grey lines a rough estimate where large structural roots were exposed. Only trees within plots are plotted.

Figure 8.17: Picture of test location at Hallyburton Hill forest.

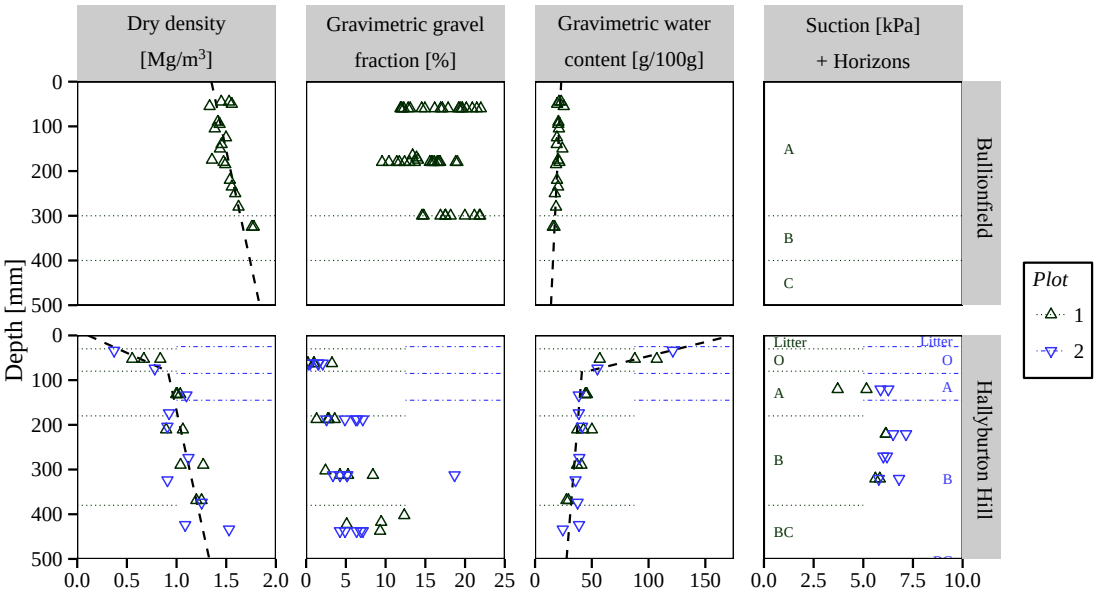

Figure 8.18: Water content, dry density, gravel content (>2 mm), suction pressures and soil horizon depths at Bullionfield and Hallyburton Hill. 'O' indicates the organic soil horizon or forest floor, 'A' the topsoil layer, 'B' the subsoil layer, 'C' the layer of parent rock material and 'BC' a mixture of 'B' and 'C'.

Root mechanical characteristics

A large number of roots were sampled to determine biomechanical strength and stiffness properties, both in uniaxial tension and 3-point bending. Sampled roots were bagged after collection and stored in a fridge at 4°C for a maximum of 4 days prior to testing to minimise potential decomposition effects. The methods and results for biomechanical testing for Sitka spruce roots from Hallyburton Hill forest were described earlier in Chapter 7.

Depending on the root diameter, a universal testing machine (Instron 5966) was fitted with a 50 N, 500 N or 2 kN load cell, using the smallest load cell possible without risk of overloading.

Sixty blackcurrant roots with diameter d_r ranging between 0.45 and 9.17 mm and a length of 40, 60, 80 or 100 mm were tested in uniaxial tension. Root length over diameter ratio was at least 10 to minimise the influence of clamping. All roots were tested at a rate of 5% strain per minute, in line with loading rates reported in literature (1–10 mm min^{-1}, e.g. Genet et al. (2008); Loades et al. (2010)). Root ends were clamped using pneumatic clamps with a pressure of 100 kPa ($0 \leq d_r \leq 2$ mm), 200 kPa ($2 \leq d_r \leq 5$ mm) or 300 kPa ($d_r > 5$ mm). For roots with diameters exceeding approximately 3 mm it was necessary to peel off bark at root ends prior to testing to ensure good grip. Removing bark was unlikely to have influenced results with observations during testing showing that, similar to the Sitka spruce roots tested before, all load carrying was concentrated in the central stele region of roots.

Forty-eight blackcurrant roots ($0.64 \leq d_r \leq 11.75$ mm) were tested in three-point bending, using a loading rate of 5 mm min^{-1}, a maximum displacement of 50 mm and a support span of at least 10 L/d_r. Although a value of $L/d_r \geq 20$ is recommended for testing of wood and timber (Rowe et al., 2006), sampled root lengths and/or changing root properties over the length of the root, e.g. excessive tapering, made this inappropriate.

For all roots, the peak strength, Young's modulus (E, stiffness over the elastic region) and secant stiffness at 90% of the peak strength (E_{90}) was determined. The latter parameter provided some insight into the non-linear stress–strain behaviour of the roots.

Root properties versus diameter relationships were fitted using conventional power law fits, see Equations 2.1 or 2.2.

Corkscrew data collection

At Bullionfield, corkscrew tests were gathered over the course of two days. Tests were performed at 0–120, 120–240 mm and 240–360 mm depth sequentially with each test at increasing depth within the hole left open by the previous test at shallower depth. If the target installation depth could not be reached, e.g. because of large stones, the actual installation depth was recorded and the results calculated taking the smaller shear plane area into account, but only if more than half of the corkscrew could be installed.

At Hallyburton Hill, on day 1 results were gathered on plot 1. On days 2 to 4, tests

were done on plot 2. Corkscrew test data from day 3 were lost due to data logger errors. The range of distances between test points and the nearest tree varied: on day 1 it ranged between 1.2 and 2.0 m, on day 2 between 0.9 and 1.5 m and on day 4 between 0.3 and 1.1 m. On the first two days, at every one of the five measurement locations tests were performed at 0–125, 125–250, 250–375 and 375–500 mm depth. On day 4, a further 11 locations were tested but measurements were only taken at 0–125 and 125–250 depth. It was decided to increase the number of tests at shallow depths on day 4 because work done on the first two days indicated that root quantities were low at depths below 250 mm at this site. In Figure 8.16 the locations of test plots, corkscrew tests and nearby trees are given.

All corkscrew tests were spaced at least $10d_{cs}$ apart, so that there was no interaction between tests. The potential zone of influence resulting from testing was calcuated using the model of Chattopadhyay and Pise (1986) for soil deformation around foundation piles tested in tension. Assuming a soil angle of internal friction of $\phi' = 30°$, soil–'pile' interface friction angle $\delta = \phi'$ and 'pile' depth of 500 mm, the radius of the uplifted soil wedge at the surface was estimated to be $4.47d_{cs}$.

At both sites, a number of standard shear vane measurements were collected using a 50 mm high 34 mm diameter cruciform blade (Edeco Pilcon). Both peak and residual strengths were recorded. At Bullionfield, 16 successful tests were performed over a depth range of 0–300 mm. At Hallyburton Hill a total number of 43 measurements were taken at depths ranging between 0 and 500 mm.

At both sites, a number of standard penetrometer tests was performed using the same penetrometer tip as used in previous experiments, i.e. a 12 mm diameter 30° cone connected to a 10 mm diameter shaft. Per site and plot an average trace was constructed by averaging individual measurements at each depth.

Sampling and processing of extracted samples

After each corkscrew test, the extracted corkscrew soil cores were wrapped in cling film and subsequently stored in a freezer (-30°C). After samples were frozen the volume of the frozen cores was measured using a ruler (1 mm divisions) and weighed using a balance (accurate to 0.01 g). Each sample was analysed for broken root ends protruding from the sides of the core. To make these more visible, the sides of the frozen cores were sprayed with hot water to remove soil, exposing the roots. Root end depths were recorded and their diameters measured using a microscope fitted with an eyepiece graticule (with 100 0.1 mm ticks). The largest magnification, 4.0, 3.0, 2.0, 1.0 or 0.7×, for which the whole root diameter could be captured in the graticule was used. Thus an accuracy of roughly $d_r/100$ was achieved. Only roots with diameters exceeding 0.5 mm were measured as it proved difficult to establish whether thinner roots were broken.

After quantifying all root ends, samples were carefully washed, collecting all root material and larger soil particles on a 2 mm sieve. All roots were subsequently scanned

and analysed using WinRhizo (version 2003b) using 0.1 mm wide uniform diameter classes. Soil particles retained on the 2 mm sieve were oven-dried and dry sieved using 2, 4, 8 and 20 mm sieves and their mass measured. To establish particle size mass fractions, the dry weight of the sampled cores was required. This required the soil water content, which could not be directly measured in every core due to the root sampling procedure. Therefore the (bi)linear soil water content–depth fit from Figure 8.18 was used to estimate the water content in each sample.

Since water expands during freezing, the measured densities using the frozen core dimensions and mass underestimated the real densities *in situ*. Therefore a correction factor was established by averaging the ratio between frozen densities and density measured in the field using the linear density–depth fits established using steel core samples (Figure 8.18). For every depth and site a different correction factor was determined. In this way realistic densities were acquired for each extracted corkscrew core while maintaining information about the natural variation in corkscrew sample densities. These densities were used to estimate the total vertical soil stress in the field at the centre of each corkscrew test.

Holes in the soil left open after corkscrew testing were filled with polyurethane expanding foam to trap broken root ends left in the external wall of the extracted cylinder. At Bullionfield, foam was applied one week after testing to allow soil to drain following heavy rain. However, at this site no foam could be applied below approximately 250 mm because of the water table level. These problems did not arise at Hallyburton Hill because of a deeper water table. After the foam had set, foam casts and the surrounding soil were dug up. Excess soil was washed away, and subsequently for all root ends sticking out of the foam core ((Figure 8.19)) the depths and root diameter were established in a similar fashion as for extracted corkscrew samples.

The root end count results from both extracted corkscrew samples and foam cores were summed to get a full set of all root ends passing though the shear surface. Since only root ends with diameters exceeding 0.5 mm were counted, the results from root scanning were used to fill the gap between $0 \leq d_r < 0.5$ mm. The WinRhizo root volumes were transformed to root area ratios by assuming random orientations of the roots, so $RAR = 0.5RV$ (Bengough et al., 1992), where RAR is the root area ratio [m^2 m^{-2}] and RV the measured root volume fraction [m^3 m^{-3}].

Force drops

During previous corkscrew testing in the lab, during preliminary field trials and also during the testing described here, discrete root breakages could be identified as sudden drops in resistance in the load–displacement trace. Where these drops could easily be identified, they were compared with the diameter of identified root ends. The largest drop was linked to the largest diameter root found, the second largest drop to the second largest root etc.

Figure 8.19: Example of a foam core after washing away surrounding soil, used to identify roots broken during corkscrew testing.

Blade penetrometer tests and modelling showed before that the magnitude of these drops was related to root and soil properties. The two analytical models were developed in Chapter 5, one assuming roots broke in pure bending (analytical bending model) and one assuming they broke in pure tension (analytical cable model). For both models, solutions for roots loaded by a point load and roots loaded by shearing soil along part of the root length were used (summarised in Table 8.1). For thick roots, considering the corkscrew loading as a point load might be important due to the limited diameter of the corkscrew with respect to the length of the displacing root.

Values for the root–soil interface friction τ_i were estimated based on the measured standard vane shear strength and multiplied by $f = 0.5$ (after Mickovski et al., 2009) to take into account that the root–soil interface friction is lower than soil–soil interface friction. Values for the ultimate soil–root perpendicular resistance p_u were based on standard penetrometer tests performed at both sites. The measured resistance was multiplied by $\alpha_2 = 0.623$ to account for shape differences between penetrometer and root. This factor had been determined before in dry sand by comparing standard penetrometer resistance to the model for soil resistance against laterally displacing piles derived by Reese and Van Impe (2011) for dry sand (Figure 6.6).

As a final model, the measured drops in corkscrew resistance were directly compared with the tensile strength of the breaking roots.

Whenever these models require a root stiffness value, the secant stiffness E_{90} was used instead of the stiffness over the linear-elastic region E to capture the non-linear stress–strain behaviour more accurately.

Table 8.1: Analytical solutions for root displacement and reinforcement. d_r is the root diameter, σ_t and σ_b are the root tensile and bending strength, E_t and E_b the root tensile and bending stiffness, p_u the (constant) soil resistance against root displacement and τ_i the interface friction between root and soil.

Model		Multiplication factor		Multiplication factor ξ
		Point load	Shear load	
Bending	Peak force	1.3027 ξ	0.5642 ξ	$\frac{\pi}{4} \cdot d_r^2 \cdot \sigma_b^{0.5} \cdot p_u^{0.5}$
	Peak displacement	0.1249 ξ	1.3360 ξ	$\frac{\pi}{4} \cdot d_r \cdot \sigma_b^2 \cdot E_b^{-1} \cdot p_u^{-1}$
Cable	Peak force	2 ξ	1 ξ	$\frac{\pi}{4} \cdot d_r^2 \cdot \sigma_t \cdot \frac{2 \cdot \sqrt{\eta}}{1+\eta}$
	Peak displacement	1 ξ	2 ξ	$\frac{\pi}{4} \cdot d_r \cdot \sigma_t \cdot p_u^{-1} \cdot \zeta^{0.5}$

$\zeta = \frac{1}{8} \cdot \frac{\sigma_t \cdot p_u}{E_t \cdot \tau_i}$

$\eta = \sqrt{\frac{\zeta - 2 \cdot \sqrt{\zeta + 1} + 2}{\zeta}}$

Comparison to existing root-reinforcement models

The experimental results were compared with a range of existing models of root-reinforcement, including the Wu/Waldron model (WWM), fibre bundle models (FBM) with various load sharing parameters (a = 0, 1 or 2, see Section 2.5.2) as well as a fibre bundle model using a load sharing criterion based on displacements of roots perpendicularly crossing the shear plane (FBM cable). This model used the cable solution described in Table 8.1. When it was assumed that the load in the root increases linearly with shear displacement, for every arbitrary shear displacement u the fraction of the root-reinforcement mobilised could be expressed as u/u_u. When $u/u_u > 1$, the root was considered broken and therefore the reinforcement set to zero. The maximum value for k'' could then be found by iterating over u.

Since both the tensile strength and root elasticity can be expressed as functions of root diameter (Equations 2.1 and 2.2), the root peak displacement in the cable model (u_u) using shear loading is correlated to the root diameter:

$$u_u \sim d_r^{1+1.5 \cdot \beta_{\sigma_t} - 0.5 \cdot \beta_{E_{90,t}}} \tag{8.2}$$

where $\beta_{\sigma,t}$ is the power coefficient in the tensile strength–diameter fit and $\beta_{E_{90,t}}$ the power coefficient in the E_{90}–diameter fit (tensile). Therefore the load sharing criterion in the FBM cable model could be expressed in terms of the conventional FBM using a load sharing parameter (Equation 2.5) equal to:

$$a = 1 + 1.5 \cdot \beta_{\sigma_t} - 0.5 \cdot \beta_{E_{90,t}} \tag{8.3}$$

Therefore, $a \approx 1.0185$ for blackcurrant roots at Bullionfield and $a \approx 1.219$ for Sitka spruce roots at Hallyburton Hill.

For every corkscrew measurement, simulations were run for every model using the

measured root area ratios and root properties to find k'', the reduction factor for mechanical reinforcement due to progressive root failure, see Equation 2.6.

Statistical analysis

Statistical analyses were performed using R statistical software (R Core Team, 2013). Statistical significance of p-values was reported as three levels: $p > 0.05$: n.s.; $p \leq 0.05$: *; $p \leq 0.01$: **; $p \leq 0.001$: ***.

8.4.3 Results

Root mechanical properties

In general, root strength and stiffness both in bending and tension increased with increasing diameters (Figure 8.20). The only statistically significant ($p \leq 0.05$) values for the power coefficient β were found for all Sitka spruce bending properties and E_{90} measured for Sitka spruce in tension.

Root distributions

Root quantities decreased rapidly with depth at both sites (Figure 8.21). At both sites, the majority of the root volume consisted of fine roots (d_r = 0–2 mm) although at Hallyburton roots with diameters exceeding 2 mm were more abundant than at Bullionfield. The total amount of large roots (> 5 mm) was highly variable between samples.

Root area ratios determined using WinRhizo (assuming uniform distributions of the roots with random orientations) generally yielded higher results compared with measuring root ends sticking out of the corkscrew and foam cores, especially for thin (0.5–2 mm) roots (Figure 8.22). There may be a number of explanations for this: 1) roots may have grown preferentially vertically, resulting in fewer intersections with the vertical shear plane. 2) Root ends not found during counting of roots in corkscrew and foam cores, or 3) inaccuracies in WinRhizo.

Root–reinforced shear strength

At every standard shear vane measurement depth, the average penetrometer trace derived for that site and plot was interpolated to find the penetrometer resistance corresponding with this depth. Good correlations were found between standard penetrometer resistance and soil peak strength measured with the standard shear vane with similar correlations for both sites (Figure 8.23).

On average, corkscrew peak strengths were slightly lower than standard vane readings (Figure 8.24), but both followed similar depth trends. Standard vane peak strength readings showed considerable scatter. Residual shear strengths were significantly lower than peak strengths for both measurement methods, indicating that both soils possessed some measure of sensitivity, commonly defined as the ratio between peak and residual strength.

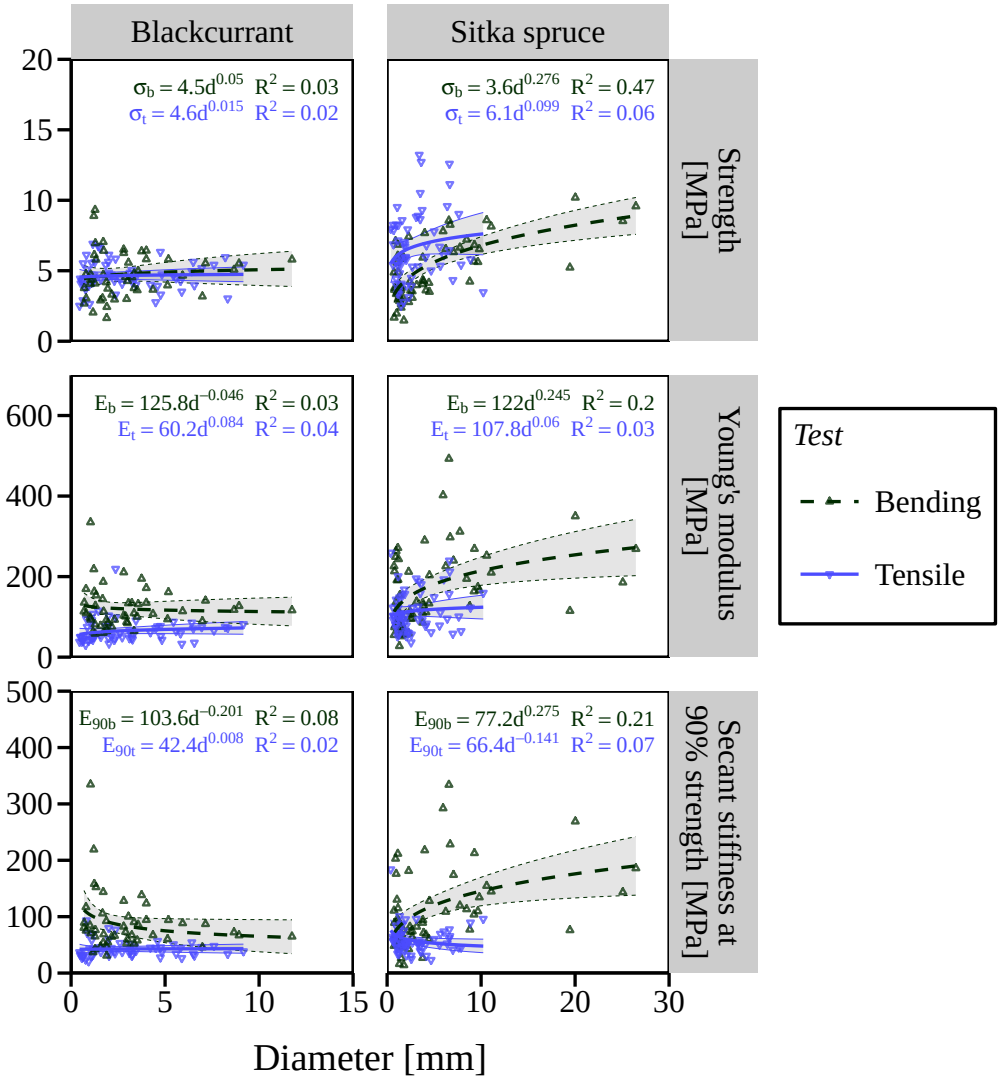

Figure 8.20: Root strength and stiffness for blackcurrant and Sitka spruce roots tested in both uniaxial tension and three-point bending. Points indicate individual measurements, lines the best power law fit and shaded areas the 95% confidence interval of these fits.

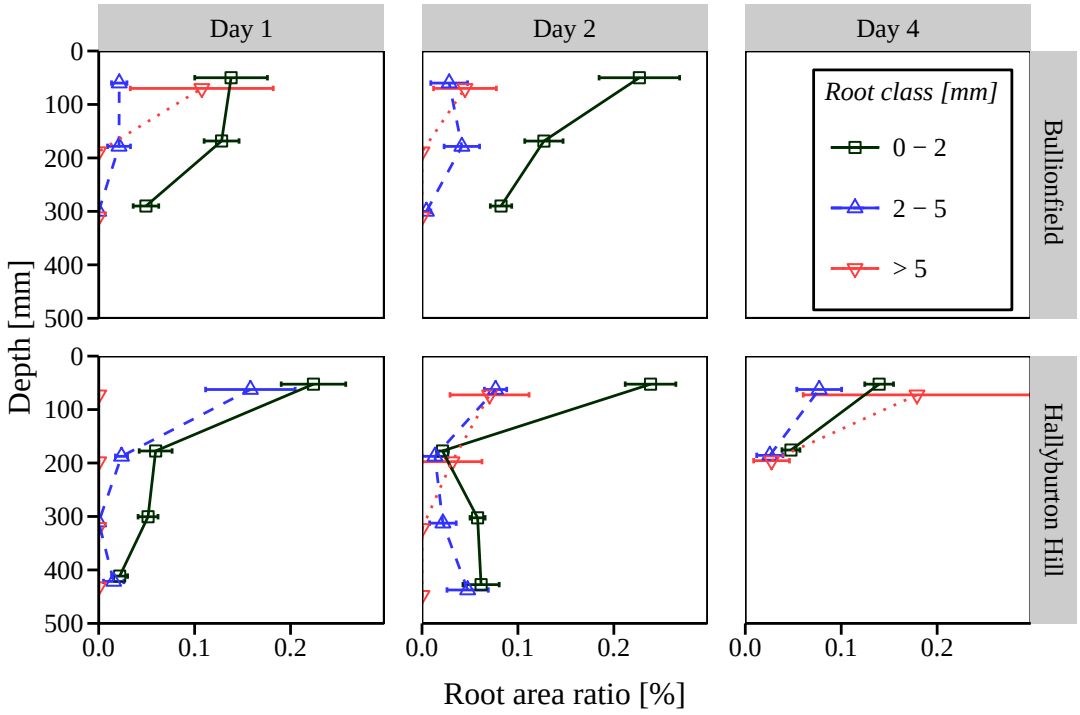

Figure 8.21: Root area ratio (determined by summing counted root ends ($d_r > 2$ mm) and WinRhizo data ($d_r \leq 2$ mm, uniform distribution assumed) for various root size classes versus depth at both sites. Error bars indicate the size of one standard error.

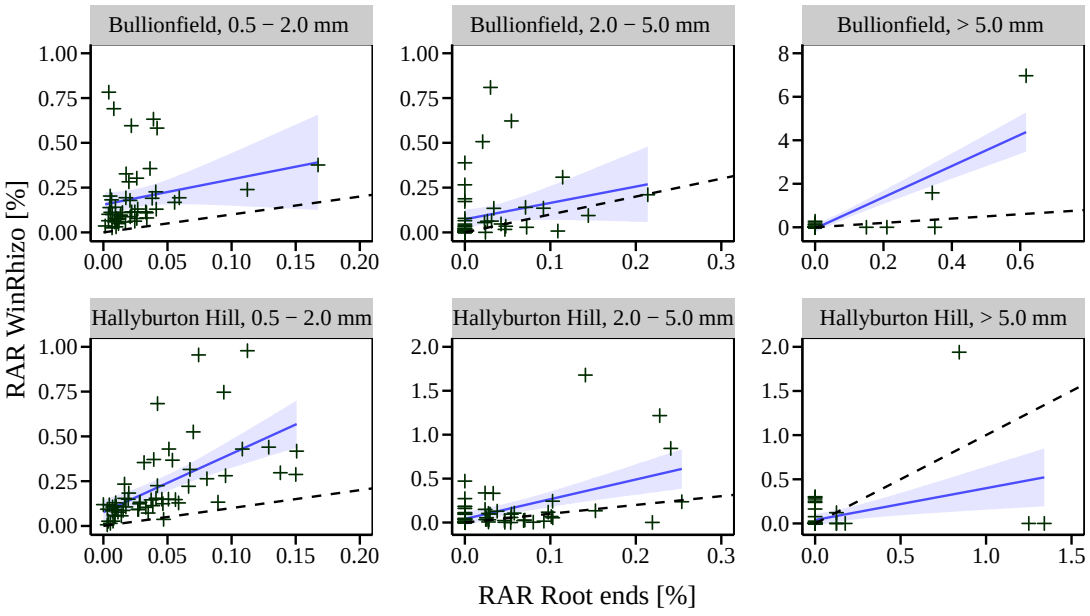

Figure 8.22: Comparison between root area ratios determined using WinRhizo and by counting root ends sticking out of corkscrew samples and foam cores. The dotted line indicates parity, solid lines the best linear fit and shaded areas the 95% confidence interval of this fit.

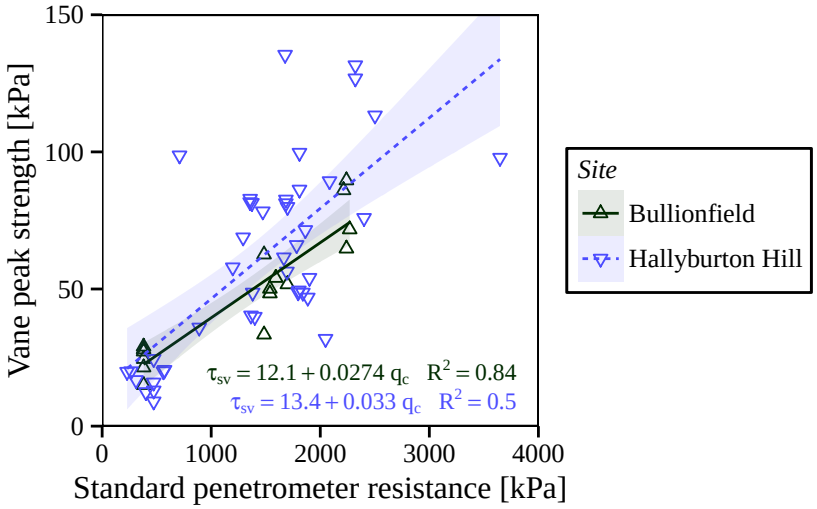

Figure 8.23: Soil penetration resistance versus standard vane peak strength at Bullionfield and Hallyburton Hill.

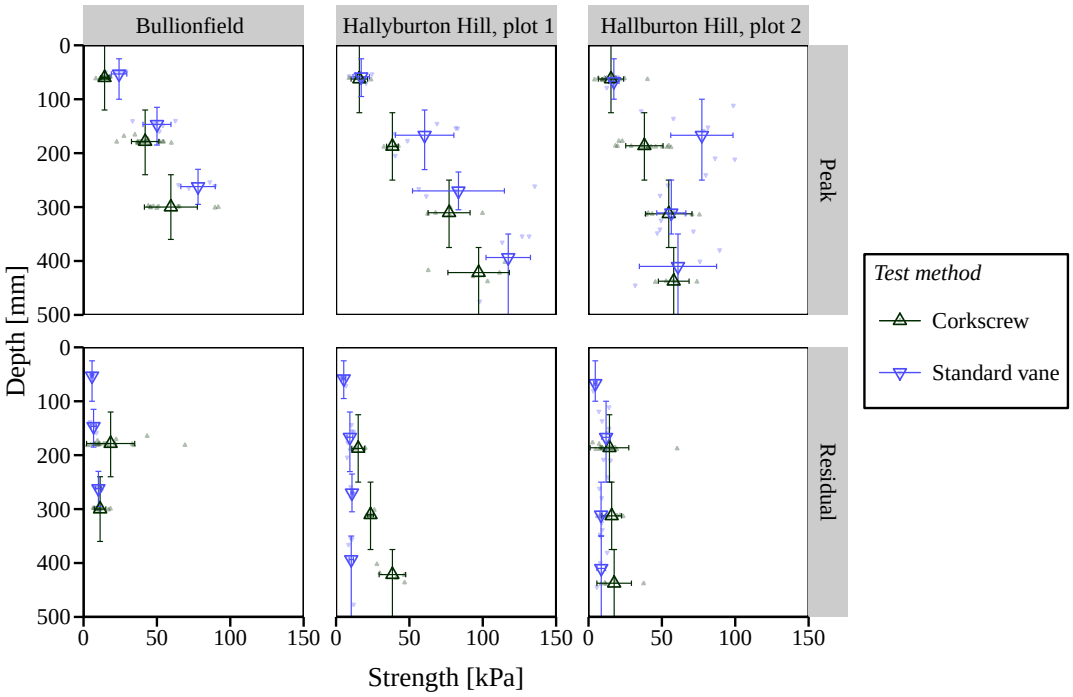

Figure 8.24: Comparison of corkscrew and standard vane peak strengths at Bullionfield and Hallyburton Hill. Small symbols indicate individual measurements. Large symbols indicate averages. Horizontal error bars indicate one standard deviation, and vertical error bars the depth range over which mean values are computed.

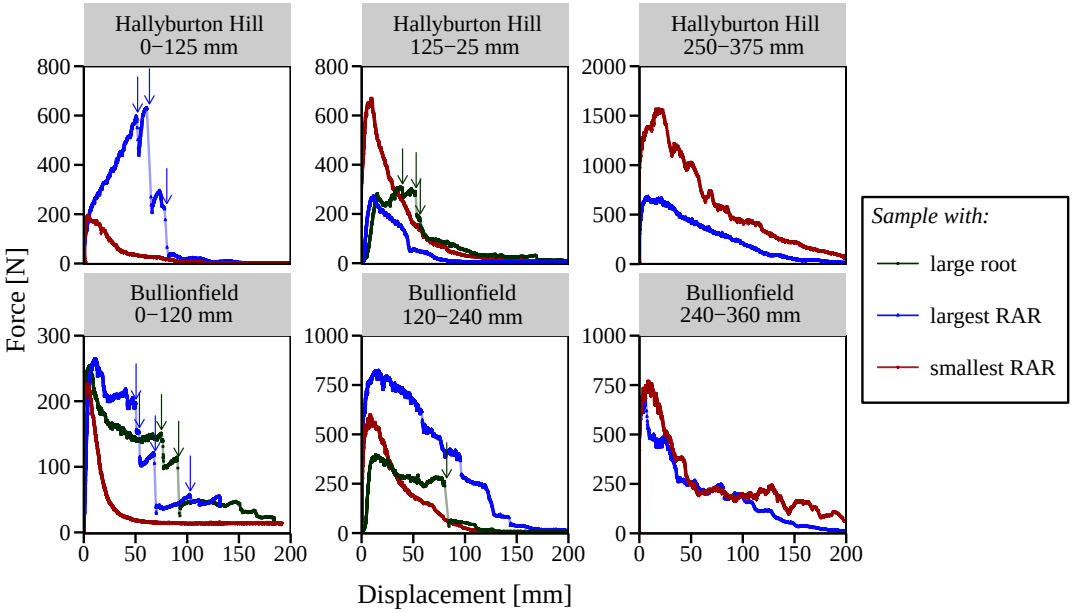

Figure 8.25: Example corkscrew force–displacement traces. Individual points, measured at f_s = 100 Hz, are indicated with darker symbols. Arrows indicate sudden drops in resistance associated with root breakages.

Measured sensitivities were S_t = 2–6 in the surface layer (0–120/125 mm depth) and S_t = 5–13 at larger depths at both sites.

A number of example corkscrew force–displacement traces for each site and measurement depth level are shown in Figure 8.25. In some traces, individual root failures could be distinguished as areas in the trace where the force suddenly dropped rapidly over the course of 10–50 ms.

A strong positive correlation between measured corkscrew peak strength and the sum of root strength ($\sum \sigma_t \cdot RAR$) was found in the surface layers (0–120/125 mm depth) at both sites (Figure 8.26). In deeper layers (> 125 mm) however, no significant or negative correlations were found.

At Hallyburton Hill positive correlations were found between total vertical soil stress and peak strength at depths > 125 mm, some of these statistically significant. However, although results appear to indicate that variations in peak strength at depths > 125 mm were mainly caused by variations in soil stress, the low stress values were unlikely to have caused such a great variation in soil shear strength when realistic values for the soil angle of internal friction are assumed. At Bullionfield these correlations were weaker.

When the peak strength was compared to the quantity of gravel ($d \geq 2$ mm) measured in extracted corkscrew cores from Hallyburton Hill, positive but non-significant correlations were found. Especially at 375–500 mm depth a steep gradient was found. At Bullionfield, peak strength and gravel appeared to be uncorrelated, except at 240–360 mm depth where a weak negative correlation was found.

Part of the negative relationship between peak strength and root quantity at greater

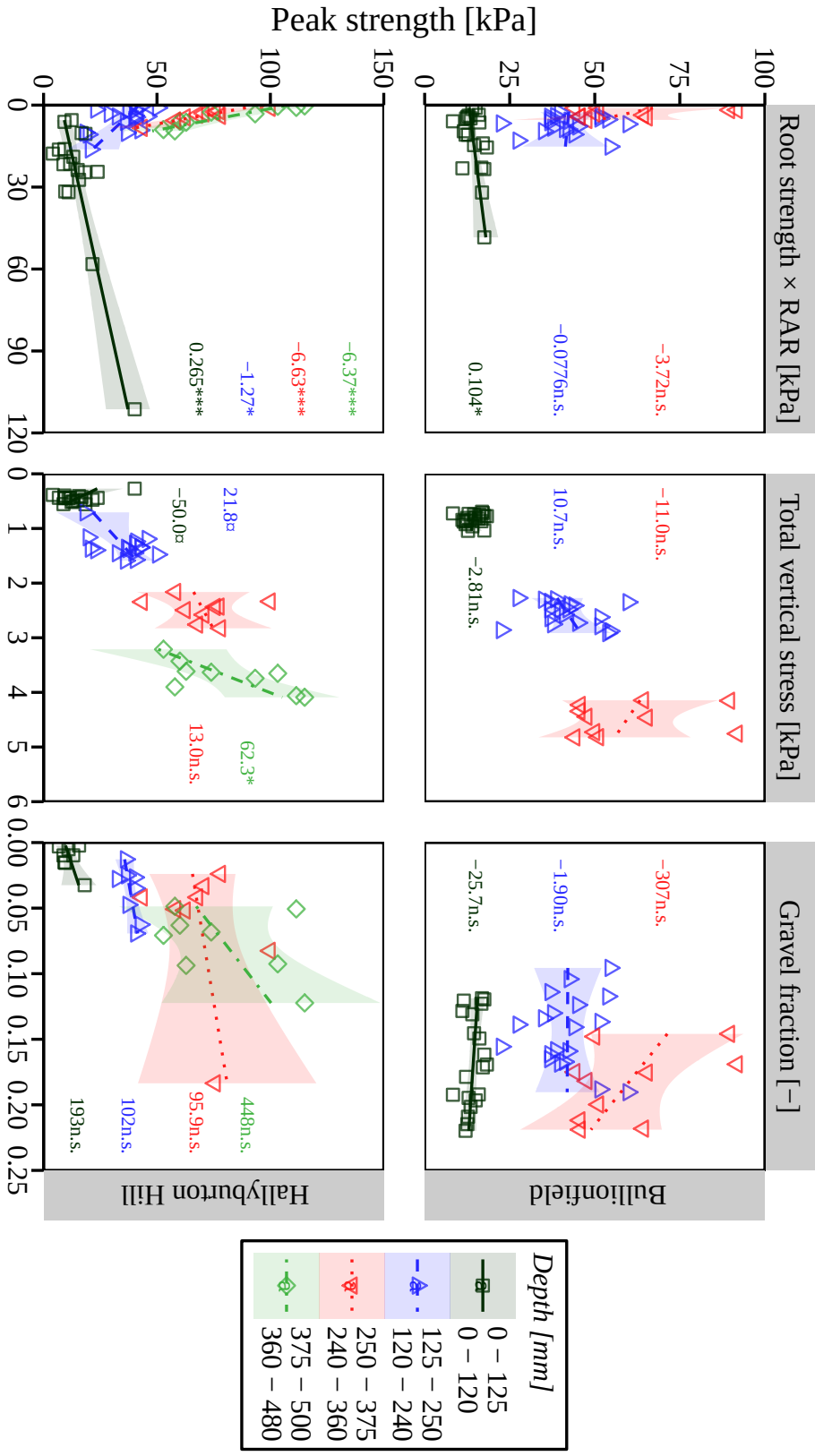

Figure 8.26: Corkscrew peak strength versus total root tensile strength (normalised for shear surface area), vertical total soil stress and gravel mass fraction for each site and depth level. *b* denotes the gradient of the linear fit. Shaded areas indicate the 95% confidence interval of the fit.

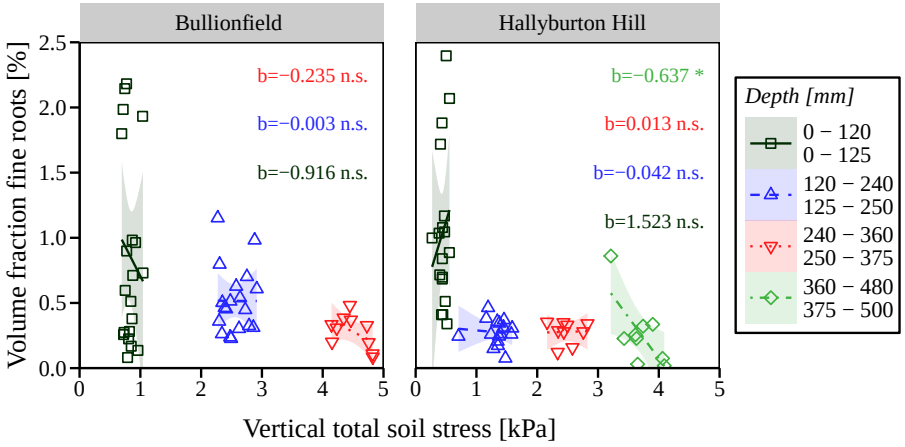

Figure 8.27: Root volume fraction for fine roots ($d_r \leq 2$ mm, determined using WinRhizo) as a function of total vertical soil stress. Numbers denote the gradient of the linear fit. Shaded areas indicate the 95% confidence interval of the fit.

depths may be explained by looking at the relation between soil stresses and root volumes (Figure 8.27). Only fine roots ($d_r \leq 2$ mm) were analysed to obtain a more reliable estimate of distribution of roots in the soil as large individual thick roots would have had a very large influence on the results. At 375–500 mm depth at Hallyburton Hill, a significant negative correlation was found between fine root volume and soil stress. At depths >120–125 mm at both sites, either no correlation or a non-significant negative correlation was found. These results suggest that in stronger, deeper layers, the roots preferentially have grown where the soil stress was low.

The encountered variation in soil parameters at depths greater than 120/125 mm made it difficult to relate soil strength to the effects of root inclusions, as the variation in reinforced soil strength was not only being related to variations in roots but also to variations in soil stress levels and gravel content. These factors could not be treated as independent, since root growth does depend on soil impedance and it is likely that gravel content relates to both soil strength (different material behaviour) and soil density (different soil structure). Only where the soil strength was low and roots plentiful, i.e. near the surface, a strong and significant positive relation between roots and soil strength was found.

Normalised energy dissipation

An example graph for the normalised energy dissipation parameter W_n for the heaviest and least rooted soil at 120–240 mm depth at Bullionfield can be found in Figure 8.28, showing distinct differences in the shape of the extraction curve and therefore in W_n between samples with few and abundant roots.

At both sites, for the surface layers (0–125 mm) strong and significant positive correlations were obtained between root strength and W_n, and positive trends were also found at 125–250 mm depth. Below 250 mm, root quantities were small and did not significantly affect W_n (Figure 8.29). The positive correlation between W_n and root strength showed

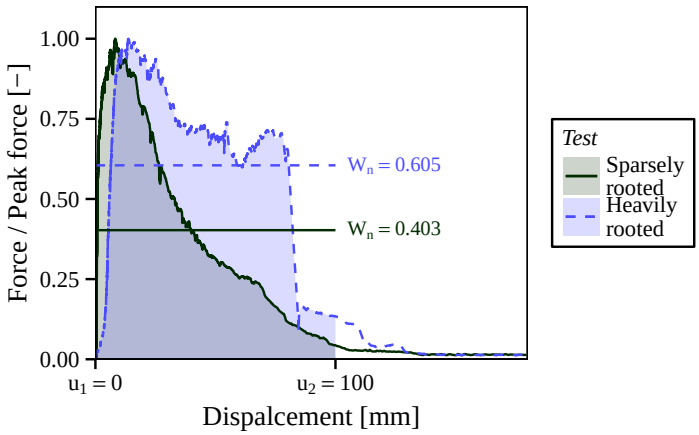

Figure 8.28: Visualisation of the normalised energy dissipation parameter W_n for a heavily and sparsely rooted test at 120–240 mm depth at Bullionfield.

Table 8.2: ANOVA results for τ_{cs} and W_n in the surface layer (0–120/125 mm). Numbers indicate the percentage of variance explained by each factor.

		Day [%]		Roots 0–2 mm [%]		Roots 2–5 mm [%]		Roots >5 mm [%]	
τ_{cs}	Bullionfield	16.7	.	18.3	.	0.1		2.6	
	Hallyburton Hill	14.4	*	0.4		1.5		64.6	***
W_n	Bullionfield	8.5	**	30.8	***	28.9	***	18.6	**
	Hallyburton Hill	1.1		0.1		1.7		57.7	***

that the soil behaved with increased ductility when roots were present, this feature being independent from the effect roots have on the peak strength. Total vertical soil stress did not significantly affect W_n. However, at Bullionfield the presence of gravel was found to affect W_n between 0 and 240 mm depth, where more gravel resulted in significantly smaller values for W_n.

Which root size class affects the results most?

Type I ANOVA results (Table 8.2) showed that in the surface layers of Bullionfield variations in the content of small roots (d_r = 0–2 mm) explained more of the encountered variation in soil strength than larger roots. However, although larger roots barely influenced the peak strength, they had considerable influence on W_n. At Hallyburton Hill, the large roots (>5 mm) were the main contributors to both soil strength and W_n.

Estimation of force drops from interpretive models

46 clear sudden drops in extraction force were identified in the measured corkscrew traces. Comparing the magnitude of the measured force drops to the various predictive models yielded highly variable results (Figure 8.30). For Bullionfield the bending model with point loading provided the best prediction, whereas for Hallyburton Hill any of the cable models, even simply assuming the force drop is equal to root tensile strength, yielded

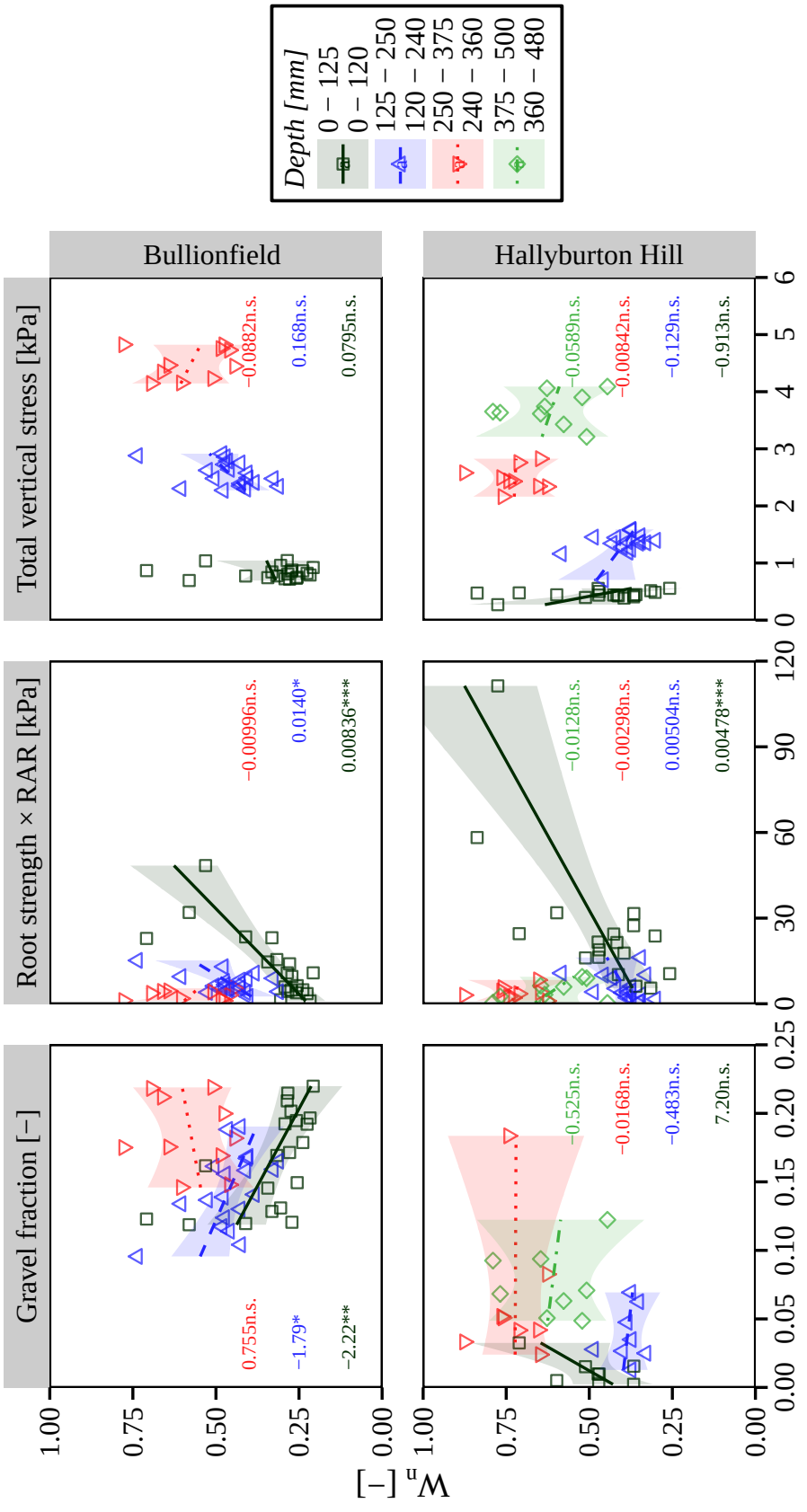

Figure 8.29: Normalised energy dissipation (W_n) as a function of total root tensile strength (normalised for shear surface area), estimated total vertical soil stress and gravel mass fraction for each site and depth level. Numbers denote the gradient of the linear fit. Shaded areas indicate the 95% confidence interval of the fit.

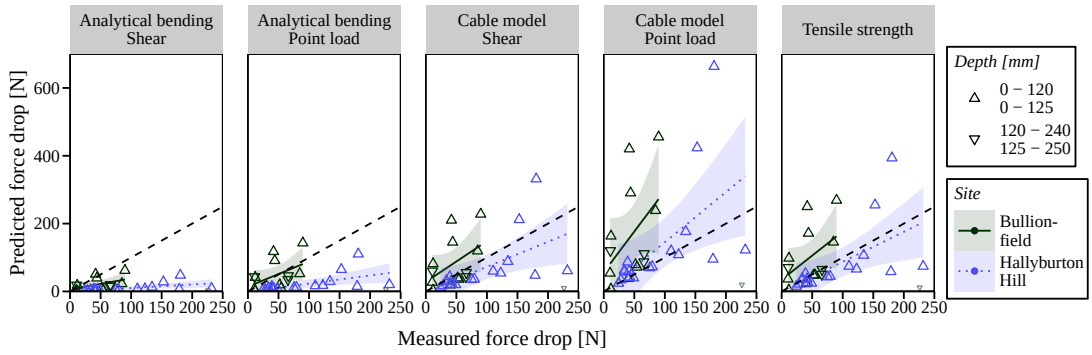

Figure 8.30: Measured magnitudes of corkscrew force drops compared with various interpretive model results. The dashed lines indicate parity, coloured lines linear fits and shading the 95% confidence interval of these fits. Points indicated with small symbols were considered to be outliers when fitting the data.

reasonably good correlations. However, these results are inconclusive about the best model because of the large scatter in the data.

Comparison to existing root-reinforcement models

Various existing analytical root–soil reinforcement models were used to make predictions for root-reinforcement. Different models yielded very different predictions (Figure 8.31). With increasing model complexity, predictions became smaller and closer to field measurements. However, all models overestimated the actual measured reinforcement.

All fibre bundle models predicted thinner roots to break before thicker roots (Figure 8.32). However, the diameter of the root breaking while reaching peak reinforcement varied between models. Higher values for the load sharing parameter (a) results in FBM predictions closer to the WWM. When α was high, the influence of thin roots was more pronounced. The cable FBM results were very close to the results of the FBM with $a = 1$. Figure 8.32 shows that for the experiments with high RAR values, when $a \geq 2$ (Bullionfield) or any value of a (Hallyburton Hill), the predicted reinforcement was completely dependent on the influence of large roots.

8.4.4 Discussion

Root mechanical properties

It is widely reported that decreasing tensile strength is associated with increasing root diameter, e.g. see Mao et al. (2012). Values for *Picea abies* reported by Vergani et al. (2014b) showed a range between $-0.17 \leq a_\sigma \leq 0.13$, depending on the sampling site (original fits reported in terms of force), more in line with values found in this study, indicating negative power law relationships are not always suitable. Data on tensile stiffness is very scarce, and no data on bending properties was found in the literature apart from a study by Stokes et al. (1996) using 5 mm diameter core samples taken from first order lateral tree roots.

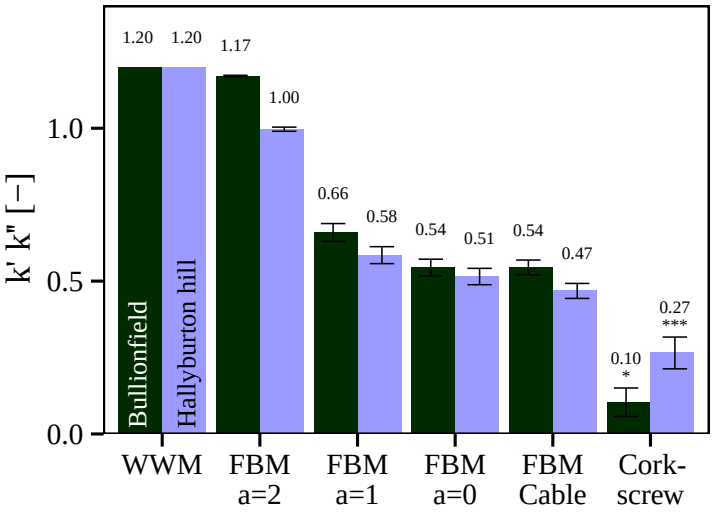

Figure 8.31: Comparison of model and experimental root-reinforcement results. Root reinforcement is normalised over the product of root tensile strength σ_t and root area ratio *RAR* in terms of $k' \cdot k''$, see Equation 2.6. For experimental results, the gradient, standard error and statistical significance of the linear fit between $\sum \sigma_t \cdot RAR$ and τ_{cs} is given. For model results, the mean and standard error (error bars) of predicted values for $k' \cdot k''$ is given, assuming $k' = 1.2$.

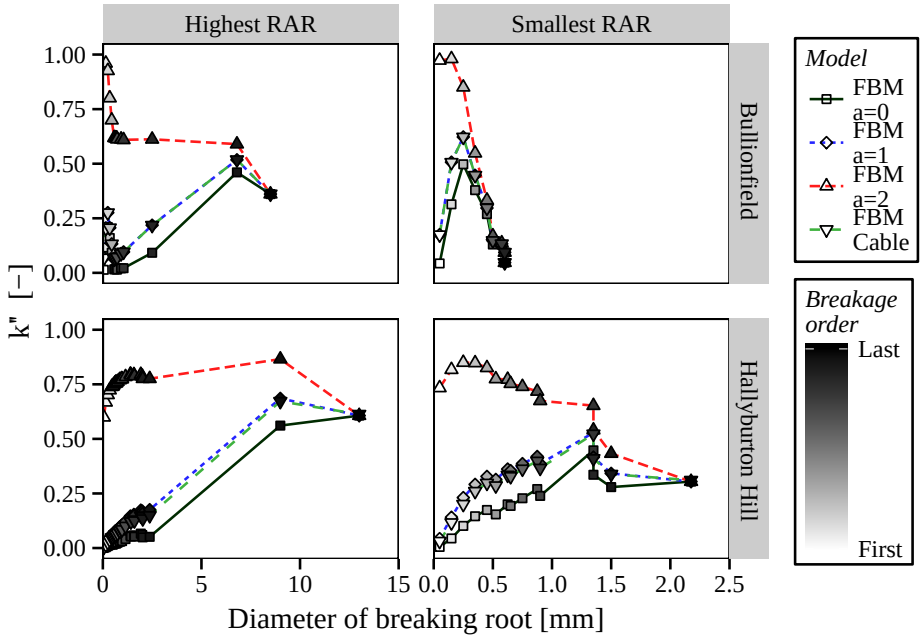

Figure 8.32: FBM force as function of diameter of breaking roots for some example tests in the surface layer (0–120/125 mm depth). Root data used corresponds with some of the test traces in Figure 8.25

Root biomechanical properties are not just a function of species and diameter. Root strength was shown to vary as function of root water content and root age (Burylo et al., 2011; Genet et al., 2008), decomposition (e.g. O'Loughlin and Ziemer, 1982), soil conditions such as the water content (Loades et al., 2010), root type (Loades et al., 2013) or environmental condition (e.g. trees on slopes; Stokes et al., 2002; Abdi et al., 2010). More work is required to yield more accurate predictions for root biomechanical properties.

Comparison of corkscrew to shear vane

The corkscrew showed a cone-like failure mechanism during testing in the surface layer (0–120/125 mm), likely to have resulted in an underestimation of the actual shear strength. Therefore corkscrew testing can be considered to yield conservative results near the surface. At larger depths, vane tests showed more variability compared with corkscrew testing, probably caused by the smaller size of the device, making it more sensitive to spatial variability in the soil, especially where pockets of gravel were present.

At increased depths, corkscrew test peak strength could have been slightly smaller than vane results because of the sensitive nature of the soil and the stiffness of the corkscrew: high soil strengths at depth result in greater strain during extraction, resulting in a slight gradient of soil strain over the test depth and therefore variation in the mobilised soil strength. Therefore the measured peak will always be slightly smaller than the actual maximum peak. The vane device is much less sensitive to this effect since it was stiffer.

The large difference between peak and residual strength indicated cementation of and/or structure within the soil. The measured vane residual strengths were comparable to values expected using a simple model (after Fredlund and Rahardjo, 1993) to estimate the shear strength of unsaturated soil on a vertical plane (Figure 8.33):

$$\tau = c' + \sigma_v \cdot \tan\phi' + s \cdot \tan\phi^b \tag{8.4}$$

where σ_v is the total vertical soil stress, s the suction pressure, c' the soil cohesion (assumed as 5 kPa), ϕ' the soil angle of internal friction (assumed as 30°), ϕ^b the angle indicating the rate of increase in shear strength relative to the matric suction (ϕ^b was assumed to be equal to ϕ' due to lack of experimental data) and K_0 the coefficient of lateral earth pressure ($1 - \sin\phi'$). At Bullionfield, suctions were assumed to be negligible because of the high rainfall prior to testing and the high water table. At Hallyburton Hill, a constant $s \approx 6$ kPa was assumed, based on field measurements (Figure 8.18), but only below 80 mm depth. At depths < 80 mm soil measured densities were very low resulting in large voids and capillaries which were considered to be too wide to hold significant suctions. Although Equation 8.4 predicts the shear strength for horizontal planes while the vane device largely measures shear strength on vertical ones, Figure 8.33 suggests that the vane residual strengths measured were accurate and not just an artefact of the measurement procedure.

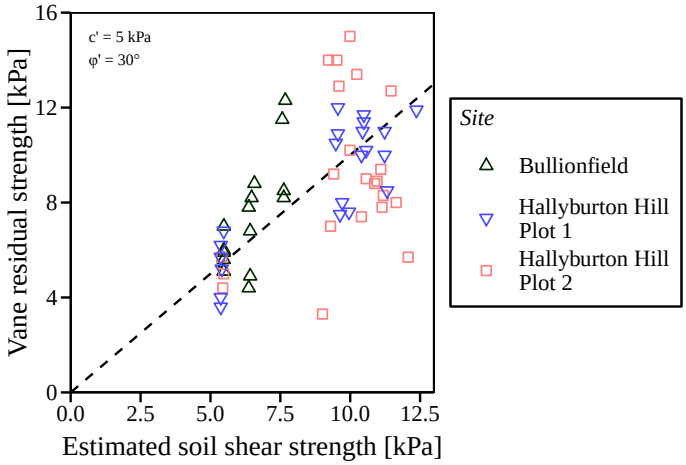

Figure 8.33: Comparison between measured vane residual strength and model predictions. The dashed line indicates parity. Suction levels were taken as $s = 0$ kPa at Bullionfield. At Hallyburton Hill, $s = 0$ kPa and 6 kPa below 80 mm depth.

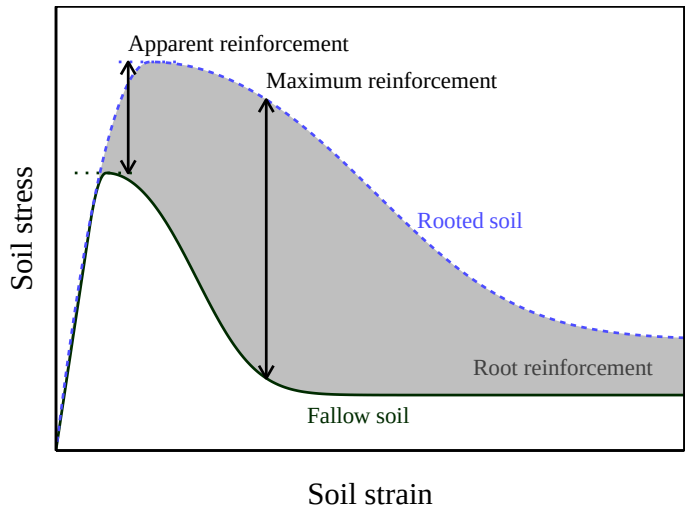

Figure 8.34: Schematic stress–strain curves for rooted and non-rooted soil.

Comparison of measured reinforcement to model predictions

The experimentally measured reinforcement was much lower than conventional model predictions. Several potential reasons were identified:

1) The soil was shown to possess sensitivity, i.e. the ratio between peak and residual strength is pronounced. Since roots mobilise resistance at much larger displacements than soil (e.g. Ekanayake et al., 1997; Mickovski et al., 2009), it is likely that the full reinforcement only mobilises when the soil strength is declining towards residual strength. This will result in a smaller apparent root reinforcing effect when the peak strengths of unrooted and rooted soil are compared, see Figure 8.34. This effect will be more pronounced in more sensitive soils. Natural field soils may age-harden in time through reorientation or cementation (Utomo and Dexter, 1981; Dexter, 1988; Mitchell and Soga,

2005) and therefore sensitivity may increase over time. In such soils, the root-reinforced peak strength will be lower than the sum of fallow soil peak strength and root cohesion. It is suggest here that this effect should be studied in more detail in future work.

2) All existing models assume that all roots with similar diameters fail simultaneously, even in FBMs. However, this ignores the effect of different root orientations. Variation in root orientation means that roots with similar diameters will mobilise resistance progressively rather than simultaneously, potentially resulting in lower predicted reinforcements. This discrepancy will be more pronounced when most of the reinforcement is caused by roots in a small diameter range. Furthermore, when the soil is rooted with predominantly fine roots, models predict a high reinforcement peak present over only a short displacement interval since cable model predicts fine roots only need small displacements to fully mobilise their strength. However, in reality, instead of one big peak the reinforcement is present over much larger displacements and the soil behaved in a very ductile way (e.g. Comino et al., 2010; Operstein and Frydman, 2000). This suggests that predictive models do not capture the right root reinforcement mobilisation mechanism, especially for finer roots.

3) Both the example corkscrew traces (Figure 8.25) and FBM examples (Figure 8.32) show that thick roots have a large effect on the reinforcement results (Vergani et al., 2014b). All reinforcement models assumed that these large roots break in tension. However, in reality they might have failed in bending resulting in potential model overestimations. Furthermore, it might have been the case that these thicker roots slipped out of the side of the corkscrew during the test rather than breaking, providing another potential reason for measured reinforcements being lower than predicted.

Experimental root-reinforcement results in the surface layers (0–120/125 mm) were compared against direct shear studies found in the body of literature. Values for k' were similar but at the lower end of those found in the literature (Figure 8.35). Interestingly, k' values acquired in controlled conditions (laboratory) were smaller than those found in the field testing. Laboratory values were all derived from saturated (Pollen and Simon, 2005; Operstein and Frydman, 2000) or near-saturated (Loades et al., 2010, saturated and subsequently drained at 5 kPa suction) conditions. All field data was derived from soil at natural water contents, apart from Docker and Hubble (2008) who tested in saturated conditions. Therefore it can be hypothesised that field studies yielded larger values because of simultaneously measuring both mechanical and hydrological root-reinforcement.

Both the corkscrew and pin vane device measure the combined effect of soil strength, root mechanical reinforcement and the hydrological reinforcement, so the measured reinforcement is the sum of root mechanical and root hydrological reinforcement. However, the hydrological contribution was thought to be small because of the low matric suctions measured during the experiments ($s < 2$ kPa in Bullion field, $s < 10$ kPa in Hallyburton Hill). Only a fraction of this will be additional suction caused by plant roots. However,

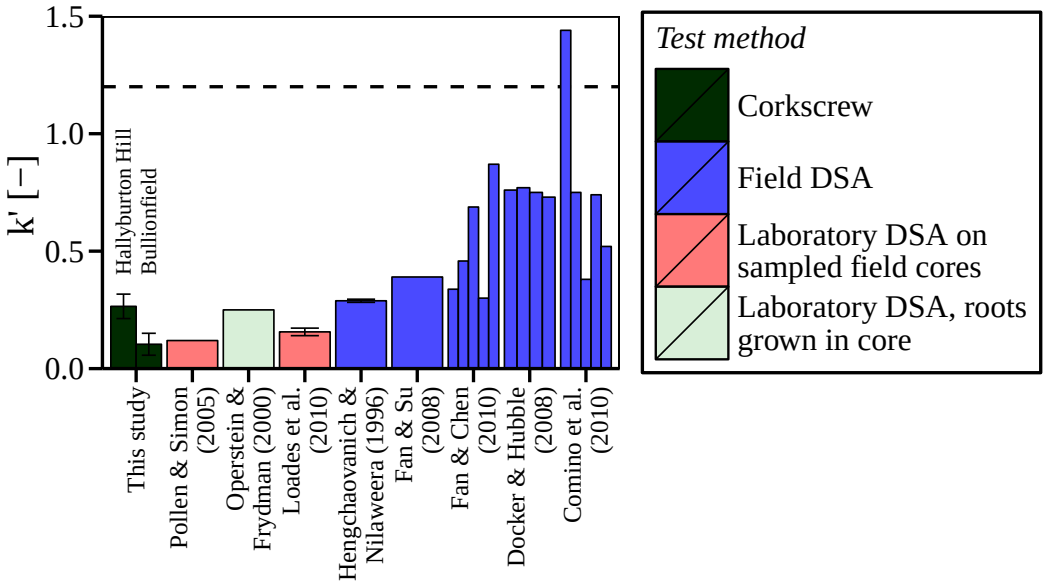

Figure 8.35: Comparison of values for k' found in the surface layer at Bullionfield (0–120 mm) and Hallyburton Hill (0–125 mm) with shear box testing reported in the literature. k' is defined as $c_r/(\sum \sigma_t \cdot RAR)$, see Equation 2.3. The dotted line indicated the WWM solution where $k' = 1.2$. Field core data from Loades et al. (2010) was re-analysed to find k'. Values for k' for Hengchaovanich and Nilaweera (1996) were found by re-analysing their reported data and the value for Pollen and Simon (2005) by analysing the gradients in their plotted data.

even in the unlikely scenario that all of the suction was thought to be caused by plant roots, and when the air entry value is assumed as $s_e \approx 0.7$ kPa (based on Bullionfield soil measurements, see Figure 4.3) and the soil friction angle as $\phi' = 30°$, a maximum increase in shear strength due to root suction effects of only ~0.6 kPa (Bullionfield) or ~1.3 kPa (Hallyburton Hill) was estimated (using the approach by Khalili et al. to calculate the increase in soil effective stress due to suction: $\Delta\sigma' = s \cdot (s_e/s)^{0.55}$ (Khalili and Khabbaz, 1998; Khalili et al., 2004)). These estimated maximum hydrological reinforcements were small compared to the total maximum root-reinforcement measured (~6 kPa in Bullionfield and ~30 kPa in Hallyburton Hill.

8.4.5 Conclusions

- The corkscrew method measured root-reinforcement in surface layers, in which there was an abundance of roots. Peak strength values were greater where more roots were present. Deeper in soil mechanical reinforcement was hidden by spatial variations in soil properties, as shown by variation in soil stress and gravel content.
- Negative correlations between soil strength and root presence indicate roots grow where the soil is locally weak. This means that root cohesion is not merely a constant factor in slope stability modelling but reinforces the soil where it needs it most. The

corkscrew test, because it is much faster than field DSA testing, offers a relatively rapid way of obtaining shear strength data of root-reinforced soil at varying depths.

- The shape of the force-displacement extraction curve was affected by roots, independent from the increase in peak strength. The roots not only increased the soil peak strength, but also provide reinforcement over a much wider range of strain levels, i.e. they increase ductility.
- Various existing reinforcement prediction models yield very different results depending on the model and model parameters chosen. However, all overestimated the measured reinforcement. This is probably caused by stress–strain behaviour of the soil, as large differences between peak and residual shear strength were identified. Roots were observed to mobilise their strength at much larger shear displacements than the soil. This means the peak strength of the root-reinforced soil is not simply equal to the sum of the non-rooted soil peak strength and the calculated root cohesion, in contrast to common practice. It is suggested that in future studies both root and soil stress–strain behaviour is investigated in more detail.
- Sudden drops in force may be used to estimate the diameter of the associated root, similar to blade penetrometer testing, although the precise root loading mechanism in corkscrew testing could not be derived from the result because of variation in the experimental data.
- The corkscrew proved a useful tool for measuring root-reinforcement. It is quick and simple to use, yields similar values to standard vane tests where numbers of roots are low and is able to pick up the additional resistance introduced by roots. Future work should focus on extending the database of field data, preferably at a site with less sensitive soil (i.e. with a smaller difference between peak and residual strength). Other suggestions include studying the influence of wedge formation near the surface, as well as the precise mechanism of root mobilisation.

8.5 Application of simplified corkscrew method on a steep slope

8.5.1 Introduction

Previous field experiments focussed on relating corkscrew results to root and soil parameters, and were performed on relatively small areas (plots of $\lesssim$ 50 m^2) on flat or gently-sloping terrain. In this final set of trials, the corkscrew method was used on steep slopes overgrown with different types of vegetation, covering larger areas of land (plots of $\approx$ 1000 m^2), thus reflecting more realistic field conditions associated with slope stability field assessments.

These trials had the following aims:

Figure 8.36: Pictures of measurement locations at QEFP: a) 'natural' unplanted slope, b) mature Sitka spruce forest and c) clearfelled site.

1. Studying whether different land uses (natural unforested slope, forested slope, clearfelled slope) influenced the soil shear strength.
2. Assessing the suitability of the corkscrew device on steep slopes.
3. Testing the performance of the corkscrew by comparing results to standard shear vane measurements to identify the potential merits of the newer technique.

8.5.2 Methods

Site location and properties

Field experiments were performed at the Queen Elizabeth forest park (QEFP) near Aberfoyle (UK) in April 2016 over the course of three days. The same 30° (approximately 1:2) south–south west facing slope (56°11'38.3"N 4°33'4.2"W) was used in all testing. Measurements were taken at three different locations on this slope, all in close proximity (<2 km), reflecting different planting treatments:

1. 'Natural' unplanted slope, where historically no forestry has taken place. This site was overgrown with grass and ferns which had died back (Figure 8.36a);
2. 'Mature forest', consisting of Sitka spruce nursed with Lodgepole pine (*Pinus contorta*), planted in 1955. The pines have since died and the spruce has completely taken over. Trees were spaced approximately 2 m apart. No significant understory vegetation was present (Figure 8.36b);
3. 'Clearfelled' site, where a Sitka spruce (*Picea sitchensis*) crop was harvested between 2007 and 2009 (i.e. 7–9 years prior to testing), leaving large tree stumps and some of the brushwood, and since left untouched. This site was overgrown with grass, moss, patchy heather and/or some natural regeneration (Figure 8.36c).

The first treatment was located on Comer Estate grounds, while the latter two were located on Forestry Commission land.

At every treatment, 3 across slope transects of 5 measurement locations were set out. Transects and measurement locations were spaced approximately 7.5 m apart. Measurements at various treatments were performed at the same altitude (210–230 m a.s.l.) to exclude altitude effects and to maximise the chance soil types were comparable between

treatments (Figure 8.37). A 400kV overhead power line runs across the slope towards the toe, such that the site is also representative of one where slope stability assessment for forestry activities may be necessary for ensuring the safety of infrastructure (in this case, part of the national strategic power distribution network).

At one point on every transect, soil bulk density and gravimetric water content were determined using 100 cm^3 steel cores. At the same locations soil suction was measured at 250 mm depth using using field tensiometers (2725ARL Jet Fill, Soilmoisture Equipment Corp.), which were left to equilibrate for at least 6 hours after installation before readings were taken. In three occasions no reliable suctions were measured. This was attributed to poor contact between the tensiometers and the surrounding soil. These measurements were therefore discarded. All soil property results can be found in Figure 8.38.

Measured suctions were highest on the clearfelled slope. This might be attributed to temperature effect. On the day before and during the three days of testing the weather was sunny with temperatures around 15–20°C. Because of soil drying, suctions measured on the clearfelled slope (measured on test day 2) were expected to be higher than those on the unplanted slope (day 1). This drying effect might have been smaller in the forest (day 3) because of the shading provided by the tree canopy.

At all treatment locations, a 10–30 mm thin layer of litter was present which was thickest in the forest and thinnest on the clearfelled site. Topsoil (A horizon) was found until approximately 150 mm depth. Below that, orange-coloured subsoil (B horizon) was found until 500 mm depth, the largest depth for which soil horizons could be reliably established based on visual observations on extracted corkscrew and core samples. In the forest however the bedrock appeared to be much more shallow, with the C horizon (substratum), containing significant amounts of rock, observed at approximately 300 mm depth.

The soil was classified as sandy silt, based on the particle size distribution of soil samples at 150–250 mm depth on the unplanted and clearfelled slope (Figure 4.2).

Corkscrew measurements

At every location corkscrew tests were performed at various depth levels (0–125, 125–250, 250–375, 375–500 and 500–625 mm depth when possible) with each test at increasing depth within the hole left open by the previous test at shallower depth. If the target installation depth could not be reached, e.g. because of large stones, the actual installation depth was recorded and the shear strength compensated for the smaller area of the shear plane. If the difference between target installation and actual installation depth exceeded $0.5 \cdot h_{cs}$, the test and all subsequent tests at greater depths were abandoned. Corkscrews were installed vertically, rather than perpendicular to the slope, as this was thought to yield more consistent results as the slope gradient varied across the site. Perpendicular installation however is possible and might be more beneficial in some cases as this makes

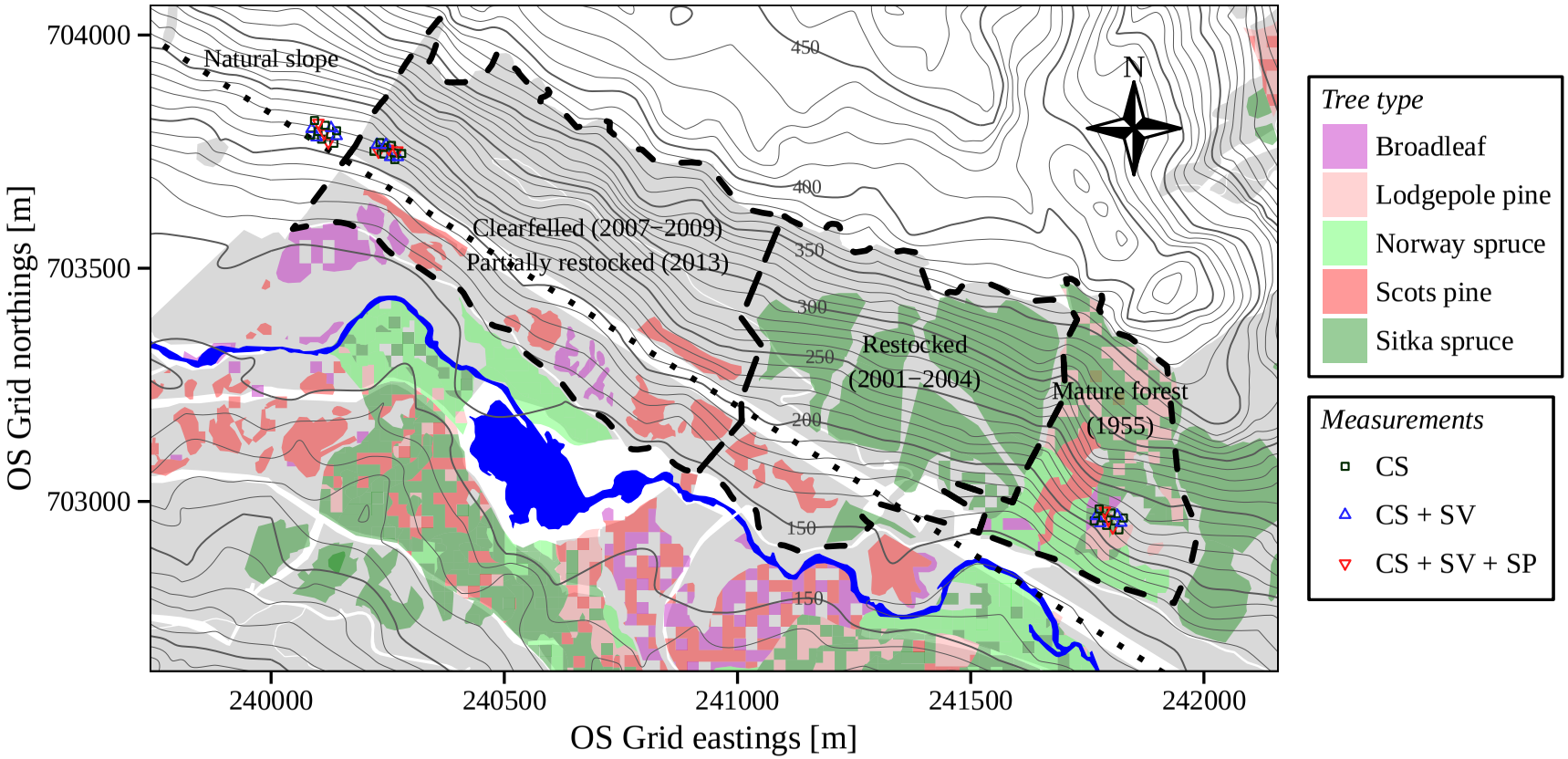

Figure 8.37: Map of measurement locations, topography and vegetation at QEFP. Coordinates are given in UK National Grid coordinates (Ordnance Survey, 2016). 'CS' = corkscrew, 'SV' = shear vane and 'SP' = soil properties (dry bulk density, water content, suction). The dotted black line indicates an overhead 400kV power line on large pylons, light grey shapes indicate areas classified by Ordinance Survey as woodland and dark blue areas surface water (data from 'OS Open Map – Local', licensed under the Open Government Licence v3.0). Contour line data (altitudes in metres) from 'OS Terrain 50' data (licensed under the Open Government Licence v3.0). Current and more detailed vegetation data (coloured shapes) from the Forestry Commission (crown copyright).

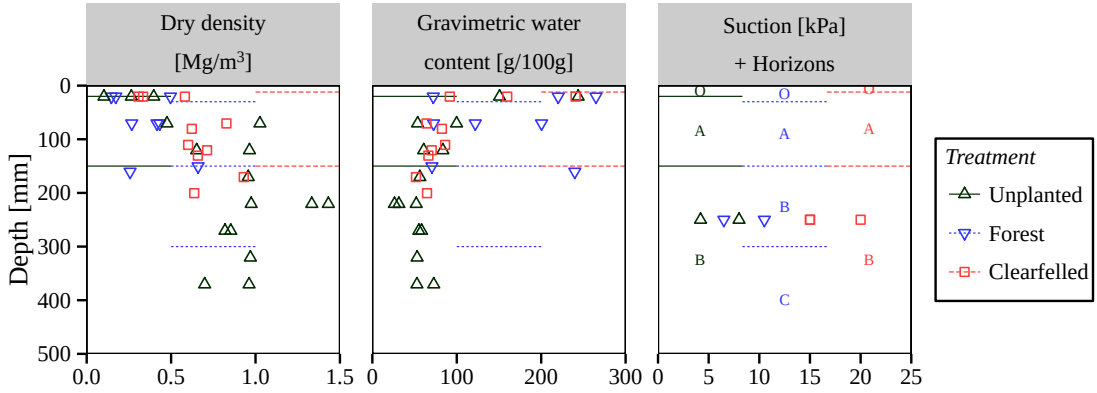

Figure 8.38: Soil bulk density, gravimetric water content and suction at QEFP site. One gravimetric water content measurement on the unplanted slope (w = 5.22 g/100g at 21 mm depth) was excluded from the graph to improve readability.

it easier to reach higher depths.

To speed up measurements for a simple and practical test procedure, in contrast to previous corkscrew experiments only the peak strength was recorded using a 500 kg load cell (DBBE-500kg-003-000, Applied Measurements Ltd.) connected to a hand-held portable strain gauge indicator (TR150). Corkscrews were installed by hand and extracted using a custom-made fulcrum and lever (Figures 8.39 and 8.40). Compared with the extraction by winching adopted in previous experiments, with this setup it proved more difficult to control the extraction rate, which was estimated as 0.75–1.50 m min^{-1}.

All extracted corkscrew soil plugs were put in sealed plastic bags and stored in a fridge at 4°C for a maximum of 7 days. Soil plug volumes were measured in the field (using a ruler) before bagging the soil. In the laboratory, the soil mass (using scales accurate to 0.01 g) was recorded and the gravimetric water content established using oven-drying of a small subsample (approximately 10% of the total mass). Soil mass and gravimetric water contents were used to estimate the average bulk density and total vertical soil stress (σ_v) at the centre of each corkscrew test. The volumetric water content (θ) in each extracted corkscrew sample was established based on the mass of water lost during evaporation and the measured soil volume.

Measurements of root volume and gravel fractions

Per treatment and depth level further, more detailed physical measurements were made for the two corkscrew samples yielding the highest shear strength and the two yielding the lowest strength. This was only done for treatments and depth levels where the number of successful corkscrew tests was 4 or higher. For the forested site at 0–125 mm depth, the four strongest samples were analysed because of large variations in strength.

For each corkscrew sample, root material was collected by careful washing of the extracted soil plug on a 2 mm sieve. This material was subsequently analysed using

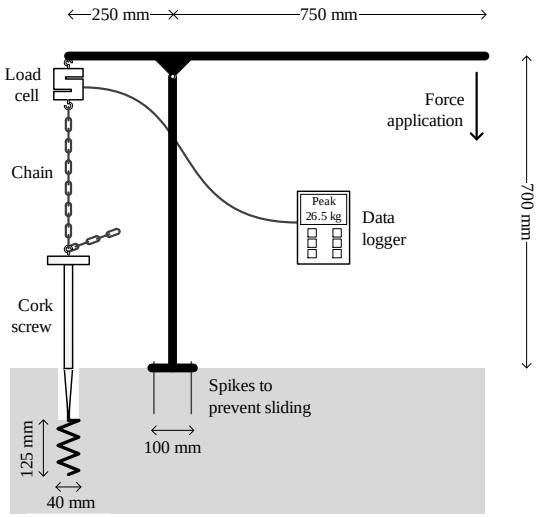

Figure 8.39: Schematic corkscrew measurement setup at QEFP site.

Figure 8.40: Picture of corkscrew testing on 'natural' slope at QEFP.

WinRhizo using 0.1 mm wide root diameter classes. The root volume fraction was expressed as the volume of roots (WinRhizo) over the measured volume of the extracted core. The soil material retained on the sieve was oven dried and the particle size mass fraction determined using 2, 4, 8 and 20 mm sieves. The gravel mass fraction was defined as the dry mass of gravel (particle size > 2 mm) divided by the dry mass of the extracted corkscrew soil plug.

Measured root volumes rapidly decreased with depth (Figure 8.41a,b). Roots at different treatments belonged to different species: on the 'unplanted' slope most of the roots consisted of (black) fern roots; on the clearfelled slope they were largely grass roots with some (thicker) roots thought to be heather or old Sitka spruce roots, and on the forested slope roots belonged to the tree species present. Especially on the forested (Sitka spruce) and 'unplanted' slope (fern) a large part of the root volume consisted of thick roots (d_r > 2 mm).

Observing overturned trees in the Sitka spruce forest (Figure 8.42) showed that the rooting depth was shallow, with roots only reaching approximately 500 mm deep. The roots in the very surface layer (approx. 0–100 mm) formed a dense root mat and accounted for the majority of roots, while below this depth mostly vertical sinker roots were observed.

A large amount of gravel (>2 mm particle size) was present in the soil apart from in the the surface layer (0–125 mm depth), especially on the forested slope (Figure 8.41c).

Although the root volume measurements of fine roots (i.e. d_r < 2 mm) were throught to reflect the real fine root volumes in the soil well, the measured root volumes of thicker roots should only be treated as indicative. For thick roots, a larger length of root will be embedded

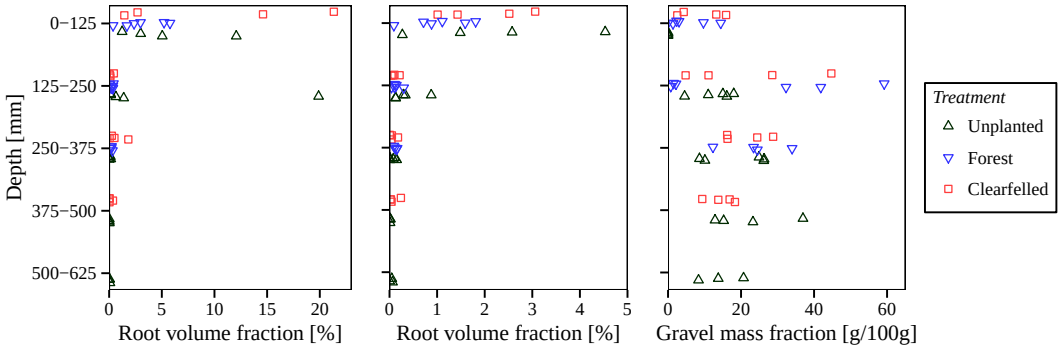

(a) Roots (all roots) **(b)** Roots ($d_r \leq 2$ mm) **(c)** Gravel (>2 mm)

Figure 8.41: Root and gravel details measured for selected extracted corkscrew cores at QEFP site.

Figure 8.42: Overturned Sitka spruce tree on the forested slope at QEFP. Black A4 clipboard for scale.

in the surrounding soil compared to in the corkscrew, causing thick roots to remain in the soil rather than to be extracted with the corkscrew, resulting in underestimations of their volumes.

Shear vane measurements

At every other corkscrew location (7 locations per treatment), standard field shear vane measurements were performed using a vane fitted with 29 mm high and 19 mm wide cruciform blades (Edeco Pilcon). 3–8 measurements of peak and residual strength were made per location covering the depth range of corkscrew testing at those locations as well as possible. The maximum depth that could be reached with the shear vane was 515 mm. On many occasions however the maximum testing depth was smaller due to the presence of stones. The actual installation depth was measured at every test and varied between 50 and 515 mm. To enable comparison between vane and corkscrew readings, standard vane readings were classed as belonging to one of five depth ranges (0–125, 125–250, 250–375, 375–500 and 500–625), equalling corkscrew depths.

Statistical analysis

To study how the corkscrew peak strength varied as a function of treatment, soil parameters and root parameters, a type III ANOVA was performed. Variables taken into account were planting treatment (unplanted, clearfelled or forested), depth level, volumetric water content, vertical soil stress, root volume fraction and gravel mass fraction. Because of the low number of replicates, measurements deeper than $z = 500$ mm were ignored, leading to a dataset of $n = 50$ measurement points. Since the depth level was taken into account as an independent variable, water content and soil stress were expressed as values relative to the average water content and soil stress at each depth level to prevent taking the effect of depth into account multiple times in the analysis.

All statistical analyses were performed using R statistical software (R Core Team, 2013).

Root biomechanics

Sitka spruce roots were sampled from the same locations as soil suction measurements in the mature forest and stored in sealed plastic bags in a fridge (4°C) for a maximum of 4 days before testing. 32 roots with a length of 100 mm were tested for tensile strength and stiffness properties using the same test conditions as described in Section 7.2.2. The root diameter range was $0.83 \leq d_r \leq 8.17$ mm. No tensile tests were performed on fern or heather roots.

8.5.3 Results

Root tensile strength and stiffness increased with increasing diameters, although the results show large scatter for both parameters (Figure 8.43). Only the power coefficient $\beta_{90,t}$ in the d_r–E_{90} fit was statistically significant ($p = 0.0071$). Compared to Sitka spruce roots

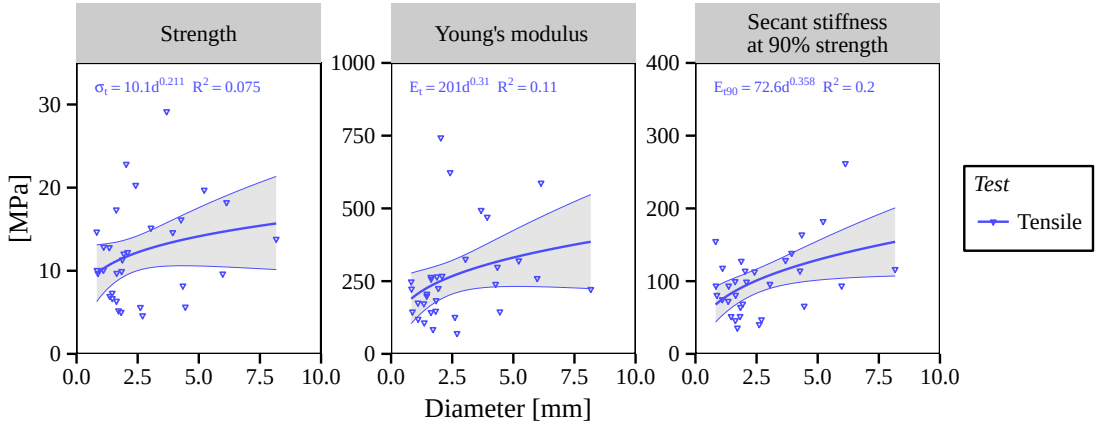

Figure 8.43: Tensile strength, Young's modulus and secant stiffness at 90% of the peak strength for Sitka spruce roots sampled at the QEFP site. The best power law fit plus 95% confidence interval of this fit are indicated by solid lines.

sampled from Hallyburton Hill (Figure 7.6), roots sampled at the QEFP were both stronger and stiffer. Comparing the best power law fits for both sites, the tensile strength was found to be 63–112% larger, the Young's modulus 77–214% larger and the secant stiffness at 90% strength 0–212% larger, all with larger differences for thicker roots.

Corkscrew testing was quick to perform, and on average approximately 10 minutes were required to measure the strength profile at one location. However, this was still noticeably longer than shear vane testing.

Corkscrew peak strength data showed an increase in strength with depth for all treatments, although per depth level large variations were found (Figure 8.44). For each depth level, none of the differences between treatments was statistically significant ($p \leq 0.05$, Welch's t-test). At 0–125 mm depth the average shear strength on the forested slope was lower than on the unplanted (27.6%) or the clearfelled slope (26.6%). At larger depths, the strength on the forested slope was similar to the unplanted slope. At 250–500 mm depth, the strength on the clearfelled slope was notably lower than on the unplanted slope (21.2% on average at 250–375 mm and 22.3% at 375–500 mm depth).

Seldom could the maximum corkscrew test depth of 625 mm or the maximum shear vane depth of 515 mm be reached (Figure 8.45). It proved slightly easier to reach larger depths using the corkscrew than using the shear vane, likely because of the larger size of the device and therefore the ability to navigate around stones.

The ANOVA results revealed that most of the variation in the corkscrew strength data stemmed from variation in measurement depth and gravel mass fraction (Table 8.3). The root volume also had a positive and significant influence on the measured peak strength. Variations in treatment, relative soil stress and relative water content were not significant. All factors together however could only account for approximately 38% of the variation in strength data, indicating other but unknown effects had a strong influence on the results.

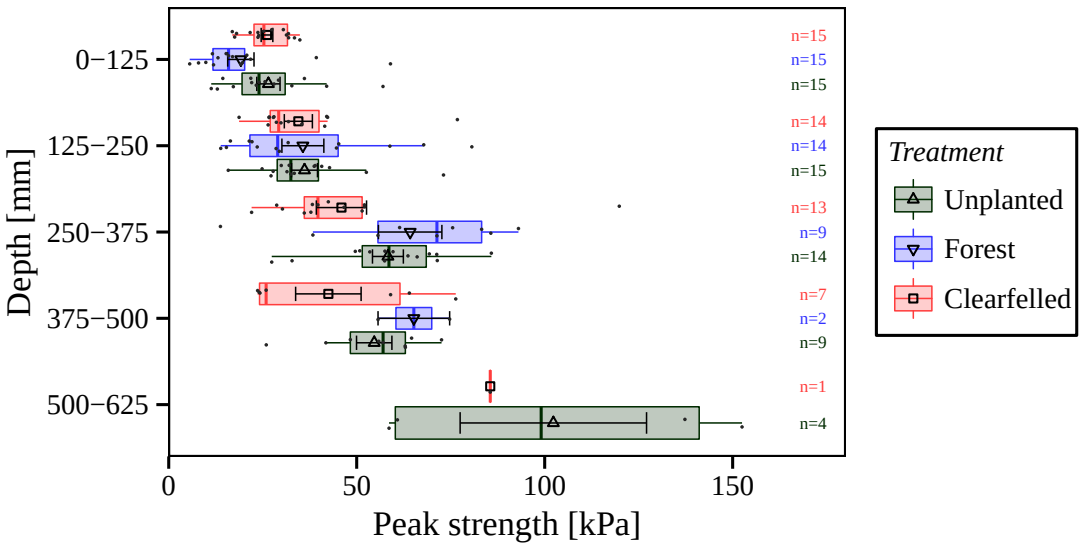

Figure 8.44: Corkscrew peak strength results at QEFP. Small grey dots indicate individual measurements. Large symbols and error bars indicate the mean and standard error per depth level and treatment. Numbers on the right (n) indicate the number of measurements taken.

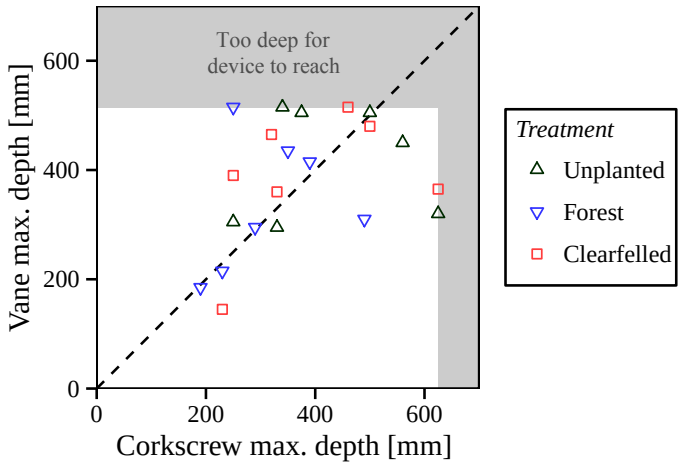

Figure 8.45: Maximum test depth reached with corkscrew and shear vane devices at QEFP.

Table 8.3: Type III ANOVA results for peak soil shear strength measured using the corkscrew device at QEFP. 'Trend' indicates whether an increase in the parameter led to an increase in strength (determined using linear fitting).

	Trend	Sum of Squares	F statistic	p-value	
Gravel (>2 mm)	+	3685.3	9.316	0.004	**
Depth level	+	3204.7	8.101	0.007	**
Root volume	+	2134.2	5.395	0.025	*
Treatment		889.7	1.125	0.335	
Water content (relative)	–	9.3	0.023	0.879	
Vertical soil stress (relative)	+	6.3	0.016	0.900	
Residual		16220			

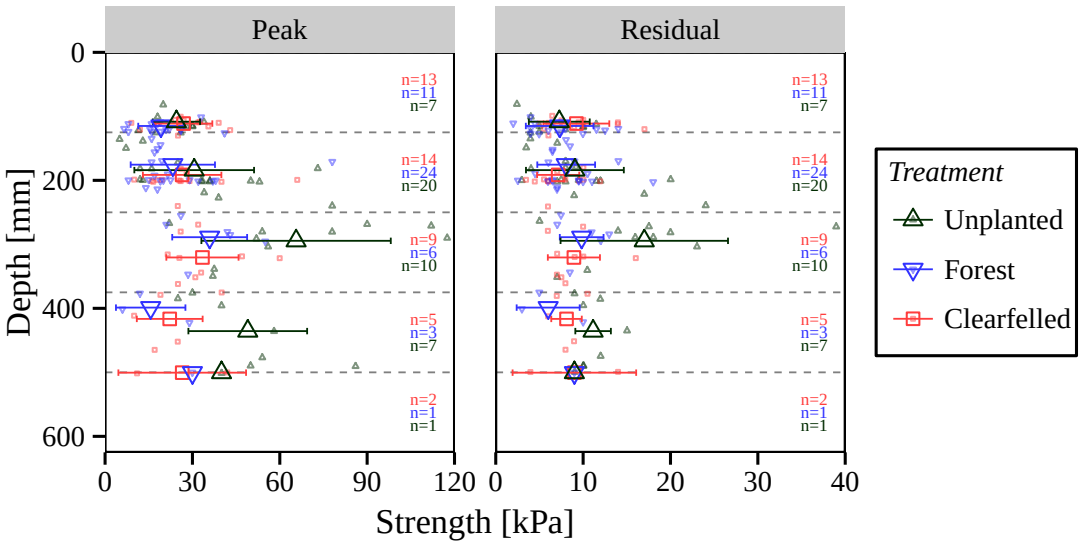

Figure 8.46: Peak and residual strengths measured using the standard vane. Small symbols indicate individual measurements. Large symbols and error bars indicate the average and standard deviation of all measurements in depth intervals separated by grey dashed lines. *n* indicates the number of successful measurements per depth interval.

No clear spatial trends could be identified in the corkscrew strength data at any depth level at any treatment. This suggests that the variation in strength is very local, and therefore demonstrates the value of a test that is quick to conduct and can therefore be conducted at many measurement points.

Similar to corkscrew readings, vane measurements showed considerable scatter for points measured at the same depth level and treatment (Figure 8.46). The average soil sensitivity was $S_t = \tau_{peak}/\tau_{residual} \approx 3.3$. The peak strength in the forest, measured with the vane device, was significantly lower than on the unplanted slope at 0–125 mm depth ($p \leq 0.05$). At both 250–375 and 375–500 mm depth, the strength on the unplanted slope was significantly higher than on both other slopes ($p \leq 0.05$). These were the only significant differences found when peak strengths between treatments were compared at each depth level.

Peak strengths measured with the vane device were comparable to those measured using the corkscrew (Figure 8.47). However, below 250 mm depth on the clearfelled and especially on the forested slope, corkscrew strengths were much higher on average. On the unplanted slope at all depths strengths measured with both devices were similar.

8.5.4 Discussion and conclusions

Sitka spruce root samples from the QEFP site were much stronger and stiffer than those encountered during testing at Hallyburton Hill (Figure 7.6). This is not surprising as it is known that roots adapt to the environment (see Section 2.3.3), e.g. to differences in soil type, hydrological conditions, wind loading or slope angle, and therefore their

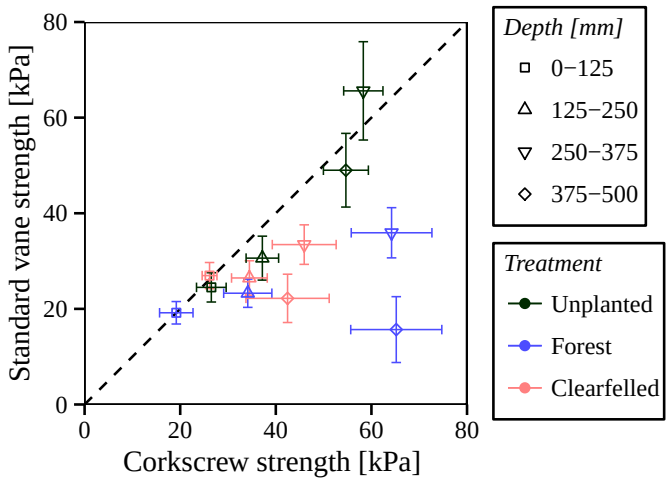

Figure 8.47: Comparison between average corkscrew and standard vane peak shear strength at QEFP site. Error bars indicate one standard error.

biomechanical properties can be different. The differences are unlikely to be caused by a difference in root age as both Sitka spruce forests had similar ages at sampling (54 and 61 years at Hallyburton Hill and QEFP respectively). These results suggest that root biomechanical properties derived at one site might not necessarily resemble those for the same species at different sites. More research is required to determine what causes the variation in root biomechanical properties apart from diameter and species.

The soil strength, measured using the corkscrew device, was not significantly different between the various treatments, largely because of the large variation within treatments and depth levels. It was largely unclear what exactly was causing this variation. Although root volume and gravel content were shown to have a significant effect on the measured soil strength, they could only explain less than half of the total variation encountered. One explanation for the poor interpretive power of the analysis could be the choice of analysis method; all data was bulked together and analysed using a type III ANOVA, thus assuming linear relationships between the soil peak strength and parameters taken into account in the analysis. However, there is no indication that all trends were linear. Furthermore other factors not taken into account in the analysis might have played a role as well, such as differences in soil structure, soil type or local variations in soil suction.

Since no significant strength differences between treatments were found, only tentative conclusions and interpretations can be drawn. On the forested slope, the strength appeared to be lower in the surface layer (z = 0–125 mm), which likely reflects the very loose top soil generally present in forest stands. Even though this layer was heavily rooted with tree roots, this might not have fully compensated for the soil component of the total shear strength being much lower than at other treatments. The clearfelled slope at the same depth was similar in strength to the unplanted slope, potentially as a result of recolonisation by heather and grasses with very shallow rooting since harvesting of the trees. By 125–250

mm the root material in the forested slope is compensating for the lower density soil, providing comparable strength to the unplanted slope. At depths exceeding 250 mm, the clearfelled site yielded lower results which might reflect a loss of strength due to a history of soil disturbance, e.g. forest operations and harvesting and subsequent tree root decay. Although the strength on the forested slope appeared to be higher than the clearfelled area once below 250 mm, this could reflect the more stony nature of the soil and might not necessarily be caused by roots as measured root volumes were very low at these depths; tree rooting was observed to be very shallow (Figure 8.41).

The large variation in data within each treatment and depth level showed that it is important to conduct a sufficient amount of tests so that this variation can be taken into account in slope stability analyses. An estimation of the required sample size was made using the experimental data. For every treatment and depth level, the shear strengths were fitted with a normal distribution. The mean and standard deviation of these were then used to estimate the sample size required to reduce to standard error to the mean of a new theoretical set of measurements to within a certain percentage of the mean. (with a 90% probability). The results (Figure 8.48) show more measurements are required to in the surface layers of the forested treatment (0–250 mm depth) compared to the other treatments, and that with increasing depth less measurements will suffice to obtain the same reliability. Based on this analysis, if a sample size of 20 would be adopted for example, the ratio between standard error and mean value will be below 10–25% with 90% certainty, depending on depth and treatment.

Near the soil surface, i.e at 0–125 mm depth, strengths measured with the standard shear vane were very similar to those measured with the corkscrew. Although on the 'unplanted' slope at increasing depths corkscrew and vane measurements were similar, on the clearfelled and especially the forested slope corkscrew strengths were comparatively higher.

Several explanations for these results are put forward. 1) Effect of large roots: Since these differences occurred in (historically) forested slopes but not on the 'natural' slope, differences might have been caused by (decaying) tree roots. Although Figure 8.41 suggested that root volumes were low at these depths, it was known that the root sampling strategy will have led to underestimation of the volume of thick roots. If these were present at greater depths, the vane device will have struggled measuring their effect while the corkscrew is more likely to have measured their reinforcement due to less disturbance during installation; 2) Effect of gravel. Soils were stony, especially on the forested slope. Corkscrew readings are likely to be higher in stony ground as during installation the screw will screw around the stones while during extraction they will increase the extraction force due their interaction with the shear plane. On the other hand, during installation of the vane stones will have been pushed aside, thus heavily disturbing the soil potentially resulting in lower strengths compared to non-stony soil; 3) Effects introduced by limited

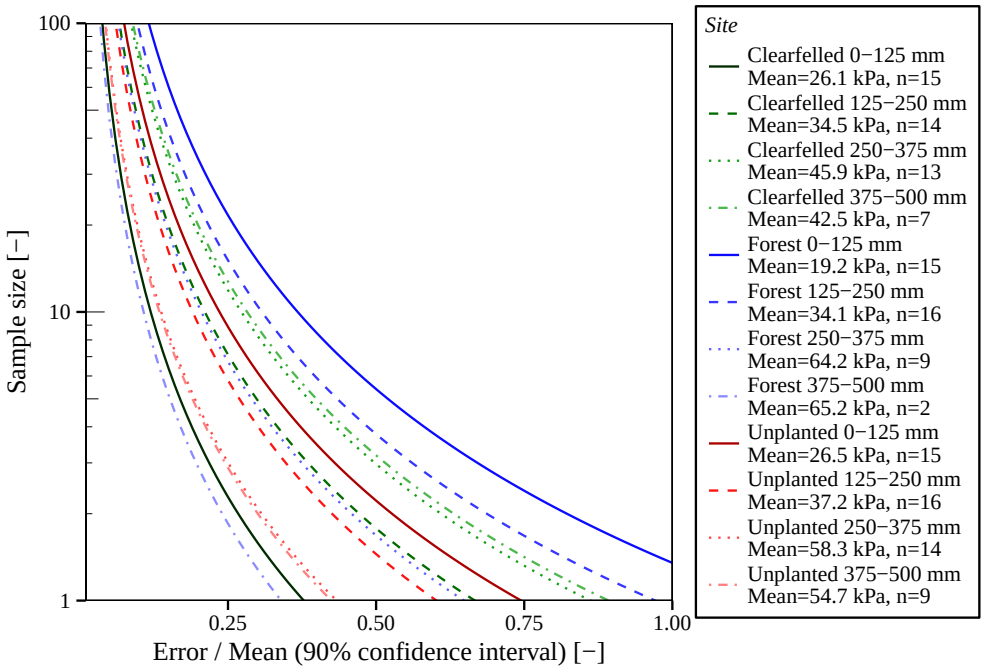

Figure 8.48: Estimation of the required sample size based experimental data from the field experiment in QEFP and the accepted normalised standard error to the mean. n indicates the sample size in field experiments.

installation depths. In many corkscrew and vane tests, the target installation depth could not be reached. Therefore, at higher depths there will be a relative overabundance of measurements in weaker, non-stony soil, since these will have been the soil that could be penetrated. Since the corkscrew was more likely to penetrate 'difficult' soil layers, average strengths were likely higher than those measured with the standard shear vane.

Although this study did not clearly show the beneficial effect of the corkscrew in rooted soil compared to the standard vane, it showed that the corkscrew has additional advantages over standard vane testing in stony soil. Since stony soils such as glacial tills are common in the UK and abroad, the corkscrew will still be a practical field testing tool.

The corkscrew was shown to be suitable for use on sites with difficult accessibility. It could be transported easily across sites and could be carried up steep (1:2 gradient) forested and non-forested slopes. Measurements were much faster than attainable using shear box testing (1 depth profile every approximately 10 minutes) although slower than shear vane testing. Large stones with sizes exceeding the pitch of the diameter ($\gtrsim$ 25 mm diameter) did however cause problems with installation, limiting the usefulness of the corkscrew in certain soils. More work is required to calibrate the corkscrew in real field conditions, covering a range of soils and vegetation types.

9

Discussion and conclusions

Using vegetation can prove a suitable and environmentally-friendly way to stabilise slopes. However, the mechanical contribution of roots to the shear strength of the soil is difficult to measure in the field. This is essential information for the engineering analysis and design of vegetated slopes. Existing test methodologies are time-consuming and therefore not suitable to quantify spatial variability on the slope. Furthermore, some methods, for example large *in situ* shear box tests, can be difficult to apply on remote sites with difficult access, e.g. steep slopes. Therefore this study set out to develop quick, small yet reliable methods to quantify mechanical root-reinforcement *in situ*.

9.1 Root biomechanical behaviour

Root biomechanical behaviour was studied to enable comparison of field data with root-reinforcement prediction models. For all species studied here (Sitka spruce, pedunculate oak and blackcurrant), no or only small positive relations were found between root diameter and root strength or stiffness. In contrast, most others have found negative relations between tensile strength and root diameter (e.g. see Bischetti et al., 2005; Operstein and Frydman, 2000; Mao et al., 2012), see Figure 9.1. The sparsely reported data on stiffness showed similar negative trends (e.g. Operstein and Frydman, 2000; Loades et al., 2013). Relatively few studies were found which showed no or slightly positive diameter–tensile strengths trends, see for example some of the results for *Picea abies* in a study by Vergani et al. (2014a).

Decreasing strengths have previously been explained by chemical changes in the root, with thinner roots containing more cellulose (Genet et al., 2005) or lignin (Zhang et al., 2014). An alternative mechanical explanation suggests the strength in thicker roots is lower due to the increased chance of imperfections in the material as the volume increases. Since failure initiates at the weakest point in the root, increased numbers of imperfections increase the chance of measuring lower strengths, as for example observed for jute fibres

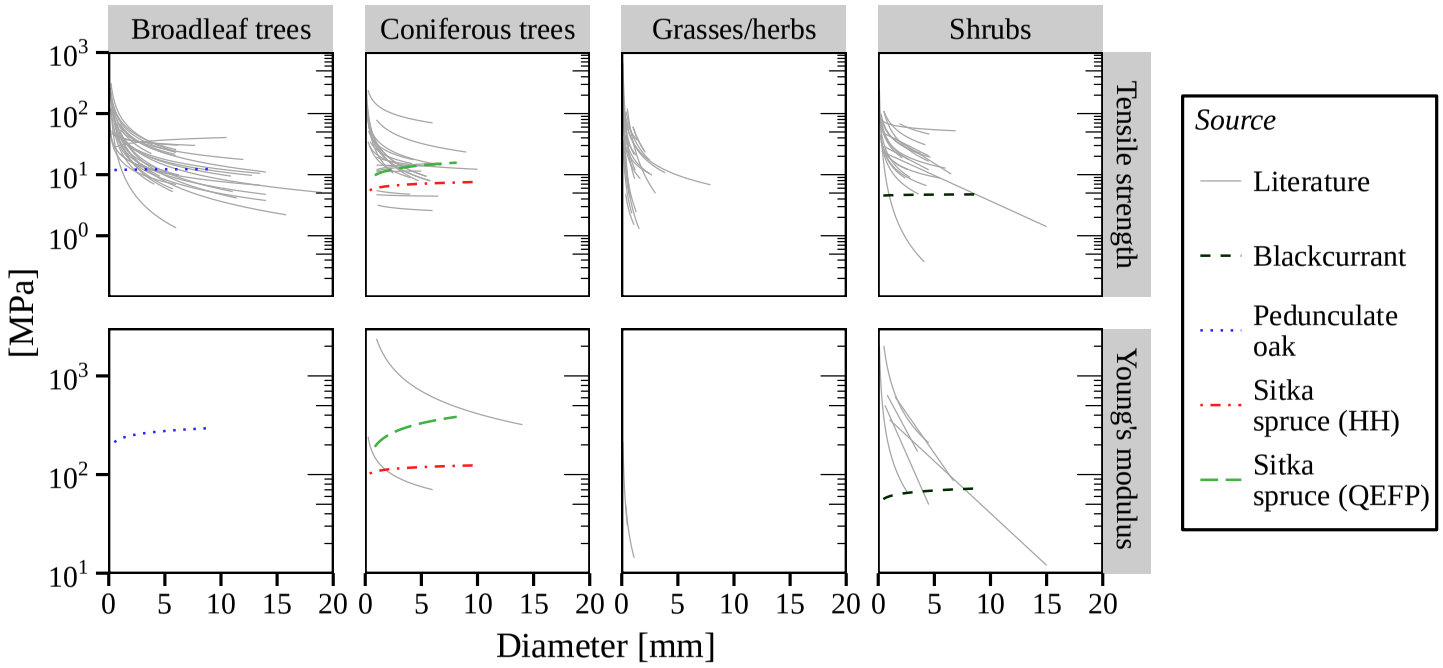

Figure 9.1: Reported relationships (literature) and experimentally measured root tensile strength and stiffness as a function of root diameter. Curves are only plotted over the diameter range of tested roots, and only sources in which this range was reported or for which it could be estimated using reported plots were used. No data was found for the Young's modulus of broadleaf tree roots. Data collated from Abernethy and Rutherfurd (2001); De Baets et al. (2008); Van Beek et al. (2005); Bischetti et al. (2005, 2009); Comino et al. (2010); Docker and Hubble (2008); Fan and Su (2008); Genet et al. (2005, 2008, 2010); Loades et al. (2010, 2013); Mattia et al. (2005); Mickovski et al. (2009); Nilaweera and Nutalaya (1999); Operstein and Frydman (2000); Simon and Collison (2002); Vergani et al. (2014a); Waldron and Dakessian (1981). Where curves are presented in terms of maximum tensile force, the curve for tensile strength was derived by dividing force fits by the root area. 'HH' denotes Hallyburton Hill, 'QEFP' denotes Queen Elizabeth Forest Park.

(Bevitori et al., 2010) or glass (Kim et al., 2013). In contrast, thicker roots are generally older and root strength has been found to increase with time (Genet et al., 2008), providing an explanation as to why thicker roots might be stronger. Another explanation for thick roots being stronger is the ratio between the cross-sectional area of bark and stele, which increases during secondary root growth. Experimental observations showed that the root strength was concentrated in the stele. For Sitka spruce in Hallyburton Hill forest the relative cross-sectional area of the stele was found to be larger in thick roots, explaining the higher tensile and bending strength and stiffness measured in thicker roots.

In this thesis new data is presented on root strength and stiffness characteristics in bending. It was shown that strength and stiffness measured in 3-point bending were different from those measured in uniaxial tension. Data for these root properties is scarce (but see Ennos et al. (1993); Stokes et al. (1996); Goodman et al. (2001), for example). However, these properties are important especially for thicker roots which might behave in bending instead of tension. Furthermore, when roots are mobilised by shearing soil, some roots might be loaded in compression first. In these cases, root bending data is required when roots are assumed to fail due to buckling effects, e.g. see modelling by Schwarz et al. (2015).

The tensile strength and stiffness of Sitka spruce roots sampled from different sites (Hallyburton Hill and Queen Elizabeth Forest Park) were different, proving that root strength and stiffness are not just a function of species and diameter. Roots adapt to the environment, e.g. to differences in soil type, hydrological conditions (e.g. Loades et al., 2013), wind loading or slope angle (e.g. Nicoll and Ray, 1996), and therefore their biomechanical properties will differ. Therefore root biomechanical properties derived at one site might not necessarily resemble those for the same species at other sites. This has important consequences for root-reinforcement predictions which generally make use of root tensile strength data. It is therefore better to establish root properties for every new site rather than to rely on values from the literature. More research is required to determine what causes the variation in root biomechanical properties apart from diameter and species.

9.2 Blade penetrometer testing and root–soil interaction models

The blade penetrometer was developed to detect the depth and diameters of roots based on characteristics of the depth–resistance penetrometer. To increase the sensitivity of the device to roots, a standard cone penetrometer tip was fitted with a thin but wide blade. This added a relatively small soil resistance while greatly increasing the chance the tip would hit a root.

Both in the lab (PP fibres and ABS root analogues) and in the field (Sitka spruce and

pedunculate oak roots) the blade penetrometer was shown to detect effects introduced by roots. A distinct difference between the behaviour of small and thicker roots was observed. Polypropylene fibres (laboratory) or numerous fine roots near the surface (field) introduced increased resistance over the whole range of the rooted zone, but without distinct root failures, i.e. without sudden drops in resistance. This lack of distinct failures corresponds with results of triaxial tests (Ibraim and Fourmont, 2007; Diambra et al., 2010) or laboratory direct shear tests (Jewell and Wroth, 1987) on fibre-reinforced soils or direct shear tests of rooted soil (e.g. Comino et al., 2010; Docker and Hubble, 2008; Fan and Su, 2008). Sampling rates in direct shear tests in the literature might however have been too low to accurately measure sudden changes in the resistance. Both blade penetrometer and corkscrew testing showed that the sudden drop in force due to root breakage occurs within only tens of milliseconds.

In the laboratory, increased resistance was found with increasing number of fibres (i.e. the volume fraction), and in the field a strong correlation was found linking root length density and root volume with resistance near the surface. However, model predictions using the newly developed 'root mat model', modelling the composite root behaviour as the sum of the effect of individual roots, did yield the right trends but resulted in inaccurate predictions for the field experiments. This indicated that the mechanism through which fine roots reinforce the soil is not captured correctly in existing models. It is hypothesised this was caused by 1) roots displacing more than predicted, 2) roots slipping rather than breaking, resulting in lower reinforcements per root but active over a much longer displacement range, or 3) root–root interaction as roots are part of an interconnected network, generally ignored in models.

These experiments provided qualitative proof suggesting that soil rooted with fine roots behaves very differently from soils rooted with thicker roots. In the first case, the rooted material behaves like a composite material where the effects from soil and roots should not be studied separately. Generally in mechanical root-reinforcement research, it is assumed that roots follow the behaviour of the soil as perfectly elastic elements, i.e. the roots have no influence on the deformations within the soil. However, the observed 'composite' behaviour suggests that this assumption is not true, as fine roots greatly increased the ductility of the soil. Even though this effect was observed during shear box testing, where rooted soils showed thicker shear bands and required larger displacements to reach failure (e.g. Ekanayake et al., 1997; Fan and Su, 2008; Mickovski et al., 2009; Shewbridge and Sitar, 1989), it has never been incorporated in predictive root-reinforcement models.

The root mat model indicated that the resistance of fine roots in a root mat to blade penetrometer penetration was related not just to the peak strength of the root but also to the root displacement, and therefore to the amount of energy dissipated by the root. This suggests it is advisable to divert more effort into studying the effect of root mobilisation and strain effects instead of exclusively focussing on strengths. The progressive mobil-

isation of a root bundle has been addressed before (e.g. Schwarz et al., 2010, 2013) but not in conjunction with simultaneous mobilisation of soil resistance and root–soil interaction. One possible route to address root and soil mobilisation simultaneously would be constitutive modelling, for example as attempted for fibre-reinforced soil (Diambra et al., 2010).

In contrast to thin roots, the breakage of thicker roots could be observed as distinct drops in force. When roots were thick (ABS roots in the laboratory testing, real roots with diameters exceeding 0.5–1 mm in field testing), the effects of individual roots on the depth–resistance trace could be noted. From the moment a root was hit the resistance gradually increased with depth until root failure, visible in the trace as a sudden decline in resistance, lasting only tens of milliseconds.

The magnitude of these drops could be predicted using newly developed analytical models. However, an assumption for how the roots will break, either in bending or tension, was required to select the right model for each species and root diameter. All ABS root analogues tested in the laboratory in dry sand (2 or 4 mm diameter) failed in bending; Sitka spruce roots at Hallyburton Hill forest all appeared to have failed in tension while small oak roots at Paddockmuir Wood ($d_r \lesssim 2$ mm) were thought to have failed in tension and thicker oak roots in bending. This implies that the biomechanical behaviour of a root needs to be known or studied before an interpretive model is selected, as roots from various species were shown to behave in different ways.

Both laboratory and field testing showed that the magnitude of the resistance, measured as the magnitude of the force drop, was a much better predictor for root diameter than the root displacement to failure. Various explanations were derived: 1) Displacement predictions are much more sensitive to variations in root strength, stiffness and soil resistance; 2) The interpretive models assume linear stress–strain behaviour, ignoring any root plasticity. Only a part of the effects of inelasticity were accounted for by using the secant stiffness at 90% of the peak strength instead of the Young's modulus of the elastic region. 3) Real roots can be tortuous, whereas the models assumed straight roots. From pull-out tests using real roots it is known that the measured 'apparent' stiffness can be much smaller than the root material stiffness because the root will straighten out during pulling (e.g. Commandeur and Pyles, 1991).

Both newly derived analytical interpretive models, the analytical bending and cable models, were easy to use and require only a small number of input parameters: root strength, root stiffness, soil resistance and for the cable model an additional estimate for root–soil interface friction. Numerical modelling showed that the soil resistance can be assumed as a constant value, independent from root lateral displacement, because root displacements are large compared to soil displacement required to reach the maximum soil resistance according to p-y theory (American Petroleum Institute, 2000; Randolph and Gourvenec, 2011; Reese and Van Impe, 2011). The analytical bending model improved

over existing models by modelling soil resistance as a constant value, in contrast to Wu et al. (1988), or by its more practical formulation (Wu, 2007, 2013). The analytical cable model improved over existing cable models for roots (Wu et al., 1988; Wu, 2007, 2013) by accounting for non-linear displacement effects and the influence of axial strain in the root.

Even though both analytical models were shown to explain the behaviour of real roots or root analogues, both suffer from large simplifications. Both assume individual, long, straight, horizontal, unbranched roots with homogeneous cross sections. Although laboratory testing suggested that the effect of diameter is larger than the influence of angle, length, loading position and branching, the effects of these parameters should be studied in future work to improve both interpretive models. Especially in soft soil, the effect of root architecture might heavily influence the results as larger parts of the root will displace and therefore the effect of root architecture (roots being connected to other roots and therefore roots influencing each other) will be more pronounced.

Yet the method was shown to perform well at real field sites. The method was quick and easy to use and yielded valuable information about both root depth and root diameter. When this testing method is to be used for practical applications, one should know the plant species involved so that the right interpretive model can be selected. Since root biomechanical properties vary significantly between species, root tensile and/or bending strength and stiffness should be measured or assumed for each species studies. To acquire accurate values for the soil resistance, penetrometer testing can be adopted. However, a correction factor is required to take the difference in shape between cone tip and root into account. This correction factor should be studied in more detail. In this work an estimation was made based on comparing penetrometer data to model results using the method of Reese and Van Impe (2011). However, this factor was only derived for dry sand and not explicitly determined in the field. Root–soil interface friction can be estimated using simple field shear strength tools such as a field shear vane. This value should be corrected since soil–soil friction is likely to be higher than soil–root interface friction (Gray and Sotir, 1996; Mickovski et al., 2009). This correction factor was not experimentally verified in this study and does depend on soil and root interface characteristics. It is advisable to study this friction in more detail, e.g. by pull-out tests of real root, to obtain a stronger experimental basis for this parameter.

Stones and debris caused difficulties in this study. Not only did they limit the maximum penetration depth but they also introduced artefacts in the force–displacement plot that were difficult to distinguish from root breakages. This has important implications for application of the method in soils such as the glacial tills present in many field sites in Scotland. Incorporation of a microphone into the blade penetrometer should help identification of snapping roots using sound so that a distinction can be made between hitting stones or roots. Blade penetrometer field testing in Paddockmuir Wood showed

promising acoustic results, showing that roots breakages could be heard as short bursts (approx 10–50 ms) of sound.

Since this method can only be used to infer root depths and root characteristics, using this measurement data to quantify root-reinforcement requires an additional modelling step to quantify effect on the root shear strength, e.g. by using the Wu/Waldron model (Wu et al., 1979) or a fibre bundle model (e.g. Pollen and Simon, 2005). Although at Hallyburton Hill both blade penetrometer resistance and cork screw shear strength were measured, these were not directly compared in this thesis because they were acquired at different times (different soil conditions) and because of the unavailability of an accurate method to quantify the effect of small roots from blade penetrometer test results.

9.3 Shear testing

In this thesis, two new methods to directly measure the root-reinforced shear strength were developed, namely the pin vane and corkscrew device. Both were shown to yield comparable results to standard vane testing in fallow field soil. Near the surface (0–125 mm depth) however and to a lesser extent at 125–250 mm depth, corkscrew testing did yield lower strengths compared to vane devices due to surface heave and the development of a conical rather than the cylindrical failure mechanisms assumed during data analysis. In surface layers heavily rooted with grass, the standard vane was shown to yield much lower strength values compared to the pin vane due to significant soil and root disturbance during installation and a different failure mechanism, similar to disturbance observed in peat during standard vane tests by Landva (1980). It was therefore concluded the pin vane is the better device when studying shallow root-reinforcement, e.g. for soil erosion susceptibility. However, the ease of use and the larger dimension of the corkscrew made this device more suitable in deeper layers, important for landslide susceptibility analyses. Because of its larger size and ability to screw around solid objects during installation, it is more useful in stony soil as long as the stones are smaller than the diameter of the device.

Field testing was mainly performed using the corkscrew device since the main interest of this study was the effect of roots on landslide susceptibility. Corkscrew field testing showed positive and significant trends between predicted and measured reinforcement in surface layers (0–125 mm) where roots were abundant and the soil relatively weak. With increasing depth however root quantities decreased significantly at the field sites used and the soil component of the overall strength increased. Local variations in soil strength and gravel made it difficult to isolate the root-reinforcement component at these depths. These complications have not been observed before in previous field shear box tests due to limited replication of most field shear box tests. The number of tests is generally much smaller due to the time required to set up a test (e.g. 25 tests per species in Docker and Hubble (2008), 8–12 tests per species in Fan and Chen (2010) or 10 tests per species in Comino

et al. (2010), compared to the 49 (Bullion Field), 62 (Hallyburton Hill) or approximately 50 (per treatment in Queen Elizabeth Forest Park) successful corkscrew tests performed in this thesis), and generally all variability in measured strengths is attributed to roots without investigating other effects which might influence the soil strength, such as soil stress levels and density, water content, suction levels or soil type and texture.

The high variability in corkscrew results likely stems from the relatively small size of the device, making it more sensitive to small local variations. Since one of the requirements for these new measurement devices was that they had to be portable, the sizes of the used corkscrew and pin vane had to be limited. Therefore the methods are sensitive to small local variations in soil and root conditions. This can be an advantage when studying the root spread of a single plant as more accurate local data is collected, but might introduce difficulties when large areas are to be assessed as a single measurement point might not be fully representative of the area in which it is taken. Therefore, when using this method care should be taken to select an appropriate amount of measurement points, reflecting the expected spatial variability.

To build up a stronger experimental basis for both new root-reinforced shear strength measurement methods, it is suggested that additional experiments should be undertaken in homogeneous field soils reinforced with real roots. Thus the 'noise' in the data resulting from variations in soil parameters can be minimised while still testing in realistic field conditions.

Compared to model predictions using the Wu/Waldron model (Waldron, 1977; Wu et al., 1979) or fibre bundle models (e.g. Pollen and Simon, 2005), measured values for corkscrew root-reinforcement were much smaller. Models with increased complexity yielded lower reinforcement predictions closer to experimentally measured values. The large variation in model predictions was in line with numerical work by Thomas and Pollen-Bankhead (2010). This suggests that, although there is good theoretical and some experimental support for the existing models predicting the behaviour of a single root, the behaviour of a bundle of roots (as measured during field tests) is not captured well in existing models. Likely explanations are variations in root architecture (e.g. angle with shear plane, anchoring) and root–root interaction, e.g. through roots being connected to each other.

Comparing experimental results with other studies revealed that while values for k' measured in this study were small, they were comparable to those found in lab or field shear box testing reported before (e.g. Comino et al., 2010; Docker and Hubble, 2008; Fan and Su, 2008; Fan and Chen, 2010; Hengchaovanich and Nilaweera, 1996; Loades et al., 2010; Operstein and Frydman, 2000; Pollen and Simon, 2005). This reinforces the conclusion that the real mechanism through which a bundle of roots reinforces the soil is poorly captured by existing models. The large variability in experimental results furthermore shows that reinforcement might not simply be a function of root tensile

strength and diameters.

Both the corkscrew and pin vane device measure the combined effect of soil strength, root mechanical reinforcement and the hydrological reinforcement (through an increase in matric suction). The various sites used throughout the field work performed in this thesis to quantify root-reinforcement were generally quite wet, with small values of matric suction ($<$ 10 kPa, apart from the clearfelled slope in the Queen Elizabeth Forest Park where $s \approx$ 10–20 kPa). Only a fraction of this will be additional suction caused by plant roots, and the hydrological effect of plant roots on the soil shear strength will have been small in this thesis. However, if the pin vane and corkscrew are to be used to quantify the mechanical reinforcement caused by roots in sites where the hydrological reinforcement is thought to be a major influence, the measured total root-reinforcement had to be corrected for the hydrological part. This can for example be done by measuring the increase in soil suction due to plant roots by comparing rooted and non-rooted sites, and subsequently calculating the effect on soil–root composite shear strength through an increase in effective stress.

Field testing indicated that understanding the full stress–strain behaviour of the soil is important. Both field soils tested showed considerable sensitivity, i.e. a marked difference between peak and residual soil shear strength. This is probably caused by a breakdown of soil structure (e.g. Utomo and Dexter, 1981; Mitchell and Soga, 2005). Since roots require much larger shear displacements than soil to reach their full reinforcement potential, the peak root-reinforced shear strength might be lower than the sum of the individual root and soil shear strength peaks. Secondly, roots were shown to add resistance over longer displacement intervals. Therefore more energy is dissipated during shearing of rooted soil, even when the apparent reinforcement effect was low. This additional ductility might be important for understanding the post-triggering consequences of landsliding in rooted soil. Because more energy is dissipated during sliding, a potential landslide in rooted soil might reach slower velocities and therefore travel less far. Future work should study this effect in more detail, as so far most research on landslides in root-reinforced soil have focussed on the triggering phase (i.e. where strength is most important) rather than the propagation phase.

A small body of experimental evidence showed a negative correlations between fine root mass and soil stress at depth (375–500 mm), indicating preferential root growth where the soil mechanical impedance is smaller (Bengough and Mullins, 1990). This might have important implications for slope stability. It indicates that roots act as ‘natural engineers’, reinforcing the soil where it is most needed. This effect has never been observed before during *in situ* shear testing of rooted soil. It also implies that the assumption that root-reinforcement is evenly distributed, often assumed in slope stability modelling, is incorrect. Since landslides tend to localise in weaker zones, understanding the spatial spread of roots and soil strength is important and more effort should be diverted in this

direction.

Individual small roots crossing the shear plane during cork screw testing can be assumed to fail due to shearing, as analytical models suggest that only a small length of the root on either side needs to displace before failure occurs. In contrast, larger roots might have been loaded in a slightly different way as they might intersect the shear plane on either side of the corkscrew device. In those cases, the 'real' loading mechanism lies somewhere between a point and shear load. Although the developed analytical models should able to estimate when this transition takes place they were not considered accurate since laboratory and field testing using the blade penetrometer showed that the displacements predicted using these models were not accurate.

Both pin vane and corkscrew devices measure root reinforcement primarily on vertical planes and therefore primarily measure the reinforcement introduced by more or less horizontally orientated roots. In landslides, however, the shear plane will be more horizontal. This issue can be partially addressed by inserting the measurement devices perpendicular to the suspected root angle. Alternatively, assumptions or measurements on the distributions of root orientations can be used to verify or correct the root reinforcement from mathematical root architecture models (e.g. see Danjon et al., 2008). In this thesis, no attempts were made to address the issue of root-reinforcement anisotropy, but this should be investigated in future work. It should be noted that varying the inclination might affect the soil component of the measured shear strengths as well when the soil is anisotropic.

No attempts were made to study the effect of the extraction rate on the shear strength measurements. Instead, the rate was chosen in line with landslide velocities obtained from the literature. Although tensile testing by Cofie and Koolen (2001) indicated that the effect of the test rate on root strength is small, rate effects are known to effect the behaviour of soil due to the potential build-up due to changes in pore water pressures. It is therefore advised that in future work the effect of the extraction rate on the measurement results is studied.

Both the pin vane and corkscrew method measure the root-reinforced shear strength at a particular time. Since soil strength depends not just on the root quantity but also for example on the water content and matric suction levels in the soil, measured values are only valid for the conditions in which they were measured. Since slope instabilities are often triggered by rainfall and increased water contents in the soil, an assessment of the (rooted) soil strength in such adverse conditions (representing critical design scenarios) should be made. It is therefore important during corkscrew or pin vane measurements that the soil water content, matric suction and density are also recorded and a record of the soil type is made. If it is not possible to take measurements in conditions similar to when the soil is expected to be prone to failure, an additional soil model is required which can use this additional soil data to make predictions for the strength of the soil in adverse conditions. The reinforcement effect of the roots can still be assessed in a wide range

of soil conditions by comparing measurements taken in both rooted and non-rooted soil when both can be found close together.

9.4 Summary

- Root biomechanical testing showed no or slight positive trends between root diameter and both root tensile or bending strength and stiffness, in contrast to data on tensile properties reported before. Data showed considerable scatter. Sitka spruce roots tested from two different sites had different properties, showing that biomechanical properties are not only a function of species and diameter.
- Several simple analytical models to predict root behaviour under point loading or loading by soil shear displacement were developed. One model assumed roots break in tension, while another assumed bending failure. Based on root strength, root stiffness, soil resistance and root–soil interface friction, both root displacements and associated forces due to relative soil–root movement could be predicted.
- Blade penetrometer depth–resistance traces could be used to detect the depth and estimate the properties of roots, both in simplified laboratory conditions and at field sites. However, the correct failure mechanism (tension or bending) must be known in advance to select the right interpretive model.
- The pin vane device, although not extensively studied, was qualitatively shown to function well in heavily rooted (surface) soil layers, both in laboratory and field conditions. It caused much less soil and root disturbance than the traditional field shear vane device.
- The corkscrew device under-predicted root–reinforced shear strength results near the surface (conservative results) but functioned well in deeper ($\gtrsim$ 250 mm) soil layers important for landslides. Relating measured reinforcement to root properties was only possible near the surface (0–125 mm depth). In deeper layers, local variation in soil stress, gravel content or water content, combined with low root volumes, made it difficult to accurately determine the effect of the roots. Measured reinforcements were small compared to existing model predictions but comparable to direct shear tests on rooted soil reported before.
- Tests with these new, quick and easy to use methods to quantify mechanical root-reinforcement showed promising results for practical field use. However, more work is required to validate and further improve the interpretive models developed and to calibrate these methods for a range of soil and root conditions.

Bibliography

Abdi, E., Majnounian, B., Genet, M., and Rahimi, H. (2010). Quantifying the effects of root reinforcement of Persian ironwood (*Parrotia persica*) on slope stability; a case study: Hillslope of Hyrcanian forests, northern Iran. *Ecological Engineering*, 36(10):1409–1416.

Abe, K., Ziemer, R. R., and Usda (1991). Effect of tree roots on shallow-seated landslides. *Proceedings of the IUFRO Technical Session on Geomorphic Hazards in Managed Forests*, 130:11–20.

Abernethy, B. and Rutherfurd, I. D. (2001). The distribution and strength of riparian tree roots in relation to riverbank reinforcement. *Hydrological Processes*, 15(1):63–79.

Adhikari, A. R., Gautam, M. R., Yu, Z., Imada, S., and Acharya, K. (2013). Estimation of root cohesion for desert shrub species in the Lower Colorado riparian ecosystem and its potential for streambank stabilization. *Ecological Engineering*, 51:33–44.

Al-Defae, A. H. (2013). *Seismic performance of pile-reinforced slopes*. PhD thesis, University of Dundee.

American Petroleum Institute (2000). *Recommended practice for planning, desdesign and constructing fixed offshore platforms – Working stress design: API recommended practice 2A-WSD, 21st edition, December 2000. Errata and supplement 1, December 2002*. American Petroleum Institute.

Ammer, C. and Wagner, S. (2005). An approach for modelling the mean fine-root biomass of Norway spruce stands. *Trees – Structure and Function*, 19(2):145–153.

Bengough, A. G., Mackenzie, C. J., and Diggle, A. J. (1992). Relations between root length densities and root intersections with horizontal and vertical planes using root growth modelling in 3-dimensions. *Plant and Soil*, 145(2):245–252.

Bengough, A. G. and Mullins, C. E. (1990). Mechanical impedance to root growth: a review of experimental techniques and root growth responses. *Journal of Soil Science*, 41(3):341–358.

Bevitori, A. B., Da Silva, I. L. A., Lopes, F. P. D., and Monteiro, S. N. (2010). Diameter dependence of tensile strength by Weibull analysis: Part II jute fiber. *Revista Matéria*, 15(2):117–123.

Bischetti, G. B., Chiaradia, E. A., Epis, T., and Morlotti, E. (2009). Root cohesion of forest species in the Italian Alps. *Plant and Soil*, 324(1-2):71–89.

Bischetti, G. B., Chiaradia, E. A., Simonato, T., Speziali, B., Vitali, B., Vullo, P., and Zocco, A. (2005). Root strength and root area ratio of forest species in Lombardy (northern Italy). *Plant and Soil*, 278(1–2):11–22.

Børja, I., De Wit, H. A., Steffenrem, A., and Majdi, H. (2008). Stand age and fine root biomass, distribution and morphology in a Norway spruce chronosequence in southeast Norway. *Tree Physiology*, 28(5):773–784.

British Standards Institution (2007). *BS 1377-9:1990: Methods of test for soils for civil engineering purposes – Part 9: In-situ tests*. British Standards Institution, London.

British Standards Institution (2010). *BS ISO 13320:2009: Particle size analysis. Laser diffraction methods*. British Standards Institution, London.

Burroughs, E. R. and Thomas, B. R. (1977). *Declining root strength in Douglas-fir after felling as a factor in slope stability, Research Paper INT-190*. US Department of Agriculture Forest Service, Ogden, Utah.

Burylo, M., Hudek, C., and Rey, F. (2011). Soil reinforcement by the roots of six dominant species on eroded mountainous marly slopes (Southern Alps, France). *Catena*, 84(1–2):70–78.

Cammeraat, E., van Beek, R., and Kooijman, A. (2005). Vegetation succession and its consequences for slope stability in SE Spain. *Plant and Soil*, 278(1–2):135–147.

Casper, B. B., Schenk, H. J., and Jackson, R. B. (2003). Defining a plant's belowground zone of influence. *Ecology*, 84(9):2313–2321.

Chattopadhyay, B. C. and Pise, P. J. (1986). Uplift capacity of piles in sand. *Journal of Geotechnical Engineering (ASCE)*, 12(9):888–904.

Chen, Y., Thompson, C. E. L., and Collins, M. B. (2012). Saltmarsh creek bank stability: Biostabilisation and consolidation with depth. *Continental Shelf Research*, 35:64–74.

Chen, Z., Mi, H., Zhang, F., and Wang, X. (2003). A simplified method for 3D slope stability analysis. *Canadian Geotechnical Journal*, 40(3):675–683.

Cofie, P. and Koolen, A. J. (2001). Test speed and other factors affecting the measurements of tree root properties used in soil reinforcement models. *Soil & Tillage Research*, 63(1–2):51–56.

Collison, A. J. C., Anderson, M. G., and Lloyd, D. M. (1995). Impact of vegetation on slope stability in a humid tropical environment – a modeling approach. *Proceedings of the Institution of Civil Engineers – Water Maritime and Energy*, 112(2):168–175.

Comino, E. and Marengo, P. (2010). Root tensile strength of three shrub species: *Rosa canina*, *Cotoneaster dammeri* and *Juniperus horizontalis*. *Catena*, 82(3):227–235.

Comino, E., Marengo, P., and Rolli, V. (2010). Root reinforcement effect of different grass species: A comparison between experimental and models results. *Soil & Tillage Research*, 110(1):60–68.

Commandeur, P. R. and Pyles, M. R. (1991). Modulus of elasticity and tensile-strength of Douglas-fir roots. *Canadian Journal of Forest Research*, 21(1):48–52.

Coppin, N. and Richards, I. (1990). *Use of vegetation in civil engineering, CIRIA book 10*. Butterworths, Kent.

Coutts, M. P. (1983). Root architecture and tree stability. *Plant and Soil*, 71(1–3):171–188.

Cruden, D. M. and Varnes, D. J. (1996). Landslide types and processes. In Turner, A. K. and Shuster, R. L., editors, *Landslides: Investiagation and mitigation, Special report 247*, pages 36–75. Transport Research Board.

Danjon, F., Barker, D. H., Drexhage, M., and Stokes, A. (2008). Using three-dimensional plant root architecture in models of shallow-slope stability. *Annals of Botany*, 101(8):1281–1293.

Danjon, F., Bert, D., Porté, A., Meredieu, C., Trichet, P., Lagane, F., and Issenhuth, B. (2007). Effect of fertilization on 3D root architecture in 12-year-old *Pinus pinaster* trees. In *Proceedings 4th International Symposium on Dynamics of Physiological Processes in Roots of Woody Plants, 16th–19th September 2007, Bangor, UK, p. 36*.

Davies, M. C. R., Bowman, E. T., and White, D. J. (2010). Physical modelling of natural hazards. In Springman, S., Laue, J., and Seward, L., editors, *Physical modelling in geotechnics, ICPMG 2010*, pages 3–22, London. Taylor and Francis.

De Baets, S., Poesen, J., Reubens, B., Wemans, K. De Baerdemaeker, J., and Muys, B. (2008). Root tensile strength and root distribution of typical Mediterranean plant species and their contribution to soil shear strength. *Plant and Soil*, 305(1):207–226.

Dexter, A. R. (1988). Advances in characterization of soil structure. *Soil & Tillage Research*, 11(3–4):199–238.

Di Iorio, A., Lasserre, B., Scippa, G. S., and Chiatante, D. (2005). Root system architecture of *Quercus pubescens* trees growing on different sloping conditions. *Annals of Botany*, 95(2):351–361.

Diambra, A., Ibraim, E., Wood, D. M., and Russell, A. R. (2010). Fibre reinforced sands: Experiments and modelling. *Geotextiles and Geomembranes*, 28(3):238–250.

Docker, B. B. and Hubble, T. C. T. (2008). Quantifying root-reinforcement of river bank soils by four Australian tree species. *Geomorphology*, 100(3–4):401–418.

Docker, B. B. and Hubble, T. C. T. (2009). Modelling the distribution of enhanced soil shear strength beneath riparian trees of south-eastern Australia. *Ecological Engineering*, 35(5):921–934.

Duckett, N. R. (2014). *Development of improved predictive tools for mechanical soil root interaction*. PhD thesis, University of Dundee.

Dupuy, L., Fourcaud, T., and Stokes, A. (2005a). A numerical investigation into factors affecting the anchorage of roots in tension. *European Journal of Soil Science*, 56(3):319–327.

Dupuy, L., Fourcaud, T., and Stokes, A. (2005b). A numerical investigation into the influence of soil type and root architecture on tree anchorage. *Plant and Soil*, 278(1–2):119–134.

Ekanayake, J. C., Marden, M., Watson, A. J., and Rowan, D. (1997). Tree roots and slope stability: a comparison between *Pinus radiata* and kanuka. *New Zealand Journal of Forestry Science*, 27(2):216–233.

Ennos, A. R., Crook, M. J., and Grimshaw, C. (1993). The anchorage mechanics of maize, *zea mays*. *Journal of Experimental Botany*, 44(1):147–153.

Fan, C.-C. and Chen, Y.-W. (2010). The effect of root architecture on the shearing resistance of root-permeated soils. *Ecological Engineering*, 36(6):813–826.

Fan, C.-C. and Su, C.-F. (2008). Role of roots in the shear strength of root-reinforced soils with high moisture content. *Ecological Engineering*, 33(2):157–166.

Farabegoli, E., Onorevoli, G., and Morandi, M. (2012). The "turf's comb", a new in situ instrument to measure the shear resistance of the grass mantle: preliminary results and applications. In *The use of vegetation to improve slope stability, 3rd International Conference on Soil Bio- and Eco-engineering, Vancouver, Canada, 23-27 July 2012*. Conference poster.

Fattet, M., Fu, Y., Ghestem, M., Ma, W., Foulonneau, M., Nespoulous, J., Le Bissonnais, Y., and Stokes, A. (2011). Effects of vegetation type on soil resistance to erosion: Relationship between aggregate stability and shear strength. *Catena*, 87(1):60–69.

Forestry Commission (2011). *The UK Forestry Standard – the governments' approach to sustainable forest management*. Forestry Commission, Edinburgh.

Forestry Commission (2015). *Forestry Statistics 2015 – A compendium of statistics about woodland, forestry and primary wood processing in the United Kingdom*. Forestry Commission, Edinburgh.

Fredlund, D. G. and Rahardjo, H. (1993). *Soil mechanics for unsaturated soils*. John Wiley & Sons Inc., New York.

Genet, M., Kokutse, N., Stokes, A., Fourcaud, T., Cai, X., Ji, J., and Mickovski, S. (2008). Root reinforcement in plantations of *Cryptomeria japonica* D. Don: effect of tree age and stand structure on slope stability. *Forest Ecology and Management*, 256(8):1517–1526.

Genet, M., Stokes, A., Fourcaud, T., and Norris, J. E. (2010). The influence of plant diversity on slope stability in a moist evergreen deciduous forest. *Ecological Engineering*, 36(3):265–275.

Genet, M., Stokes, A., Salin, F., Mickovski, S., Fourcaud, T., Dumail, J. F., and van Beek, R. (2005). The influence of cellulose content on tensile strength in tree roots. *Plant and Soil*, 278(1–2):1–9.

Giadrossich, F., Schwarz, M., Cohen, D., Preti, F., and Or, D. (2013). Mechanical interactions between neighbouring roots during pullout tests. *Plant and Soil*, 367(1–2):391–406.

Goodman, A. M., Crook, M. J., and Ennos, A. R. (2001). Anchorage mechanics of the tap root system of winter-sown oilseed rape (*Brassica napus* L.). *Annals of Botany*, 87(3):397–404.

Gray, D. H. (1991). Deformation characteristics of reinforced sand in direct shear – discussion. *Journal of Geotechnical Engineering (ASCE)*, 117(11):1810–1812.

Gray, D. H. and Ohashi, H. (1983). Mechanics of fiber reinforcement in sand. *Journal of Geotechnical Engineering (ASCE)*, 109(3):335–353.

Gray, D. H. and Sotir, R. B. (1996). *Biotechnical and soil bioengineering slope stabilization, a practical guide for erosion control*. John Wiley & Sons Inc, New York.

Gregory, P. J. (2006). *Plant roots: growth, activity and interaction with soils*. Blackwell Publishing, Oxford.

Gyssels, G., Poesen, J., Bochet, E., and Li, Y. (2005). Impact of plant roots on the resistance of soils to erosion by water: a review. *Progress in Physical Geography*, 29(2):189–217.

Hales, T. C., Ford, C. R., Hwang, T., Vose, J. M., and Band, L. E. (2009). Topographic and ecologic controls on root reinforcement. *Journal of Geophysical Research – Earth Surface*, 114(F3):n/a–n/a.

Hammond, C., Hall, D., Miller, S., and Swetik, P. (1992). *Level I stability analysis (LISA) documentation for version 2.0. General Technical Report INT-285*. USDA Forest Service Intermountain Research Station, Ogden, Utah, US.

Hamza, O., Bengough, A. G., Bransby, M. F., Davies, M. C. R., and Hallett, P. D. (2007). Mechanics of root-pullout from soil: a novel image and stress analysis procedure. In Stokes, A., Spanos, I., Norris, J. E., and Cammeraat, E., editors, *Eco- and ground bio-engineering: the use of vegetation to improve slope stability*, pages 13–20. Springer, Dordrecht, The Netherlands.

Heineck, K. S., Coop, M. R., and Consoli, N. C. (2005). Effect of microreinforcement of soils from very small to large shear strains. *Journal of Geotechnical and Geoenvironmental Engineering*, 131(8):1024–1033.

Henderson, R., Ford, E. D., and Renshaw, E. (1983a). Morphology of the structural root-system of Sitka spruce. 2. computer-simulation of rooting patterns. *Forestry*, 56(2):137–153.

Henderson, R., Ford, E. D., Renshaw, E., and Deans, J. D. (1983b). Morphology of the structural root-system of Sitka spruce: 1. analysis and quantitative description. *Forestry*, 56(2):121–135.

Hengchaovanich, D. and Nilaweera, N. S. (1996). An assessment of strength properties of vetiver grass roots in relation to slope stabilization. In *Proceedings of the International Conference on Vetiver, Chain Kai, Thailand*, pages 153–158, Bangkok, Thailand. Office of the Royal Development Projects Board.

Hibbeler, R. C. (2014). *Structural analysis (9th edition)*. Prentice Hall, Upper Saddle River, NJ, US.

Hirano, Y., Dannoura, M., Aono, K., Igarashi, T., Ishii, M., Yamase, K., Makita, N., and Kanazawa, Y. (2009). Limiting factors in the detection of tree roots using ground-penetrating radar. *Plant and Soil*, 319(1–2):15–24.

Hoyt, R. M. and Clemence, S. P. (1989). Uplift capacity of helical anchors in soil. In *Proceedings of the Twelfth International Conference on Soil Mechanics and Foundation Engineering, Vol 2*, pages 1019–1022. Taylor and Francis.

Hudek, C., Burylo, M., and Rey, F. (2010). Root system traits of *Mahonia aquifolium* and its potential use in soil reinforcement in mountain horticultural practices. *Scientia Horticulturae*, 125(3):504–511.

Ibraim, E., Diambra, A., Russell, A. R., and Wood, D. M. (2012). Assessment of laboratory sample preparation for fibre reinforced sands. *Geotextiles and Geomembranes*, 34:69–79.

Ibraim, E. and Fourmont, S. (2007). Behaviour of sand reinforced with fibres. *Soil Stress–Strain Behavior: Measurement, Modeling and Analysis*, 146:807–818.

Imaizumi, F. and Sidle, R. C. (2012). Effect of forest harvesting on hydrogeomorphic processes in steep terrain of central Japan. *Geomorphology*, 169–170:109–122.

Ito, T. and Matsui, T. (1975). Methods to estimate lateral force acting on stabilizing piles. *Soils and Foundations*, 15:43–59.

Jackson, R. B., Canadell, J., Ehleringer, J. R., Mooney, H. A., Sala, O. E., and Schulze, E. D. (1996). A global analysis of root distribution for terrestial biomes. *Oecologica*, 108(3):389–411.

James Hutton Institute (2016). Soil information for Scottish soils (SIFFS). http://sifss.hutton.ac.uk/.

Jewell, R. A. and Wroth, C. P. (1987). Direct shear tests on reinforced sand. *Géotechnique*, 37(1):53–68.

Jobbágy, E. G. and Jackson, R. B. (2001). The distribution of soil nutrients with depth: Global patterns and the imprint of plants. *Biogeochemistry*, 53(1):51–77.

John, B., Pandey, H. N., and Tripathi, R. S. (2001). Vertical distribution and seasonal changes of fine and coarse root mass in *Pinus kesiya* Royle ex. Gordon forest of three different ages. *Acta Oecologica*, 22(5–6):293–300.

Johnson, C. E., Grisso, R. D., Nichols, T. A., and Bailey, A. C. (1987). Shear measurement for agricultural soils – a review. *Transactions of the ASAE*, 30(4):935–938.

Khalili, N., Geiser, F., and Blight, G. E. (2004). Effective stress in unsaturated soils: review with new evidence. *International Journal of Geomechanics*, 4(2):115–126.

Khalili, N. and Khabbaz, M. H. (1998). A unique relationship for χ for the determination of the shear strength of unsaturated soils. *Géotechnique*, 48(2):1–7.

Kim, T., Oshima, K., and Kawada, H. (2013). Impact tensile properties and strength development mechanism of glass for reinforcement fiber. *Journal of Physics: Conference Series*, 451(1):1–6.

Knappett, J. A. and Craig, R. F. (2012). *Craig's soil mechanics*. Spon, Abingdon, Oxfordshire, UK.

Landva, A. O. (1980). Vane testing in peat. *Canadian Geotechnical Journal*, 17(1):1–19.

Lauder, K. (2010). *The performance of pipeline ploughs*. PhD thesis, University of Dundee.

Liang, T. (2015). *Seismic performance of vegetated slopes*. PhD thesis, University of Dundee.

Liang, T., Knappett, J., and Bengough, A. (2014). Scale modelling of plant root systems using 3-D printing. In Gaudin, C. and White, D., editors, *ICPMG2014 – Physical Modelling in Geotechnics*, volume 1, pages 361–366, Leiden, The Netherlands. CRC.

Liang, T., Knappett, J., and Duckett, N. (2015). Modelling the seismic performance of rooted slopes from individual root–soil interaction to global slope behaviour. *Géotechnique*, 65(12):995–1009.

Loades, K. W., Bengough, A. G., Bransby, M. F., and Hallett, P. D. (2010). Planting density influence on fibrous root reinforcement of soils. *Ecological Engineering*, 36(3):276–284.

Loades, K. W., Bengough, A. G., Bransby, M. F., and Hallett, P. D. (2013). Biomechanics of nodal, seminal and lateral roots of barley: effects of diameter, waterlogging and mechanical impedance. *Plant and Soil*, 370(1):407–418.

Lunne, T., Robertson, P. K., and Powell, J. J. M. (1997). *Cone penetration testing in geotechnical practice*. Blackie Academic/Routledge Publishing, New York.

Mao, Z., Bourrier, F., Stokes, A., and Fourcaud, T. (2014). Three-dimensional modelling of slope stability in heterogeneous montane forest ecosystems. *Ecological Modelling*, 273:11–22.

Mao, Z., Saint-Andre, L., Genet, M., Mine, F.-X., Jourdan, C., Rey, H., Courbaud, B., and Stokes, A. (2012). Engineering ecological protection against landslides in diverse mountain forests: Choosing cohesion models. *Ecological Engineering*, 45:55–69.

Mattia, C., Bischetti, G. B., and Gentile, F. (2005). Biotechnical characteristics of root systems of typical Mediterranean species. *Plant and Soil*, 278(1–2):23–32.

Meijer, G. J., Bengough, A. G., Knappett, J. A., Loades, K. W., and Nicoll, B. C. (2015). Comparison of new in situ root-reinforcement measuring devices to existing techniques. In Winter, M., Smith, D., Eldred, P., and Toll, D., editors, *Proceedings of the 16th European Conference on Soil Mecanics and Geotechnical Engineering (XVI ECSMGE): Geotechnical Engineering for Infrastructure and Development*, pages 1621–1626, London. Institution of Civil Engineers.

Meijer, G. J., Bengough, A. G., Knappett, J. A., Loades, K. W., and Nicoll, B. C. (2016a). In situ root identification through blade penetrometer testing – part 1: interpretative models and laboratory testing. *Géotechnique*. Under review.

Meijer, G. J., Bengough, A. G., Knappett, J. A., Loades, K. W., and Nicoll, B. C. (2016b). In situ root identification through blade penetrometer testing – part 2: field testing. *Géotechnique*. Under review.

Meijer, G. J., Bengough, A. G., Knappett, J. A., Loades, K. W., and Nicoll, B. C. (2016c). New in-site techniques for measuring the properties of root-reinforced soil – laboratory evaluation. *Géotechnique*, 66(1):27–40.

Michalowski, R. L. (2008). Limit analysis with anisotropic fibre-reinforced soil. *Géotechnique*, 58(6):489–501.

Michalowski, R. L. and Çermák, J. (2002). Strength anisotropy of fiber-reinforced sand. *Computers and Geotechnics*, 29(4):279–299.

Michalowski, R. L. and Çermák, J. (2003). Triaxial compression of sand reinforced with fibers. *Journal of Geotechnical and Geoenvironmental Engineering*, 129(2):125–136.

Mickovski, S. B., Bengough, A. G., Bransby, M. F., Davies, M. C. R., Hallett, P. D., and Sonnenberg, R. (2007). Material stiffness, branching pattern and soil matric potential affect the pullout resistance of model root systems. *European Journal of Soil Science*, 58(6):1471–1481.

Mickovski, S. B., Hallett, P. D., Bransby, M. F., Davies, M. C. R., Sonnenberg, R., and Bengough, A. G. (2009). Mechanical reinforcement of soil by willow roots: Impacts of root properties and root failure mechanism. *Soil Science Society of America Journal*, 73(4):1276–1285.

Mickovski, S. B., Stokes, A., van Beek, R., Ghestem, M., and Fourcaud, T. (2011). Simulation of direct shear tests on rooted and non-rooted soil using finite element analysis. *Ecological Engineering*, 37(10):1523–1532.

Mickovski, S. B. and Van Beek, L. P. H. (2009). Root morphology and effects on soil reinforcement and slope stability of young vetiver (Vetiveria zizanioides) plants grown in semi-arid climate. *Plant and Soil*, 324(1):43–56.

Mitchell, J. K. and Soga, K. (2005). *Fundamentals of Soil Behavior*. John Wiley & Sons Inc., New York.

Moos, C., Bebi, P., Graf, F., Mattli, J., Rickli, C., and Schwarz, M. (2016). How does forest structure affect root reinforcement and susceptibility to shallow landslides? *Earth Surface Processes and Landforms*, 41(7):951–960.

Nicoll, B. C. and Ray, D. (1996). Adaptive growth of tree root systems in response to wind action and site conditions. *Tree Physiology*, 16(11–12):891–898.

Nilaweera, N. S. and Nutalaya, P. (1999). Role of tree roots in slope stabilisation. *Bulletin of Engineering Geology and the Environment*, 57(3):337–342.

Nindl, D. and Wiebking, M. (2010). *Surveying tripods – White paper. Characteristics and influences*. Leica Geosystems, Heerbrugg, Switzerland.

Normaniza, O., Faisal, H. A., and Barakbah, S. S. (2008). Engineering properties of *Leucaena leucocephala* for prevention of slope failure. *Ecological Engineering*, 32(3):215–221.

Norris, J. E. (2005). Root reinforcement by hawthorn and oak roots on a highway cut-slope in southern England. *Plant and Soil*, 278(1–2):43–53.

Norris, J. E., Stokes, A., Mickovski, S. B., Cammeraat, E., Van Beek, R., Nicoll, B. C., and Achim, A. (2008). *Slope stability and erosion control: Ecotechnical solutions*. Springer, Dordrecht, The Netherlands.

O'Loughlin, C. and Ziemer, R. R. (1982). The importance of root strength and deterioration rates upon edaphic stability in steepland forests. In *I.U.F.R.O. Workshop P.1.07-00 Ecology of Subalpine Ecosystems as a Key to Management*, pages 70–78, Courvallis, Oregon. Oregon State University.

Operstein, V. and Frydman, S. (2000). The influence of vegetation on soil strength. *Ground Improvement*, 4:81–89.

Ordnance Survey (2016). The national grid. https://www.ordnancesurvey.co.uk/resources/maps-and-geographic-resources/the-national-grid.html, accessed on 26/05/2016.

Osman, N. and Barakbah, S. S. (2006). Parameters to predict slope stability – soil water and root profiles. *Ecological Engineering*, 28(1):90–95.

Pack, J. S. (2009). *Practical Design and Inspection Guide for Helical Piles and Helical Tension Anchors, fourth edition*. I.M.R. Inc., Denver, Colorado, US.

Petley, D. (2012). Global patterns of loss of life from landslides. *Geology*, 40(10):927–930.

Pierret, A., Moran, C. J., McLachan, C. B., and Kirby, J. M. (2000). Measurement of root length density in intact samples using x-radiography and image analysis. *Image Analysis & Stereology*, 19(2):145–149.

Pohl, M., Alig, D., Koerner, C., and Rixen, C. (2009). Higher plant diversity enhances soil stability in disturbed alpine ecosystems. *Plant and Soil*, 324(1–2):91–102.

Pohl, M., Graf, F., Buttler, A., and Rixen, C. (2012). The relationship between plant species richness and soil aggregate stability can depend on disturbance. *Plant and Soil*, 355(1–2):87–102.

Pollen, N. (2007). Temporal and spatial variability in root reinforcement of streambanks: Accounting for soil shear strength and moisture. *Catena*, 69(3):197–205.

Pollen, N. and Simon, A. (2005). Estimating the mechanical effects of riparian vegetation on stream bank stability using a fiber bundle model. *Water Resources Research*, 41(7):W07025.

Pollen-Bankhead, N. and Simon, A. (2009). Enhanced application of root-reinforcement algorithms for bank-stability modeling. *Earth Surface Processes and Landforms*, 34(4):471–480.

Pollen-Bankhead, N. and Simon, A. (2010). Hydrologic and hydraulic effects of riparian root networks on streambank stability: Is mechanical root-reinforcement the whole story? *Geomorphology*, 116(3–4):353–362.

Preti, F. (2006). Stabilità dei versanti vegetati. In Sauli, G., Cornelini, P., and Preti, F., editors, *Manuale 3 Ingegneria Naturalistica Sistemazione dei versanti*, pages 137–168. Regione Lazio. in Italian.

Preti, F. (2013). Forest protection and protection forest: Tree root degradation over hydrological shallow landslides triggering. *Ecological Engineering*, 61, Part C:633–645.

R Core Team (2013). *R: A Language and Environment for Statistical Computing*. R Foundation for Statistical Computing, Vienna, Austria.

Randolph, M. and Gourvenec, S. (2011). *Offshore geotechnical engineering*. Spon, New York, US.

Reese, L. C. and Van Impe, W. F. (2011). *Single piles and pile groups under lateral loading, 2nd edition*. CRC, Leiden, The Netherlands.

Reubens, B., Poesen, J., Danjon, F., Geudens, G., and Muys, B. (2007). The role of fine and coarse roots in shallow slope stability and soil erosion control with a focus on root system architecture: a review. *Trees-Structure and Function*, 21(4):385–402.

Riestenberg, M. M. (1994). *Anchoring of thin colluvium by roots of sugar maple and white ash on hillslopes in Cincinnati, US Geological Survey Bulletin 2059-E*. US Government Print Office, Washington, US.

Roering, J. J., Schmidt, K. M., Stock, J. D., Dietrich, W. E., and Montgomery, D. R. (2003). Shallow landsliding, root reinforcement, and the spatial distribution of trees in the Oregon Coast Range. *Canadian Geotechnical Journal*, 40(2):237–253.

Rowe, N. P., Isnard, S., Gallebmüller, F., and Speck, T. (2006). Diversity of mechanical architectures in climbing plants: an ecological perspective. In Herrel, A., Speck, T., and Rowe, N., editors, *Ecology and biomechanics: a mechanical approach to the ecology of animals and plants*, pages 35–60. CRC, Boca Raton, FL, US.

Schenk, H. J. and Jackson, R. B. (2002). The global biogeography of roots. *Ecological Monographs*, 72(3):311–328.

Schiechtl, H. M. (1980). *Bioengineering for Land Reclamation and Conservation*. University of Alberta Press, Edmonton, Alberta, Canada.

Schmidt, K. M., Roering, J. J., Stock, J. D., Dietrich, W. E., Montgomery, D. R., and Schaub, T. (2001). The variability of root cohesion as an influence on shallow landslide susceptibility in the Oregon Coast Range. *Canadian Geotechnical Journal*, 38(5):995–1024.

Schwarz, M., Giadrossich, F., and Cohen, D. (2013). Modeling root reinforcement using a root-failure Weibull survival function. *Hydrology and Earth System Sciences*, 17:4367–4377.

Schwarz, M., Lehmann, P., and Or, D. (2010). Quantifying lateral root reinforcement in steep slopes – from a bundle of roots to tree stands. *Earth Surface Processes and Landforms*, 35(3):354–367.

Schwarz, M., Rist, A., Cohen, D., Giadrossich, F., Egorov, P., Büttner, D., Stolz, M., and Thormann, J.-J. (2015). Root reinforcement of soils under compression. *Journal of Geophysical Research: Earth Surface*, 120(10):2103–2120.

Scippa, G. S., Di Michele, M., Di Iorio, A., Costa, A., Lasserre, B., and Chiatante, D. (2006). The response of *Spartium junceum* roots to slope: Anchorage and gene factors. *Annals of Botany*, 97(5):857–866.

Scott, J., Loveridge, F., and O'Brien, A. S. (2007). Influence of climate and vegetation on railway embankments. In Cuellar, V., Dapena, E., Alonso, E., Echave, J. M., Gens, A., de Justo, J. L., Oteo, C., Rodriguez-Ortiz, J. M., Sagaseta, C., Sola, P., and Soriano, A., editors, *Proceedings of the 14th European Conference on Soil Mechanics and Geotechnical Engineering (XIV ECSMGE), Madrid*, pages 659–664, Amsterdam. IOS Press.

SEPA (2008). *Engineering in the water environment: good practice guide – Bank protection: rivers and lochs*. Scottish Environment Protection Agency (SEPA).

Shewbridge, S. E. and Sitar, N. (1989). Deformation characteristics of reinforced sand in direct shear. *Journal of Geotechnical Engineering (ASCE)*, 115(8):1134–1147.

Shewbridge, S. E. and Sitar, N. (1991). Deformation characteristics of reinforced sand in direct shear – closure. *Journal of Geotechnical Engineering (ASCE)*, 117(11):1812–1817.

Sidle, R. C. and Ochiai, H. (2006). *Landslides: Processes, Prediction, and Land Use*, volume 18 of *Water Resources Monograph*. AGU, Washington D.C.

Simon, A. and Collison, A. J. C. (2002). Quantifying the mechanical and hydrologic effects of riparian vegetation on streambank stability. *Earth Surface Processes and Landforms*, 27(5):527–546.

Smucker, A. J. M. (2005). Structure and roots. In Lal, R., editor, *Encyclopedia of soil science, second edition – volume 2*, pages 1695–1697. CRC, Boca Raton, FL, US.

Sonnenberg, R. (2008). *Centrifuge modelling of root reinforced slopes*. PhD thesis, Univerisity of Dundee.

Sonnenberg, R., Bransby, M. F., Hallett, P. D., Bengough, A. G., Mickovski, S. B., and Davies, M. C. R. (2010). Centrifuge modelling of soil slopes reinforced with vegetation. *Canadian Geotechnical Journal*, 47(12):1415–1430.

Steele, S. J., Gower, S. T., Vogel, J. G., and Norman, J. M. (1997). Root mass, net primary production and turnover in aspen, jack pine and black spruce forests in Saskatchewan and Manitoba, Canada. *Tree Physiology*, 17(8–9):577–587.

Stokes, A. (2002). Biomechanics of tree root anchorage. In Waisel, Y., Eshel, A., and Kafkafi, U., editors, *Plant Roots: The Hidden Half*, pages 269–286. Marcel Dekker Inc., New York.

Stokes, A., Abd. Ghani, M., Salin, F., Danjon, F., Jeannin, H., Berthier, S., Kokutse, A. D., and Frochot, H. (2007). Root morphology and strain distribution during tree failure on mountain slopes. In Stokes, A., Spanos, I., Norris, J. E., and Cammeraat, E., editors, *Eco- and ground bio-engineering: the use of vegetation to improve slope stability*, pages 165–173. Springer.

Stokes, A., Atger, C., Bengough, A. G., Fourcaud, T., and Sidle, R. C. (2009). Desirable plant root traits for protecting natural and engineered slopes against landslides. *Plant and Soil*, 324(1–2):1–30.

Stokes, A., Ball, J., Fitter, A. H., Brain, P., and Coutts, M. P. (1996). An experimental investigation of the resistance of model root systems to uprooting. *Annals of Botany*, 78(4):415–421.

Stokes, A., Fourcaud, T., Hruska, J., Çermák, J., Nadyezdhina, N., Nadyezhdin, V., and Praus, L. (2002). An evaluation of different methods to investigate root system architecture of urban trees in situ: I. ground-penetrating radar. *Journal of Arboriculture*, 28(1):2–10.

Stokes, V. (2011). *The impact of forests and forest management on slope stability. Can continuous cover forestry management improve slope stability?* Forestry Commission.

Tang, C., Shi, B., Gao, W., Chen, F., and Cai, Y. (2007). Strength and mechanical behavior of short polypropylene fiber reinforced and cement stabilized clayey soil. *Geotextiles and Geomembranes*, 25(3):194–202.

Tarantino, A., Mongiovi, L., and McDougall, J. (2002). Analysis of hydrological effects of vegetation on slope stability. In Juca, J., de Campos, T., and Marinho, A., editors, *Unsaturated Soils: Proceedings of the third international conference on unsaturated soils, UNSAT 2002, 10–13 March 2002, Recife, Brazil, Volume 2*, pages 749–754. CRC.

Thomas, R. E. and Pollen-Bankhead, N. (2010). Modeling root-reinforcement with a fiber-bundle model and Monte Carlo simulation. *Ecological Engineering*, 36(1):47–61.

Tiwari, R. C., Bhandary, N. P., Yatabe, R., and Bhat, D. R. (2013). New numerical scheme in the finite-element method for evaluating the root-reinforcement effect on soil slope stability. *Géotechnique*, 63(2):129–139.

Tosi, M. (2007). Root tensile strength relationships and their slope stability implications of three shrub species in the northern Apennines (Italy). *Geomorphology*, 87(4):268–283.

Transport Scotland (2016a). Known landslide areas. http://www.transport.gov.scot/road/maintenance/known-landslide-areas, accessed on 7/4/2016.

Transport Scotland (2016b). Previous landslides at the A83 Rest and Be Thankful. http://www.transport.gov.scot/road/a83-rest-and-be-thankful/previous-landslides-a83-rest-and-be-thankful, accessed on 21/03/2016.

UKCIP (2009). UK climate projections, 2009 (UKCP09). http://ukclimateprojections.metoffice.gov.uk/, accessed on 7/4/2016.

USGS (2016). Landslides faq. http://www.usgs.gov/faq/taxonomy/term/9752, accessed on 8/4/2016.

Utomo, W. H. and Dexter, A. R. (1981). Age hardening of agricultural top soils. *Journal of Soil Science*, 32(3):335–350.

Van Beek, L. P. H., Wint, J., Cammeraat, L. H., and Edwards, J. P. (2005). Observation and simulation of root reinforcement on abandoned Mediterranean slopes. *Plant and Soil*, 278(1–2):55–74.

Van Genuchten, M. T. (1980). A closed-form equation for predicting the hydraulic conductivity of unsaturated soils. *Soil Science Society of America Journal*, 44(5):892–898.

Vergani, C., Chiaradia, E. A., Bassanelli, C., and Bischetti, G. B. (2014a). Root strength and density decay after felling in a silver fir–Norway spruce stand in the Italian Alps. *Plant and Soil*, 377(1–2):63–81.

Vergani, C., Chiaradia, E. A., and Bischetti, G. B. (2012). Variability in the tensile resistance of roots in alpine forest tree species. *Ecological Engineering*, 46:43–56.

Vergani, C., Schwarz, M., Cohen, D., Thormann, J. J., and Bischetti, G. B. (2014b). Effects of root tensile force and diameter distribution variability on root reinforcement in the Swiss and Italian Alps. *Canadian Journal of Forest Research*, 44(11):1426–1440.

Verruijt, A. (2012). *Soil mechanics*. Delft University of Technology, Delft. Online accessible via: http://geo.verruijt.net/software/SoilMechBook2012.pdf.

Waldron, L. J. (1977). Shear resistance of root-permeated homogeneous and stratified soil. *Soil Science Society of America Journal*, 41(5):843–849.

Waldron, L. J. and Dakessian, S. (1981). Soil reinforcement by roots – calculation of increased soil shear resistance from root properties. *Soil Science*, 132(6):427–435.

Wang, Z., Guo, D., Wang, X., Gu, J., and Mei, L. (2006). Fine root architecture, morphology, and biomass of different branch orders of two Chinese temperate tree species. *Plant and Soil*, 288(1–2):155–171.

Watson, A., Phillips, C., and Marden, M. (1999). Root strength, growth, and rates of decay: root reinforcement changes of two tree species and their contribution to slope stability. *Plant and Soil*, 217(1–2):39–47.

Weisstein, E. W. (2016). Parabolic segment. http://mathworld.wolfram.com/ParabolicSegment.html, accessed on 08/03/2016.

Winter, M. G., Macgregor, F., and Shackman, L. (2005). *Scottish Road Network Landslides Study*. The Scottish Executive, Edinburgh.

Wroth, C. P. and Wood, D. M. (1978). The correlation of index properties with some basic engineering properties of soils. *Canadian Geotechnical Journal*, 15(2):137–145.

Wu, T. H. (1976). *Investigation of landslides on Prince of Wales Island. Geotechnical Engineering Report 5*. Civil Engineering Department, Ohio State University, Columbus, Ohio.

Wu, T. H. (2007). *Root reinforcement: analyses and experiments*, volume 103 of *Eco- and Ground Bio-Engineering: The Use of Vegetation to Improve Slope Stability*. Springer, Dordrecht.

Wu, T. H. (2013). Root reinforcement of soil: review of analytical models, test results and applications to design. *Canadian Geotechnical Journal*, 50(3):259–274.

Wu, T. H., McKinnell III, W. P., and Swanston, D. N. (1979). Strength of tree roots and landslides on Prince of Wales Island, Alaska. *Canadian Geotechnical Journal*, 16(1):19–33.

Wu, T. H., McOmber, R. M., Erb, R. T., and Beal, P. E. (1988). Study of soil–root interaction. *Journal of Geotechnical Engineering (ASCE)*, 114(12):1351–1375.

Wu, T. H. and Watson, A. (1998). In situ shear tests of soil blocks with roots. *Canadian Geotechnical Journal*, 35(4):579–590.

Yang, Y., Chen, L., Li, N., and Zhang, Q. (2016). Effect of root moisture content and diameter on root tensile properties. *PLoS ONE*, 11:1–17.

Zhang, C. B., Chen, L. H., and Jiang, J. (2014). Why fine tree roots are stronger than thicker roots: The role of cellulose and lignin in relation to slope stability. *Geomorphology*, 206:196–202.

Zhang, C.-B., Chen, L.-H., Liu, Y.-P., Ji, X.-D., and Liu, X.-P. (2010). Triaxial compression test of soil–root composites to evaluate influence of roots on soil shear strength. *Ecological Engineering*, 36(1):19–26.

Ziemer, R. R. and Swanston, D. N. (1977). *Root strength changes after logging in southeast Alaska, USDA Forest Service Research Note PNW-306*. US Departement of Agriculture Forest Service, Portland, Oregon.

Ziemian, C., Sharma, M., and Ziemian, S. (2012). Anisotropic mecanical properties of ABS parts fabricated by fused deposition modelling. In Gokcek, M., editor, *Mechanical Engineering*, pages 159–180. InTech. Available from: http://www.intechopen.com/books/mechanical-engineering/anisotropic-mechanical-properties-of-abs-parts-fabricated-by-fused-deposition-modeling-.

Appendices

A

Pin vane spacing

When using the pin vane device, different failure mechanisms might develop depending on the adopted prong spacing. To assure cylindrical soil failure, the torque resistance induced by soil resistance acting on the cylindrical interface should be lower than the torque resistance caused by soil resistance acting on individual prongs. The torque required to reach soil yield on this interface, T_{soil} [kNm], is estimated as:

$$T_{soil} = A \cdot \frac{d_{pv}}{2} \cdot \tau = \frac{1}{2} \cdot \pi \cdot h_{pv} \cdot d_{pv}^2 \cdot \tau \tag{A.1}$$

where h_{pv} and d_{pv} are the height and diameter of the soil cylinder [m] and τ the soil shear strength, defined using the Mohr-Coulomb model:

$$\tau = \sigma_v' \cdot K_0 \cdot \tan\phi' + c' \tag{A.2}$$

where σ_v' is the effective vertical soil pressure [kPa], K_0 the coefficient of lateral earth pressure at rest $(1 - \sin\phi')$, and ϕ' [°] and c' [kPa] the soil angle of internal friction and soil cohesion respectively. To allow for a dimensionless analysis, the resistance acting on the top and bottom interfaces of the coil cylinder was neglected. For the adopted pin vane design, where there will be no soil resistance acting on the top interface because of excavation prior to testing, this introduced an underestimation of ≈10% in soil resistance. This was deemed to be an acceptable simplification.

The torque resistance caused by soil resisting individual prong movement was estimated using the plastic deformation model derived by Ito and Matsui (1975) to estimate lateral soil forces acting on stabilizing piles in slopes. In this model, equilibrium of forces is analysed assuming a bilinear failure surface around the pile, see Figure A.1. Soil is assumed to become plastic only in a small area around the pile/prong according to the Mohr-Coulomb yield criterion. This model can be applied to the pin vane, because the forces applied by moving soil on stationary piles are the same as those caused by moving

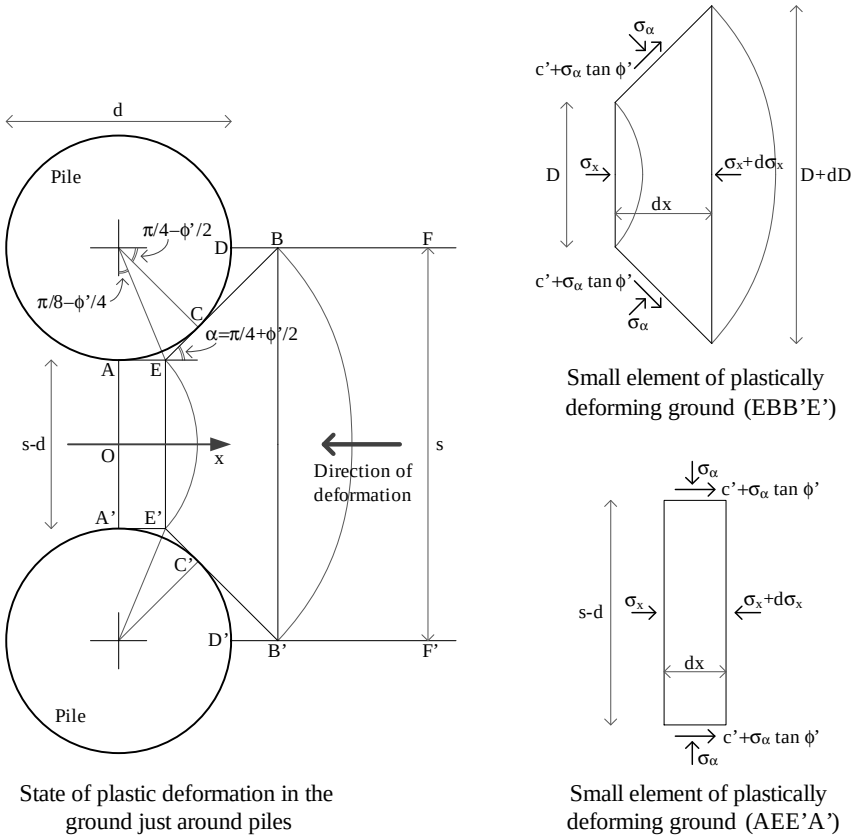

Figure A.1: Model definition and force equilibrium assumptions for the plastic deformation model derived by Ito and Matsui (1975) to calculate the lateral soil forces acting on stabilizing pile wall in slopes.

piles through stationary soil. The diameter of the pile is defined as d [m] and the pile centre-to-centre distance as s [m]. The resistance F_{pile} [kNm^{-1}] acting over width s per unit length of pile, according to Ito and Matsui's plastic deformation model, is equal to:

$$F_{pile} = c' \cdot s \cdot \left(\frac{s}{d-s}\right)^{\left(\sqrt{N_\phi}\cdot\tan\phi' + N_\phi - 1\right)} \cdot \left[\frac{1}{N_\phi \cdot \tan\phi'} \cdot \left\{\exp\left(\frac{d}{d-s} \cdot N_\phi \cdot \tan\phi' \cdot \tan\left(\frac{\pi}{8} + \frac{\phi'}{4}\right)\right) - 2 \cdot \sqrt{N_\phi} \cdot \tan\phi' - 1\right\} + \frac{2 \cdot \tan\phi' + 2 \cdot \sqrt{N_\phi} + N_\phi^{-0.5}}{\sqrt{N_\phi} \cdot \tan\phi' + N_\phi - 1}\right] - c' \cdot \left\{s \cdot \frac{2 \cdot \tan\phi' + 2 \cdot \sqrt{N_\phi} + N_\phi^{-0.5}}{\sqrt{N_\phi} \cdot \tan\phi' + N_\phi - 1} - 2 \cdot (d-s) \cdot N_\phi^{-0.5}\right\} + \frac{\sigma'_v}{N_\phi} \cdot \left\{s \cdot \left(\frac{s}{d-s}\right)^{\left(\sqrt{N_\phi}\cdot\tan\phi' + N_\phi - 1\right)} \cdot \exp\left(\frac{d}{d-s} \cdot N_\phi \cdot \tan\phi' \cdot \tan\left(\frac{\pi}{8} + \frac{\phi'}{4}\right)\right) - (d-s)\right\}$$

where $N_\phi = \tan^2(\pi/4 + \phi'/2)$ [-] and σ'_v the vertical effective stress [kPa].

Then, the torque required to overcome the soil resistance of the prongs is calculated as

follows:

$$T_{prongs} = \underbrace{F_{pile} \cdot h_{pv}}_{\substack{\text{Force} \\ \text{per} \\ \text{prong}}} \cdot \underbrace{\frac{2 \cdot d_{pv}}{s}}_{\substack{\text{Number of} \\ \text{prongs,} \\ \text{cruciform} \\ \text{pattern}}} \cdot \underbrace{\frac{d_{pv}}{4}}_{\substack{\text{Average} \\ \text{moment} \\ \text{arm}}} \tag{A.3}$$

In this analysis, the difference in displacement between prongs on the outside and those closer to the centre, caused by rotational movement, is neglected. Every point in the device is considered to have the same displacement so that Ito and Matsui's pile 'wall' model can be adopted.

When $T_{soil} < T_{prongs}$, the desired cylindrical soil failure will take place. When $T_{soil} > T_{prongs}$ however, soil yield will take place around each individual prong. From the model formulation it follows that the ratio between T_{soil} and T_{prongs} is independent of the dimensions of the device, and only a function of the soil strength parameters ϕ' and c', vertical soil stress level σ'_v and the relative prong spacing s/d.